doi.org/10.26434/chemrxiv.12912455.v1

Aryl Amination with Soluble Weak Base Enabled by a Water-Assisted Mechanism

Sii Hong Lau, Peng Yu, Liye Chen, Christina B. Madsen-Duggan, Michael Williams, Brad Carrow

Submitted date: 03/09/2020 • Posted date: 04/09/2020

Citation information: Lau, Sii Hong; Yu, Peng; Chen, Liye; Madsen-Duggan, Christina B.; Williams, Michael; Carrow, Brad (2020): Aryl Amination with Soluble Weak Base Enabled by a Water-Assisted Mechanism. ChemRxiv. Preprint. https://doi.org/10.26434/chemrxiv.12912455.v1

Amination of aryl halides has become one of the most commonly practiced C–N bond-forming reactions in pharmaceutical and laboratory synthesis. The widespread use of strong or poorly soluble inorganic bases for amine activation nevertheless complicates the compatibility of this important reaction class with sensitive substrates as well as applications in flow and automated synthesis, to name a few. We report a palladium-catalyzed C–N coupling using Et_3N as a weak, soluble base, which allows a broad substrate scope that includes bromo- and chloro(hetero)arenes, primary anilines, secondary amines, and amide type nucleophiles together with tolerance for a range of base-sensitive functional groups. Mechanistic data have established a unique pathway for these reactions in which water serves multiple beneficial roles. In particular, ionization of a neutral catalytic intermediate via halide displacement by H_2O generates, after proton loss, a coordinatively-unsaturated Pd–OH species that can bind amine substrate triggering intramolecular N–H heterolysis. This water-assisted pathway operates efficiently with even weak terminal bases, such as Et_3N. The use of a simple, commercially available ligand, PAd_3, is key to this water-assisted mechanism by promoting coordinative unsaturation in catalytic intermediates responsible for the heterolytic activation of strong element-hydrogen bonds, which enables broad compatibility of carbon-heteroatom cross-coupling reactions with sensitive substrates and functionality.

File list (3)

Water-Assisted C-N Coupling_Final_TOC.pdf (43.82 KiB)	view on ChemRxiv	download file
Water-Assisted C-N Coupling_Final.pdf (1.76 MiB)	view on ChemRxiv	download file
Water-Assisted C-N Coupling_SUPPORTING INFORMA... (11.70 MiB)	view on ChemRxiv	download file

H_2O-assisted mechanism · soluble weak base · base sensitive functionality

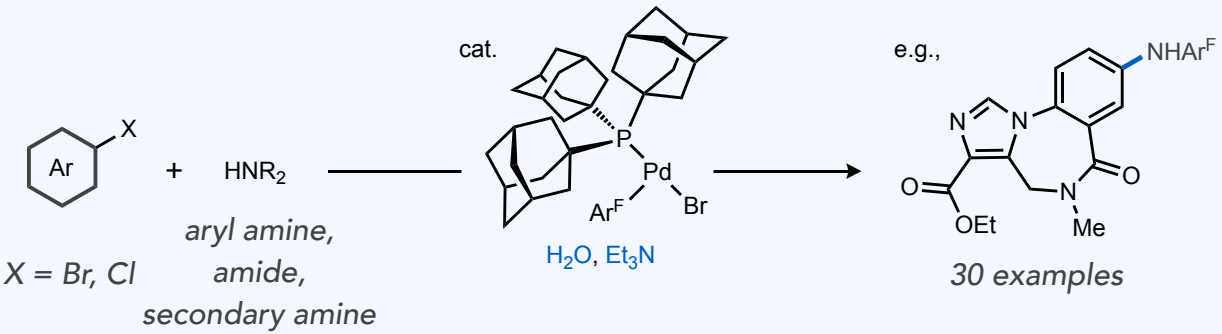

Lewis acid & Brønsted base synergism

Aryl Amination with Soluble Weak Base Enabled by a Water-Assisted Mechanism

Sii Hong Lau,[†] Peng Yu,[†] Liye Chen,[†] Christina B. Madsen-Duggan,[¶] Michael J. Williams,[¶] and Brad P. Carrow[†,*]

[†]Department of Chemistry, Princeton University, Princeton, New Jersey 08544, United States

[¶]Chemical Process Development, Bristol Myers Squibb, 556 Morris Avenue, Summit, NJ 07902, United States

ABSTRACT: Amination of aryl halides has become one of the most commonly practiced C–N bond-forming reactions in pharmaceutical and laboratory synthesis. The widespread use of strong or poorly soluble inorganic bases for amine activation nevertheless complicates the compatibility of this important reaction class with sensitive substrates as well as applications in flow and automated synthesis, to name a few. We report a palladium-catalyzed C–N coupling using Et_3N as a weak, soluble base, which allows a broad substrate scope that includes bromo- and chloro(hetero)arenes, primary anilines, secondary amines, and amide type nucleophiles together with tolerance for a range of base-sensitive functional groups. Mechanistic data have established a unique pathway for these reactions in which water serves multiple beneficial roles. In particular, ionization of a neutral catalytic intermediate via halide displacement by H_2O generates, after proton loss, a coordinatively-unsaturated Pd–OH species that can bind amine substrate triggering intramolecular N–H heterolysis. This water-assisted pathway operates efficiently with even weak terminal bases, such as Et_3N. The use of a simple, commercially available ligand, PAd_3, is key to this water-assisted mechanism by promoting coordinative unsaturation in catalytic intermediates responsible for the heterolytic activation of strong element-hydrogen bonds, which enables broad compatibility of carbon-heteroatom cross-coupling reactions with sensitive substrates and functionality.

INTRODUCTION

Carbon-nitrogen cross-coupling reactions using palladium and related late transition metal catalysts are some of the most widely utilized methods for the synthesis of pharmaceuticals, agrochemicals, organic electronic materials, and fine chemicals.[1] Over that past two decades, numerous innovations in the ligand(s) and precatalyst structure of palladium complexes have been made that have expanded the diversity of organic electrophile and amine nucleophile classes applicable to this transformation.[2] On the other hand, the bases used for Buchwald-Hartwig amination have evolved to a lesser extent; modern C–N coupling methods still rely heavily on ionic bases, such as sodium *tert*-butoxide or lithium hexamethyldisilazide (LiHMDS).[3] Such strong ionic bases impose compatibility issues with functional groups susceptible to nucleophilic attack, such as carboxylic acids, esters, nitriles, nitro groups, and carbonyl groups with enolizable sites, to name a few.[4] Amination reactions conducted on scale in organic solvents using common inorganic bases, such as hydroxide, carbonate and phosphate salts, also frequently incur reproducibility issues.[5] High-throughput experimentation (HTE)[6] and continuous flow chemistry[7] face similar issues where base insolubility can present either an inconvenience or major hurdle, respectively.[8] The development of new methods that operate efficiently with weak, soluble, and inexpensive bases could circumvent all of these issues and broaden the applicability of C–N coupling in industrial applications.

The difficulty of transitioning C–N coupling toward the use of weak, soluble bases can be attributed, at least in part, to a mechanistic challenge using conventional Pd catalysts, such as those ligated by BINAP as a prototypical example. A combined computational and experimental mechanistic study by Norrby found that soluble neutral bases such as the phosphazene *tert*-butylimino-

Scheme 1. Base effects in Pd-catalyzed C–N coupling.

A. Conventional conditions (strong ionic bases)

Norrby, 2014:

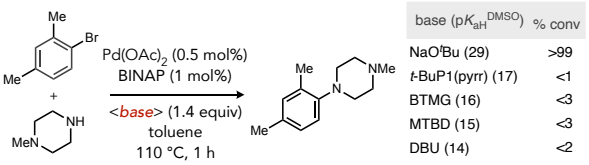

B. Ionic pathway (soluble amine bases)

Buchwald, 2018:

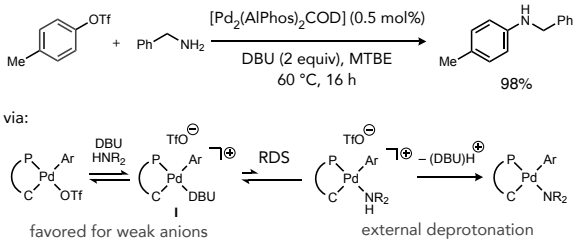

C. Ambiphilic, water-assisted pathway (*this work*)

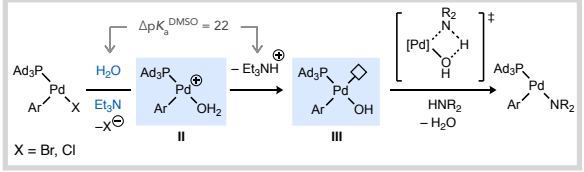

- Coordination-induced acidification (**II**)
- Lewis acid & Brønsted base synergism (**III**)
- Base inhibition (i.e., **I**) mitigated by H_2O
- Amination of ArBr and ArCl enabled with a soluble weak base

tri(pyrrolidino)phosphorene (*t*-BuP1(pyrr)), Barton's guanidine base 2-*tert*-butyl-1,1,3,3-tetramethylguanidine (BTMG), or the amidines 7-methyl-1,5,7-triazabicyclo[4.4.0]dec-5-ene (MTBD) and 1,8-diazabicyclo[5.4.0]undec-7-ene (DBU) perform poorly relative to NaO^{t}Bu as a prototypical strong ionic base (Scheme 1a).[9] This striking difference was correlated to the preference of the system to maintain neutral reaction pathways in nonpolar organic solvents because ionization of neutral metal halide complexes is too energetically unfavorable. Ionic bases are more reactive in the neutral manifold, either by deprotonating a neutral amine-coordinated Pd intermediate or through salt metathesis to generate a basic Pd-alkoxo intermediate that can deprotonate an amine substrate.[10] Furthermore, amine bases such as DBU were implicated in catalyst inhibition by competitively binding Pd to form off-cycle intermediates.

Several studies have recently demonstrated that newer generation Pd complexes featuring hindered phosphines can catalyze C–N coupling reactions with soluble bases. The phosphazene superbase P_2Et enabled homogeneous aminations suitable for HTE screening on micro- or nanomole scale.[11] However, phosphazene bases are prohibitively expensive for large scale applications. Buchwald developed a well-defined Pd precatalyst coordinated by the hindered terphenyl phosphine AlPhos, which catalyzes amination reactions of aryl triflates or some halides with unhindered primary amines and amides using DBU as base.[12] Palladium catalysts featuring other phosphine ligands, such as Xantphos, DPEphos, and Josiphos have also emerged for DBU-promoted C–N coupling.[13,5] Additionally, photoredox[14] or electrochemical[15] conditions have been demonstrated to provide sufficient driving force to utilize weak bases, such as DABCO.

Importantly in the (AlPhos)Pd-catalyzed reactions, a ligand-enabled mechanism change from a typical neutral to an ionic pathway for N–H cleavage was identified, which facilitates efficient turnover with a weak base (Scheme 1b).[16] Dissociation of a triflate anion and coordination of amine leads to acidification of the bound substrate to such an extent that the cationic intermediate is susceptible to external N–H deprotonation by even moderate bases, like DBU. Furthermore, the turnover-limiting step of these reactions was found to be dissociation of DBU from an off-cycle intermediate coordinated by this base, which highlights another challenge facing weak base amination reactions involving Lewis basic (strongly coordinating) reagents. Extending the applicable weak base further to tertiary amines remains highly desirable in this area due to their low cost, tunable properties, and low basicity in comparison to other soluble bases such as amidines, guanidines, or phosphazenes. To this end, a Ni-catalyzed amination of aryl triflates with anilines and triethylamine as base was recently reported by Buchwald.[17] An ionic catalytic pathway is also believed to operate in this system for which aryl bromides and chlorides are more challenging substrates, possibly due to stronger halide coordination to the transition metal that inhibits ionization and amine binding. An outstanding need thus remains for the identification of new catalysts that can promote weak base coupling with widely available halo(hetero)arene electrophiles, as opposed to specialty aryl triflates, with a variety of amine nucleophile classes using an "ideal" soluble weak base, such as Et_3N.[18]

Our group previously reported a coordinatively-unsaturated organopalladium catalyst, $Pd(PAd_3)(Ar^F)Br$ **1** (Ar^F = 4-FC_6H_4), which functions as an on-cycle catalyst for Suzuki-Miyaura coupling with organoboronic acids prone to fast base-catalyzed protodeboronation (PDB).[19] A key aspect of this development was achieving efficient catalytic turnover using the combination of H_2O and a weak, soluble amine base (Et_3N). Stoichiometric mechanistic experiments implicated ionization of $Pd(PAd_3)(Ar^F)X$ (X = Br, Cl) complexes to cationic species $[Pd(PAd_3)(Ar^F)(S)]^+$ (S = water, solvent),[20] which undergo facile deprotonation of the acidified aqua ligand even by mild bases (Scheme 1c).[21] It is thus possible to access coordinatively unsaturated Pd-hydoxo intermediates (**III**, Scheme 1c) that feature both Lewis acidic (open coordination site) and Lewis/Brønsted basic properties in the absence of stoichiometric ionic bases (i.e., hydroxide or alkoxides).[22] Because palladium hydroxo and alkoxo complexes have been implicated in numerous other catalytic processes but are classically accessed by reactions involving stoichiometric strong bases (e.g., NaOH, NaO^{t}Bu), it may be possible to leverage the water-assisted pathway we uncovered to promote a range of catalytic transformations under conditions milder than what was possible using traditional catalysts.

The Brønsted basicity of species such as **III** should also be reactive toward activation of strong element-hydrogen bonds, such as in the amine activation step (N–H heterolysis) of Buchwald-Hartwig amination.[23] While such species can be generated from stoichiometric reactions of Pd(II)-halide complexes with hydroxide,[25] the intermediacy of palladium hydroxo complexes in N–H bond activation has to our knowledge not been unambiguously established in a catalytic setting.[24] We hypothesized that the coordination of amine to the catalyst open site should strongly acidify the N–H bond, and the *cis*-hydroxo ligand would then be poised for intramolecular deprotonation to extrude water and generate the penultimate Pd-amido catalytic intermediate. Here we report a method for aryl amination of bromo- and chloro(hetero)arenes using the on-cycle catalyst **1** and Et_3N as a soluble weak base. Water is an essential component for these reactions, and mechanistic data implicate three complementary roles by which water can facilitate the overall catalytic process: i) acceleration of an inner sphere heterolysis of the substrate N–H bond, ii) driving an unfavorable ionization of neutral palladium halide species by sequestering halide into an aqueous phase, and iii) shunting catalyst away from an inhibited, base-coordinated state.

RESULTS AND DISCUSSION

High-throughput experimentation (HTE) techniques were used to assess the multi-dimensional influence of solvent, amine base, and water on a model reaction between 4-chlorobiphenyl and 4-nitroaniline catalyzed by complex **1** (1 mol%) to form amine **2**.[26] Representative results of this three-dimensional screening are visualized in the heat plot shown in Figure 1 (see Tables S1 and S2 for tabular data). The solvent dimension did not indicate a clear contrast in conversion as a function of solvent polarity. Both polar (a)protic (e.g., *t*-amyl alcohol, DMF) and relatively non-polar (e.g., toluene, DME, 2-methyl tetrahydrofuran) solvents were associated with significant conversion. On the other hand, Et_3N (pK_{aH}^{DMSO} = 9) gave the best average conversion versus other tertiary amines (e.g., diisopropylethylamine, *N*-methyl morpholine) in the base dimension. Counterintuitively, stronger bases (pK_a^{DMSO}) such as MTBD (15), DBU (14), or tetramethylguanidine (13) were generally inferior to Et_3N, which contrasts the base trends typically observed in C–N coupling, even compared to a recently-developed weak base method using AlPhos-coordinated Pd catalysts.[16] Importantly, reactions conducted with more water performed better regardless of the choice of base.

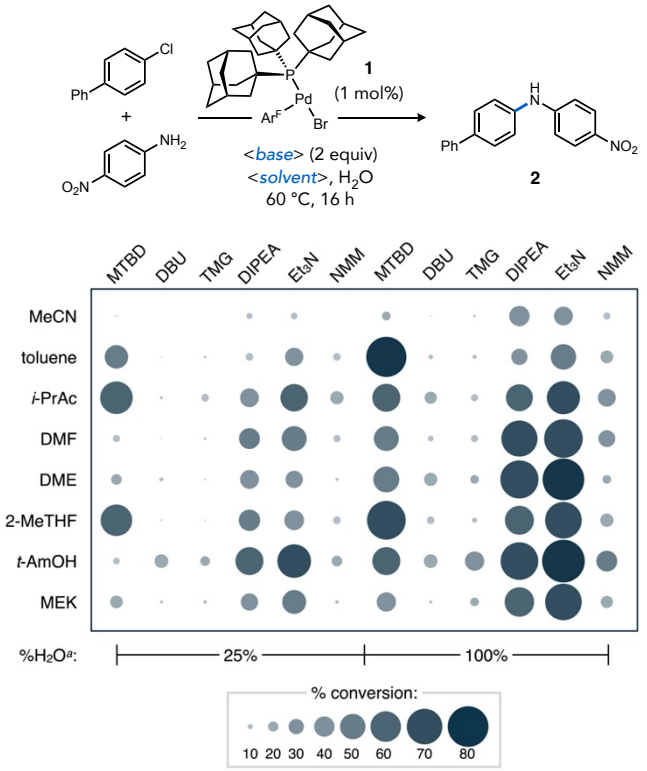

Figure 1. Heat plot for survey of soluble amine bases under Buchwald-Hartwig amination conditions with water co-solvent. Ar^F = 4-FC_6H_4. [a]Versus total solvent volume.

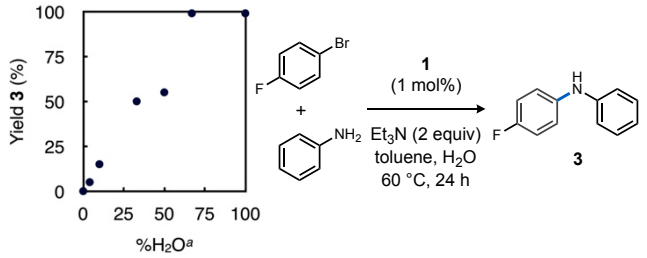

Figure 2. Optimization of water assistance during weak base Buchwald-Hartwig amination. Yield determined by ^{19}F NMR versus $CF_3C_6H_5$ as internal standard. [a]Versus total toluene volume.

Additional optimization confirmed water loading as a crucial dimension for achieving high reaction conversions (Figure 2), as determined by formation of **3** by ^{19}F NMR spectroscopy during reactions of 1-bromo-4-fluorobenzene with aniline. Together with an increase in reaction temperature from 60 to 80 °C, adjusting the solvent/water ratio to at least 2:3 gave markedly improved yields after 6 h. It is worth noting we believe the better performance of toluene in this model reaction versus the HTE screen may reflect a solubility artifact during catalyst dosing (compare Tables S1 and S2). In subsequent methodology studies (Tables S3–S5), a 1:4 mixture of toluene and water was ultimately selected as the most versatile mixture across different haloarene and amine combinations.

A variety of chloro- and bromo(hetero)arene electrophiles and nucleophiles were tested to explore the scope of a method featuring this (Ad_3P)Pd-catalyzed, water-assisted reaction pathway (Table 1). For primary aryl amines, products generated from an electron-poor nucleophile (**4**), which are more challenging versus simple amines,[14,27] and hindered aniline (**5**) occurred in 92% and 72% isolated yield, respectively, suggesting good tolerance to variations in aniline electronic and steric properties. Chemoselective oxidative addition favoring bromide over triflate or chloride is confirmed by formation of **6**, **12**, **13**, **18**, and **27** in 61–87% isolated yields. This orthogonality makes bond constructions at different C–X bonds viable and also complements previous C–N coupling methods favoring activation of aryl triflates. Heteroaryl chlorides, such as those containing thiophene (**7**) and pyrimidine (**8**) motifs, were compatible substrates under the reaction conditions. Reactions using heterocyclic amines such as 5-aminoindole (**9**) and 3-amino-2-methoxypyridine (**10**) underwent arylation in high yield (84% and 91%, respectively).

Secondary anilines that underwent arylation in good to excellent yields (79–98%) include carbazole (**12**), phenothiazine (**13**), indoline (**14**), and *N*-methylaniline (**15**). Aliphatic secondary amines are also competent nucleophiles to generate **16**–**18** in 61–83% isolated yields, the latter of which involved the drug amoxapine as the nucleophile. As a point of comparison, secondary amines were shown to be poor substrates in previous C–N coupling strategies with organic base, presumably due to steric clash with the extremely hindered ligands used.[13,17] The amide nucleophile 2-azetidinone or the protected ammonia equivalent *t*-butyl carbamate generated **19** and **20** in 89% and 97% yields, respectively. Hydrazine derivatives that are useful functional handles for heterocycle synthesis,[1a] such as 1-Boc-1-methylhydrazide or benzophenone hydrazone, were also suitable nucleophiles for this method generating **21** and **22** in 69% and 80% isolated yields, respectively. These results highlight versatility of this water-assisted method across a spectrum of nucleophile classes that sample a broad range of N–H pK_a and size.

Drug-like electrophiles were also explored to gauge the tolerance of the catalyst and water-assisted method to more complex functionality. Reaction of 4-fluoroaniline with the Merck informer compounds X2, X3, X4, X6, or X8 generated amination products **23**–**27** in 76–98% isolated yields.[28] The high yields in these reactions indicate the synthetic utility of a weak base strategy compared against established catalytic or stoichiometric C–N coupling of these substrates using strong bases.[11d,29]

Importantly, we envisioned this weak base method should engender improved compatibility toward base-sensitive functionality. Ketone and ester functional groups with enolizable sites were well-tolerated, as exemplified by the moderate to good yields obtained for formation of products **7** (45%), **19** (89%), **25** (94%), **26** (98%), **28** (90%), and **31** (58%). Formation of **17** and **18** in 89% and 61% yield, respectively, demonstrate tolerance of nitrile and nitro groups. Functionalization of the commercial drugs indomethacin, fenofibrate, and haloperidol in 51%, 90%, and 58% isolated yields, respectively, further highlight both the compatibility of this weak base amination method with chloroarenes as well as with protic functional groups (e.g., carboxylic acid in **29** and alcohol in **31**). Several amination reactions were also conducted in neat water (e.g., **4**, **6**, and **14**), which demonstrate that catalyst **1** can operate under single phase conditions that could be advantageous for green chemistry[30,31] or biorthogonal[32] applications and also hints that the beneficial role(s) of water may extend beyond just sequestration of halide away from the organic solvent phase where catalyst resides.

Amination of the chloroarene fenofibrate was selected to evaluate the scalability of the method. Preliminary reactions (Table S7) on half-gram scale at 98 °C indicated comparably high conversions for reactions in toluene, anisole, cyclopropyl methyl ether, or *t*-amyl

Table 1. Substrate Scope of Water-Assisted Amination Using Triethylamine as a Soluble Weak Base.[a]

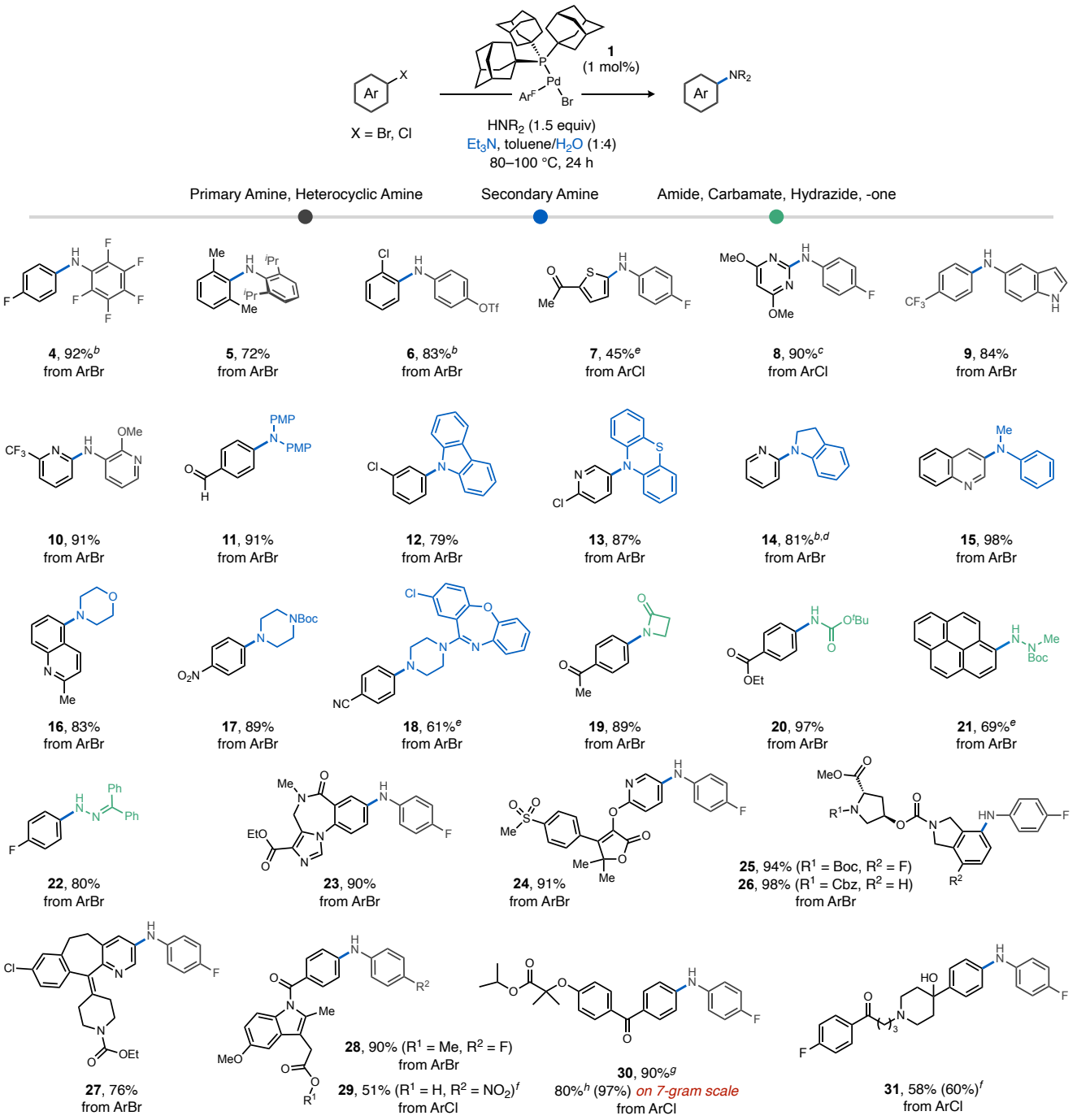

[a]Standard conditions: Aryl halide (0.2 M), amine (1.5 equiv), Et_3N (2 equiv), and catalyst **1** (1 mol%) were stirred in a toluene/H_2O (1:4) mixture at 80 °C (X = Br) or 100 °C (X = Cl) in a sealed vial over 24 h. Isolated yields shown unless noted otherwise; parentheses denote yields determined by ^{19}F NMR vs. $CF_3C_6H_5$ as internal standard or calibrated UPLC analysis. [b]Neat water. [c]16 h. [d]3 mol% **1**. [e]48 h. [f]2 mol% **1**, 48 h. [g]36 h. [h]*t*-AmOH/H_2O (1:3), 85 °C for 12 h. Ar^F = 4-FC_6H_4. PMP = 4-$MeOC_6H_4$.

alcohol as solvent. At a lower temperature (80 °C), *t*-AmOH was superior giving 94% conversion within 21 h. Further increasing the reaction in *t*-AmOH to 20-mmol scale gave an excellent solution yield (97%) of **30** within 12 h at 85 °C yielding 7.0 g (80%) of analytically pure (>99%) product after crystallization. Kinetic profiling of the reaction (Figure S3) indicated 100% conversion was actually achieved within 45 min at 1 mol% catalyst loading.

The effectiveness of the combination of a $(Ad_3P)Pd$ catalyst and water in enabling catalytic turnover of bromo- and chloroarenes raised several mechanistic questions. For instance, it was not clear *a priori* if a similar or distinct catalytic mechanism might be operative compared to what has been proposed using an (AlPhos)Pd catalyst and DBU under anhydrous conditions (Scheme 1b).[12,16] A switch in mechanism could potentially account for the improved reactivity toward bromo- and chloroarene electrophiles in this method versus

aryl triflates as well as the lack of base inhibition observed previously. Experiments were thus conducted to interrogate the role(s) water plays in the catalytic mechanism, such as the initially hypothesized potential for on-cycle Pd intermediates to be generated from coordinated water.

Observation of the reaction of neutral complex **1** with water and Et_3N in toluene by ^{31}P NMR spectroscopy indicated clean formation of a new palladium complex after 1 min (Figure 3a). Based on comparison to an independently prepared sample, this new species was assigned as the μ-hydroxo complex **32**. A dimeric solution structure for **32** is suggested by the observation in the ^1H NMR spectrum of a single upfield resonance virtually coupled to phosphorus (δ_H = -2.12 ppm, $J(^{31}P–^1H)$ = 3.2 Hz) corresponding to a μ-OH ligand and an *anti* disposition of PAd_3 ligands. Importantly, the time frame for this stoichiometric reaction is far less than that required for the respective catalytic aminations in Table 1 even at a much lower temperature, which suggests formation of Pd hydroxo species from water and Et_3N is a kinetically viable step during catalysis. On the other hand, addition of water or Et_3N individually to **1** led to no detectable changes in the ^{31}P NMR spectra. Based on the above data together with the observation that substitution of water and Et_3N for phosphate buffer (pH 8.0) in the catalytic reaction completely suppressed conversion, we propose **32** forms through initial equilibrium hydrolysis of **1** to generate a cationic Pd intermediate rather than by direct substitution of halide at palladium by a low concentration of free hydroxide ions.

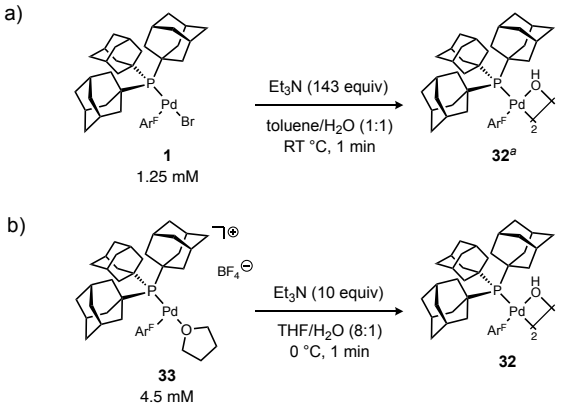

Figure 3. Stoichiometric O–H heterolysis reactions initiated from (a) neutral or (b) cationic aryl-palladium complexes using water and Et_3N. [a]No conversion was observed in the absence of added H_2O or Et_3N. Ar^F = 4-FC_6H_4.

Deprotonation of a strongly acidified aqua ligand by Et_3N in a cationic Pd species would be expected to be facile. An analogous cationic pathway for B-to-Pd transmetalation was postulated in our previous study of weak base Suzuki-Miyaura coupling.[20] To further probe if such a process could be operative in the present amination reactions, a discrete cationic species $[Pd(PAd_3)(Ar^F)(THF)]^+ BF_4^-$ (**33**) was prepared at low temperature according to a reported procedure.[20] Treatment of **33** with water and Et_3N at 0 °C in THF for 1 min again led to clean formation of the Pd hydroxo complex **32** (Figure 3b). This faster reaction is consistent with a cationic aqua complex being a competent intermediate in the conversion of the palladium halide complex **1** to the palladium hydroxo complex **32**, considering that exchange of the labile solvento ligand in **33** for water should occur readily. Furthermore, water could also play a role in driving the reaction forward by sequestering the resulting ammonium salts. Finally, the presumed basicity of the hydroxo ligand was confirmed by the immediate reversion of **32** back to **33** upon treatment with HBF_4 etherate in THF at –25 °C (Figure S10).

While palladium hydroxo complexes have been proposed as intermediates in numerous cross-coupling reactions, their formation is generally believed to require anion exchange processes using stoichiometric ionic bases. Hydrolysis of halide ligands in a nonpolar organic solvent represents a unique and much milder pathway to access these versatile intermediates, yet such ionization processes have been proposed to be energetically prohibitive.[9] This issue has been mitigated by moving away from halide electrophiles to those with weaker anions (e.g., triflate) or by addition of halide abstracting reagents (i.e., Ag^+, Tl^+), such as in methods that access the cationic pathway for the Mizoroki-Heck reaction.[33] Our data suggest that an appropriate coordinatively-unsaturated metal intermediate, such as the T-shaped $(Ad_3P)Pd(II)$ species in this work, can in fact undergo facile ionization through hydrolysis even in toluene, which allows deprotonation of the resultant acidified aqua ligand in the cationic complex using very mild bases. To our knowledge, such a process represents a novel pathway for a key catalytic step of Buchwald-Hartwig amination reactions that activates the substrate amine, which engenders advantages in the electrophile scope to include more strongly coordinating anions (e.g., Br, Cl) without the need for halide scavengers.

Scheme 2. Proposed catalytic cycle for $(Ad_3P)Pd$-catalyzed, water-assisted amination.

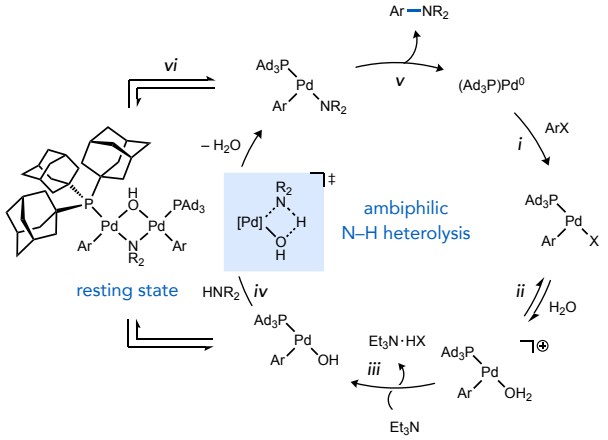

A catalytic cycle is proposed for $(Ad_3P)Pd$-catalyzed aryl amination of aryl halides in Scheme 2, which incorporates a water-assisted mechanism to generate an ambiphilic Pd hydroxo species. To probe the turnover-limiting step, the experimental rate law (eq 1) was determined using either Burés' variable time normalization analysis[34]

$$\frac{d[\mathbf{3}]}{dt} = k_{obs}\,[Ar^FBr]^0\,[H_2NPh]^0\,[Et_3N]^0\,[\mathbf{1}]^1 \qquad (1)$$

or initial rate measurements for reactions of 4-BrC_6H_4F (Ar^FBr) with aniline under the standard conditions of Table 1 (see Figures S31–S34). The observation of a zeroth-order dependence of the initial rates on $[Ar^FBr]$ and $[Et_3N]$ suggest neither oxidative addition (step *i*) nor deprotonation of water (step *iii*) are turnover-limiting, respectively, in the catalytic reaction. These results contrast prior work on amination of aryl triflates where either a positive order dependence on [DIPEA] signified rate-determining N–H deprotonation using a

tertiary amine base, or a negative order dependence on [DBU] under different conditions indicated catalyst poisoning by this base.[16]

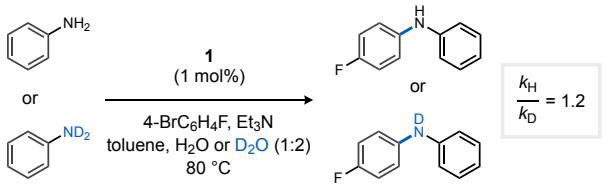

Figure 4. Determination of kinetic isotope effect from independent catalytic amination reactions of aniline or aniline-*d*$_2$.

While the zeroth-order dependence of the rate on [amine] is consistent with fast N–H heterolysis (step *iv*), it could also be manifested in a scenario in which amine coordination to Pd occurred reversibly and the equilibrium saturated in the range of concentrations tested. To distinguish between these possibilities, the kinetic isotope effect (KIE) was determined for independent reactions of Ar^{F}Br with aniline in toluene/H_2O or aniline-*d*$_2$ in toluene/D_2O (Figure 4). The absence of a primary KIE in these reactions is inconsistent with turnover-limiting N–H heterolysis regardless of potential reversibility in amine substrate coordination.

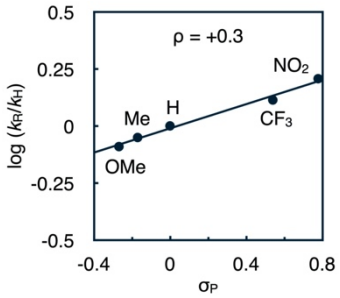

Figure 5. Hammett plot for catalytic amination of 4-BrC$_6$H$_4$F with a *para*-substituted aniline under the optimized conditions of Table 1 as determined by the method of initial rates.

The kinetic and isotope effect data above seem to implicate C–N reductive elimination as the likely turnover-limiting step of catalysis. However, analysis of the initial rates for reactions using a series of *para*-substituted anilines (Figure 5) suggest C–N bond formation (step *v*) is not rate-determining. The slope of this Hammett plot (ρ = +0.3) is inconsistent with literature data for stoichiometric reductive elimination reactions from arylpalladium amido complexes, which are generally faster for complexes with more electron-rich amido ligands (ρ < 0).[35] Considering also that stoichiometric reactions (see Figure 3) suggest hydrolysis is kinetically facile (step *ii*), the available data are not consistent with any on-cycle catalytic step being turnover-limiting. An alternative kinetic scenario must then be operative during these catalytic reactions, and spectroscopic data from additional stoichiometric experiments at low temperature with isolated organometallic complexes provided several key insights in this regard.

The stoichiometric N–H heterolysis of $H_2NC_6F_5$ by Pd hydroxo complex **32** in THF occurred with full conversion of **32** within 1 min at –25 °C to generate a new palladium species (δ_P 58.8 ppm) in 84% yield (Figure 6a). The stoichiometry of μ-OH and μ-NHC$_6$F$_5$ resonances versus Pd(PAd$_3$) and Pd(4-FC$_6$H$_4$) resonances (1:2, respectively) in the ^{1}H NMR and single resonance in the ^{31}P NMR spectra suggests a *syn*-dinuclear complex (**34**), which is structurally analogous to a {Pd$_2$(PPh$_3$)$_2$Ph$_2$(μ-OH)(μ-NHtBu)} species that was crystallographically characterized by Hartwig.[23,36] When **34** was allowed to warm to room temperature, C–N reductive elimination occured completely to form **4** in 93% yield, relative to both [Pd]–Ar^F equivalents in the starting dimer complex **32**, as determined by ^{19}F NMR versus octafluorotoluene as standard. A yield of product **4** in excess of 50% necessitates the μ-OH ligand in the dinuclear intermediate **34** further reacts with the remaining $H_2NC_6F_5$ in solution after C–N bond formation is triggered. The identification of this dinuclear species (**34**) can also resolve the issue of the turnover-limiting step during catalysis. Specifically, the observed reaction constant of ρ = +0.3 is consistent with rate-determining fragmentation of the μ-anilido ligand in species analogous to **34**, which should be faster with decreasing ligand σ-donicity induced by withdrawing anilido substituents. Fragmentation of this dinuclear catalyst resting state is still consistent with a first-order dependence of the rate on [**1**] because dissociation of the dinuclear species into one equivalent of Pd(PAd$_3$)(Ar)NR$_2$ (plus a Pd(PAd$_3$)(Ar)OH fragment) generates only one equivalent of product per turnover.

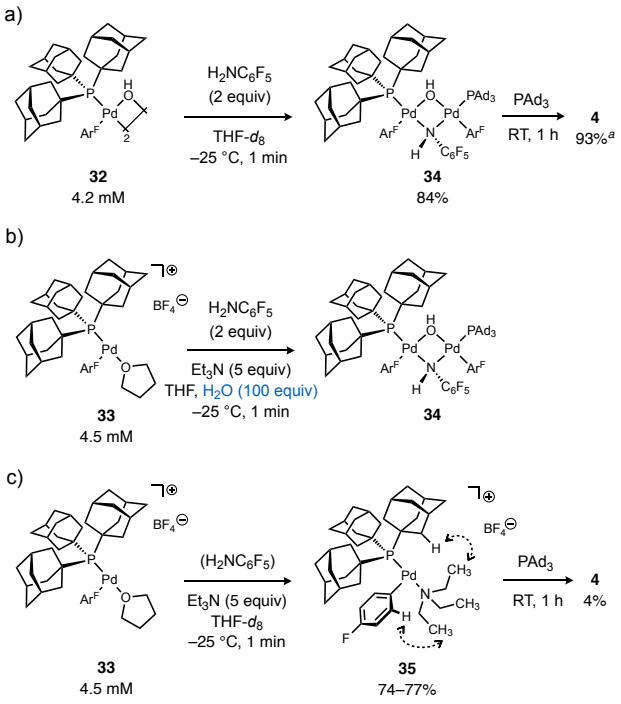

Figure 6. Stoichiometric N–H heterolysis reactions between aryl-palladium complexes, $H_2NC_6F_5$, and Et$_3$N with or without added water and characterization of the resulting amido-Pd or amino-Pd intermediates. Dashed lines indicate NOE-correlated ^{1}H nuclei. [a]Relative to both [Pd]–Ar^F equivalents in **32**. Ar^F = 4-FC$_6$H$_4$.

The reaction of cationic complex **33** with $H_2NC_6F_5$, excess water, and Et$_3$N in THF also occurred within 1 min at –25 °C to generate the same dinuclear intermediate **34** (Figure 6b). In contrast, an analogous reaction of **33** with Et$_3$N *in the absence of added water* (Figure 6c) led to the consumption of starting material but generated a distinct product (δ_P 41.5 ppm) as shown in Figure 7. Characterization of this species by ^{1}H and ^{1}H–^{1}H NOESY NMR is consistent with a cationic, Et$_3$N-coordinated structure (**35**). Importantly, repetition of the reaction with added $H_2NC_6F_5$ led to formation of the same species (Figure 7), but upon warming to room temperature only a trace (4%) of C–N coupling product **4** formed after 1 h. We interpret these results as suggesting that aniline substrates struggle to displace coordinated Et$_3$N at Pd, and catalyst inhibition should

occur using a soluble base as was observed previously by Buchwald.[16] Because this does not appear to occur during the catalytic reactions

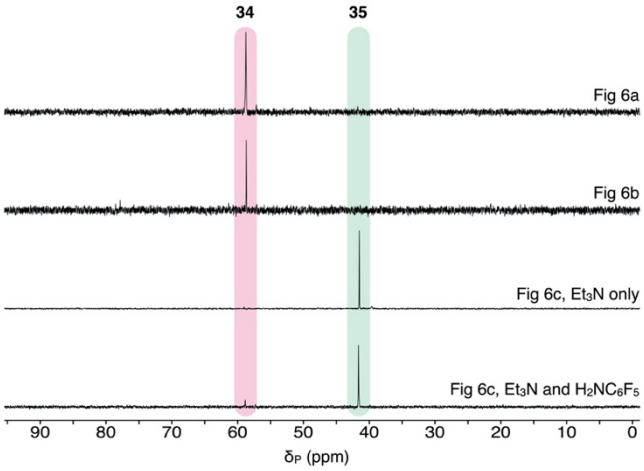

Figure 7. ^{31}P NMR spectra of stoichiometric reactions of aryl-Pd complexes **32** or **33** with amines shown in Figure 6.

of this work (reactions are zeroth- rather than inverse-order in [Et_3N]), we postulate that another role of excess water can be to shunt catalyst away from an inactive state (e.g., **35**) toward active intermediates, such as [$Pd(PAd_3)Ar(OH_2)]^+$ and $Pd(PAd_3)Ar(OH)$. In total, these mechanistic data strongly support a catalytic pathway unique from previous work on amination of aryl triflates using weak base for which the resting state is an off-cycle base-coordinated Pd species – an undesirable poisoned state that can be circumvented by the action of water together with the coordinative unsaturation of $(Ad_3P)Pd$ catalytic species.

CONCLUSION

A method for amination of chloro- and bromo(hetero)arenes has been developed that operates efficiently with Et_3N as a mild, soluble base in combination with water in toluene. The nucleophile classes applicable to this transformation span a wide pK_a range from relatively acidic amides and electron-deficient anilines to poorly acidic aliphatic secondary amines. The mild conditions are also compatible with range of base sensitive functional groups that can be problematic under classic strong base conditions, which includes carboxylic acids, esters, nitrile, nitro, and enolizable keto groups. Amination in complex settings was validated by reactions of the chloroaryl group in the pharmaceuticals indomethacin, fenofibrate, and haloperidol as well as in five drug-like bromo(hetero)arenes from the Merck informer library. Reactions can also be conducted in neat water for applications requiring single phase conditions.

Mechanistic experiments support multiple roles for water assistance in the catalytic mechanism. An initial hydrolysis of the organopalladium halide complex formed after oxidative addition is facilitated kinetically by the PAd_3-enforced coordinative unsaturation of the complex, as well as thermodynamically driven through sequestration of the halide byproduct into the aqueous phase of a biphasic system. Importantly, this ionization occurs even for more strongly coordinated halide ions derived from commercially abundant bromo- and chloroarenes, which contrasts the typically difficult task of ionization Pd(II) complexes in nonpolar media that traditionally requires organic electrophiles with better leaving groups or halide scavengers. Deprotonation of an acidified aqua ligand in the cationic intermediate can occur readily even with Et_3N, which corresponds to a considerable influence of the catalyst on relative acidities (ΔpK_a^{DMSO} = 22). The ambiphilic $Pd(PAd_3)(Ar)OH$ intermediate that is readily accessible from water and Et_3N in these reactions features both Lewis acidic and Brønsted basic properties that, upon coordination of amine substrate, triggers an intramolecular N–H cleavage under very mild conditions.

Stoichiometric experiments with aryl-palladium complexes implicate another unanticipated role of water in shunting catalyst speciation away from inactive, base-coordinated intermediates, which has been a challenge in other recently developed weak base amination methods. To our knowledge, this water-assisted mechanism for C–N coupling reactions has not been previously observed and could potentially be effective in promoting other catalytic processes involving element-hydrogen bond activation under weak base conditions. The persistent coordinative unsaturation of the $(Ad_3P)Pd$ catalyst thus appears to engender a number of kinetic benefits in accessing unique catalytic mechanisms for carbon-carbon and now carbon-heteroatom bond forming reactions that are attractive for catalysis in the most sensitive settings.

ASSOCIATED CONTENT

Supporting Information. This material is available free of charge via the Internet at http://pubs.acs.org.
Experimental procedures. Reaction optimization details, kinetics data, and spectral data for new compounds.

Corresponding Author

* bcarrow@princeton.edu

Notes

The authors declare the following competing financial interest(s): A patent was filed by Princeton University: Carrow, B. P.; Chen, L. WO2017/075581 A1, May 4, 2017.

ACKNOWLEDGMENT

Support was provided by the National Institutes of Health (R35GM128902). We thank Kiwoon Baeg and Lucy Wang for assistance with preliminary catalyst development and Michael Peddicord for HR-MS analyses.

REFERENCES

(1) (a) Ruiz-Castillo, P.; Buchwald, S. L.; Applications of Palladium-Catalyzed C–N Cross-Coupling Reactions. *Chem. Rev.* **2016**, *116*, 12564-12649; (b) Torborg, C.; Beller, M.; Recent Applications of Palladium-Catalyzed Coupling Reactions in the Pharmaceutical, Agrochemical, and Fine Chemical Industries. *Adv. Synth. Catal.* **2009**, *351*, 3027-3043; (c) Devendar, P.; Qu, R.-Y.; Kang, W.-M.; He, B.; Yang, G.-F.; Palladium-Catalyzed Cross-Coupling Reactions: A Powerful Tool for the Synthesis of Agrochemicals. *J. Agric. Food Chem.* **2018**, *66*, 8914-8934.

(2) (a) Surry, D. S.; Buchwald, S. L.; Biaryl Phosphane Ligands in Palladium-Catalyzed Amination. *Angew. Chem., Int. Ed.* **2008**, *47*, 6338-6361; (b) Hartwig, J. F.; Evolution of a Fourth Generation Catalyst for the Amination and Thioetherification of Aryl Halides. *Acc. Chem. Res.* **2008**, *41*, 1534-1544; (c) Valente, C.; Çalimsiz, S.; Hoi, K. H.; Mallik, D.; Sayah, M.; Organ, M. G.; The Development of Bulky Palladium NHC Complexes for the Most-Challenging Cross-Coupling Reactions. *Angew. Chem., Int. Ed.* **2012**, *51*, 3314-3332; (d) Chartoire, A.; Nolan, S. P. CHAPTER 4 Advances in C–C and C–X Coupling Using Palladium–N-Heterocyclic Carbene (Pd–NHC) Complexes. In *New Trends in Cross-Coupling: Theory and Applications*; The Royal Society of Chemistry: 2015, p 139-227; (e) Stradiotto, M. Ancillary Ligand Design in the Development of Palladium

Catalysts for Challenging Selective Monoarylation Reactions. In *New Trends in Cross-Coupling: Theory and Applications*; Colacot, T., Ed.; The Royal Society of Chemistry: 2015, p 228-253; (f) Ingoglia, B. T.; Wagen, C. C.; Buchwald, S. L.; Biaryl monophosphine ligands in palladium-catalyzed C–N coupling: An updated User's guide. *Tetrahedron* **2019**, *75*, 4199-4211; (g) Forero-Cortés, P. A.; Haydl, A. M.; The 25th Anniversary of the Buchwald–Hartwig Amination: Development, Applications, and Outlook. *Org. Process Res. Dev.* **2019**, *23*, 1478-1483; (h) Shaughnessy, K. H.; Development of Palladium Precatalysts that Efficiently Generate LPd(0) Active Species. *Isr. J. Chem.* **2020**, *60*, 180-194.

(3) (a) Old, D. W.; Wolfe, J. P.; Buchwald, S. L.; A highly active catalyst for palladium-catalyzed cross-coupling reactions: Room-temperature Suzuki couplings and amination of unactivated aryl chlorides. *J. Am. Chem. Soc.* **1998**, *120*, 9722-9733; (b) Hartwig, J. F.; Kawatsura, M.; Hauck, S. I.; Shaughnessy, K. H.; Alcazar-Roman, L. M.; Room-Temperature Palladium-Catalyzed Amination of Aryl Bromides and Chlorides and Extended Scope of Aromatic C–N Bond Formation with a Commercial Ligand. *J. Org. Chem.* **1999**, *64*, 5575-5580; (c) Wolfe, J. P.; Buchwald, S. L.; A Highly Active Catalyst for the Room-Temperature Amination and Suzuki Coupling of Aryl Chlorides. *Angew. Chem., Int. Ed.* **1999**, *38*, 2413-2416; (d) Huang, J.; Grasa, G.; Nolan, S. P.; General and Efficient Catalytic Amination of Aryl Chlorides Using a Palladium/Bulky Nucleophilic Carbene System. *Org. Lett.* **1999**, *1*, 1307-1309; (e) Stauffer, S. R.; Lee, S.; Stambuli, J. P.; Hauck, S. I.; Hartwig, J. F.; High Turnover Number and Rapid, Room-Temperature Amination of Chloroarenes Using Saturated Carbene Ligands. *Org. Lett.* **2000**, *2*, 1423-1426; (f) Wolfe, J. P.; Tomori, H.; Sadighi, J. P.; Yin, J.; Buchwald, S. L.; Simple, Efficient Catalyst System for the Palladium-Catalyzed Amination of Aryl Chlorides, Bromides, and Triflates. *J. Org. Chem.* **2000**, *65*, 1158-1174; (g) Stambuli, J. P.; Kuwano, R.; Hartwig, J. F.; Unparalleled rates for the activation of aryl chlorides and bromides: coupling with amines and boronic acids in minutes at room temperature. *Angew. Chem., Int. Ed.* **2002**, *41*, 4746-4748; (h) Shen, Q.; Shekhar, S.; Stambuli, J. P.; Hartwig, J. F.; Highly Reactive, General, and Long-Lived Catalysts for Coupling Heteroaryl and Aryl Chlorides with Primary Nitrogen Nucleophiles. *Angew. Chem., Int. Ed.* **2005**, *44*, 1371-1375; (i) Marion, N.; Navarro, O.; Mei, J.; Stevens, E. D.; Scott, N. M.; Nolan, S. P.; Modified (NHC)Pd(allyl)Cl (NHC = N-Heterocyclic Carbene) Complexes for Room-Temperature Suzuki-Miyaura and Buchwald-Hartwig Reactions. *J. Am. Chem. Soc.* **2006**, *128*, 4101-4111; (j) Navarro, O.; Marion, N.; Mei, J.; Nolan, S. P.; Rapid room temperature Buchwald-Hartwig and Suzuki-Miyaura couplings of heteroaromatic compounds employing low catalyst loadings. *Chem.--Eur. J.* **2006**, *12*, 5142-5148; (k) Biscoe, M. R.; Fors, B. P.; Buchwald, S. L.; A New Class of Easily Activated Palladium Precatalysts for Facile C–N Cross-Coupling Reactions and the Low Temperature Oxidative Addition of Aryl Chlorides. *J. Am. Chem. Soc.* **2008**, *130*, 6686-6687; (l) Shen, Q.; Hartwig, J. F.; [(CyPF-tBu)PdCl2]: An Air-Stable, One-Component, Highly Efficient Catalyst for Amination of Heteroaryl and Aryl Halides. *Org. Lett.* **2008**, *10*, 4109-4112; (m) Fors, B. P.; Watson, D. A.; Biscoe, M. R.; Buchwald, S. L.; A Highly Active Catalyst for Pd-Catalyzed Amination Reactions: Cross-Coupling Reactions Using Aryl Mesylates and the Highly Selective Monoarylation of Primary Amines Using Aryl Chlorides. *J. Am. Chem. Soc.* **2008**, *130*, 13552-13554; (n) Organ, M. G.; Abdel-Hadi, M.; Avola, S.; Dubovyk, I.; Hadei, N.; Kantchev, E. A. B.; O'Brien, C. J.; Sayah, M.; Valente, C.; Pd-Catalyzed Aryl Amination Mediated by Well Defined, N-Heterocyclic Carbene (NHC)–Pd Precatalysts, PEPPSI. *Chem. Eur. J.* **2008**, *14*, 2443-2452; (o) Lundgren, R. J.; Sappong-Kumankumah, A.; Stradiotto, M.; A Highly Versatile Catalyst System for the Cross-Coupling of Aryl Chlorides and Amines. *Chem. Eur. J.* **2010**, *16*, 1983-1991; (p) Crawford, S. M.; Lavery, C. B.; Stradiotto, M.; BippyPhos: A Single Ligand With Unprecedented Scope in the Buchwald–Hartwig Amination of (Hetero)aryl Chlorides. *Chem. Eur. J.* **2013**, *19*, 16760-16771; (q) Weber, P.; Scherpf, T.; Rodstein, I.; Lichte, D.; Scharf, L. T.; Gooßen, L. J.; Gessner, V. H.; A Highly Active Ylide-Functionalized Phosphine for Palladium-Catalyzed Aminations of Aryl Chlorides. *Angew. Chem., Int. Ed.* **2019**, *58*, 3203-3207; (r) Tappen, J.; Rodstein, I.; McGuire, K.; Großjohann, A.; Löffler, J.; Scherpf, T.; Gessner, V. H.; Palladium Complexes Based on Ylide-Functionalized Phosphines (YPhos): Broadly Applicable High-Performance Precatalysts for the Amination of Aryl Halides at Room Temperature. *Chem. Eur. J.* **2020**, *26*, 4281-4288.

(4) Reactions using LiHMDS as base can in certain circumstances tolerate hydroxyl, amide, and carbonyl groups. See: Harris, M. C.; Huang, X.; Buchwald, S. L.; Improved Functional Group Compatibility in the Palladium-Catalyzed Synthesis of Aryl Amines. *Org. Lett.* **2002**, *4*, 2885-2888.

(5) Beutner, G. L.; Coombs, J. R.; Green, R. A.; Inankur, B.; Lin, D.; Qiu, J.; Roberts, F.; Simmons, E. M.; Wisniewski, S. R.; Palladium-Catalyzed Amidation and Amination of (Hetero)aryl Chlorides under Homogeneous Conditions Enabled by a Soluble DBU/NaTFA Dual-Base System. *Org. Process Res. Dev.* **2019**, *23*, 1529-1537.

(6) Shevlin, M.; Practical High-Throughput Experimentation for Chemists. *ACS Med. Chem. Lett.* **2017**, *8*, 601-607.

(7) (a) Noël, T.; Buchwald, S. L.; Cross-coupling in flow. *Chem. Soc. Rev.* **2011**, *40*, 5010-5029; (b) Schoenitz, M.; Grundemann, L.; Augustin, W.; Scholl, S.; Fouling in microstructured devices: a review. *Chem. Commun.* **2015**, *51*, 8213-8228.

(8) (a) Meyers, C.; Maes, B. U. W.; Loones, K. T. J.; Bal, G.; Lemière, G. L. F.; Dommisse, R. A.; Study of a New Rate Increasing "Base Effect" in the Palladium-Catalyzed Amination of Aryl Iodides. *J. Org. Chem.* **2004**, *69*, 6010-6017; (b) Dooleweerdt, K.; Birkedal, H.; Ruhland, T.; Skrydstrup, T.; Irregularities in the Effect of Potassium Phosphate in Ynamide Synthesis. *J. Org. Chem.* **2008**, *73*, 9447-9450.

(9) Sunesson, Y.; Limé, E.; Nilsson Lill, S. O.; Meadows, R. E.; Norrby, P.-O.; Role of the Base in Buchwald–Hartwig Amination. *J. Org. Chem.* **2014**, *79*, 11961-11969.

(10) (a) Shekhar, S.; Ryberg, P.; Hartwig, J. F.; Mathew, J. S.; Blackmond, D. G.; Strieter, E. R.; Buchwald, S. L.; Reevaluation of the Mechanism of the Amination of Aryl Halides Catalyzed by BINAP-Ligated Palladium Complexes. *J. Am. Chem. Soc.* **2006**, *128*, 3584-3591; (b) Shekhar, S.; Hartwig, J. F.; Effects of Bases and Halides on the Amination of Chloroarenes Catalyzed by Pd(PtBu3)2. *Organometallics* **2007**, *26*, 340-351.

(11) (a) Buitrago Santanilla, A.; Christensen, M.; Campeau, L.-C.; Davies, I. W.; Dreher, S. D.; P2Et Phosphazene: A Mild, Functional Group Tolerant Base for Soluble, Room Temperature Pd-Catalyzed C–N, C–O, and C–C Cross-Coupling Reactions. *Org. Lett.* **2015**, *17*, 3370-3373; (b) Buitrago Santanilla, A.; Regalado, E. L.; Pereira, T.; Shevlin, M.; Bateman, K.; Campeau, L.-C.; Schneeweis, J.; Berritt, S.; Shi, Z.-C.; Nantermet, P.; Liu, Y.; Helmy, R.; Welch, C. J.; Vachal, P.; Davies, I. W.; Cernak, T.; Dreher, S. D.; Nanomole-scale high-throughput chemistry for the synthesis of complex molecules. *Science* **2015**, *347*, 49-53; (c) Ahneman, D. T.; Estrada, J. G.; Lin, S.; Dreher, S. D.; Doyle, A. G.; Predicting reaction performance in C–N cross-coupling using machine learning. *Science* **2018**, *360*, 186; (d) Uehling, M. R.; King, R. P.; Krska, S. W.; Cernak, T.; Buchwald, S. L.; Pharmaceutical diversification via palladium oxidative addition complexes. *Science* **2019**, *363*, 405-408; (e) Baumgartner, L. M.; Dennis, J. M.; White, N. A.; Buchwald, S. L.; Jensen, K. F.; Use of a Droplet Platform To Optimize Pd-Catalyzed C–N Coupling Reactions Promoted by Organic Bases. *Org. Process Res. Dev.* **2019**, *23*, 1594-1601.

(12) Dennis, J. M.; White, N. A.; Liu, R. Y.; Buchwald, S. L.; Breaking the Base Barrier: An Electron-Deficient Palladium Catalyst Enables the Use of a Common Soluble Base in C–N Coupling. *J. Am. Chem. Soc.* **2018**, *140*, 4721-4725.

(13) Kashani, S. K.; Jessiman, J. E.; Newman, S. G.; Exploring Homogeneous Conditions for Mild Buchwald–Hartwig Amination in Batch and Flow. *Org. Process Res. Dev.* **2020**, ASAP. doi.org/10.1021/acs.oprd.0c00018

(14) Corcoran, E. B.; Pirnot, M. T.; Lin, S.; Dreher, S. D.; DiRocco, D. A.; Davies, I. W.; Buchwald, S. L.; MacMillan, D. W. C.; Aryl amination using ligand-free Ni(II) salts and photoredox catalysis. *Science* **2016**, *353*, 279-283.

(15) Li, C.; Kawamata, Y.; Nakamura, H.; Vantourout, J. C.; Liu, Z.; Hou, Q.; Bao, D.; Starr, J. T.; Chen, J.; Yan, M.; Baran, P. S.; Electrochemically Enabled, Nickel-Catalyzed Amination. *Angew. Chem., Int. Ed.* **2017**, *56*, 13088-13093.

(16) Dennis, J. M.; White, N. A.; Liu, R. Y.; Buchwald, S. L.; Pd-Catalyzed C–N Coupling Reactions Facilitated by Organic Bases: Mechanistic Investigation Leads to Enhanced Reactivity in the Arylation of Weakly Binding Amines. *ACS Catal.* **2019**, *9*, 3822-3830.

(17) Liu, R. Y.; Dennis, J. M.; Buchwald, S. L.; The Quest for the Ideal Base: Rational Design of a Nickel Precatalyst Enables Mild, Homogeneous C–N Cross-Coupling. *J. Am. Chem. Soc.* **2020**, *142*, 4500-4507.

(18) Murthy Bandaru, S. S.; Bhilare, S.; Chrysochos, N.; Gayakhe, V.; Trentin, I.; Schulzke, C.; Kapdi, A. R.; Pd/PTABS: Catalyst for Room Temperature Amination of Heteroarenes. *Org. Lett.* **2018**, *20*, 473-476.

(19) Chen, L.; Francis, H.; Carrow, B. P.; An "On-Cycle" Precatalyst Enables Room-Temperature Polyfluoroarylation Using Sensitive Boronic Acids. *ACS Catal.* **2018**, *8*, 2989-2994.

(20) Chen, L.; Sanchez, D. R.; Zhang, B.; Carrow, B. P.; "Cationic" Suzuki–Miyaura Coupling with Acutely Base-Sensitive Boronic Acids. *J. Am. Chem. Soc.* **2017**, *139*, 12418-12421.

(21) Lennox, A. J. J.; Lloyd-Jones, G. C.; Transmetalation in the Suzuki–Miyaura Coupling: The Fork in the Trail. *Angew. Chem., Int. Ed.* **2013**, *52*, 7362-7370.

(22) (a) Thomas, A. A.; Denmark, S. E.; Pre-transmetalation intermediates in the Suzuki-Miyaura reaction revealed: The missing link. *Science* **2016**, *352*, 329-332; (b) Thomas, A. A.; Wang, H.; Zahrt, A. F.; Denmark, S. E.; Structural, Kinetic, and Computational Characterization of the Elusive Arylpalladium(II)boronate Complexes in the Suzuki–Miyaura Reaction. *J. Am. Chem. Soc.* **2017**, *139*, 3805-3821.

(23) Driver, M. S.; Hartwig, J. F.; Energetics and Mechanism of Alkylamine N-H Bond Cleavage by Palladium Hydroxides: N-H Activation by Unusual Acid-Base Chemistry. *Organometallics* **1997**, *16*, 5706-5715.

(24) (a) Kuwano, R.; Utsunomiya, M.; Hartwig, J. F.; Aqueous Hydroxide as a Base for Palladium-Catalyzed Amination of Aryl Chlorides and Bromides. *J. Org. Chem.* **2002**, *67*, 6479-6486; (b) Huang, X.; Anderson, K. W.; Zim, D.; Jiang, L.; Klapars, A.; Buchwald, S. L.; Expanding Pd-Catalyzed C–N Bond-Forming Processes: The First Amidation of Aryl Sulfonates, Aqueous Amination, and Complementarity with Cu-Catalyzed Reactions. *J. Am. Chem. Soc.* **2003**, *125*, 6653-6655; (c) Urgaonkar, S.; Verkade, J. G.; Scope and Limitations of Pd2(dba)3/P(i-BuNCH2CH2)3N-Catalyzed Buchwald–Hartwig Amination Reactions of Aryl Chlorides. *J. Org. Chem.* **2004**, *69*, 9135-9142.

(25) Nelson, D. J.; Nolan, S. P.; Hydroxide complexes of the late transition metals: Organometallic chemistry and catalysis. *Coord. Chem. Rev.* **2017**, *353*, 278-294.

(26) These substrates were selected based on good HPLC resolution of starting materials and product in the high throughput assay.

(27) (a) Pompeo, M.; Farmer, J. L.; Froese, R. D. J.; Organ, M. G.; Room-Temperature Amination of Deactivated Aniline and Aryl Halide Partners with Carbonate Base Using a Pd-PEPPSI-IPentCl- o-Picoline Catalyst. *Angew. Chem., Int. Ed.* **2014**, *53*, 3223-3226; (b) Brusoe, A. T.; Hartwig, J. F.; Palladium-Catalyzed Arylation of Fluoroalkylamines. *J. Am. Chem. Soc.* **2015**, *137*, 8460-8468.

(28) Note that X4 and X8 are supplied as a mixture of diastereomers, which complicates analysis of potential epimerization of the enolizable stereocenter during the reaction.

(29) Kutchukian, P. S.; Dropinski, J. F.; Dykstra, K. D.; Li, B.; DiRocco, D. A.; Streckfuss, E. C.; Campeau, L.-C.; Cernak, T.; Vachal, P.; Davies, I. W.; Krska, S. W.; Dreher, S. D.; Chemistry informer libraries: a chemoinformatics enabled approach to evaluate and advance synthetic methods. *Chem. Sci.* **2016**, *7*, 2604-2613.

(30) (a) Dallas, A. S.; Gothelf, K. V.; Effect of Water on the Palladium-Catalyzed Amidation of Aryl Bromides. *J. Org. Chem.* **2005**, *70*, 3321-3323; (b) Xu, C.; Gong, J.-F.; Wu, Y.-J.; Amination of aryl chlorides in water catalyzed by cyclopalladated ferrocenylimine complexes with commercially available monophosphinobiaryl ligands. *Tetrahedron Lett.* **2007**, *48*, 1619-1623; (c) Lipshutz, B. H.; Chung, D. W.; Rich, B.; Aminations of Aryl Bromides in Water at Room Temperature. *Adv. Synth. Catal.* **2009**, *351*, 1717-1721; (d) Pithani, S.; Malmgren, M.; Aurell, C.-J.; Nikitidis, G.; Friis, S. D.; Biphasic Aqueous Reaction Conditions for Process-Friendly Palladium-Catalyzed C–N Cross-Coupling of Aryl Amines. *Org. Process Res. Dev.* **2019**, *23*, 1752-1757.

(31) (a) Shaughnessy, K. H.; Beyond TPPTS: New Approaches to the Development of Efficient Palladium-Catalyzed Aqueous-Phase Cross-Coupling Reactions. *Eur. J. Org. Chem.* **2006**, *2006*, 1827-1835; (b) Shaughnessy, K. H. Cross-Coupling Reactions in Aqueous Media. In *Palladium - Catalyzed Coupling Reactions*; Wiley - VCH Verlag GmbH & Co. KGaA: Weinheim, 2013, p 235-286; (c) Carril, M.; SanMartin, R.; Domínguez, E.; Palladium and copper-catalysed arylation reactions in the presence of water, with a focus on carbon–heteroatom bond formation. *Chem. Soc. Rev.* **2008**, *37*, 639-647; (d) Shaughnessy, K. H. Greener Approaches to Cross-Coupling. In *New Trends in Cross-Coupling: Theory and Applications*; The Royal Society of Chemistry: 2015, p 645-696.

(32) Zhang, C.; Vinogradova, E. V.; Spokoyny, A. M.; Buchwald, S. L.; Pentelute, B. L.; Arylation Chemistry for Bioconjugation. *Angew. Chem., Int. Ed.* **2019**, *58*, 4810-4839.

(33) Jutand, A. Mechanisms of the Mizoroki–Heck Reaction. In *The Mizoroki–Heck Reaction*; Oestreich, M., Ed.; John Wiley & Sons, Ltd: West Sussex, 2009, p 1-50.

(34) Burés, J.; Variable Time Normalization Analysis: General Graphical Elucidation of Reaction Orders from Concentration Profiles. *Angew. Chem., Int. Ed.* **2016**, *55*, 16084-16087.

(35) (a) Hartwig, J. F.; Electronic Effects on Reductive Elimination To Form Carbon–Carbon and Carbon–Heteroatom Bonds from Palladium(II) Complexes. *Inorg. Chem.* **2007**, *46*, 1936-1947; (b) Arrechea, P. L.; Buchwald, S. L.; Biaryl Phosphine Based Pd(II) Amido Complexes: The Effect of Ligand Structure on Reductive Elimination. *J. Am. Chem. Soc.* **2016**, *138*, 12486-12493; (c) Peacock, D. M.; Jiang, Q.; Hanley, P. S.; Cundari, T. R.; Hartwig, J. F.; Reductive Elimination from Phosphine-Ligated Alkylpalladium(II) Amido Complexes To Form sp3 Carbon–Nitrogen Bonds. *J. Am. Chem. Soc.* **2018**, *140*, 4893-4904.

(36) Driver, M. S.; Hartwig, J. F.; Carbon–Nitrogen-Bond-Forming Reductive Elimination of Arylamines from Palladium(II) Phosphine Complexes. *J. Am. Chem. Soc.* **1997**, *119*, 8232-8245.

Authors are required to submit a graphic entry for the Table of Contents (TOC) that, in conjunction with the manuscript title, should give the reader a representative idea of one of the following: A key structure, reaction, equation, concept, or theorem, etc., that is discussed in the manuscript. Consult the journal's Instructions for Authors for TOC graphic specifications.

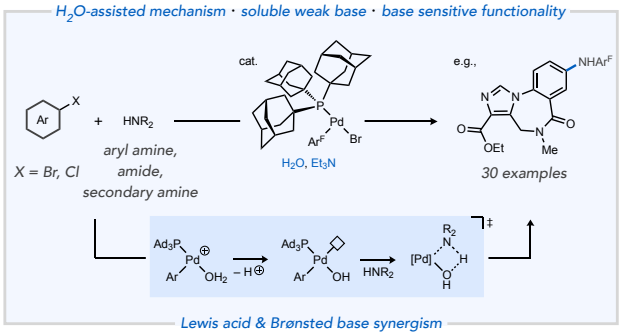

Supporting Information

Aryl Amination with Soluble Weak Base Enabled by a Water-Assisted Mechanism

Sii Hong Lau,[†] Peng Yu,[†] Liye Chen,[†] Christina B. Madsen-Duggan,[¶] Michael J. Williams,[¶] and Brad P. Carrow [†,*]

[†]*Department of Chemistry, Princeton University, Princeton, NJ 08544, United States*

[¶]*Chemical Process Development, Bristol Myers Squibb, 556 Morris Avenue, Summit, NJ 07902, United States*

*Email: bcarrow@princeton.edu

General Remarks

All reactions were performed inside a dry nitrogen filled glovebox or using standard Schlenk techniques unless otherwise noted. Solvents (tetrahydrofuran, toluene, diethyl ether, dichloromethane, *n*-pentane, *tert*-amyl alcohol (*t*-AmOH), cyclopentyl methyl ether (CPME), and anisole) were purified in a solvent purification system by percolation through neutral alumina under positive pressure of nitrogen or purchased from Millipore Sigma in Sure/Seal® containers. Deuterated solvents (chloroform-d_3, benzene-d_6, tetrahydrofuran-d_8) were stored over 4Å molecular sieves. All chemicals purchased from commercial suppliers were used as received unless otherwise noted. PAd_3,[1] $Pd(PAd_3)(4\text{-}FC_6H_4)Br$ (**1**),[2] and $[Pd(PAd_3)(4\text{-}FC_6H_4)]^+ BF_4^-$ (**33**)[3] were prepared according to literature. ^1H, ^{13}C, ^{19}F, and $^{31}P\{^1H\}$ nuclear magnetic resonance spectra (NMR) were obtained on a Bruker Avanche III 500 MHz, Bruker NanoBay 400 MHz or Bruker NanoBay 300 MHz spectrometers recorded in ppm (δ), referenced to residual solvent ($CHCl_3$, $CHDCl_2$, etc.).[4] Spin-spin coupling is described as singlet (s), doublet (d), triplet (t), quartet (q), quintet (quint), broad (br) or multiplet (m); coupling constants (*J*) are reported in Hz. Purity values were utilized from commercial sources or determined via ^1H NMR spectroscopy (300 MHz, delay = 30 s) implementing 1,3,5-trimethoxybenzene as the external standard. All analysis was performed on a mixture of accurately weighed (0.01 mg) standard and substrate in deuterated solvents. HR-MS was obtained from either Agilent 6320B LC TOF-MS with 0.01M ammonium acetate in 95:5 and 5:95 mixtures of acetonitrile and water as mobile phases or Waters GCT Premier Spectrometer using the desorption chemical ionization probe (DCI) with methane as CI reagent gas. UPLC analysis was performed on a Waters I-Class instrument (MP-A: 0.05% TFA in 95:5 water:acetonitrile; MP-B: 0.05% TFA in 95:5 acetonitrile:water; Column: Agilent Zorbax Eclipse C18+ (2.1x50 mm; 1.8 um); Temperature: 40 °C; flow: 0.8 mL/min; wavelength: specified for experiment; and gradient: 100 % MPA to 100% MPB over 1.2 min, hold at 100% MPB for 0.4 min, and return to initial conditions). Measurement of pH was accomplished using a Mettler Toledo Seven Excellence meter (with pH electrode) and calibrated using commercially available buffer standards (pH = 4, 7, and 10; slope $\geq$ 99%).

Methodology Optimization

General procedure for high-throughput screening. A 96-well aluminum microvial plate (Analytical Sales & Services cat. no. 96973) was equipped with 1 mL microvials (Analytical Sales & Services cat. no. 884001). In all reactions, stock solutions of reagents were used. In cases where reagents were only partially soluble, slurry additions were employed. Catalyst $Pd(PAd_3)(4\text{-}C_6H_4F)Br$ **1** (0.2 mmol, 0.004 M) and 4-propyl-1,1'-biphenyl (internal standard, 2 mmol, 0.04 M) were loaded by one of two methods: (*i*) a THF solution (50 µL) was transferred to all vials in the reaction plate then the plate was evaporated to dryness using a Genevac, at RT, 15 min, 20 Torr; (*ii*) a THF solution (50 µL) was transferred to all vials in the reaction plate last after all other reagents and solvent. Eight stock solutions containing 4-chloro-1,1'-biphenyl (20 mmol, 0.2 M) and 4-nitroaniline (24 mmol, 0.24 M) were dispensed into the appropriate wells, as shown in Figure S1, from stock solutions using pipettors so that each well received 100 µL of the appropriate solvent. To the left half of the plate (wells A1:A6, B1:B6, C1:C6, D1:D6, E1:E6, F1:F6, G1:G6, H1:H6) an additional appropriate solvent (50 µL) was added. Degassed water (50 µL) was added to the same left half of the plate (wells A1:A6, B1:B6, C1:C6, D1:D6, E1:E6, F1:F6, G1:G6, H1:H6), (solvent / H_2O (3:1) = 150 µL solvent, 50 µL water total added per well). Degassed water (100 µL) was also added to the right half of the plate (wells A7:A12, B7:B12, C7:C12, D7:D12, E7:E12, F7:F12, G1:G12, H7:H12), (solvent / H_2O (1:1) = 100 µL solvent, 100 µL water total added per well). The organic base (40 mmol) was added neat, as diagrammed in Figure S1, the microvial plate was sealed, removed from the glove box and shaken at 1000 rpm for 16 h at 60°C on an Eppendorf Thermomixer C with plate adapter. After aging, the reactions were diluted with MeCN: DMSO: H2O (3:1:1) with 1% HOAc (0.5 mL) and the plate was sealed and shaken at 1000 rpm an additional 15 minutes, at RT. The quenched reaction mixtures (30 mL) were sampled into a diluted sample plate occupied by 750 mL of 2:1 MeCN: Water. The plate was filtered and analyzed on Acquity I-class plus, Zorbax Eclipse plus C18, 2.1x50mm, 1.8um, TFA, 2 mins methods, 284 nm.

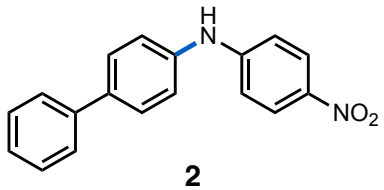

2

Reaction mixture from wells in columns B1:H1, B2:H2, B7:H7, B8:H8 and B10:H10 in the HTE screen were pooled and diluted with EtOAc (7 mL) and brine (7 mL) and transferred to a separatory funnel. Layers were split and the organics were collected, and solvents evaporated. The solid residue was redissolved in CH_2Cl_2 and the mixture was purified via silica, eluted with 0-40 % EA/heptane. Evaporation of desired product, followed by drying under vacuum, provided an analytical sample of **2**, as a yellow solid.

^{1}H NMR (500 MHz, $CDCl_3$) δ (ppm) = 8.19 - 8.10 (m, 2H), 7.63 - 7.57 (m, 4H), 7.53 - 7.34 (m, 3H), 7.28 (d, *J* = 7.6 Hz, 2H), 7.04 - 6.94 (m, 2H), 6.34 (s, 1H)

^{13}C NMR (126 MHz, $CDCl_3$) δ (ppm) = 150.0, 140.2, 139.9, 138.8, 137.5, 128.9, 128.3, 127.3, 126.8, 126.3, 122.0, 113.9

HRMS (ESI+) Calcd. for $[C_{18}H_{15}N_2O_2^+]$ ($M+H^+$), 291.1128; Found, 291.1130.

HPLC (Zorbax Eclipse plus C18, 2.1x50mm, 1.8um, TFA, 2 mins methods, 284 nm): 1.184 mins

96 total reaction conditions (6 bases x 8 solvents x 2 solvent / H_2O ratios)

Bases: Et_3N, DIPEA, DBU, MTBD, NMM, TMG

Solvents: MeCN, Anisole, IPAc, DMF, DME, 2-MeTHF, t-AmOH, MEK

Solvent / H_2O ratios: (3:1) and (1:1)

	MTBD	DBU	TMG	DIPEA	Et_3N	NMM	MTBD	DBU	TMG	DIPEA	Et_3N	NMM
MeCN												
toluene												
IPAc	**Left half of screen**						**Right half of screen**					
DMF	Solvent / H_2O (3:1)						Solvent / H_2O (1:1)					
DME	20 μmol / reaction						20 μmol / reaction					
2-MeTHF	200 μL scale in microvials						200 μL scale in microvials					
t-AmOH												
MEK												

Figure S1. Plate design for HTE screening of soluble base and solvent combinations at two different solvent/water ratios.

Table S1. Tabular reaction conversions (%) for HTE screen shown in Figure 1 using catalyst loading method *i*.[a]

		Solvent / H_2O (3:1)						Solvent / H_2O (1:1)					
		MTBD	DBU	TMG	DIPEA	Et_3N	NMM	MTBD	DBU	TMG	DIPEA	Et_3N	NMM
		1	2	3	4	5	6	7	8	9	10	11	12
MeCN	A	4	0	0	12	13	0	17	3	5	40	37	14
toluene	B	46	3	5	15	36	15	79	8	9	32	50	25
IPAc	C	64	6	15	37	54	26	55	24	14	53	65	35
DMF	D	14	3	5	41	49	14	49	11	14	71	76	33
DME	E	21	8	4	37	34	6	51	17	26	75	82	26
2-MeTHF	F	62	4	3	42	39	15	76	15	10	57	72	26
t-AmOH	G	13	27	19	55	66	21	55	27	38	74	84	41
MEK	H	25	6	7	34	47	7	38	6	17	58	72	24

Conversion Yields (%):	10	20	30	40	50	60	70	80

[a]Normalized conversions, versus 4-propyl-1,1'-biphenyl as internal standard, are reported as a single run.

Table S2. Tabular reaction conversions (%) for HTE screen using catalyst loading method *ii*.[a]

		Solvent / H_2O (3:1)						Solvent / H_2O (1:1)					
		MTBD	DBU	TMG	DIPEA	Et_3N	NMM	MTBD	DBU	TMG	DIPEA	Et_3N	NMM
		1	2	3	4	5	6	7	8	9	10	11	12
MeCN	A	4	0	0	9	5	2	13	4	3	52	45	16
anisole	B	49	0	0	56	67	26	65	1	5	62	71	38
IPAc	C	66	21	34	46	58	39	57	37	35	59	69	39
DMF	D	17	3	4	50	60	14	38	11	9	50	57	16
DME	E	30	9	7	49	58	9	54	18	22	84	82	32
2-MeTHF	F	37	0	0	60	70	48	70	5	7	72	82	57
t-AmOH	G	32	21	26	59	66	26	44	23	34	81	87	41
MEK	H	39	3	17	41	54	10	52	9	22	62	72	24

Conversion Yields (%):	10	20	30	40	50	60	70	80	90

[a]Normalized conversions, versus 4-propyl-1,1'-biphenyl as internal standard, are reported as a single run.

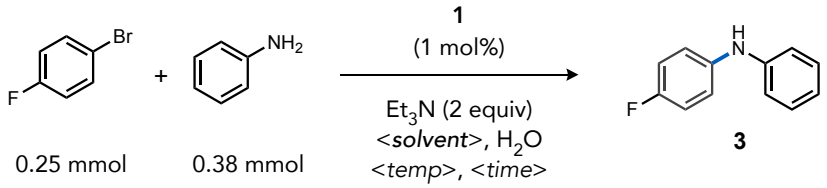

Representative procedure for non-parallel reaction optimizations. In a nitrogen filled glovebox, to an oven-dried 4 mL scintillation vial equipped with a stir bar was charged with 1-bromo-4-fluorobenzene (27 µL, 0.25 mmol, 1.0 equiv), aniline (34 µL, 0.375 mmol, 1.5 equiv), triethylamine (70 µL, 0.50 mmol, 2.0 equiv), trifluorotoluene (internal standard, 10 µL, 0.083 mmol, 0.33 equiv), Pd(PAd$_3$)(4-C$_6$H$_4$F)Br (**1**) (1.8 mg, 2.5 µmol, 1 mol%) and solvent. The vial was capped with a puncturable PTFE-lined cap and taken out of the glovebox. Under N_2 atmosphere, degassed deionized water was injected into the vial and the reaction mixture was left stirring at a certain temperature for the desired time period. After cooling down to room temperature, the mixture was diluted with $CDCl_3$ (1 mL) and the organic layer was separated for NMR characterization. The yield of **3** was obtained from the relative ^{19}F resonance integration of product and standard.[5]

Table S3. Effect of water on C–N coupling yield.

Entry	Variation from standard condition	Yield (%)
1	None (1:2 tol:H_2O)	>99
2	No water (1.0/0.0 mL)	0
3	25:1 tol:H_2O (1.0/0.04 mL)	5
4	10:1 tol:H_2O (1.0/0.1 mL)	18
5	2:1 tol:H_2O (1.0/0.5 mL)	50
6	1:1 tol:H_2O (1.0/1.0 mL)	55
7	0:1 tol:H_2O (0.0/1.0 mL)	>99

Conditions: toluene (0.5 mL):H_2O (1 mL), 60 ºC, 24 h.

Table S4. Effect of amine identity on the C–N coupling yield.

Entry	Variation from standard condition	Yield (%)
1	none	61
2	1:4 tol:H_2O (0.25/1.0 mL)	92
3	NCy_2Me instead of NEt_3	25
4	$N(OEt)_3$ instead of NEt_3	33
5	With 1.1 equiv LiI as additive	11
6	*p*-F-C_6H_4OTf instead of *p*-F-C_6H_4Br	3

Conditions: toluene (0.5 mL):H_2O (1 mL), 60 ºC, 6 h.

Table S5. Effect of solvent choice on the C–N coupling yield.

Entry	Variation from standard condition	Yield (%)
1	None	59
2	THF instead of toluene	52
3	Dioxane instead of toluene	44
4	2-MeTHF instead of toluene	53
5	DMF instead of toluene	45
6	DMA instead of toluene	35
7	K Phosphate Buffer pH 7.0 (0.1M) instead of water, no NEt_3	0
8	K Phosphate Buffer pH 6.0 (0.1M) instead of water	44
9	K Phosphate Buffer pH 7.0 (0.1M) instead of water	46
10	K Phosphate Buffer pH 8.0 (0.1M) instead of water	26

Conditions: toluene (0.25 mL):H_2O (1 mL), 60 ºC, 1 h.

General procedures for C–N coupling reactions

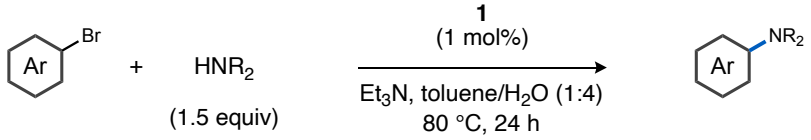

Procedure A (bromoarenes). To an oven-dried 20 mL scintillation vial equipped with a stir bar was charged with Pd(PAd$_3$)(4-C$_6$H$_4$F)Br (**1**) (5.4 mg, 7.5 μmol, 1 mol%), aryl bromide (0.75 mmol), amine nucleophile (1.13 mmol, 1.5 equiv), triethylamine (0.20 mL, 1.5 mmol, 2.0 equiv), and toluene (0.75 mL) under nitrogen (a 4 mL scintillation vial was used as reaction vessel for reactions conducted on 0.05 or 0.25 mmol-scale). The vial was capped with a puncturable PTFE-lined cap and taken out of the glovebox. Degassed deionized water (3.0 mL) was injected into the vial *via* a syringe. The reaction mixture was stirred at 80 °C for 24 h. After cooling to room temperature, the mixture was extracted with dichloromethane (3 x 5 mL) and the organic layer was dried over Na_2SO_4. After evaporation, the crude product was purified by column chromatography.

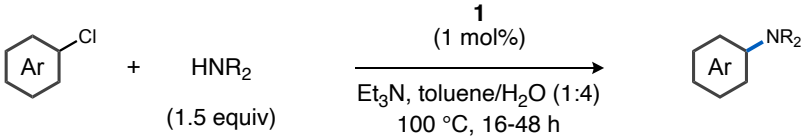

Procedure B (chloroarenes). To an oven-dried 4 mL scintillation vial equipped with a stir bar was charged with Pd(PAd$_3$)(4-C$_6$H$_4$F)Br (**1**) (1.8 mg, 2.5 μmol, 1 mol%), aryl chloride (0.25 mmol), amine nucleophile (0.38 mmol, 1.5 equiv), triethylamine (70 μL, 0.50 mmol, 2.0 equiv), and toluene (0.25 mL) under nitrogen. The vial was capped with a puncturable PTFE-lined cap and taken out of the glovebox. Degassed deionized water (1.0 mL) was injected into the vial via a syringe. The reaction mixture was left stirring at 100 °C for the indicated time. After cooling to room temperature, the mixture was extracted with dichloromethane (3 x 5 mL) and the organic layer was dried over Na_2SO_4. After evaporation, the crude product was purified by column chromatography.

Compound Characterization:

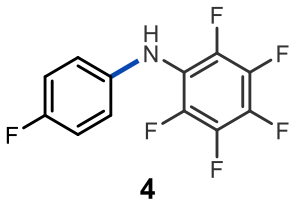

4

General procedure A was used, except using neat water (3.0 mL), on 0.75 mmol scale, and 191 mg of **4** (92%) was obtained as a pink solid.

^{1}H NMR (500 MHz, $CDCl_3$) δ 7.07–6.96 (m, 2H), 6.83–6.81 (m, 2H), 5.37 (s, 1H).

^{13}C NMR (126 MHz, $CDCl_3$) δ 158.6 (d, J = 241.4 Hz), 141.0 (dm, J = 246.3 Hz), 138.4 (dm, J = 250.2 Hz), 138.2 (d, J = 2.5 Hz), 137.0 (dm, J = 249.6 Hz), 118.8 (d, J = 8.1 Hz), 118.4–118.2 (m), 116.0 (d, J = 22.9 Hz).

^{19}F NMR (376 MHz, $CDCl_3$) δ -121.3 (m, 1F), -150.5 – -150.6 (m, 2F), -162.7 (td, J = 21.8, 5.3 Hz, 2F), -164.3 (tt, J = 21.8, 3.4 Hz, 1F).

HRMS (DCI) Calcd. for [$C_{12}H_6F_6N$] (M), 277.0326; Found, 277.0338.

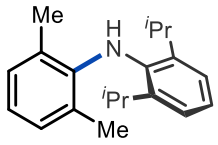

5

General procedure A was used on 0.75 mmol scale, and 152 mg (72%) of **5** was obtained as a colorless liquid.

^{1}H NMR (500 MHz, $CDCl_3$) δ 7.16–7.10 (m, 3H), 6.94 (d, J = 7.5 Hz, 2H), 6.72 (t, J = 7.5 Hz, 1H), 4.79 (s, 1H), 3.15 (hept, J = 7.0 Hz, 2H), 1.98 (s, 6H), 1.12 (d, J = 7.0 Hz, 12H).

^{13}C NMR (126 MHz, $CDCl_3$) δ 144.3, 143.3, 138.9, 129.6, 125.7, 124.9, 123.4, 119.7, 28.2, 23.6, 19.5.

HRMS (ESI+) Calcd. for [$C_{20}H_{28}N^+$] ($M+H^+$), 282.2216; Found, 282.2222.

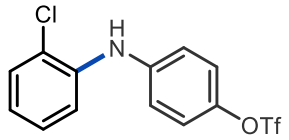

6

General procedure A was used, except using neat water (3.0 mL), on 0.75 mmol scale, and 219 mg (83%) of **6** was obtained as a colorless liquid.

^{1}H NMR (500 MHz, $CDCl_3$) δ 7.40 (dd, *J* = 8.0, 1.5 Hz, 1H), 7.30 (dd, *J* = 8.0, 1.5 Hz, 1H), 7.22–7.13 (m, 5H), 6.91 (td, *J* = 7.5, 1.5 Hz, 1H), 6.14 (s, 1H).

^{13}C NMR (126 MHz, $CDCl_3$) δ 143.9, 142.3, 139.0, 130.2, 127.7, 123.0, 122.6, 122.1, 119.8, 118.9 (q, *J* = 321.3 Hz), 117.2.

HRMS (ESI+) Calcd. for [$C_{13}H_{10}ClF_3NO_3S^+$] ($M+H^+$), 352.0017; Found, 352.0020.

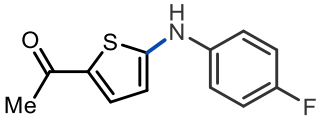

7

General procedure B was used on 0.25 mmol scale (48 h reaction time), and 26.5 mg (45%) of **7** was obtained as a grey solid.

^{1}H NMR (500 MHz, $CDCl_3$) δ 7.45 (d, *J* = 4.0 Hz, 1H), 7.18–7.16 (m, 2H), 7.04 (t, *J* = 9.0 Hz, 2H), 6.50 (s, 1H), 6.39 (d, *J* = 4.0 Hz, 1H), 2.46 (s, 3H).

^{13}C NMR (126 MHz, $CDCl_3$) δ 189.6, 159.0 (d, *J* = 243.2 Hz), 158.4, 137.5 (d, *J* = 2.6 Hz), 134.2, 130.3, 120.5 (d, *J* = 7.8 Hz), 116.5 (d, *J* = 22.9 Hz), 109.3, 25.7.

^{19}F NMR (376 MHz, $CDCl_3$) δ -119.2.

HRMS (DCI) Calcd. for [$C_{12}H_{11}FNOS$] (M), 236.0545; Found, 236.0536.

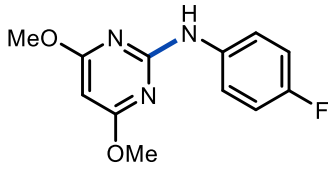

8

General procedure B was used on 0.25 mmol scale (16 h reaction time), and 56 mg (90%) of **8** was obtained as a white solid.

^{1}H NMR (500 MHz, $CDCl_3$) δ 7.58–7.54 (m, 2H), 7.03–6.99 (m, 2H), 6.97 (s, 1H), 5.58 (s, 1H), 3.90 (s, 6H)

^{13}C NMR (126 MHz, $CDCl_3$) δ 172.1, 158.4 (d, J = 240.0 Hz), 157.5, 135.8 (d, J = 2.5 Hz), 120.83 (d, J = 7.5 Hz), 115.5 (d, J = 21.3 Hz), 81.2, 54.0.

^{19}F NMR (282 MHz, $CDCl_3$) δ -121.1.

HRMS (ESI+) Calcd. for [$C_{12}H_{13}FN_3O_2^+$] ($M+H^+$), 250.0986; Found, 250.0995.

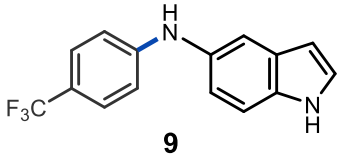

9

General procedure A was used on 0.75 mmol scale, and 174 mg (84%) of **9** was obtained as a brown solid.

^{1}H NMR (500 MHz, $CDCl_3$) δ 8.17 (s, 1H), 7.47 (d, J = 2.5 Hz, 1H), 7.40 (t, J = 8.5 Hz, 3H), 7.25 (d, J = 3.0 Hz, 1H), 7.05 (dd, J = 8.5, 2.0 Hz, 1H), 6.88 (d, J = 9.0 Hz, 2H), 6.53 (t, J = 2.0 Hz, 1H), 5.87 (s, 1H).

^{13}C NMR (126 MHz, $CDCl_3$) δ 149.6, 133.5, 133.3, 128.7, 126.7 (q, J = 3.8 Hz), 125.4, 125.0 (q, J = 270.6 Hz), 120.0 (q, J = 32.6 Hz), 119.5, 115.5, 113.6, 112.0, 102.8.

HRMS (ESI+) Calcd. for [$C_{15}H_{12}F_3N_2^+$] ($M+H^+$), 277.0947; Found, 277.0955.

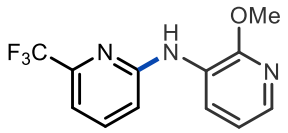

10

General procedure A was used on 0.25 mmol scale, and 61.2 mg (91%) of **10** was obtained as a white solid.

^{1}H NMR (500 MHz, $CDCl_3$) δ 8.71 (dd, *J* = 7.9, 1.7 Hz, 1H), 7.78 (d, *J* = 1.7 Hz, 1H), 7.65 (t, *J* = 8.0 Hz, 1H), 7.17 (s, 1H), 7.14 (d, *J* = 7.3 Hz, 1H), 6.94 (dd, *J* = 7.8, 5.0 Hz, 1H), 6.91 (d, *J* = 8.4 Hz, 1H), 4.05 (s, 3H).

^{13}C NMR (126 MHz, $CDCl_3$) δ 155.06, 153.04, 146.36 (q, *J* = 34.3 Hz), 138.36, 138.01, 124.91, 124.30, 121.68 (q, *J* = 274.1 Hz), 117.54, 113.99, 111.62, 53.81.

^{19}F NMR (376 MHz, $CDCl_3$) δ -68.64.

HRMS (ESI+) Calcd. for [$C_{12}H_{11}F_3N_3O^+$] ($M+H^+$), 270.0849; Found, 270.0858.

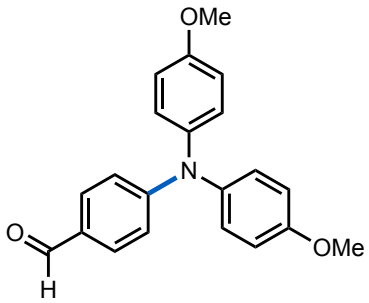

11

General procedure A was used on 0.75 mmol scale, and 228 mg (91%) of **11** was obtained as a yellow oil.

^{1}H NMR (500 MHz, $CDCl_3$) δ 9.76 (s, 1H), 7.64–7.62 (m, 2H), 7.14–7.12 (m, 4H), 6.91–6.84 (m, 6H), 3.82 (s, 6H).

^{13}C NMR (126 MHz, $CDCl_3$) δ 190.43, 157.43, 154.19, 138.94, 131.56, 128.20, 127.89, 116.87, 115.18, 55.64.

HRMS (ESI+) Calcd. for [$C_{21}H_{20}NO_3^+$] ($M+H^+$), 334.1438; Found, 334.1445.

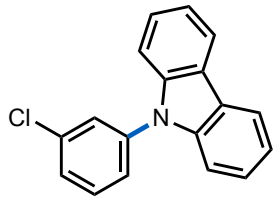

12

General procedure A was used on 0.75 mmol scale, and 165 mg (79%) of **12** was obtained as a yellow oil.

^{1}H NMR (500 MHz, $CDCl_3$) δ 8.15 (d, *J* = 8.0 Hz, 2H), 7.60 (t, *J* = 2.0 Hz, 1H), 7.55 (t, *J* = 8.0 Hz, 1H), 7.50 – 7.48 (m, 1H), 7.47 – 7.44 (m, 1H), 7.44 – 7.41 (m, 4H), 7.33 – 7.29 (m, 2H).

^{13}C NMR (126 MHz, $CDCl_3$) δ 140.7, 139.1, 135.5, 131.0, 127.7, 127.4, 126.3, 125.4, 123.6, 120.5, 120.5, 109.8.

HRMS (ESI+) Calcd. for [$C_{18}H_{13}ClN^+$] ($M+H^+$), 278.0731; Found, 278.0737.

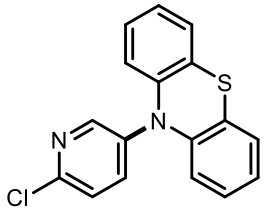

13

General procedure A was used on 0.25 mmol scale, and 67.6 mg (87%) of **13** was obtained as a white solid.

^{1}H NMR (500 MHz, $CDCl_3$) δ 8.40 – 8.39 (m, 1H), 7.66 (dd, *J* = 8.5, 3.0 Hz, 1H), 7.49 – 7.47 (m, 1H), 7.18 – 7.16 (m, 2H), 7.04 – 7.00 (m, 2H), 6.99 – 6.95 (m, 2H), 6.48 – 6.46 (m, 2H).

^{13}C NMR (126 MHz, $CDCl_3$) δ 148.6, 143.0, 138.2, 127.8, 127.4, 125.8, 124.5, 124.3, 118.8, 118.8.

HRMS (ESI+) Calcd. for [$C_{17}H_{12}ClN_2S^+$] ($M+H^+$), 311.0404; Found, 311.0411.

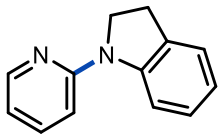

14

General procedure A was used, except using neat water (3.00 mL) and 3 mol% **1**, on 0.75 mmol scale, and 119 mg (81%) of **14** was obtained as an off-white solid.

^{1}H NMR (500 MHz, $CDCl_3$) δ 8.37 – 8.35 (m, 1H), 8.22 – 8.19 (m, 1H),), 7.61 – 7.56 (m, 1H), 7.21 – 7.17 (m, 2H), 6.87 (t, *J* = 9.0 Hz, 1H), 6.79 – 6.76 (m, 2H), 4.04 (t, *J* = 10.5 Hz, 2H), 3.21 (t, *J* = 10.5 Hz, 2H).

^{13}C NMR (126 MHz, $CDCl_3$) δ 155.6, 148.1, 145.0, 137.4, 131.5, 127.4, 124.7, 120.5, 114.5, 113.4, 108.7, 49.5, 27.8.

HRMS (ESI+) Calcd. for [$C_{13}H_{13}N_2^+$] ($M+H^+$), 197.1073; Found, 197.1080.

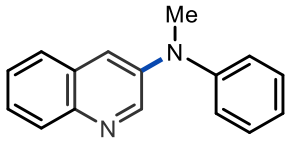

15

General procedure A was used on 0.25 mmol scale, and 57.4 mg (98%) of **15** was obtained as a yellow oil.

^{1}H NMR (500 MHz, $CDCl_3$) δ 8.69 (d, *J* = 3.0 Hz, 1H), 7.99 (d, *J* = 8.5 Hz, 1H), 7.67 (dd, *J* = 8.0, 2.0 Hz, 1H), 7.52 – 7.50 (m, 2H), 7.49 – 7.46 (m, 1H), 7.36 – 7.33 (m, 2H), 7.16 – 7.13 (m, 2H), 7.11 – 7.08 (m, 1H), 3.44 (s, 3H).

^{13}C NMR (126 MHz, $CDCl_3$) δ 148.2, 146.4, 143.3, 142.6, 129.8, 129.1, 129.1, 127.1, 126.7, 126.6, 123.4, 122.3, 119.6, 40.6.

HRMS (ESI+) Calcd. for [$C_{16}H_{15}N_2^+$] ($M+H^+$), 235.1230; Found, 235.1233.

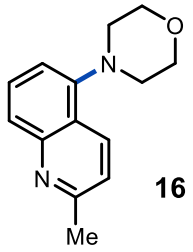

16

General procedure A was used on 0.25 mmol scale, and 47.4 mg (83%) of **16** was obtained as an orange solid.

^{1}H NMR (500 MHz, $CDCl_3$) δ 7.91 (dd, *J* = 9.0, 3.0 Hz, 2H), 7.45 (dd, *J* = 9.0, 3.0 Hz, 1H), 7.22 (d, *J* = 8.0 Hz, 1H), 7.01 (d, *J* = 7.5 Hz, 1H), 3.93–3.91 (m, 4H), 3.28 – 3.26 (m, 4H), 2.70 (s, 3H).

^{13}C NMR (126 MHz, $CDCl_3$) δ 156.4, 148.9, 143.7, 135.2, 129.6, 127.5, 122.5, 122.1, 109.4, 67.0, 49.8, 25.2.

HRMS (ESI+) Calcd. for [$C_{14}H_{17}N_2O^+$] ($M+H^+$), 229.1335; Found, 229.1343.

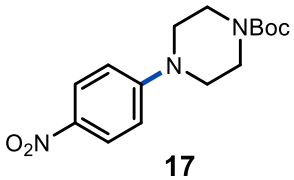

17

General procedure A was used on 0.75 mmol scale, and 205 mg (89%) of **17** was obtained as an orange solid.

^{1}H NMR (500 MHz, $CDCl_3$) δ 8.14 (d, *J* = 9.5 Hz, 2H), 6.82 (d, *J* = 9.0 Hz, 2H), 3.61 – 3.59 (m, 4H), 3.43 – 3.41 (m, 4H), 1.49 (s, 9H).

^{13}C NMR (126 MHz, $CDCl_3$) δ 154.8, 154.7, 138.9, 126.1, 113.0, 80.5, 47.0, 28.5.

HRMS (ESI+) Calcd. for [$C_{15}H_{22}N_3O_4^+$] ($M+H^+$), 308.1605; Found, 308.1606.

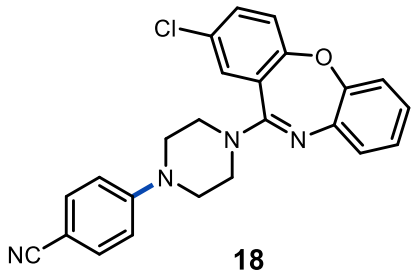

18

General procedure A was used (48 h reaction time) on 0.25 mmol scale, and 63.3 mg (61%) of **18** was obtained as an off-white solid.

^{1}H NMR (500 MHz, $CDCl_3$) δ 7.53 (d, *J* = 9.0 Hz, 2H), 7.42 (d, *J* = 9.0, 3.0 Hz, 1H), 7.36 (d, *J* = 3.0 Hz, 1H), 7.21 (d, *J* = 8.5 Hz, 1H), 7.18 – 7.16 (m, 1H), 7.12 – 7.09 (m, 2H), 7.04 – 7.01 (m, 1H), 6.91 (d, *J* = 8.5 Hz, 2H), 3.69 (s, 4H), 3.46 (s, 4H).

^{13}C NMR (126 MHz, $CDCl_3$) δ 159.5, 158.9, 153.4, 151.9, 139.9, 133.7, 133.0, 130.6, 129.0, 127.3, 126.0, 125.1, 124.9, 123.0, 120.3, 120.0, 114.7, 101.1, 47.2.

HRMS (ESI+) Calcd. for [$C_{24}H_{20}ClN_4O^+$] ($M+H^+$), 415.1320; Found, 415.1326.

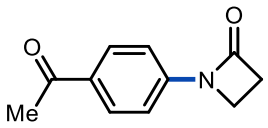

19

General procedure A was used on 0.25 mmol scale, and 42.1 mg (89%) of **19** was obtained as an off-white solid.

^{1}H NMR (500 MHz, $CDCl_3$) δ 7.96 (d, *J* = 9.0 Hz, 2H), 7.41 (d, *J* = 8.5 Hz, 2H), 3.70 (t, *J* = 4.5 Hz, 2H), 3.18 (d, *J* = 4.5 Hz, 2H), 2.58 (s, 3H).

^{13}C NMR (126 MHz, $CDCl_3$) δ 196.9, 164.9, 142.3, 132.7, 130.1, 115.9, 38.4, 36.7, 26.6.

HRMS (ESI+) Calcd. for [$C_{11}H_{12}NO_2^+$] ($M+H^+$), 190.0863; Found, 190.0870.

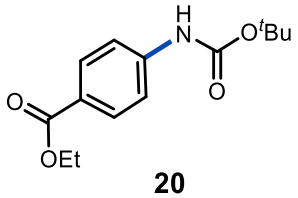

20

General procedure A was used on 0.75 mmol scale, and 193 mg (97%) of **20** was obtained as a white solid.

^{1}H NMR (500 MHz, $CDCl_3$) δ 7.98 (d, *J* = 9.0 Hz, 2H), 7.42 (d, *J* = 8.5 Hz, 2H), 6.66 (s, 1H), 4.35 (d, *J* = 7.0 Hz, 2H), 1.53 (s, 9H), 1.38 (t, *J* = 7.0 Hz, 3H).

^{13}C NMR (126 MHz, $CDCl_3$) δ 166.4, 152.3, 142.7, 131.0, 124.9, 117.4, 81.3, 60.9, 28.4, 14.5.

HRMS (ESI+) Calcd. for [$C_{14}H_{20}NO_4^+$] ($M+H^+$), 266.1387; Found, 266.1391.

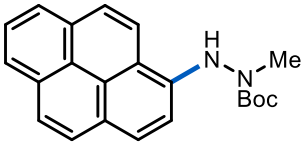

21

General procedure A was used (48 h reaction time) on 0.25 mmol scale, and 59.8 mg (69%) of **21** was obtained as an off-white solid.

^{1}H NMR (500 MHz, $CDCl_3$) δ 8.12 – 8.06 (m, 3H), 8.05 – 7.99 (m, 2H), 7.98 – 7.93 (m, 2H), 7.87 (d, *J* = 9.0 Hz, 1H), 7.43 (d, *J* = 8.4 Hz, 1H), 7.02 (s, 1H), 3.40 (s, 3H), 1.35 (s, 9H).

^{13}C NMR (126 MHz, $CDCl_3$) δ 156.2, 141.0, 132.0, 131.3, 127.6, 126.6, 126.0, 125.9, 125.7, 125.6, 125.3, 124.6, 124.5, 124.0, 119.3, 117.1, 109.9, 81.3, 37.7, 28.2.

HRMS (ESI+) Calcd. for [$C_{22}H_{23}N_2O_2^+$] ($M+H^+$), 369.1573; Found, 369.1580.

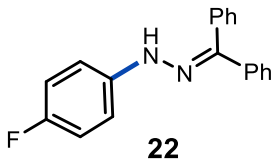

22

General procedure A was used on 0.25 mmol scale, and 58.1 mg (80%) of **22** was obtained as a brown solid.

^{1}H NMR (500 MHz, $CDCl_3$) δ 7.60 – 7.56 (m, 4H), 7.54 – 7.51 (m, 1H), 7.42 (s, br, 1H), 7.34 – 7.29 (m, 5H), 7.04 – 7.01 (m, 2H), 6.97 – 6.94 (m, 2H).

^{13}C NMR (126 MHz, $CDCl_3$) δ 157.4 (d, J = 237.8 Hz), 144.5, 141.1 (d, J = 2.1 Hz), 138.4, 132.8, 129.8, 129.4, 129.2, 128.3, 128.2, 126.6, 115.9 (d, J = 22.6 Hz), 113.9 (d, J = 7.7 Hz).

HRMS (ESI+) Calcd. for [$C_{19}H_{16}FN_2^+$] ($M+H^+$), 291.1292; Found, 291.1305.

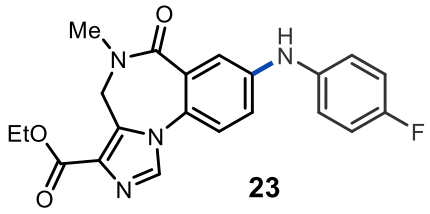

23

General procedure A was used on 50 μmol scale, and 17.7 mg (90%) of **23** was obtained as an off-white solid.

^{1}H NMR (500 MHz, $CDCl_3$) δ 7.84 (s, 1H), 7.52 (d, J = 2.7 Hz, 1H), 7.26 (d, J = 8.6 Hz, 1H, obscured by chloroform-d_6 peak), 7.17 – 7.10 (m, 3H), 7.08 – 7.02 (m, 2H), 5.93 (s, 1H), 5.25-5.07 (m, 1H), 4.51 – 4.29 (m, 3H), 3.23 (s, 3H), 1.45 (t, J = 7.2 Hz, 3H).

^{13}C NMR (126 MHz, $CDCl_3$) δ 166.6, 163.3, 159.4 (d, J = 242.9 Hz), 145.2, 136.9 (d, J = 2.9 Hz), 135.5, 134.8, 130.4, 128.3, 124.2, 123.3, 123.2 (d, J = 8.1 Hz), 118.7, 118.0, 116.6 (d, J = 22.6 Hz), 61.1, 42.6, 36.0, 14.6.

^{19}F NMR (376 MHz, $CDCl_3$) δ -118.8.

HRMS (ESI+) Calcd. for [$C_{21}H_{20}FN_4O_3^+$] ($M+H^+$), 395.1514; Found, 395.1521.

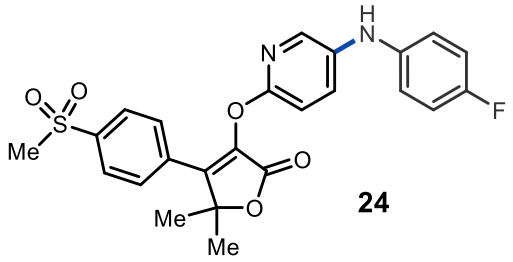

24

General procedure A was used on 50 μmol scale, and 21.3 mg (91%) of **24** was obtained as a green oil.

^{1}H NMR (500 MHz, $CDCl_3$) δ 8.03 – 7.97 (m, 2H), 7.83 – 7.81 (m, 1H), 7.80 – 7.76 (m, 2H), 7.40 (dd, J = 8.7, 2.8 Hz, 1H), 7.01 – 6.89 (m, 6H), 3.07 (s, 3H), 1.76 (s, 6H).

^{13}C NMR (126 MHz, $CDCl_3$) δ 165.9, 158.2 (d, J = 240.8 Hz), 155.6, 147.6, 141.2, 138.7, 138.1, 137.4, 136.4, 135.1, 129.7, 129.0, 127.9, 120.0 (d, J = 7.6 Hz), 116.2 (d, J = 22.6 Hz), 111.6, 84.3, 44.4, 26.5.

HRMS (ESI+) Calcd. for [$C_{24}H_{22}FN_2O_5S^+$] ($M+H^+$), 469.1228; Found, 469.1233.

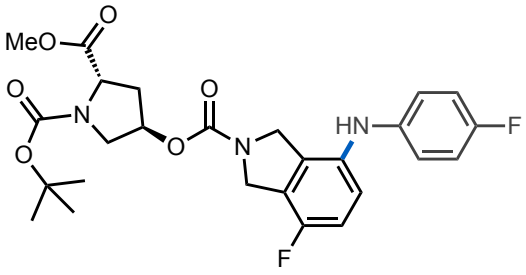

25

General procedure A was used on 50 μmol scale, and 24.3 mg (94%) of **25** was obtained as an orange solid. Note that the starting aryl bromide (X4 in Merck informer library) is supplied as a mixture of diastereomers. Flash chromatography did not separate the diastereomers of **25**, and spectral data are reported for the mixture as a result.

^{1}H NMR (500 MHz, $CDCl_3$) δ 7.01 – 6.84 (m, 6H), 5.36 – 5.26 (m, 1H), 5.18 (d, J = 28.1 Hz, 1H), 4.81 – 4.77 (m, 1H), 4.72 (s, 1H), 4.59 (s, 1H), 4.56 – 4.53 (m, 1H), 4.49 – 4.30 (m, 1H), 3.78 – 3.72 (m, 4H), 3.78 – 3.59 (m, 1H), 2.52 – 2.37 (m, 1H), 2.29 – 2.16 (m, 1H), 1.49 – 1.39 (m, 9H).

^{13}C NMR (126 MHz, $CDCl_3$) δ 173.2, 173.1, 172.9, 172.8, 159.0, 158.9, 157.1, 157.0, 154.4, 154.4, 154.1, 154.0, 153.9, 153.8, 153.7, 153.7, 152.1, 152.1, 151.9, 139.1, 139.1, 139.0, 139.0, 134.8, 134.7, 134.7, 134.6, 134.6, 129.7, 129.7, 129.5, 129.5, 129.3, 129.2, 124.7, 124.5, 124.4, 124.4, 124.3, 124.2, 119.7, 119.7, 119.6, 119.5, 119.5, 118.8, 116.2, 116.2, 116.0, 116.0, 115.4, 115.3, 115.3, 115.2, 115.2, 115.1, 80.6, 73.8, 73.8, 73.2, 73.2, 58.1, 58.0, 57.7, 57.6, 52.8, 52.7, 52.5, 52.4, 52.2, 51.5, 51.0, 51.0, 50.3, 49.8, 37.0, 37.0, 36.1, 36.0, 28.4, 28.3.

HRMS (ESI+) Calcd. for [$C_{26}H_{30}F_2N_3O_6^+$] ($M+H^+$), 540.1917; Found, 540.1925.

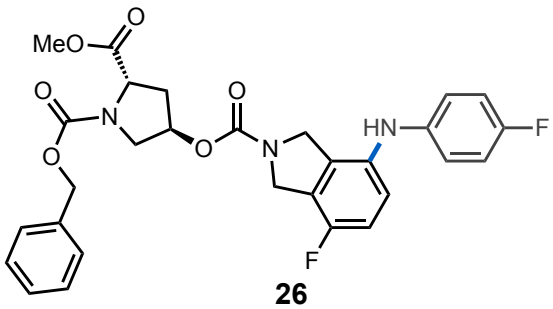

26

General procedure A was used on 50 μmol scale, and 26.1 mg (98%) of **26** was obtained as an orange solid. Note that the starting aryl bromide (X8 in Merck informer library) is supplied as a mixture of diastereomers. Flash chromatography did not separate the diastereomers of **26**, and spectral data are reported for the mixture as a result.

^{1}H NMR (500 MHz, $CDCl_3$) δ 7.38 – 7.28 (m, 5H), 7.18 (t, J = 7.8 Hz, 1H), 7.07 – 6.92 (m, 5H), 6.86 – 6.77 (m, 1H), 5.38 – 4.96 (m, 4H), 4.74 (s, 1H), 4.69 – 4.42 (m, 4H), 3.93 – 3.73 (m, 4H), 3.56 (d, J = 5.2 Hz, 1H), 2.56 – 2.45 (m, 1H), 2.32 – 2.19 (m, 1H).

^{13}C NMR (126 MHz, $CDCl_3$) δ 172.7, 172.7, 172.5, 172.5, 159.4, 159.4, 157.5, 157.5, 154.9, 154.9, 154.3, 153.9, 153.7, 139.3, 139.3, 138.2, 138.1, 138.1, 138.0, 138.0, 137.9, 137.9, 136.3, 136.3, 136.3, 136.2, 129.1, 128.5, 128.1, 128.1, 127.9, 127.9, 125.0, 124.8, 124.8, 124.7, 121.5, 121.4, 121.3, 121.3, 116.2, 116.0, 114.9, 114.8, 114.8, 114.8, 114.4, 114.2, 114.1, 73.6, 73.0, 72.9, 67.4, 58.1, 58.1, 57.8, 57.8, 53.1, 53.0, 53.0, 52.8, 52.7, 52.7, 52.5, 52.3, 51.0, 50.6, 50.5, 37.2, 37.1, 36.1, 36.1.

HRMS (ESI+) Calcd. for [$C_{29}H_{29}FN_3O_6^+$] ($M+H^+$), 534.2035; Found, 534.2038.

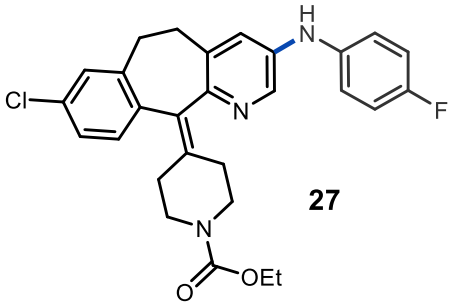

27

General procedure A was used on 50 μmol scale, and 18.7 mg (76%) of **27** was obtained as an orange solid.

^{1}H NMR (500 MHz, $CDCl_3$) δ 8.10 (d, *J* = 2.7 Hz, 1H), 7.20 – 7.07 (m, 3H), 7.06 – 6.96 (m, 5H), 5.63 (s, 1H), 4.13 (q, *J* = 7.1 Hz, 2H), 3.82 (d, *J* = 16.1 Hz, 2H), 3.41 – 3.31 (m, 1H), 3.31 – 3.20 (m, 1H), 3.18 – 3.04 (m, 2H), 2.85 – 2.68 (m, 2H), 2.55 – 2.44 (m, 1H), 2.43 – 2.35 (m, 1H), 2.35 – 2.28 (m, 2H), 1.25 (t, *J* = 7.1 Hz, 3H).

^{13}C NMR (126 MHz, $CDCl_3$) δ 158.5 (d, *J* = 241.5 Hz), 155.5, 148.6, 139.7, 139.3, 138.5, 137.7 (d, *J* = 2.9 Hz), 137.2, 136.0, 133.8, 133.6, 132.7, 130.2, 128.7, 126.2, 123.8, 121.2 (d, *J* = 7.9 Hz), 116.2 (d, *J* = 22.6 Hz), 61.3, 44.9, 44.9, 32.0, 31.5, 30.8, 30.6, 14.7.

HRMS (ESI+) Calcd. for [$C_{28}H_{28}ClFN_3O_2^+$] ($M+H^+$), 492.1849; Found, 492.1855.

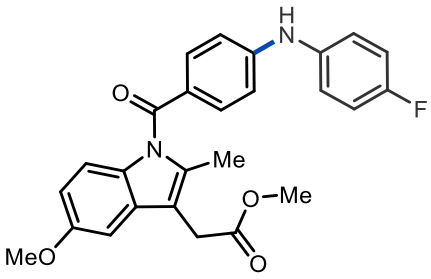

28

General procedure A was used on 0.25 mmol scale, and 100 mg (90%) of **28** was obtained as a brown solid.

^{1}H NMR (500 MHz, $CDCl_3$) δ 7.62 (d, *J* = 9.0 Hz, 2H), 7.18 – 7.15 (m, 2H), 7.07 – 7.03 (m, 2H), 6.98 – 6.96 (m, 2H), 6.88 (d, *J* = 8.5 Hz, 2H), 6.67 (dd, *J* = 9.0, 2.5 Hz, 1H), 6.14 (s, 1H), 3.84 (s, 3H), 3.70 (s, 3H), 3.68 (s, 2H), 2.47 (s, 3H).

^{13}C NMR (126 MHz, $CDCl_3$) δ 171.8, 168.9, 159.5 (d, *J* = 242.5 Hz), 155.7, 149.5, 136.3, 136.3, 132.9, 131.3, 130.3, 125.3, 123.9 (d, *J* = 7.5 Hz), 116.5 (d, *J* = 22.5 Hz), 114.8, 113.9, 111.5, 111.1, 101.0, 55.9, 52.2, 30.4, 13.0.

^{19}F NMR (282 MHz, $CDCl_3$) δ -118.2.

HRMS (ESI+) Calcd. for [$C_{26}H_{24}FN_2O_4^+$] ($M+H^+$), 447.1715; Found, 447.1720.

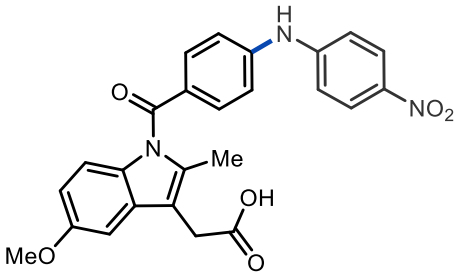

29

General procedure B was used (48 h reaction time), except using 2 mol% **1**, on 0.25 mmol scale, and 58.6 mg (51%) of **29** was obtained as a yellow solid.

^{1}H NMR (500 MHz, DMSO-d_6) δ 9.78 (s, 1H), 8.18 (d, *J* = 9.5 Hz, 2H), 7.65 (d, *J* = 8.5 Hz, 2H), 7.36 (d, *J* = 9.0 Hz, 2H), 7.31 (d, *J* = 9.0 Hz, 2H), 7.03 (d, *J* = 2.5 Hz, 1H), 6.93 (d, *J* = 9.0 Hz, 1H), 6.71 (dd, *J* = 9.0, 3.0 Hz, 1H), 3.76 (s, 3H), 3.67 (s, 2H), 2.28 (s, 3H).

^{13}C NMR (126 MHz, DMSO-d_6) δ 172.3, 168.1, 155.2, 148.6, 145.5, 139.7, 135.3, 131.9, 130.5, 130.4, 127.6, 126.0, 117.8, 116.0, 114.2, 112.5, 111.2, 101.4, 55.4, 29.6, 12.9.

HRMS (ESI+) Calcd. for [$C_{25}H_{22}N_3O_6^+$] ($M+H^+$), 460.1503; Found, 460.1505.

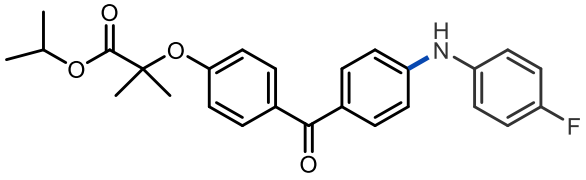

30

General procedure B was used (36 h reaction time) on 0.25 mmol scale, and 98.0 mg (90%) of **30** was obtained as a white solid.

^{1}H NMR (500 MHz, $CDCl_3$) δ 7.71 – 7.69 (m, 4H), 7.17 – 7.14 (m, 2H), 7.05 – 7.01 (m, 2H), 6.90 (d, *J* = 10 Hz, 2H), 6.85 (d, *J* = 10 Hz, 2H), 6.21 (s, 1H), 5.08 (hept, *J* = 6.5 Hz, 1H), 1.65 (s, 6H), 1.20 (d, *J* = 6.5 Hz, 6H).

^{13}C NMR (126 MHz, $CDCl_3$) δ 194.2, 173.4, 159.2 (d, *J* = 241.3 Hz), 159.0, 148.7, 136.8 (d, *J* = 2.5 Hz), 132.6, 131.7, 131.7, 128.9, 123.4 (d, *J* = 7.5 Hz), 117.3, 116.3 (d, *J* = 22.5 Hz), 113.8, 79.4, 69.4, 25.5, 21.6.

^{19}F NMR (282 MHz, $CDCl_3$) δ -118.9.

HRMS (ESI+) Calcd. for [$C_{26}H_{27}FNO_4^+$] ($M+H^+$), 436.1919; Found, 436.1907.

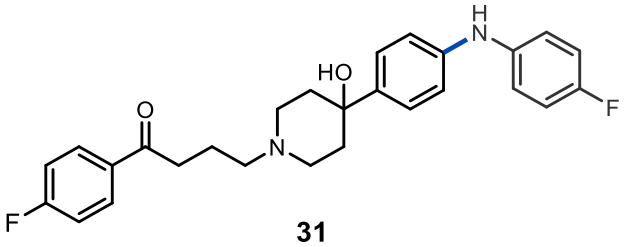

31

General procedure B was used (48 h reaction time), except using 2 mol% **1**, on 0.25 mmol scale, and 65.3 mg (58%) of **31** was obtained as a white solid. The yield of **31** was 60% as determined by ^{19}F NMR analysis versus internal standard. The product is poorly soluble in common deuterated solvents.

^{1}H NMR (500 MHz, DMSO-*d*$_6$) δ 8.13 (s, 1H), 8.09 – 8.07 (m, 2H), 7.37 (t, *J* = 9.0, 2H), 7.30 (t, *J* = 8.5, 2H), 7.06 (d, *J* = 6.5, 4H), 6.99 (d, *J* = 8.5, 2H), 6.98 (brs, 1H), 3.36 – 3.17 (m, 10H), 2.02 (s, 2H), 1.72 (s, 2H).

^{13}C NMR (126 MHz, DMSO-*d*$_6$) δ 197.6, 165.0 (d, *J* = 251.7 Hz), 156.2 (d, *J* = 236.0 Hz), 142.4, 140.0, 133.4, 130.9 (d, *J* = 9.6 Hz), 125.6, 118.4 (d, *J* = 7.7 Hz), 115.8, 115.7 (d, *J* = 21.9 Hz), 115.7 (d, *J* = 22.2 Hz), 68.2, 48.5, 35.4, 21.0.

^{19}F NMR (376 MHz, CD_2Cl_2) δ -107.1, -123.2.

HRMS (ESI+) Calcd. for [$C_{27}H_{29}FNO_4^+$] ($M+H^+$), 451.2192; Found, 451.2193.

Scale-Up of Synthesis of Fenofibrate Derivative 30:

Reaction Conversion Calibration Curve. To 4 x 8 mL vials was charged fenofibrate (MW 360.83 g/mol; measured purity 98%) and **30** (MW 435.495 g/mol; measured purity 99.5%) according to the values in the Table S6. The mixtures were then dissolved in EtOAc (7 mL), sampled (30 uL in 1.5 mL of 2:1 acetonitrile:water), and assayed via UPLC analysis. The resulting areas of each peak were measured at 304 nm and conversion (%) values were compared to the actual mass conversion values (%).

Table S6. Tabular data for detector response for substrate and product analytes.

Entry	Compound	Wt. (mg)	Corrected wt. (mg)		mmol	Measured Area (304 nm)
1	fenofibrate	159.4	156.212		0.4329	333319.00
	30	44.9	44.6755		0.103	77607
				conversion:	19%	19%
2	fenofibrate Substrate **30**	84.2	82.516		0.228	183257
		116	115.42		0.265	203654
		-	-	conversion:	54%	53%
3	fenofibrate	25.7	25.186		0.0697	58840
	30	194.0	193.03		0.4432	323089
				conversion:	86%	85%
4	fenofibrate Substrate **30**	5.4	5.292		0.014	16690
		226.8	225.666		0.5181	382633
		-	-	conversion:	97%	96%

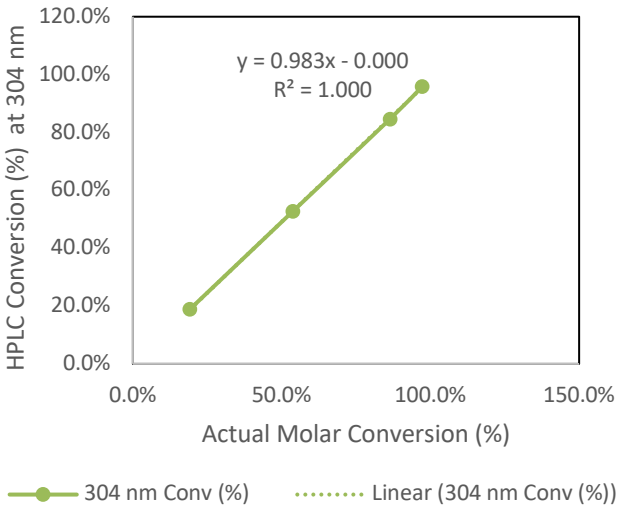

Figure S2. Calibration curve of measured versus actual conversion of fenofibrate to **30**.

Optimization of solvent and temperature in synthesis of 30. To 8 x 20 mL vials with stir bars outside of the glovebox was charged isopropyl 2-(3-(3-chlorobenzoyl)phenoxy)-2-methylpropanoate (fenofibrate) (530 mg, 1.44 mmol, 98% purity), 4-fluoroaniline (245 mg, 2.16 mmol, 1.5 equiv, 98% purity), and **1** (9.39 mg, 0.013 mmol, 0.9 mol%). The vials were then brought into the glovebox and charged with solvent (1.5 mL), degassed water (6 mL), and triethylamine (405 uL, 2.88 mmol, 2 equiv, 99% purity). The vials were sealed, removed from the glovebox, and placed into a pre-heated hotplate at the specified temperatures and aged for 21 h with vigorous stir bar agitation. Upon cooling, aliquots (50 uL) were taken with continued agitation, diluted into 2:1 acetonitrile:water (7 mL), and assayed for reaction completion using UPLC-MS analysis at 304 nm.

Table S7. Results of Temperature and Solvent Variation During Synthesis of 30.

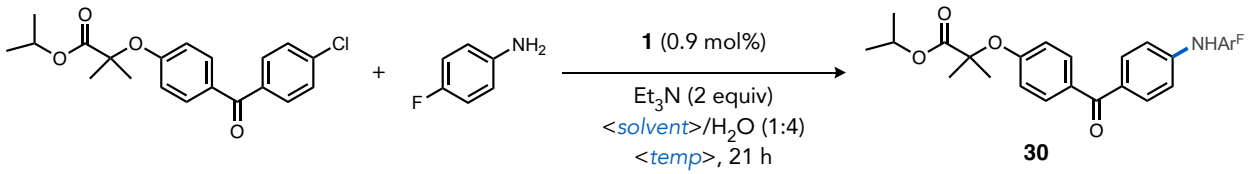

Entry	Solvent	Temperature (°C)	Conversion (%)
1	Anisole	98	89
2	CPME	98	98
3	*t*-AmOH	98	96
4	toluene	98	97
5	anisole	80	74
6	CPME	80	71
7	*t*-AmOH	80	94
8	toluene	80	83

Monitoring aqueous pH at initial reaction time. To a 20 mL vial with stir bar was charged isopropyl 2-(3-(3-chlorobenzoyl)phenoxy)-2-methylpropanoate (fenofibrate**)** (1.00 g, 2.72 mmol, 98% purity), 4-fluoroaniline (462 mg, 4.07 mmol, 1.5 equiv., 98% purity), *tert*-amyl alcohol (3 mL), degassed water (9 mL), and triethylamine (765 µL, 5.43 mmol, 2 equiv., 99% purity). The vial was agitated for ~10 min where upon the initial pH measurement was obtained (pH = 11.9) using the pH meter, electrode, and calibration procedure (*vide supra*).

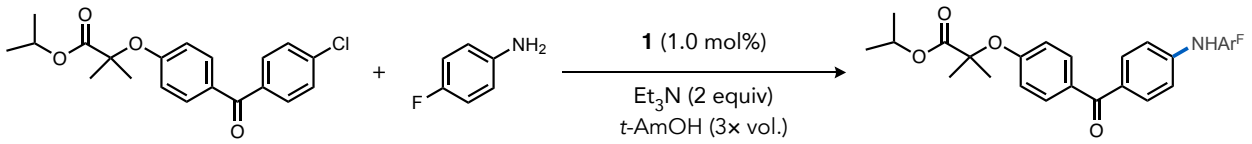

30

97% solution yield
80% Isolated yield (7.0 g)
Final pH = 8.5

Synthesis of 30 on 20-mmol Scale. To a 100 mL EasyMax vessel fitted with reflux condenser, pitched blade impeller, and nitrogen inlet was charged isopropyl 2-(3-(3-chlorobenzoyl)phenoxy)-2-methylpropanoate (fenofibrate) (7.36 g, 20.0 mmol, 98% purity) and 4-fluoroaniline (3.40 g, 30.0 mmol, 1.5 equiv, 98% purity). The vessel was sealed and purged with N_2. Degassed water (66 mL, 9× vol.), *t*-Amyl alcohol (22 mL, 3× vol., commercially available anhydrous solvent from Millipore Sigma), and degassed triethylamine (5.63 mL, 40.0 mmol, 2 equiv, 99% purity) were charged to the reactor utilizing Schlenk techniques while keeping the internal temperature at 25 °C with agitation set at 600 RPM. To the reactor was then charged complex **1** (144 mg, 200 µmol, 1 mol%) as a solid under nitrogen purge. The reaction was then ramped to 85 °C over 15 min at 600 RPM agitation rate, aged for 12 h, sampled (50 µL in 7 mL of 2:1 acetonitrile:water), and deemed complete (100% conversion). The reaction mixture was cooled to 25 °C, EtOAc (37 mL, 5× vol.) was charged, and the mixture was transferred to a separatory funnel with additional EtOAc (37 mL, 5× vol.). The resulting biphasic solution was separated (aqueous layer loss <0.1%, pH = 8.5), and the organic layer assayed (solution yield = 97%). The resulting dark organic phase was concentrated to a near oil on the rotary evaporator (70-80 mm Hg, 40 °C), and then diluted with EtOAc (37 mL, 5× vol.). To the organic mixture was then charged heptane (22 mL, 3× vol), then **30** Seed (~50 mg), and the resulting slurry was allowed to age (~30 min). Additional heptane (29 mL, 4× vol.) was charged to the dark slurry over ~ 20 min. The resulting mixture was allowed to further age (30 min) whereupon it was filtered through at disposable polypropylene filter funnel (10 µm). The wet cake was slurry washed with 20% EtOAc in heptane (2 × 22 mL, 2 × 3× vol), and the cake was allowed to dry overnight at room temperature under vacuum and a stream of N_2 to yield **30** as a light gray solid (7.02 g, 16.0 mmol, 80% yield at 99% purity by ^{1}H wt/wt NMR).

HRMS (ESI+) Calcd. for [$C_{26}H_{27}FNO_4^+$] ($M+H^+$), 436.1919; Found, 436.1938.

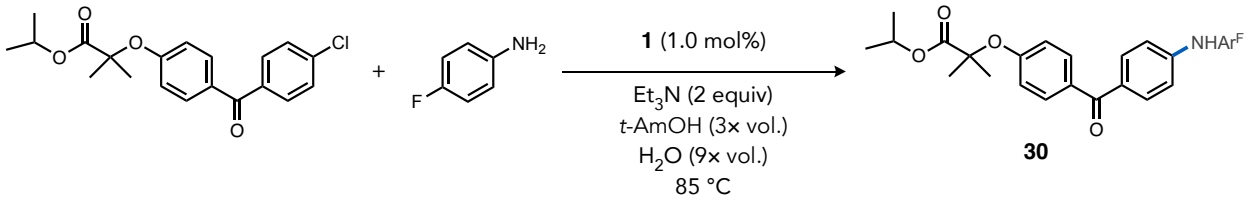

Kinetic Profile of Reaction on 20-mmol Scale. To a 100 mL EasyMax vessel fitted with reflux condenser, pitched blade impeller, nitrogen inlet, and EasySampler (Fitted with the following solvent lines: Reaction = degassed water; Quench and Diluent = 2:1 acetonitrile:water – non-degassed; Dilution Factor = 350) was charged isopropyl 2-(3-(3-chlorobenzoyl)phenoxy)-2-methylpropanoate (fenofibrate) (7.36 g, 20.0 mmol, 98% purity) and 4-fluoroaniline (3.40 g, 30.0 mmol, 1.5 equiv., 98% purity). The vessel was sealed and purged with N_2. Degassed water (66 mL, 9× vol.), *t*-Amyl alcohol (22 mL, 3× vol. - commercially available anhydrous solvent from Millipore Sigma), and degassed triethylamine (5.63 mL, 40.0 mmol, 2 equiv., 99% purity) were charged to the reactor under Schlenk conditions keeping the internal temperature at 25 °C with agitation set at 600 RPM. To the reactor was then charged complex **1** (144 mg, 0.200 mmol, 1 mole%) as a solid under nitrogen purge. The sampling times (min), temperature ramp (°C in min), and reaction conversion (%) are tabulated below.

Table S8. Tabular Data for 20-mmol Scale Amination of Fenofibrate.

Entry	Temp Ramp Time (min)	Temp (°C)	Sampling Time (min)	DP Area (304 nm)	SM Area (304 nm)	Conv. (%)	Comment
1	0	25	2	13272	240538	5%	Sampling delay of ~2 min
2	15	25	17	104215	219975	32%	Sampled after 17 min at 25 °C
3	30	85	32	448567	24593	95%	Sampled 2 min after reaching 85 °C
4	45	85	47	476641	0	100%	Sampled 17 min after reaching 85 °C
5	60	85	62	421346	0	100%	Sampled 32 min after reaching 85 °C
6	120	85	122	442854	0	100%	Sampled 1h after reaching 85 °C

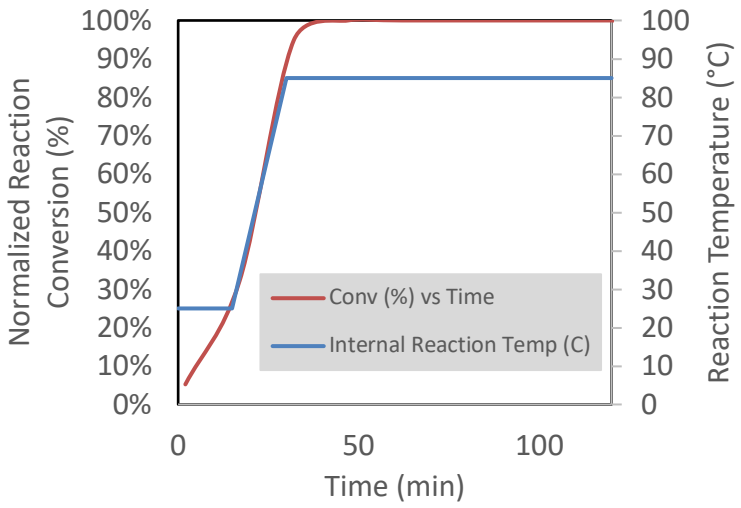

Figure S3. Reaction conversion (left-axis) and temperature (right-axis) of fenofibrate to **30** (20-mmol scale) versus time.

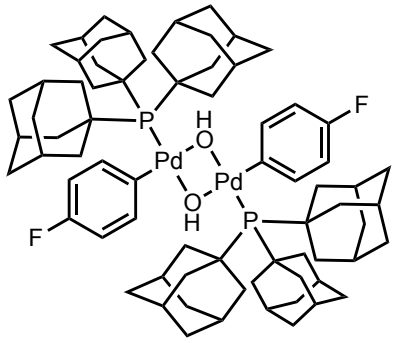

32

***anti*-[Pd(PAd$_3$)(4-C$_6$H$_4$F)(μ-OH)]$_2$ (32).** To an oven-dried 100 mL Schlenk flask equipped with a magnetic stir bar was charged with Pd(PAd$_3$)(4-C$_6$H$_4$F)Br (**1**) (90 mg, 0.13 mmol) and dichloromethane (30 mL). A solution of sodium hydroxide (50 mg, 1.3 mmol, 10 equiv) in water (30 mL) was injected into the reaction mixture. The resulting biphasic solution was stirred vigorously for 30 min at room temperature. The aqueous layer was then separated, the organic layer was concentrated, and resulting was washed with *n*-hexanes (3 x 5 mL), filtered and dried under reduced pressure to afford 64 mg (78%) of **32** an off-white solid.

^{1}H NMR (500 MHz, CD_2Cl_2) δ 7.40 (t, J = 7.1 Hz, 4H), 6.63 (t, J = 9.2 Hz, 4H), 2.42 (s, 36H), 1.88 (s, 18H), 1.72 - 1.57 (m, 36H), -2.19 (d, J = 3.2 Hz, 2H).

^{13}C{^{1}H} NMR (126 MHz, CD_2Cl_2) δ 160.91 (d, J = 238.0 Hz), 139.96, 138.68, 112.48 (d, J = 18.5 Hz), 48.83 (d, J = 5.1 Hz), 42.02, 36.97, 29.84 (d, J = 7.5 Hz).

^{19}F NMR (470 MHz, CD_2Cl_2) δ -125.2.

^{31}P{^{1}H} NMR (202 MHz, CD_2Cl_2) δ 67.1.

HRMS (ESI) m/z calculated for $C_{38}H_{52}FNPPd$ (M/2−OH+MeCN), 678.28562, found 678.28588.

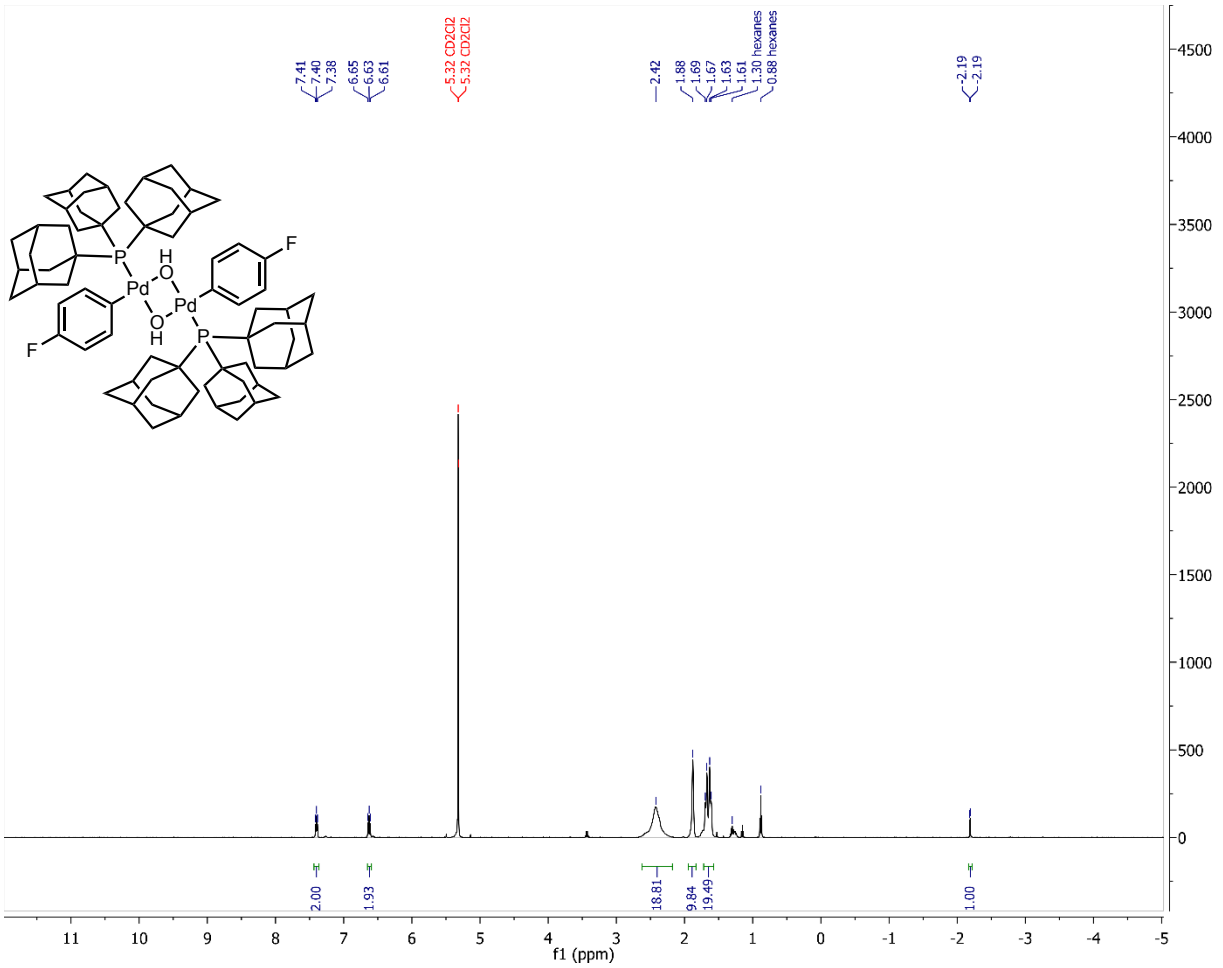

Figure S4. ^{1}H NMR spectrum (CD_2Cl_2, 500 MHz) of **32**.

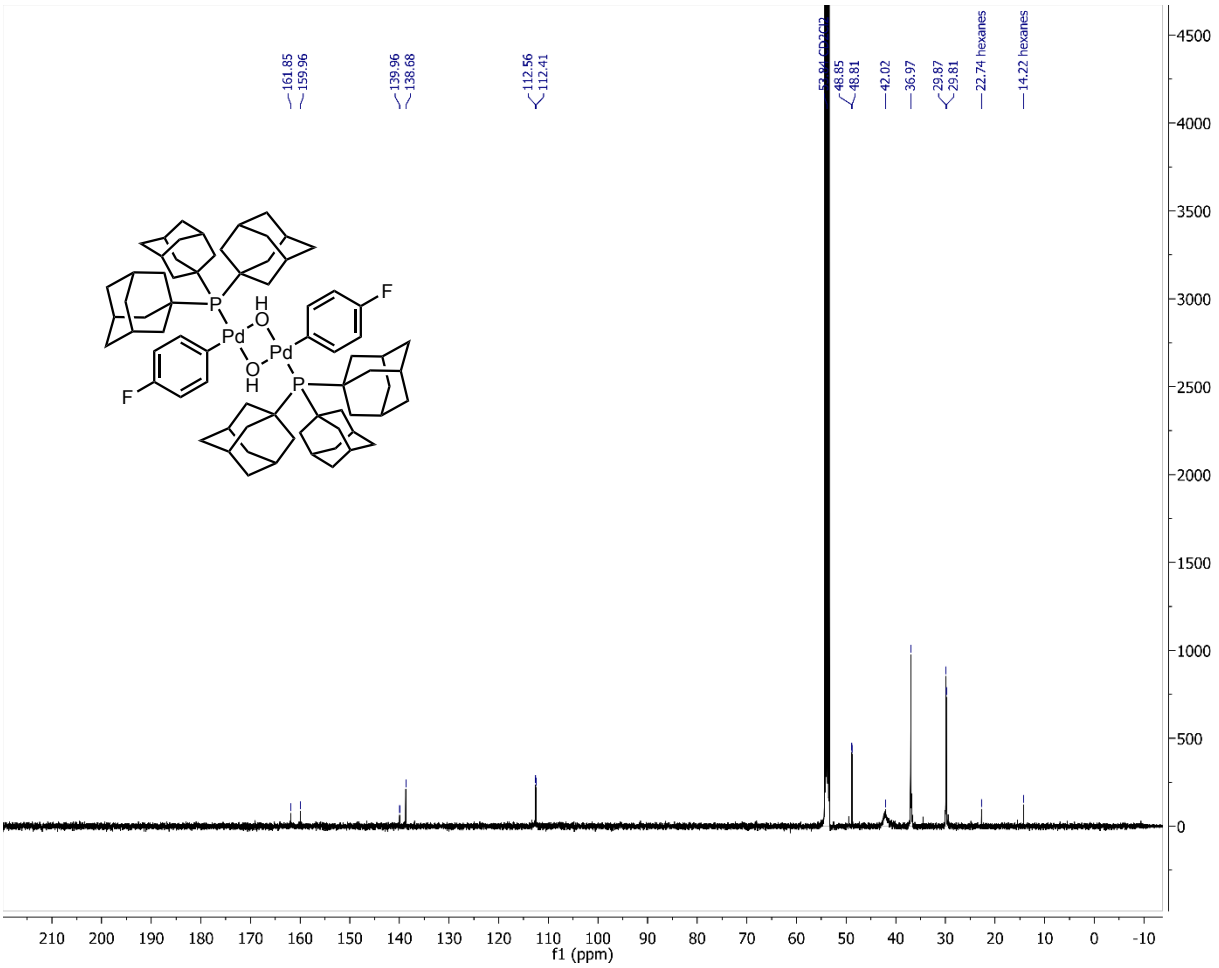

Figure S5. ^{13}C NMR spectrum (CD_2Cl_2, 126 MHz) of **32**.

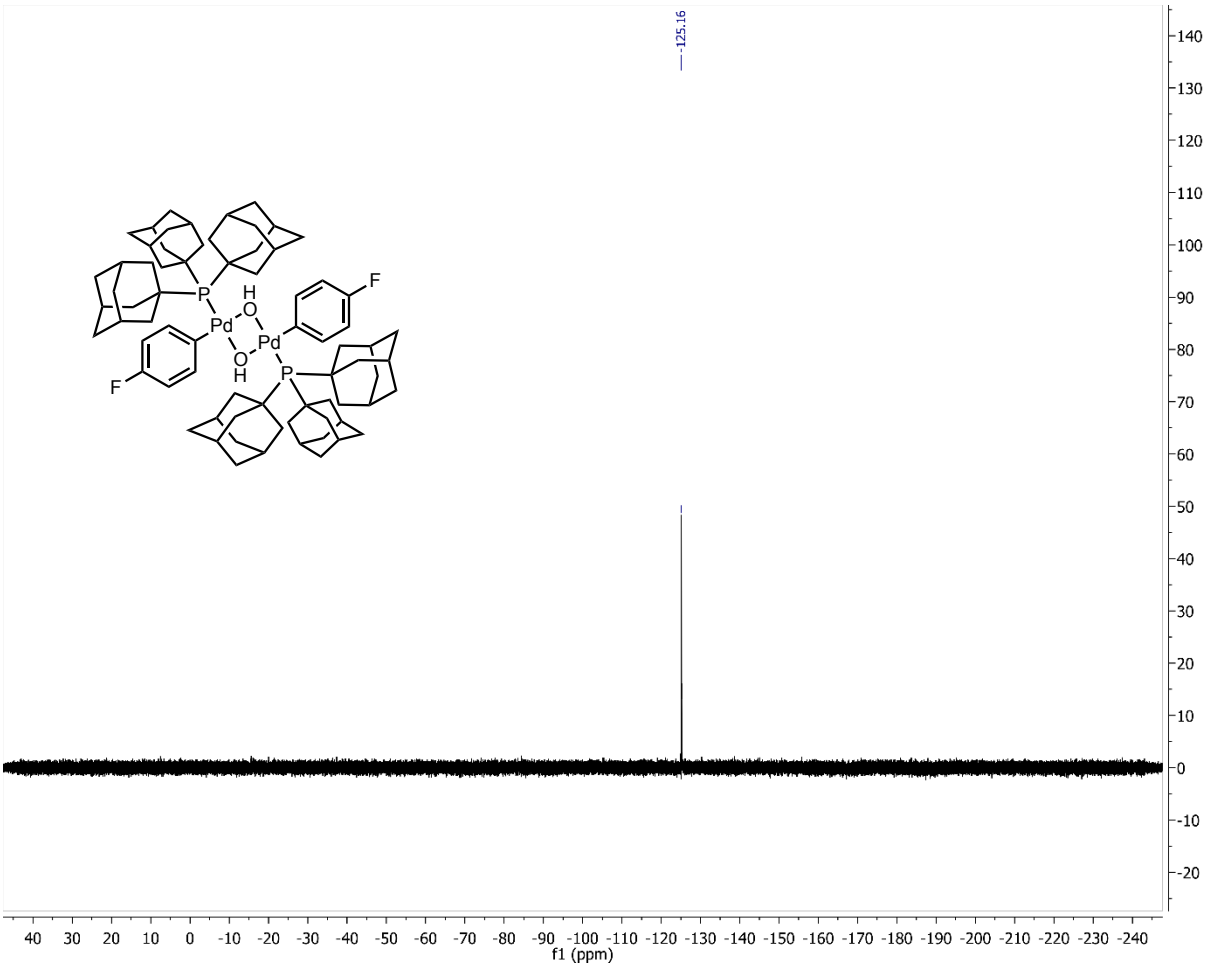

Figure S6. ^{19}F NMR spectrum (CD_2Cl_2, 470 MHz) of **32**.

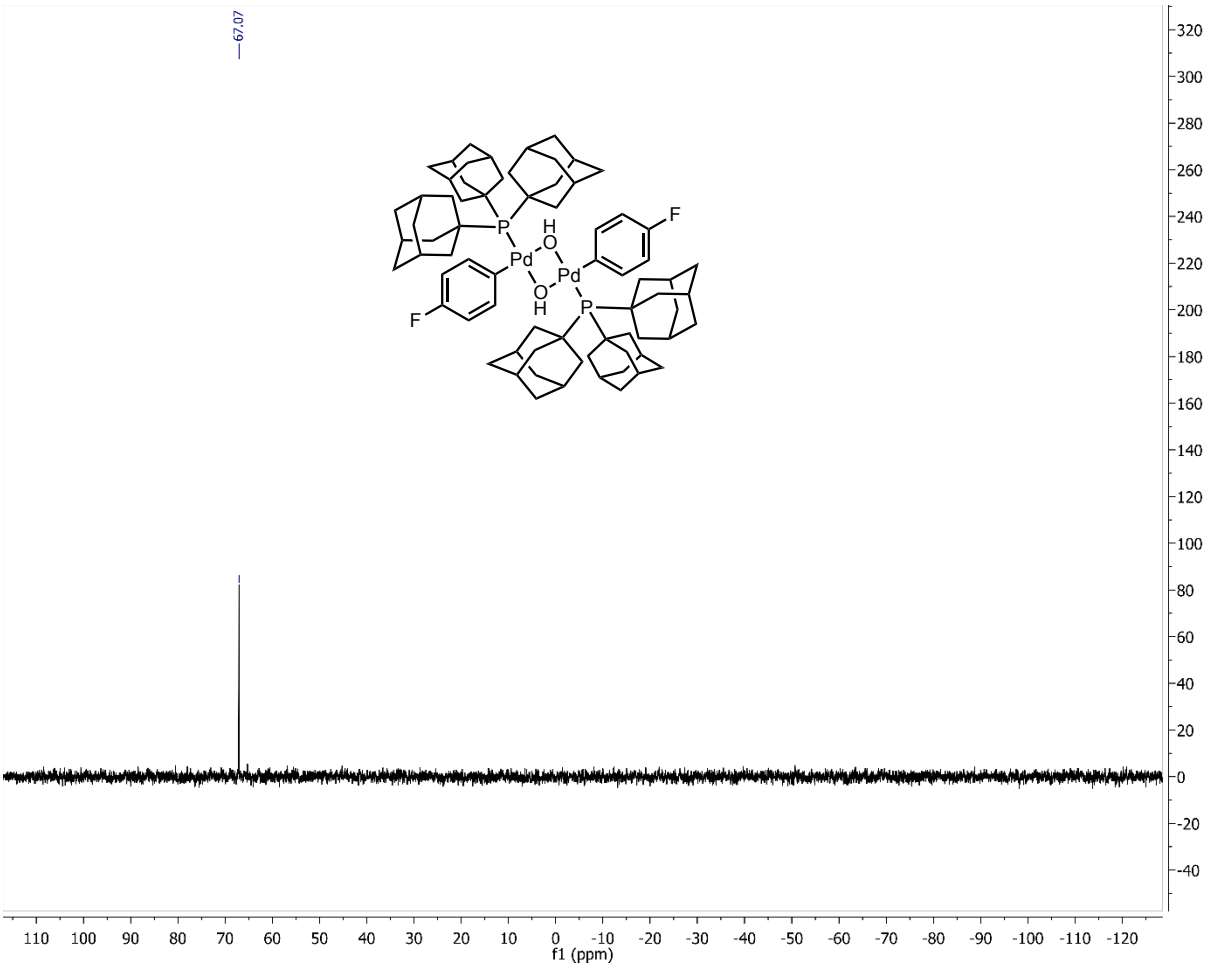

Figure S7. $^{31}P\{^{1}H\}$ NMR spectrum (CD_2Cl_2, 202 MHz) of **32**.

Kinetic and Mechanistic Experiments:

Independent route to 32 under catalytically-relevant conditions. A solution of $Pd(PAd_3)(4\text{-}C_6H_4F)Br$ (**1**) (1.8 mg, 2.5 μmol) in toluene (1.0 mL) was transferred to an NMR tube capped with a rubber septum. Triethylamine (50 μL, 359 μmol, 143 equiv) and water (1.0 mL) were injected and the reaction mixture was shaken gently for 1 min at room temperature. A $^{31}P\{^1H\}$ spectrum of the resulting solution indicated complete consumption of **1**, and **32** was cleanly formed. Analogous reactions that omitted water or triethylamine showed no conversion of **1**.

$^{31}P\{^1H\}$ NMR (202 MHz, toluene) δ 66.9.

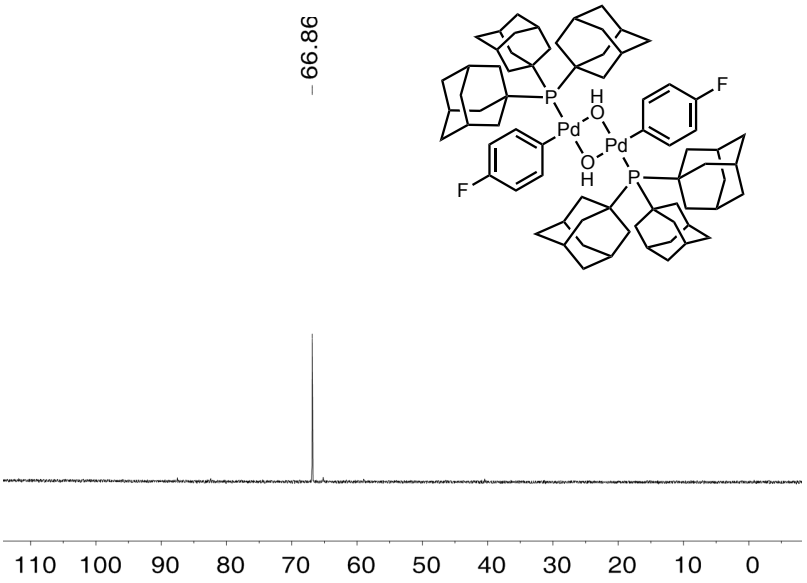

Figure S8. $^{31}P\{^1H\}$ NMR spectrum (202 MHz, toluene) of reaction of 1 with Et_3N and water in toluene after 1 min at RT.

Independent route to 32 from an independently prepared cationic aryl-Pd complex:

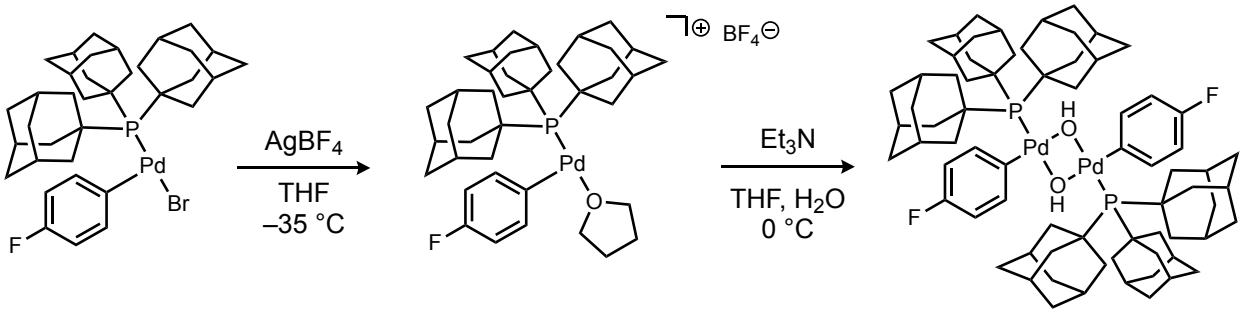

33 **32**

Generation of $[Pd(PAd_3)(4\text{-}FC_6H_4)]^+$ BF_4^- (33). The generation of **33** was adapted from a published procedure.[3] $Pd(PAd_3)(p\text{-}FC_6H_4)Br$ **1** (9.0 mg, 12.5 μmol) was dissolved in THF (2.5 mL). Separately, $AgBF_4$ (20 mg, 0.10 mmol) was dissolved in THF (2 mL). Both solutions were chilled at -35 °C (MeOH/H_2O dry ice bath). The latter solution ($AgBF_4$, 2.5 μmol, 50 μL) was then added to an aliquot of the solution of **1** (2.5 μmol, 0.5 mL) in a 4 mL vial at -35 °C. The mixture (0.55 mL) was quickly shaken, left in the cooling bath for 10 min, and transferred under nitrogen into an NMR tube capped with a rubber septum. Generation of **33** was confirmed by $^{31}P\{^1H\}$ spectrum at -25 °C before proceeding to the next step.

Generation of 32 from 33. Triethylamine (10 μL, 72 μmol, 29 equiv) and water (68 μL) were injected into the solution of **32** and the resulting mixture was shaken gently for 1 min at 0 °C. A $^{31}P\{^1H\}$ spectrum was acquired at 0 °C, which showed full conversion of **33** and clean formation of **32**.

$^{31}P\{^1H\}$ NMR (202 MHz, THF, 0 °C) δ 66.2.

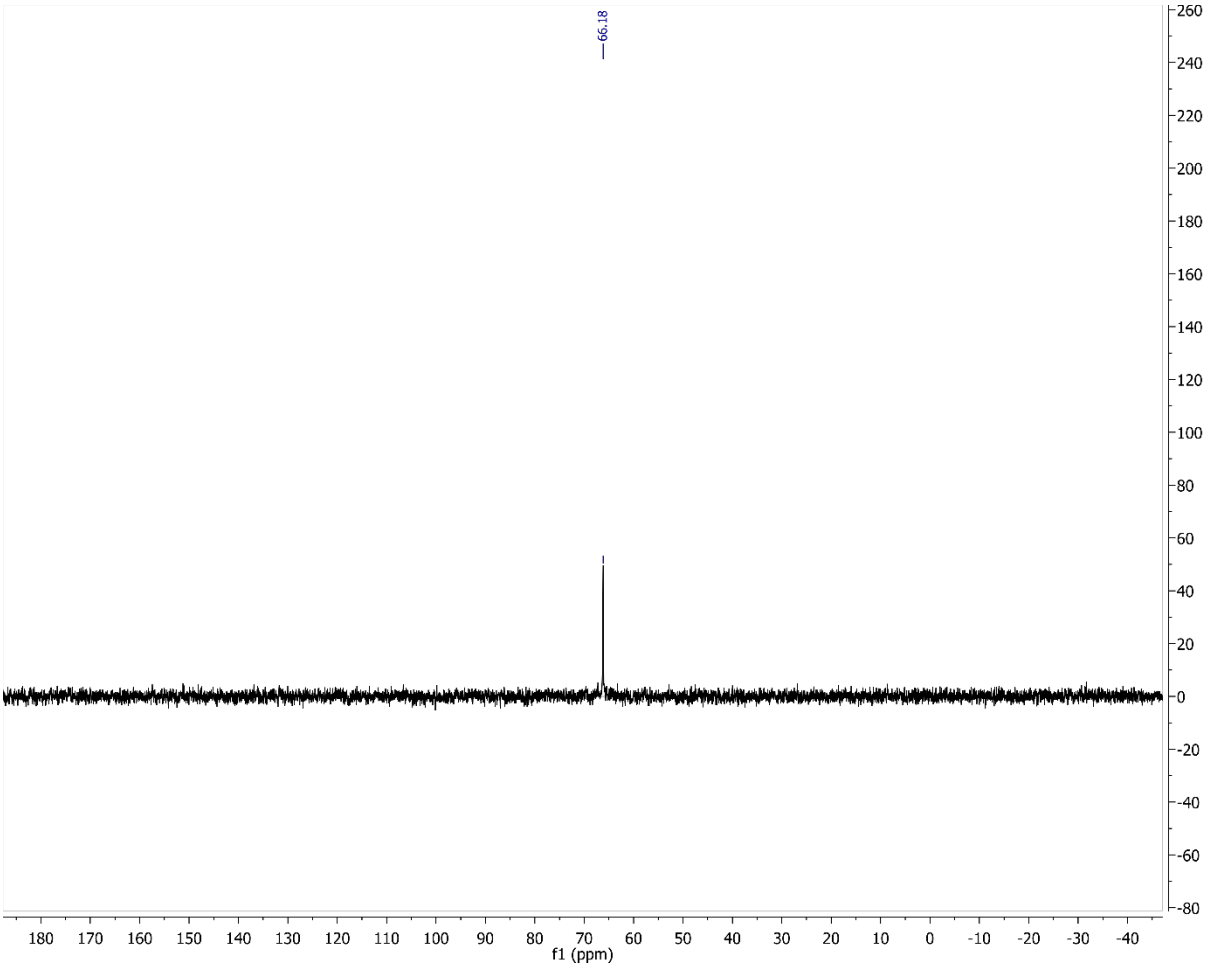

Figure S9. $^{31}P\{^{1}H\}$ NMR spectrum (202 MHz, THF, 0 °C) of the reaction of **33** with Et_3N and H_2O in THF.

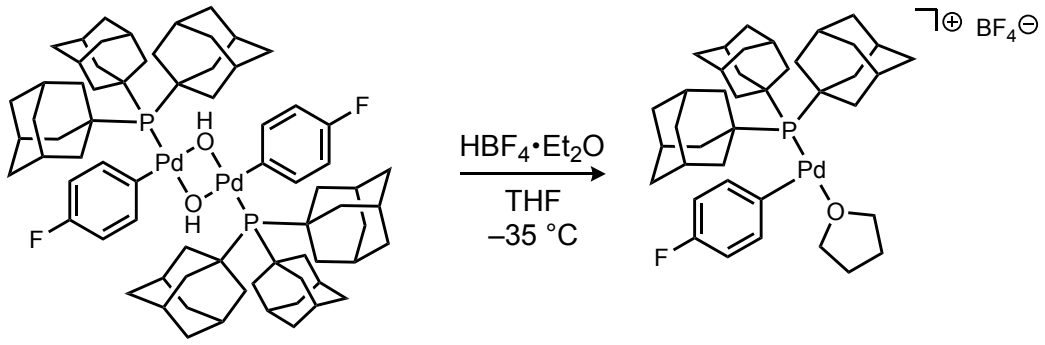

32 **33**

Conversion of 32 to 33. A solution of **32** (1.8 mg, 1.34 μmol) in THF-*d*$_8$ (0.5 mL) was transferred to an NMR tube capped with a rubber septum. Tetrafluoroboric acid diethyl ether complex (0.5 μL, 3.7 μmol, 1.3 equiv to Pd) was injected and the reaction mixture was shaken gently for 1 min at -35 °C. ^{1}H, ^{19}F, and ^{31}P{^{1}H} NMR spectra acquired at -25 °C, which indicated full conversion of **32** and clean formation of **33**.[3]

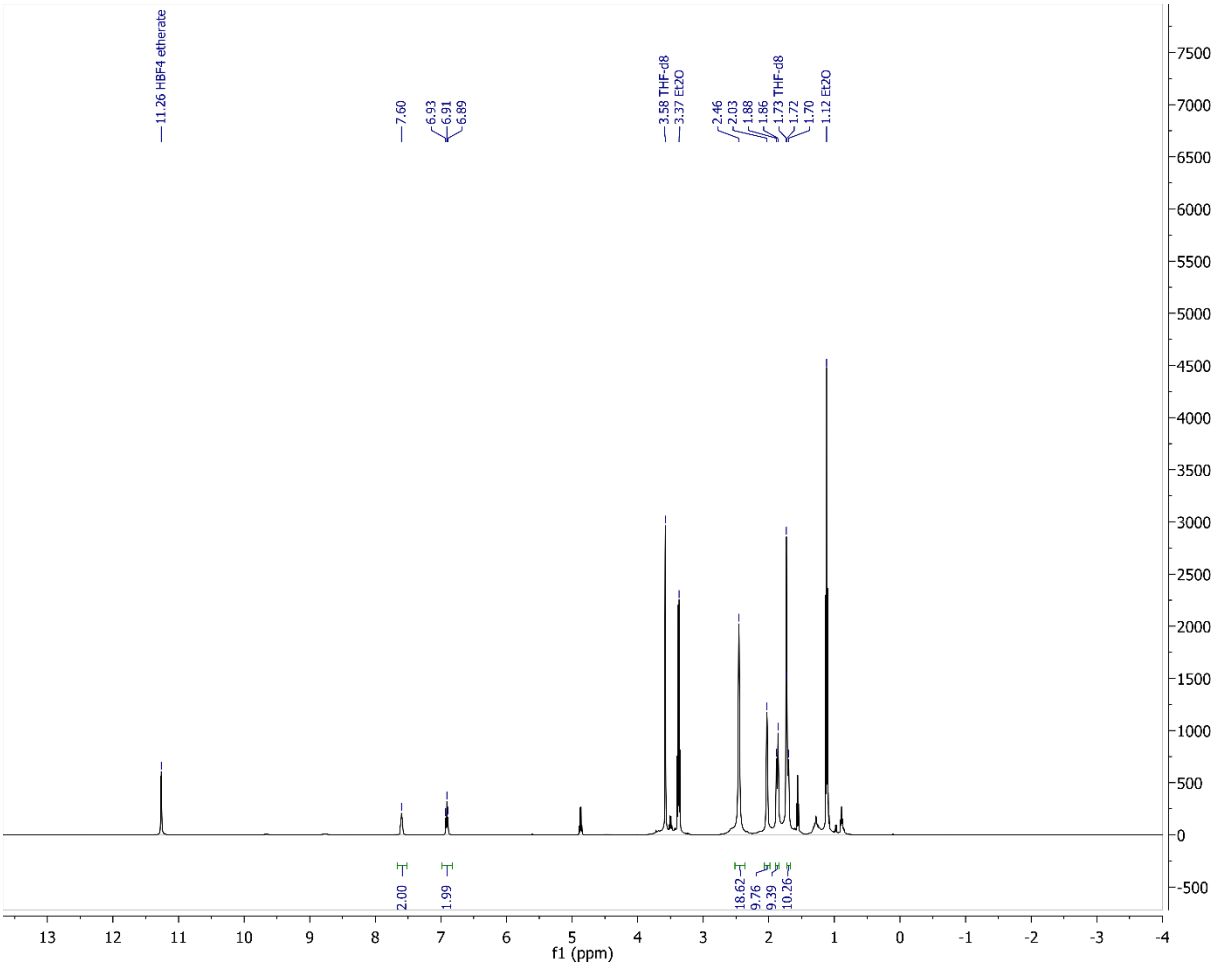

Figure S10. ^{1}H NMR spectrum (500 MHz, THF-d_8) of the mixture generated by reaction of **32** with $HBF_4{\cdot}Et_2O$ in THF at –35 °C.

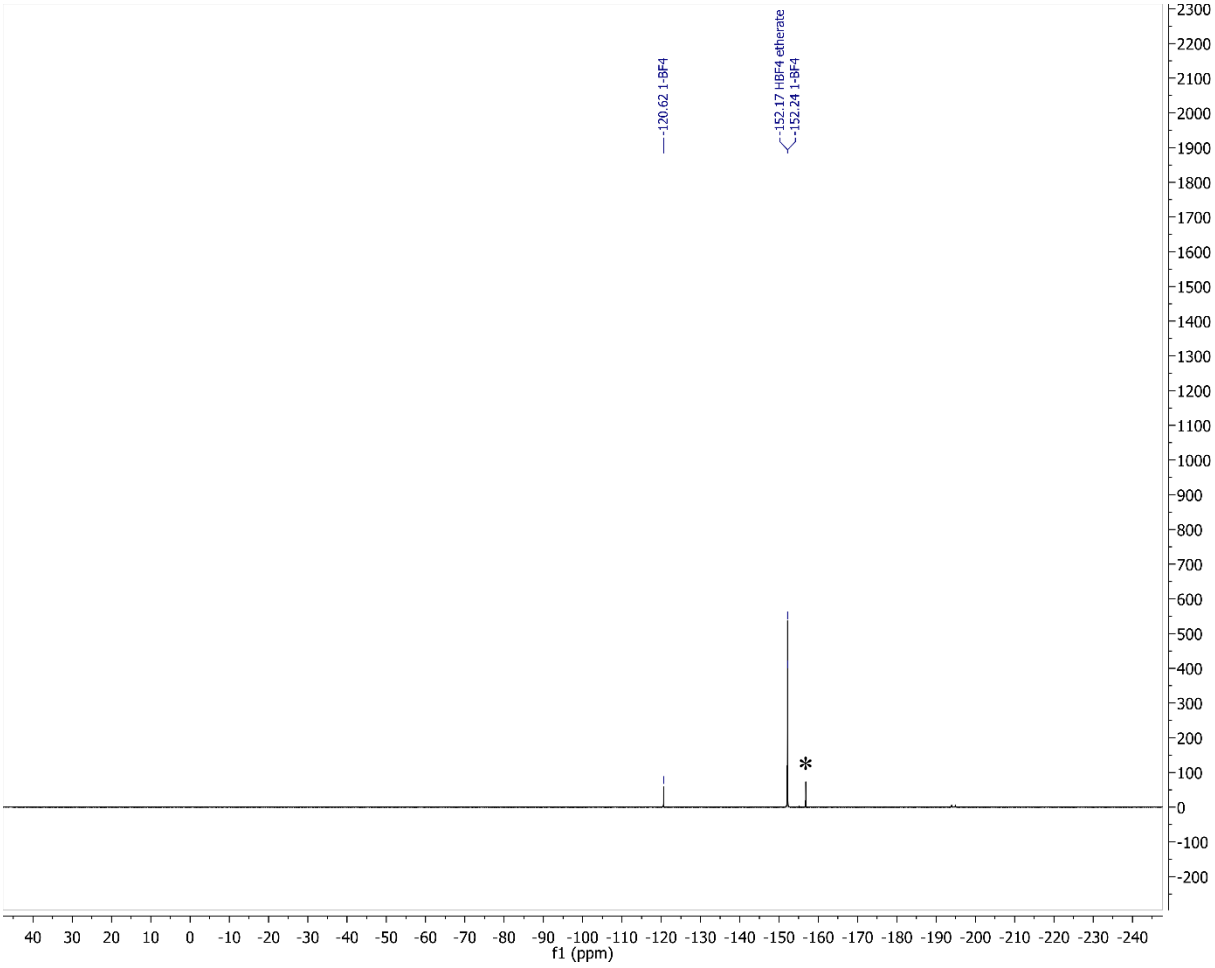

Figure S11. ^{19}F NMR spectrum (470 MHz, THF-d_8) of the mixture generated by reaction of **32** with $HBF_4{\cdot}Et_2O$ in THF at –35 °C (* = unidentified).

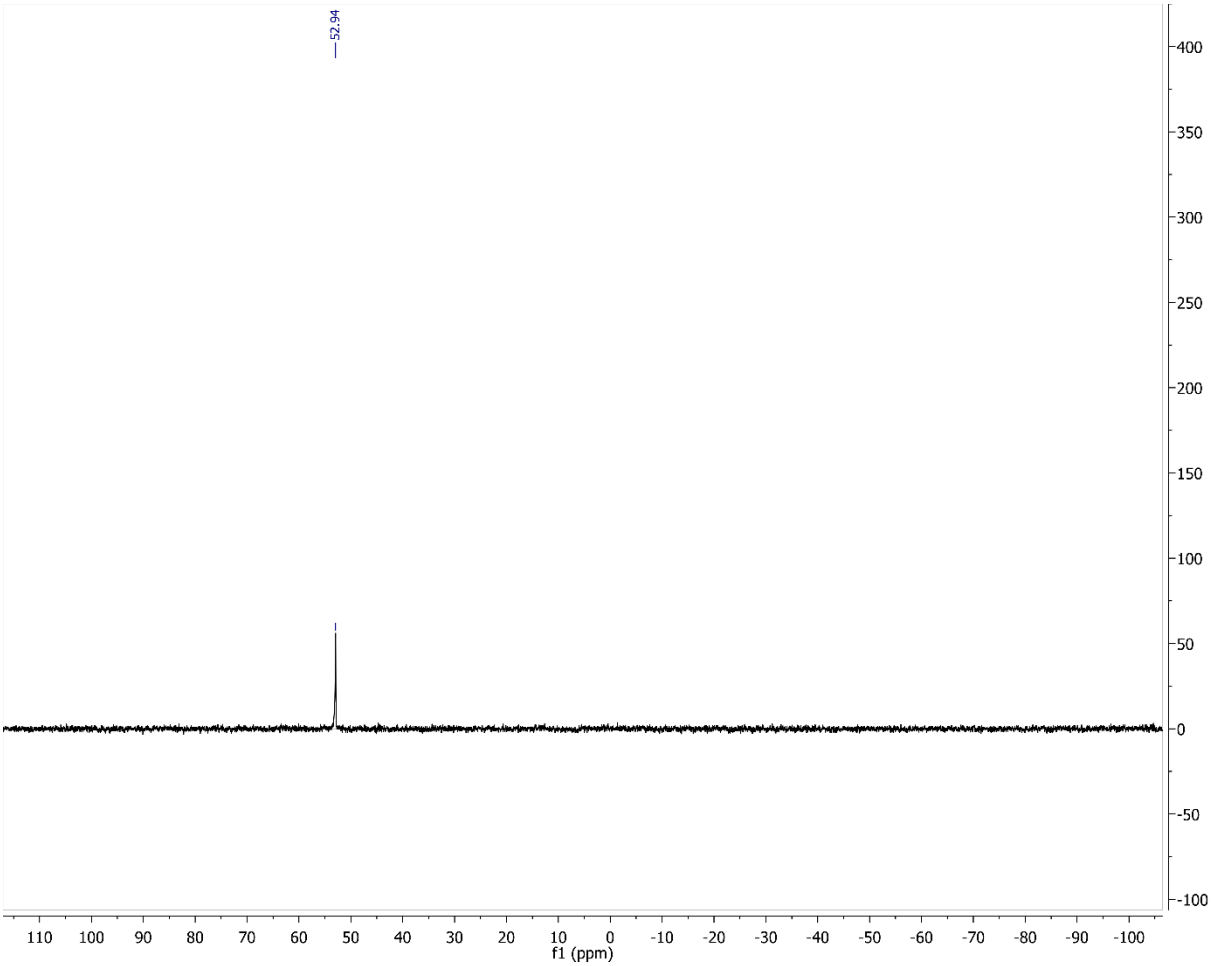

Figure S12. $^{31}P\{^{1}H\}$ NMR spectrum (202 MHz, THF-d_8) of the mixture generated by reaction of **32** with $HBF_4{\cdot}Et_2O$ in THF at –35 °C .

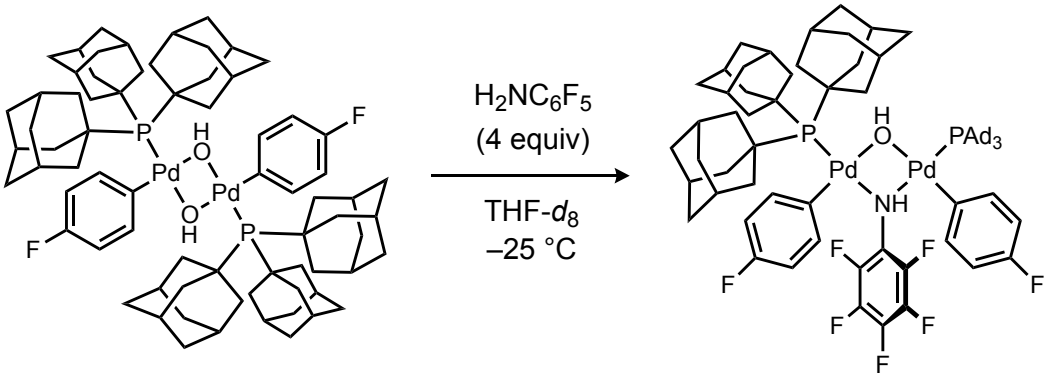

32 **34**

Synthesis and characterization of catalyst resting state, *syn*-[Pd$_2$(PAd$_3$)$_2$(4-C$_6$H$_4$F)$_2$(μ-OH)(μ-NH$_2$C$_6$F$_5$)] (34). A solution of **32** (4.9 mg, 3.8 μmol) in THF-*d*$_8$ (0.5 mL) was transferred to an NMR tube under nitrogen and capped with a rubber septum. Separately, pentafluoroaniline (2.8 mg, 15 μmol, 4 equiv) was dissolved in THF-*d*$_8$ (0.1 mL) in a 4 mL vial, and the resulting solution was added to the solution of **32** via a 1 mL syringe at low temperature (acetone/dry ice bath). The NMR tube was then shaken gently for 1 min. ^{1}H, ^{19}F, and ^{31}P{^{1}H} NMR spectra acquired at –25 °C indicated full conversion of **32** and clean formation of **34**. An EXSY NMR analysis indicated exchange between free $C_6F_5NH_2$ and the μ-anilido ligand in **34** during NMR time scale suggesting formation of **34** can occur reversibly.

^{1}H NMR (500 MHz, THF-*d*$_8$) δ 7.33 (t, *J* = 7.2 Hz, 2H), 6.51 (td, *J* = 8.9, 3.1 Hz, 2H), 6.46 (t, *J* = 7.6 Hz, 2H), 6.20 (td, *J* = 8.7, 3.1 Hz, 2H), 2.74 (s, 2H), 2.70 – 2.53 (m, 36H), 2.46 – 2.27 (m, 18H), 2.03 – 1.58 (m, 36H, partly obscured by THF residual peak), -3.84 (s, 1H).

^{19}F NMR (470 MHz, THF-*d*$_8$) δ -125.09 (2F), -147.73 (1F), -158.18 (1F), -170.71 (1F), -171.42 (1F), -176.06 (1F).

^{31}P{^{1}H} NMR (202 MHz, THF-*d*$_8$) δ 58.8.

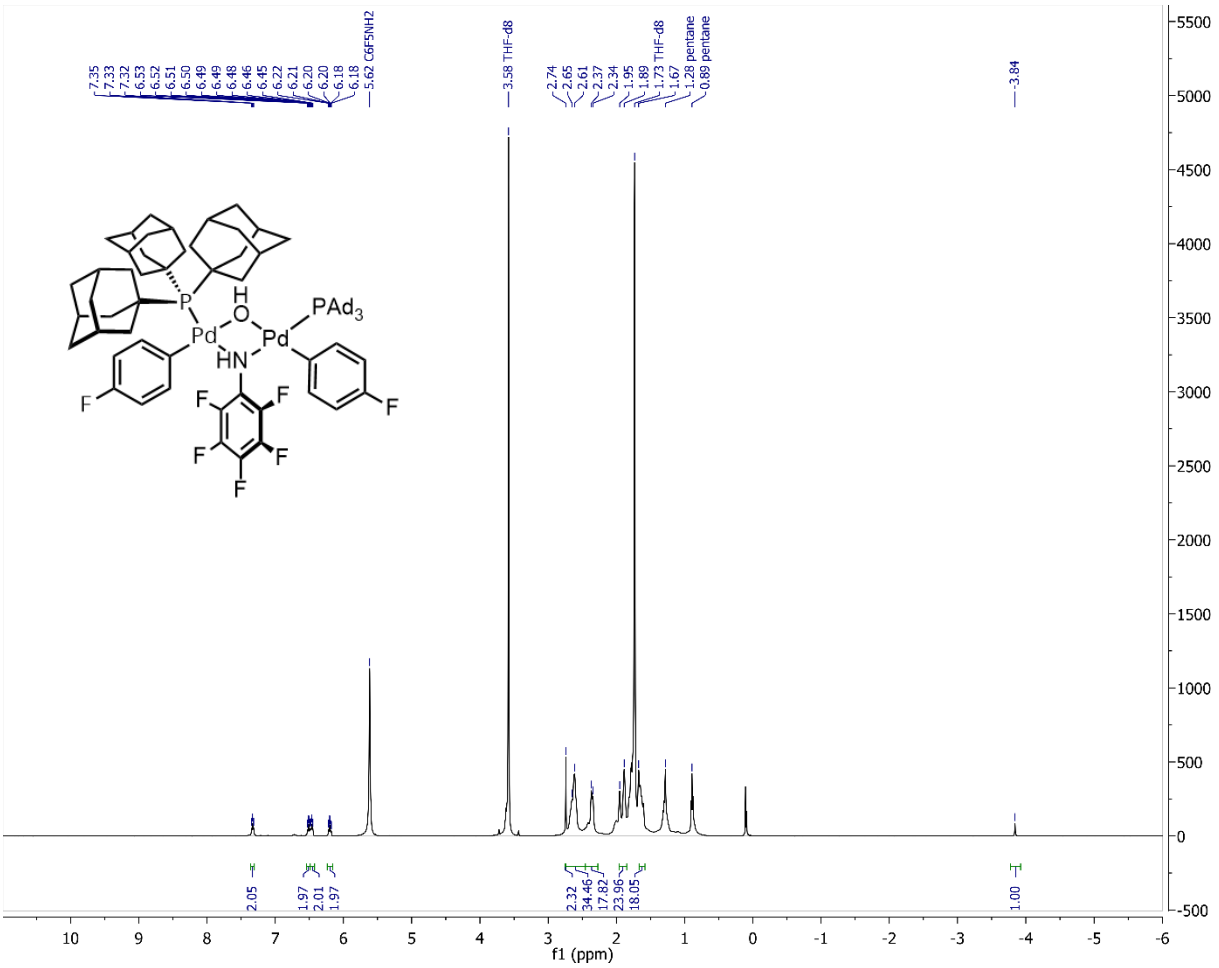

Figure S13. ^{1}H NMR spectrum (500 MHz, THF-d_8) of **34**.

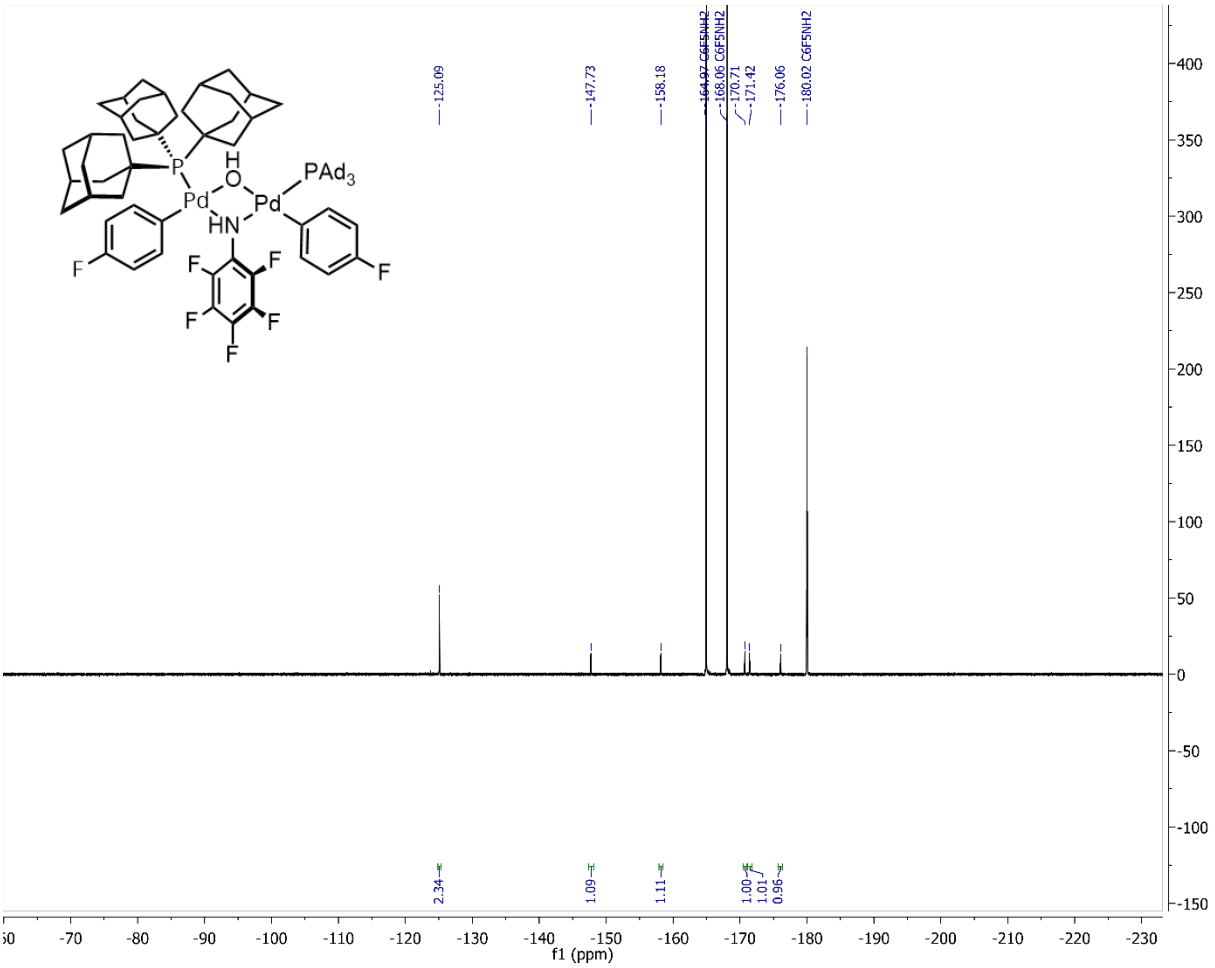

Figure S14. ^{19}F NMR spectrum (470 MHz, THF-d_8) of **34**.

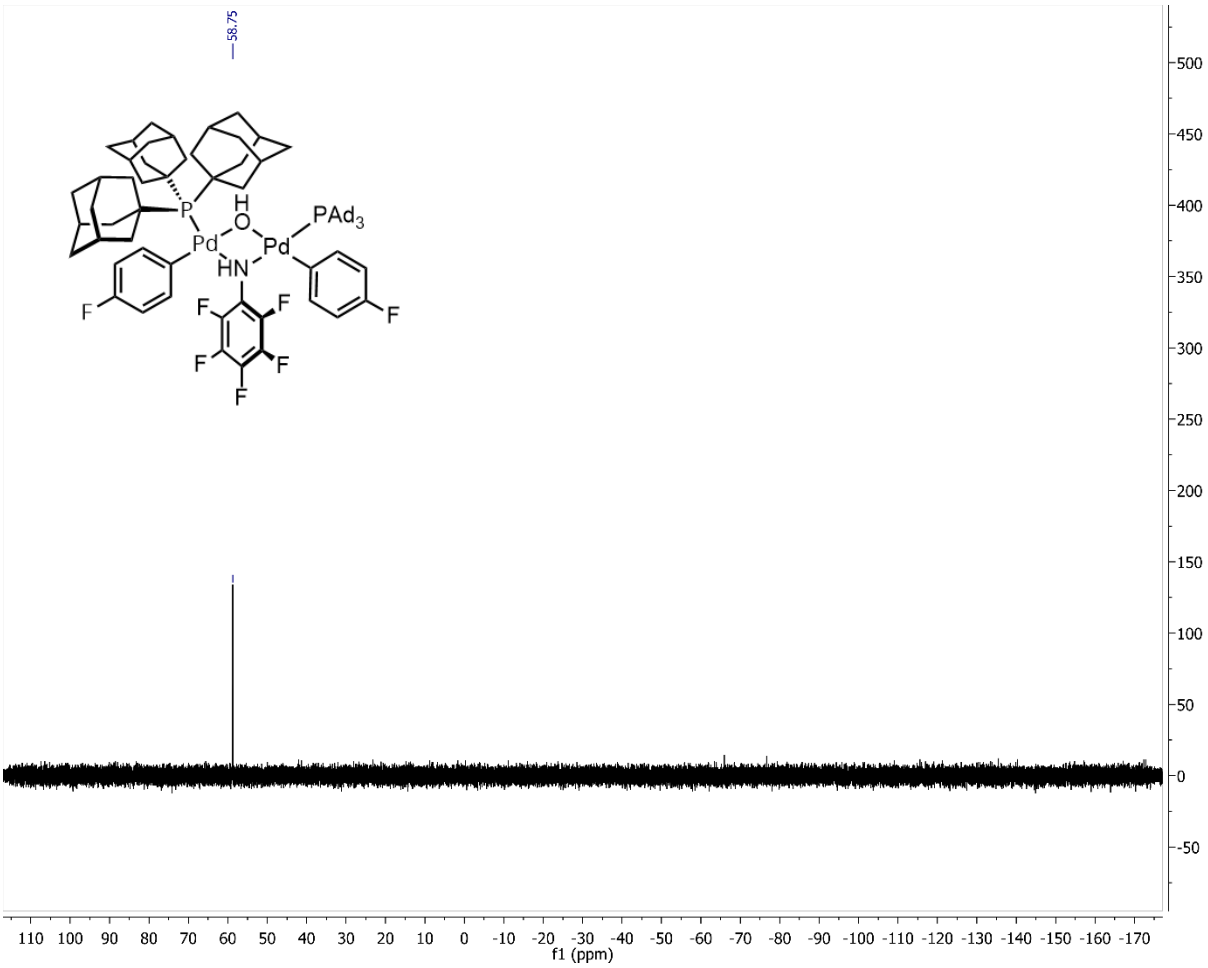

Figure S15. $^{31}P\{^{1}H\}$ NMR spectrum (202 MHz, THF-d_8) of **34**.

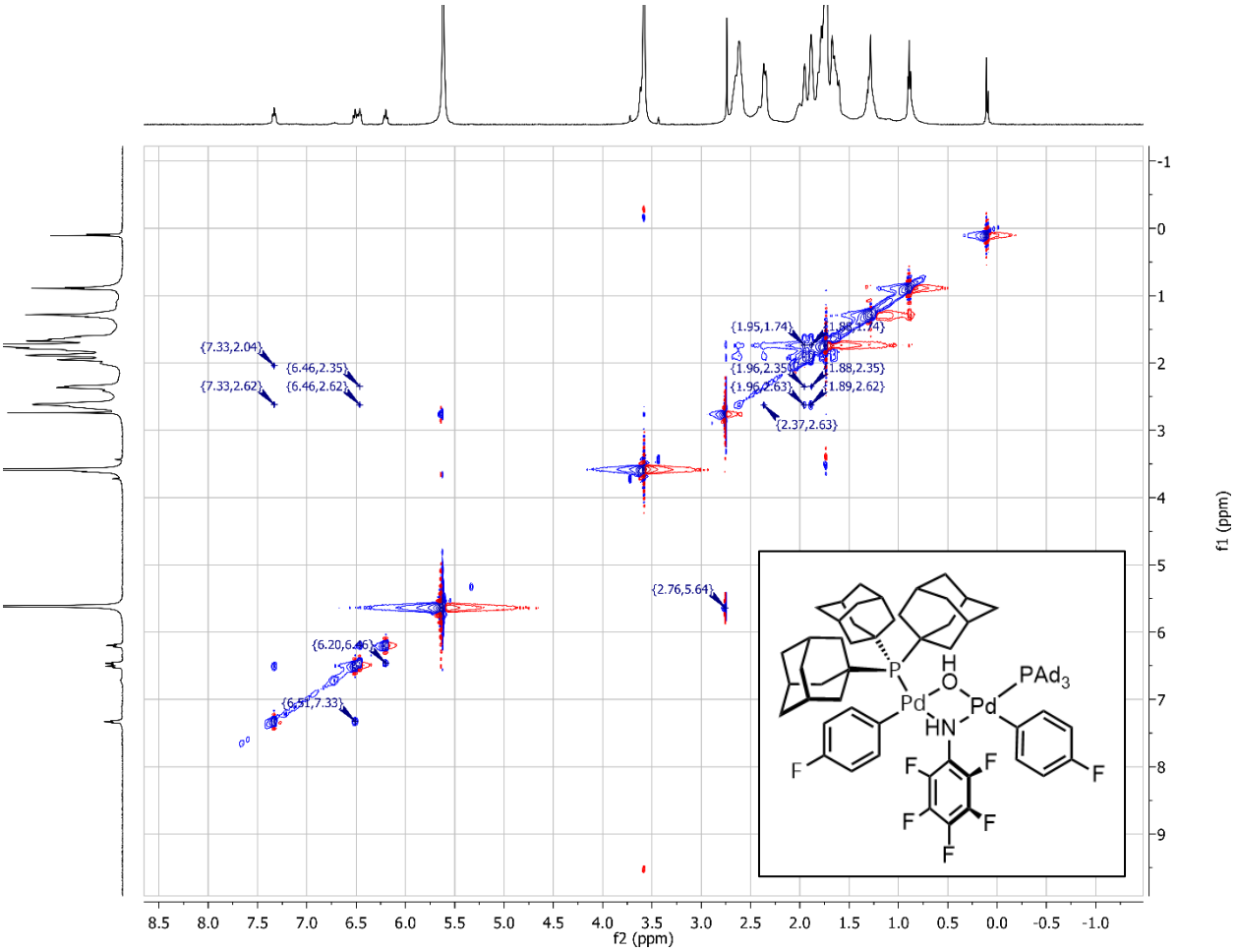

Figure S16. ^{1}H-^{1}H NOESY/EXSY NMR spectrum (500 MHz, THF-d_8) of **34**.

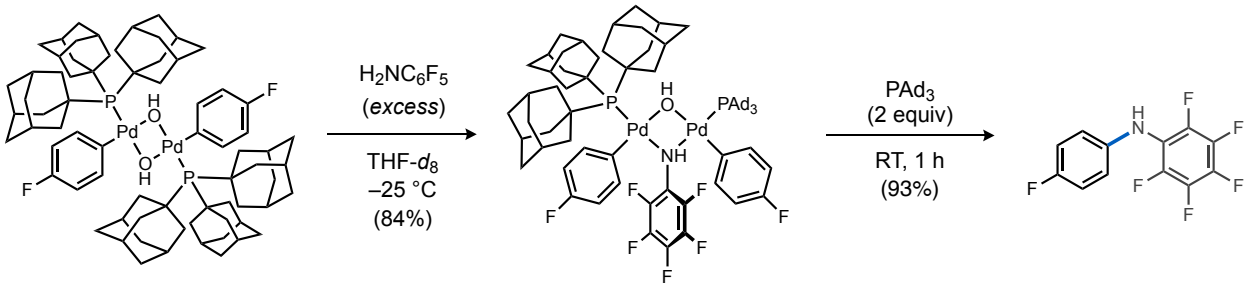

32 **34** **4**

Stoichiometric C–N bond formation from resting state complex 34. In a glove box, **32** (3.3 mg, 2.5 μmol) and octafluorotoluene (internal standard, 15 μL, 106 μmol) were dissolved in THF (0.5 mL) in a 4 mL vial. The resulting solution was transferred into an NMR tube capped with a rubber septum. Separately, pentafluoroaniline (10 mg, 55 μmol) was dissolved in THF (1 mL) in a 4 mL vial, and the resulting solution (0.1 mL, 5.5 μmol) was drawn into a 1 mL syringe. A solution of PAd_3 (4.4 mg, 10 μmol) in THF (0.2 mL) was drawn into another 1 mL syringe. The syringe needles were sealed by insertion into a rubber septum to prevent exposure to air. Both the NMR tube and syringes were taken out of the box, and the $C_6F_5NH_2$ solution was then injected into the NMR tube cooled in an acetone/dry ice bath. The NMR tube was shaken gently for 1 min after the addition. ^{19}F and $^{31}P\{^1H\}$ NMR spectra acquired at –25 °C, which confirmed full conversion of **32** and formation of **34** (84%). Next, the PAd_3 solution (to stabilize $(Ad_3P)Pd^0$) was injected into the NMR tube at -78 °C, and the mixture was warmed up to room temperature. ^{19}F and $^{31}P\{^1H\}$ NMR spectra acquired after 1 h, which indicated full conversion of **34** and formation of **4** in 93% yield.

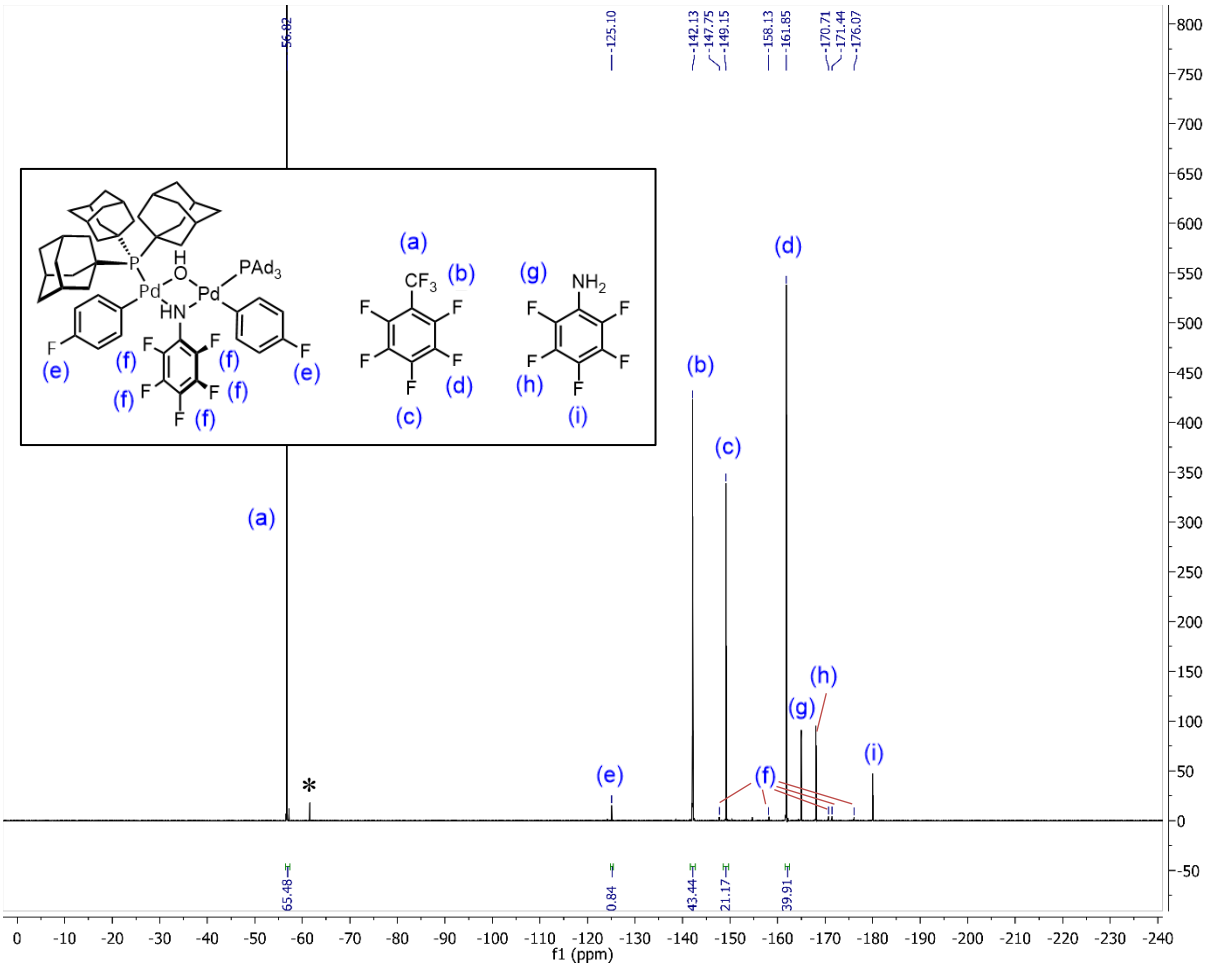

Figure S17. ^{19}F NMR spectrum (470 MHz, THF) of **34** generated in presence of internal standard (* = unidentified).

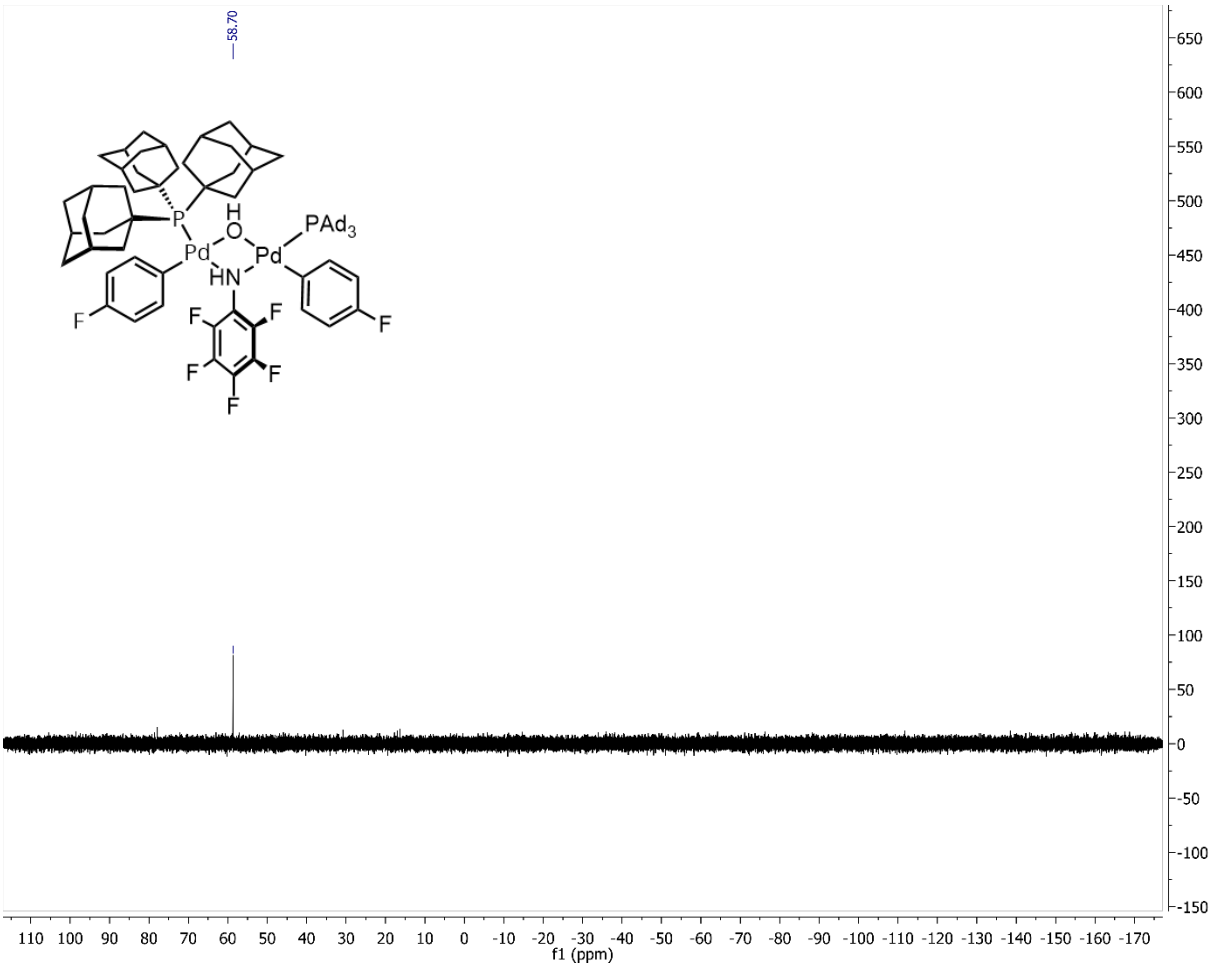

Figure S18. $^{31}P\{^{1}H\}$ NMR spectrum (202 MHz, THF) of **34** generated in presence of internal standard.

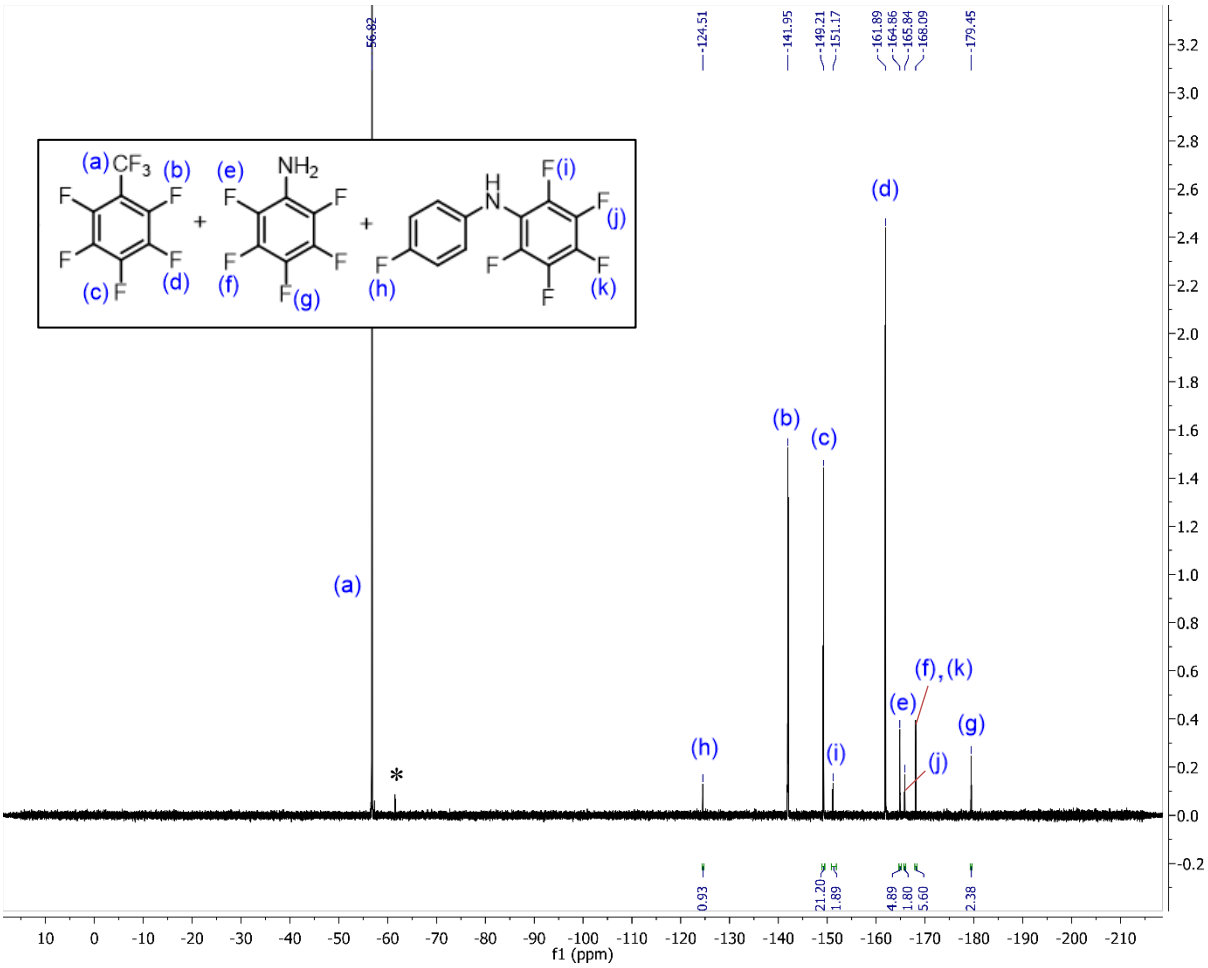

Figure S19. ^{19}F NMR spectrum (470 MHz, THF) of **4** generated upon warming a solution of **34** (* = unidentified).

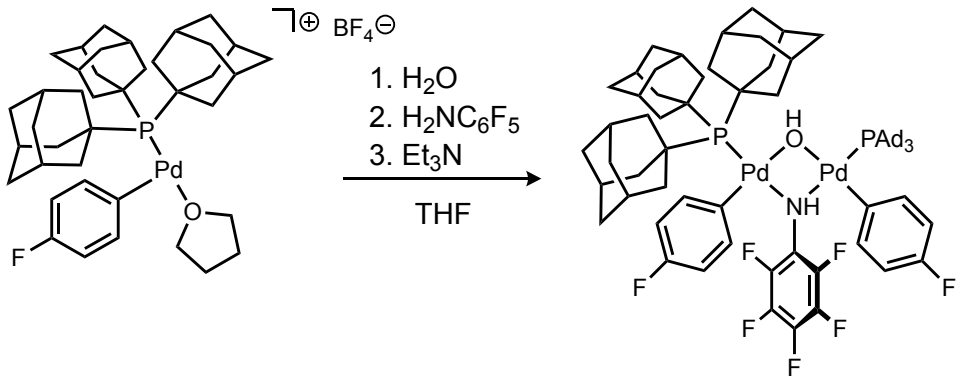

33 **34**

Independent synthesis of 34 from 33 in the presence of H_2O. The generation of $[Pd(PAd_3)(4\text{-}FC_6H_4)]^+$ BF_4^- (**33**) was adapted from a known procedure.[3] $Pd(PAd_3)(4\text{-}FC_6H_4)Br$ (9.0 mg, 12.5 μmol) was dissolved in THF (2.5 mL). Separately, $AgBF_4$ (20 mg, 0.10 mmol) was dissolved in THF (2 mL). Both solutions were chilled at -35 °C ($MeOH/H_2O$ dry ice bath). The latter solution ($AgBF_4$, 2.5 μmol, 50 μL) was then added to the solution of **1** (2.5 μmol, 0.5 mL) in a 4 mL vial at -35 °C. The mixture (0.55 mL) was quickly shaken, left in the cooling bath for 10 min, and transferred into an NMR tube capped with a rubber septum. Next, degassed deionized water (14 μL, 0.75 mmol, 300 equiv), pentafluoroaniline (0.1 mL from a 15 mM stock solution in THF, 15 μmol, 6 equiv), and triethylamine (5 μL, 38 μmol, 15 equiv) were injected into the NMR tube sequentially at -78 °C. The reaction mixture was shaken gently for 1 min, then a $^{31}P\{^1H\}$ NMR spectrum was acquired at -25 °C, which indicated clean formation of **34**.

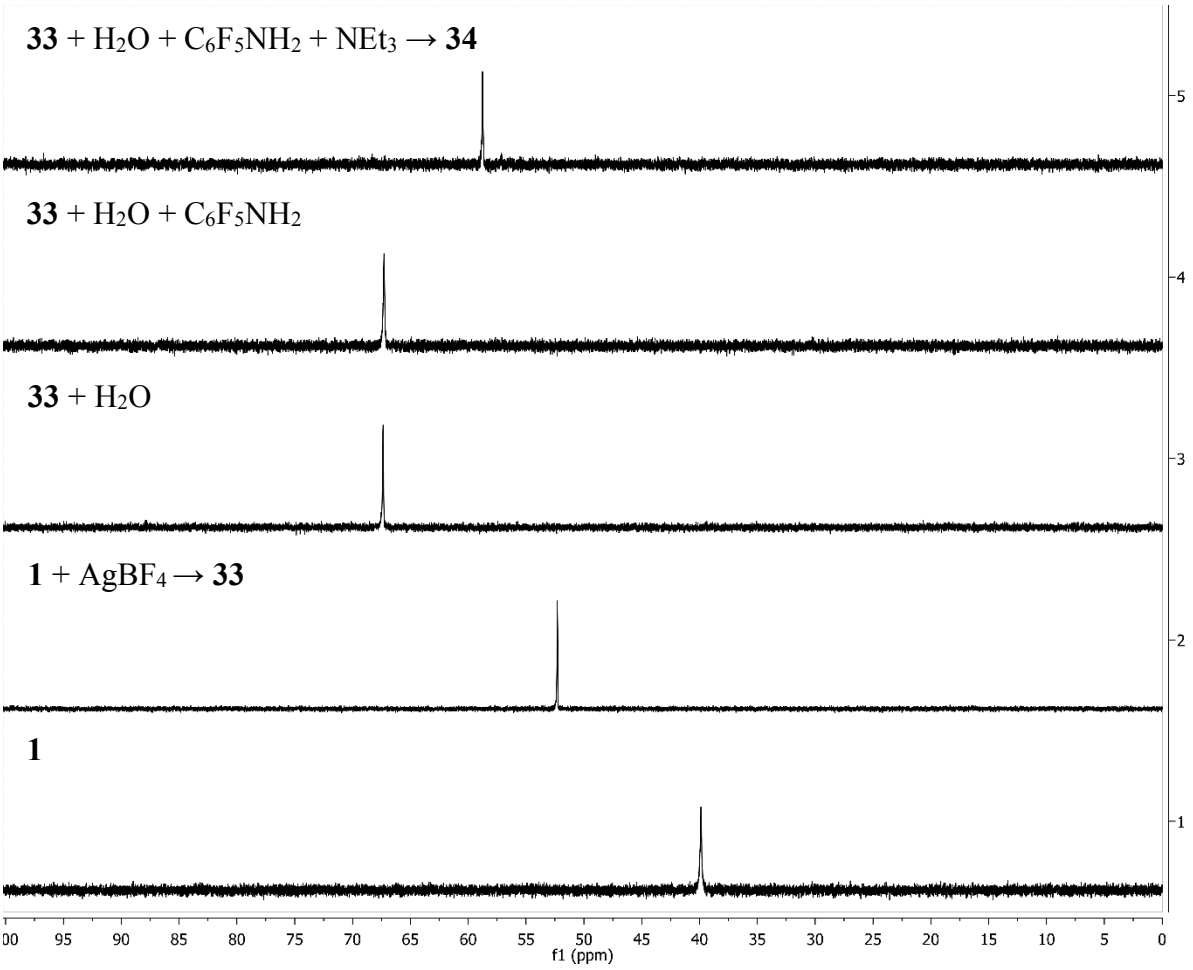

Figure S20. Stacked $^{31}P\{^{1}H\}$ NMR spectra (202 MHz, THF) for generation of **34** from **1** (via **33**) by sequential addition of (top to bottom) $AgBF_4$, water, pentafluoroaniline, then Et_3N.

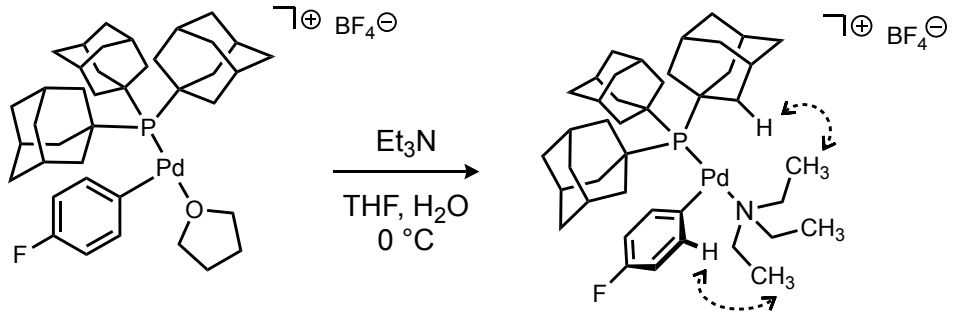

Synthesis and characterization of [Pd(PAd$_3$)(4-FC$_6$H$_4$)(NEt$_3$)]$^+$ BF$_4^-$ (35). The generation of [Pd(PAd$_3$)(4-FC$_6$H$_4$)]$^+$ BF$_4^-$ (**33**) was adapted from a known procedure.[3] Pd(PAd$_3$)(4-FC$_6$H$_4$)Br (5.4 mg, 7.5 μmol) was dissolved in THF-*d*$_8$ (1.5 mL). Separately, AgBF$_4$ (9.8 mg, 50 μmol) was dissolved in THF-*d*$_8$ (1 mL). Both solutions were chilled at -35 °C (MeOH/H$_2$O dry ice bath). The latter solution (AgBF$_4$, 2.5 μmol, 50 μL) was then added to the solution of **1** (2.5 μmol, 0.5 mL) in a 4 mL vial at -35 °C. Octafluorotoluene (internal standard, 0.3 μL, 1.9 μmol) was added to the solution. The mixture (0.55 mL) was quickly shaken, left in the cooling bath for 10 min, and transferred into an NMR tube capped with a rubber septum. ^{1}H, ^{19}F, and ^{31}P{^{1}H} NMR spectra were acquired at -25 °C to confirm clean formation of **33** prior to proceeding to the next step. Next, triethylamine (5.0 μL, 38 μmol, 15 equiv) was injected and the reaction mixture was shaken gently for 1 min at -35 °C. ^{1}H, ^{19}F, and ^{31}P{^{1}H} NMR spectra were acquired at -25 °C, which indicated formation of a new complex (**35**) in 74% yield along with an unidentified side product (19%). Analysis by EXSY NMR indicated exchange between free and Pd-bound NEt$_3$ on the NMR time scale; signals corresponding to the 4-fluorophenyl group on **35** and the unidentified side product supports an equilibrium process involving the two compounds. NOE correlations (dashed lines) between the 4-fluorophenyl on Pd and coordinated Et$_3$N, and also between PAd$_3$ resonances and coordinated Et$_3$N, support the structure assignment of **35** shown above.

^{1}H NMR (500 MHz, THF-*d*$_8$) δ 7.55 – 7.49 (m, 2H), 6.96 (t, *J* = 8.7 Hz, 2H), 2.47 (6H, obscured by NEt$_3$ peak), 2.43 (18H, obscured by NEt$_3$ peak), 2.07 (br, 9H), 1.87 – 1.69 (m, 18H, obscured by THF peak), 1.51 (br, 9H).

^{19}F NMR (470 MHz, THF-*d*$_8$) δ 120.5, 153.8

^{31}P{^{1}H} NMR (202 MHz, THF-*d*$_8$) δ 41.5.

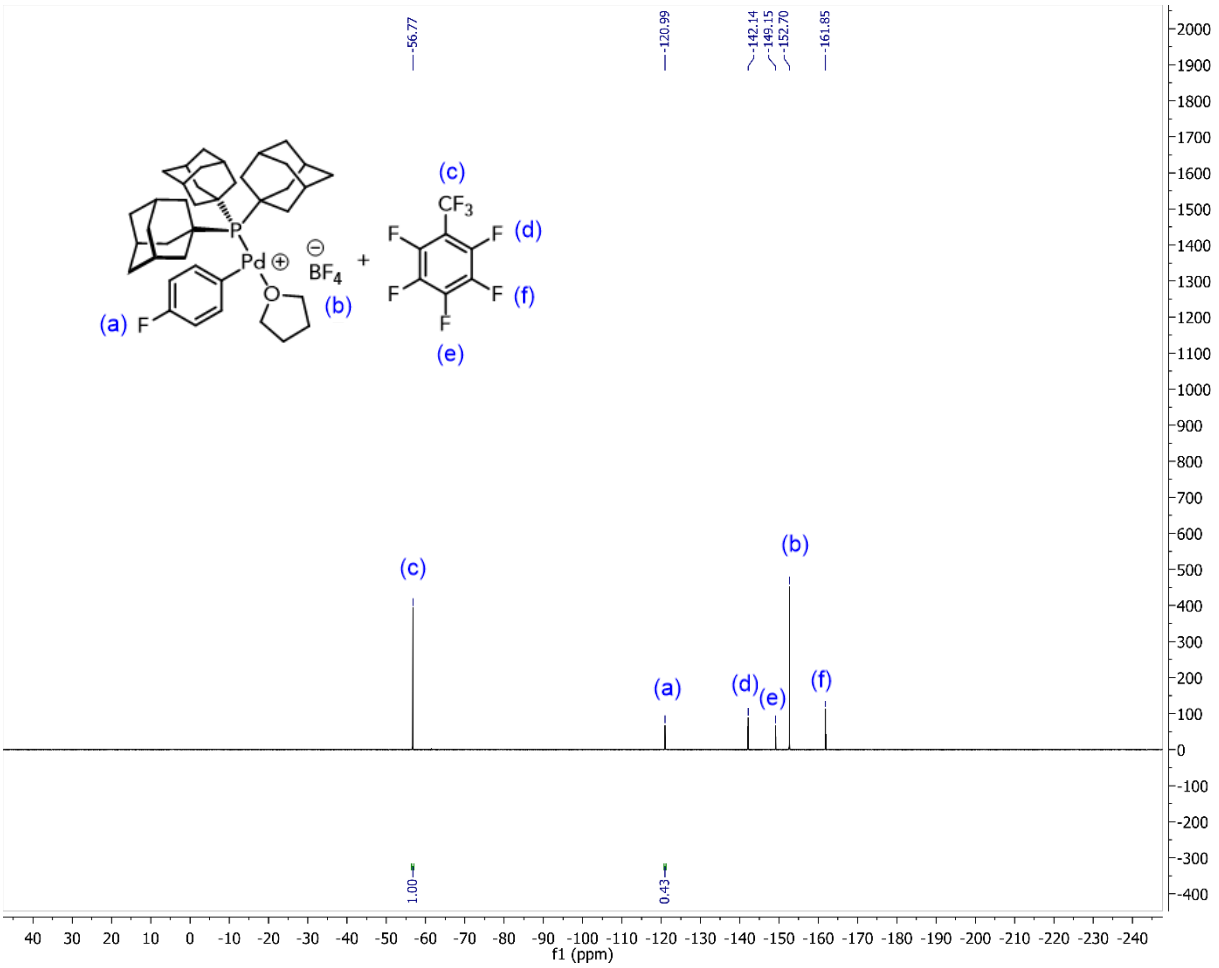

Figure S21. ^{19}F NMR spectrum (470 MHz, THF-d_8) of **33** generated prior to addition of Et_3N and formation of **35**.

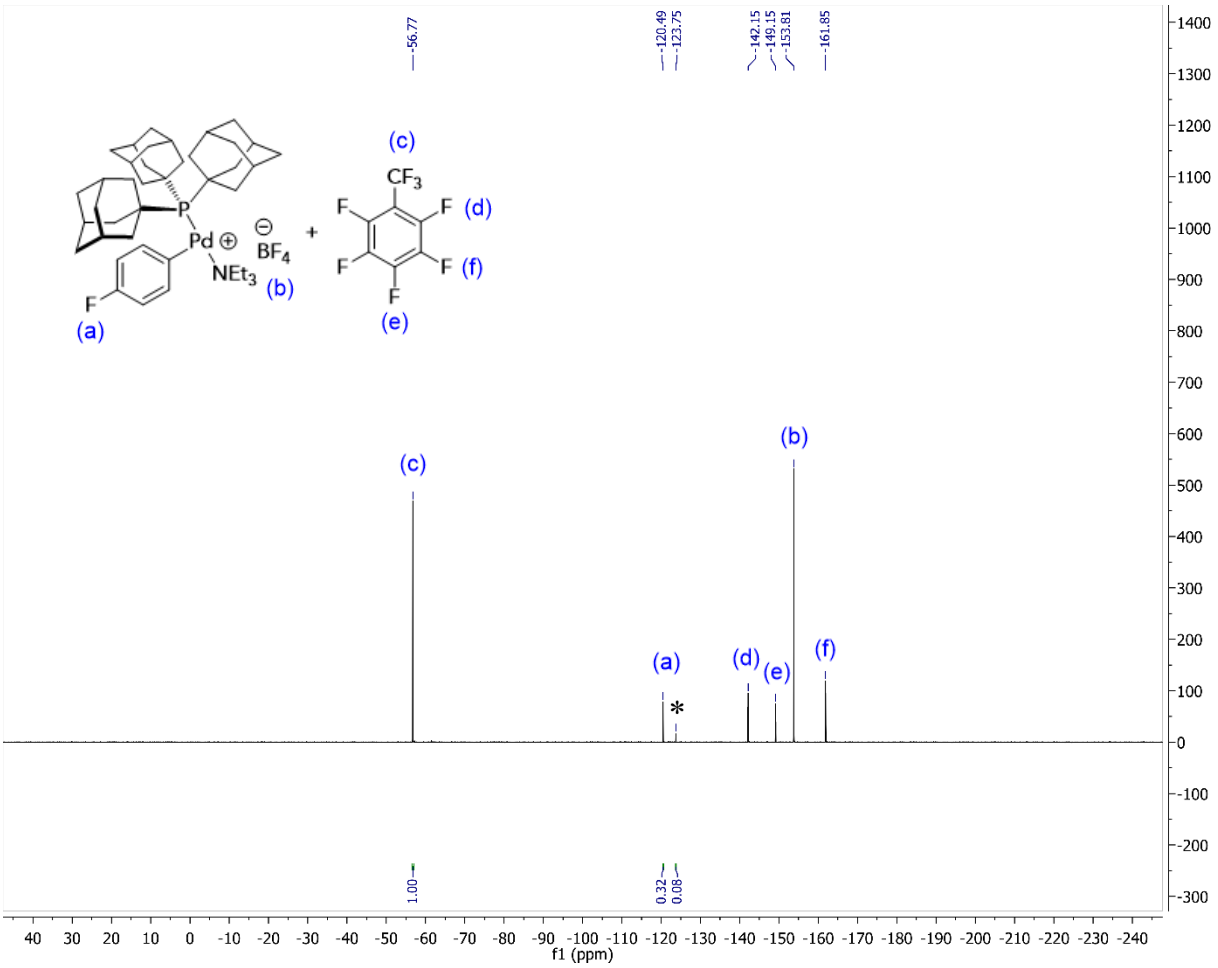

Figure S22. ^{19}F NMR spectrum (470 MHz, THF-d_8) of **35** (* = unidentified).

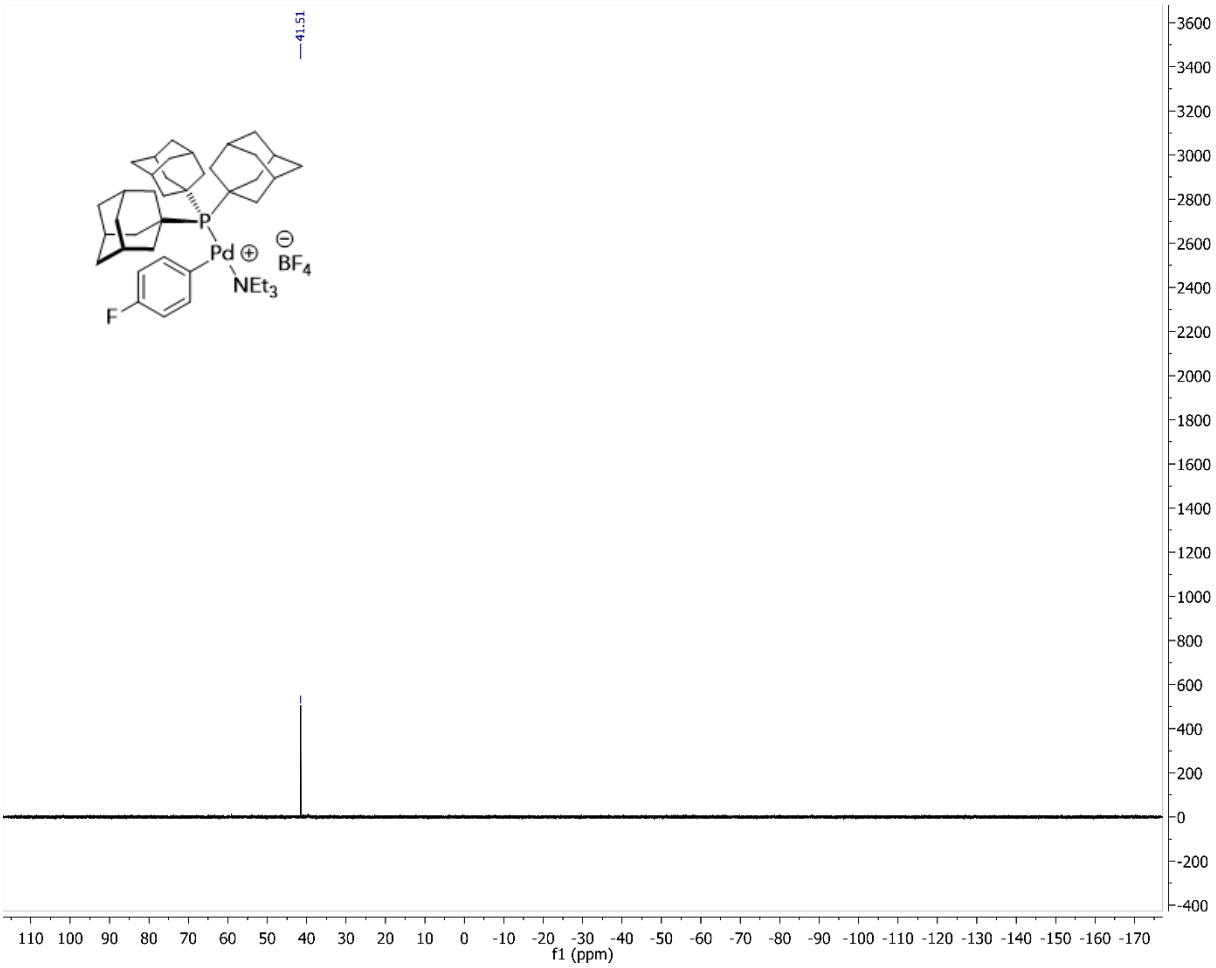

Figure S23. $^{31}P\{^{1}H\}$ NMR spectrum (202 MHz, THF-d_8) of **35**.

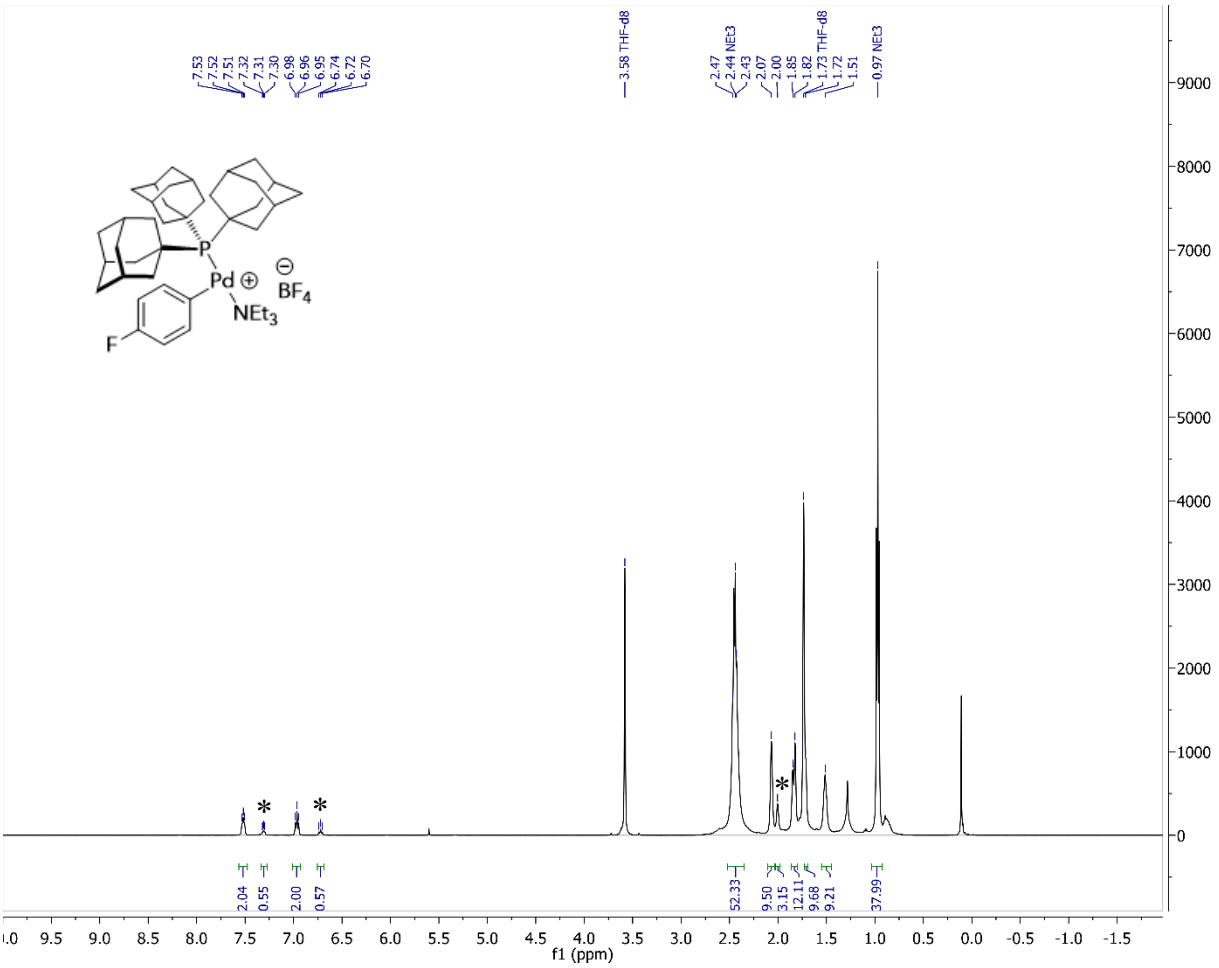

Figure S24. ^{1}H NMR spectrum (500 MHz, THF-d_8) of **35** (* = unidentified).

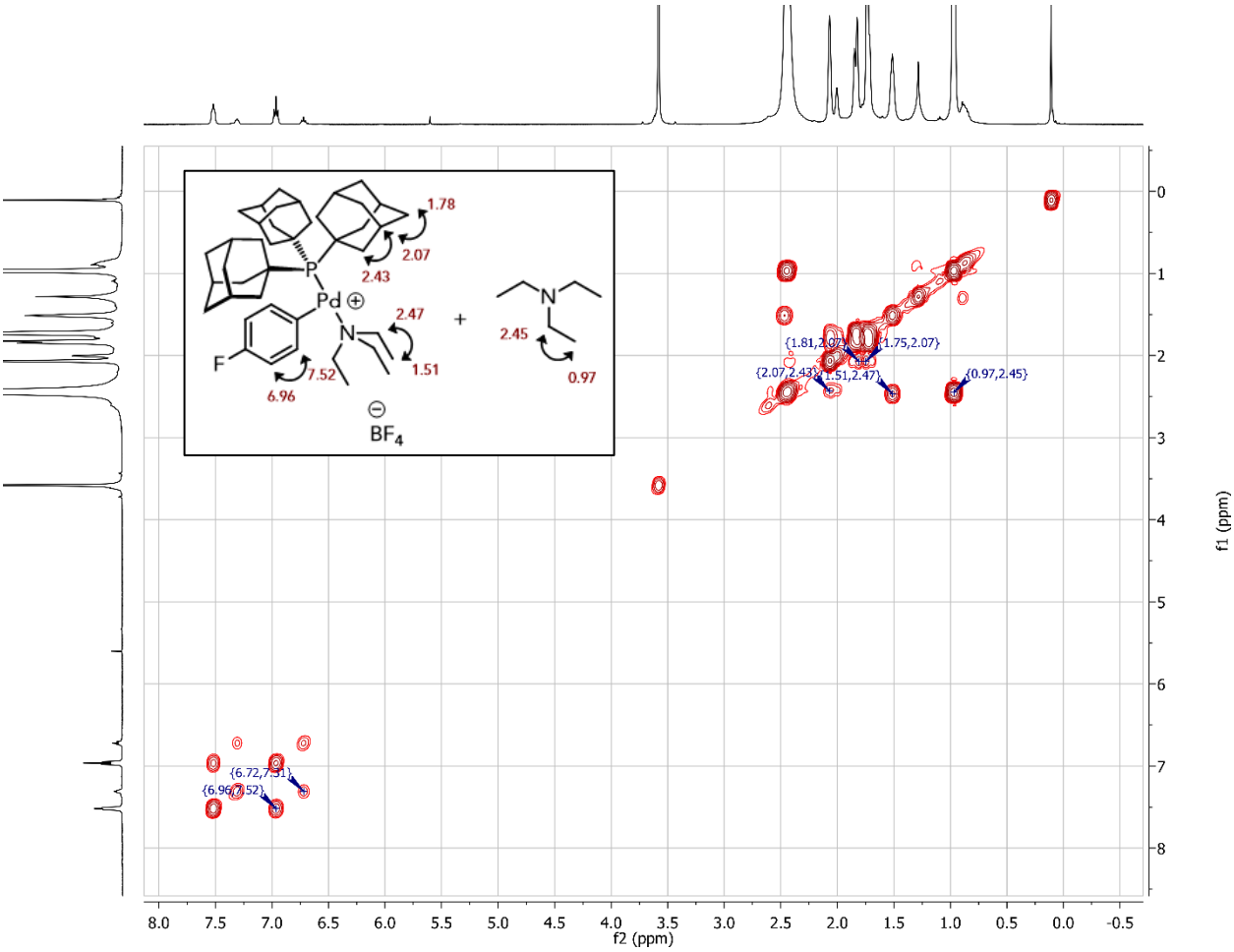

Figure S25. ^{1}H-^{1}H COSY NMR spectrum (500 MHz, THF-d_8) of **35**.

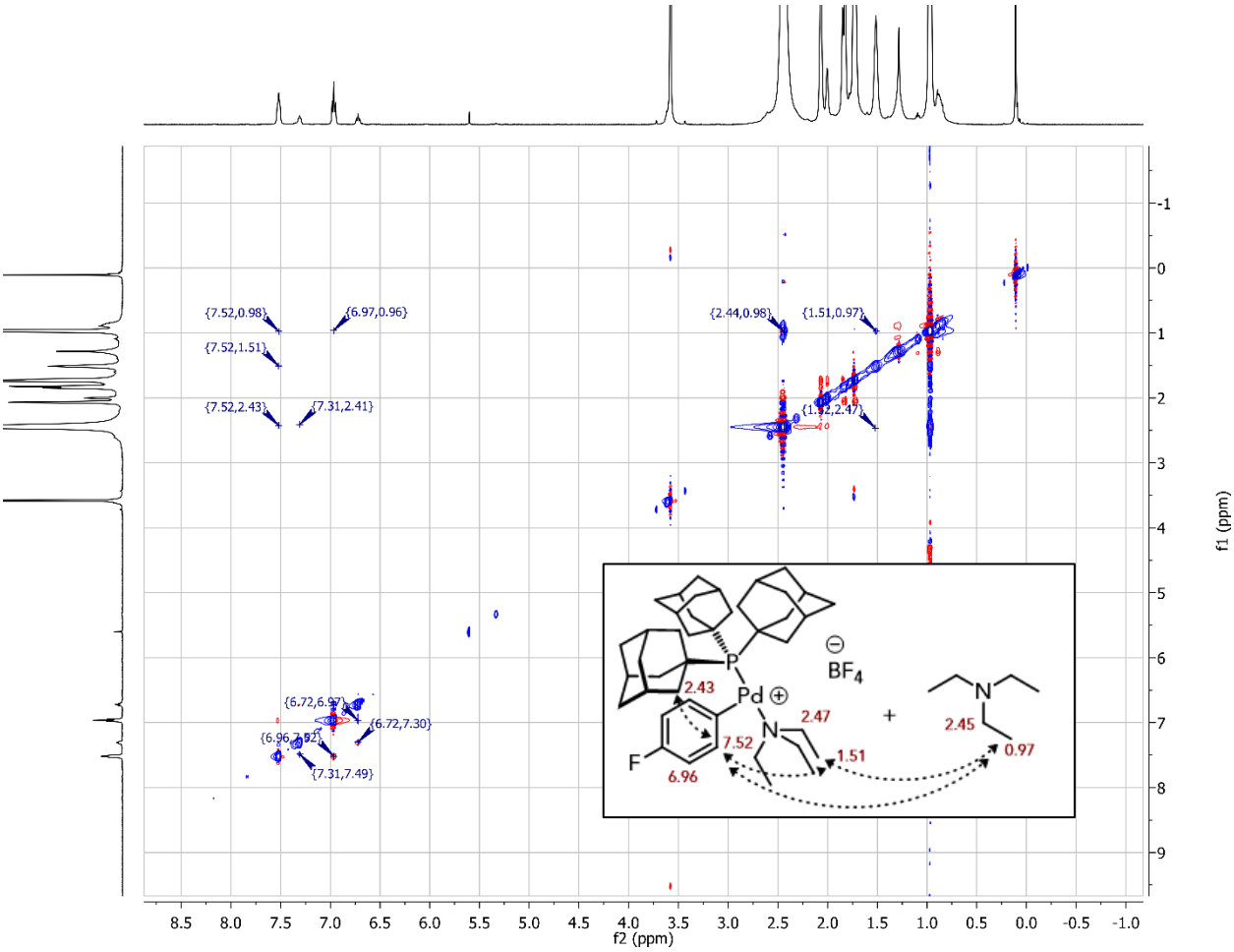

Figure S26. ^{1}H-^{1}H NOESY/EXSY NMR spectrum (500 MHz, THF-d_8) of **35**.

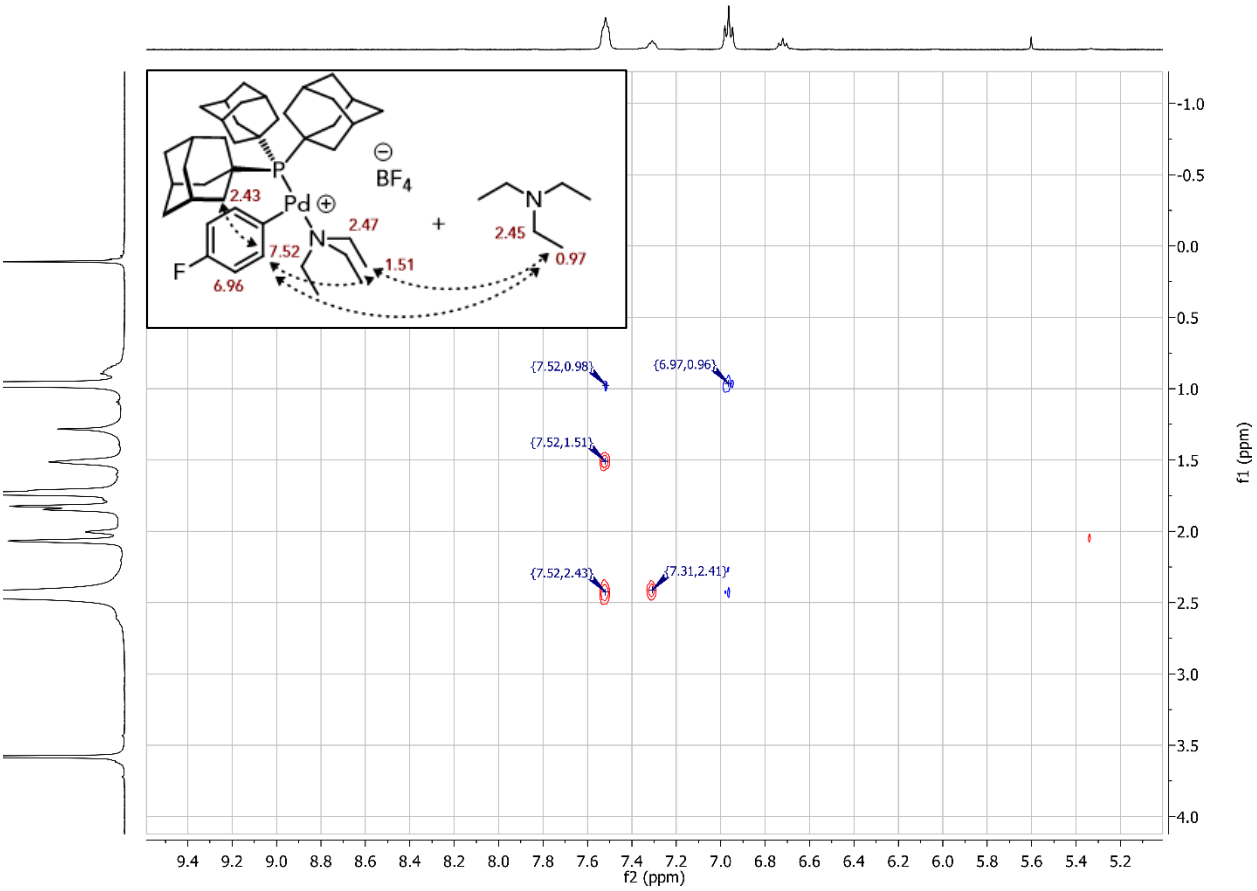

Figure S27. Inset of ^{1}H-^{1}H NOESY/EXSY NMR spectrum (500 MHz, THF-d_8) of **35**.

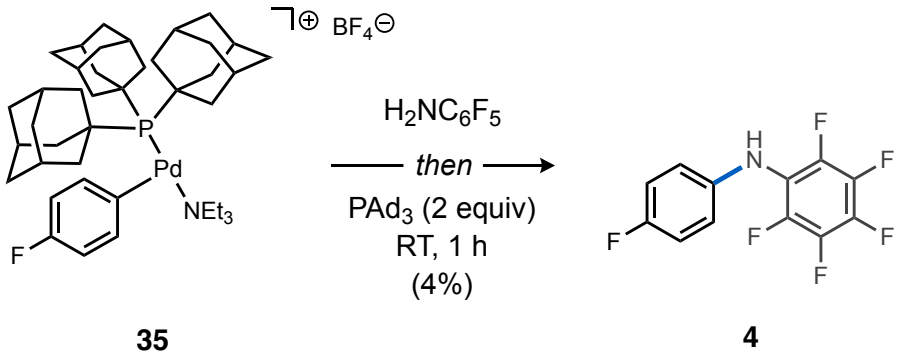

35 **4**

Attempted conversion of 35 into 4 in the absence of water. The generation of $[Pd(PAd_3)(4\text{-}FC_6H_4)]^+ BF_4^-$ (**33**) was adapted from a known procedure.[3] $Pd(PAd_3)(4\text{-}FC_6H_4)Br$ (5.4 mg, 7.5 μmol) and trifluorotoluene (internal standard, 1 μL, 8.2 μmol) were dissolved in THF-d_8 (1.5 mL). Separately, $AgBF_4$ (10 mg, 50 μmol) was dissolved in THF-d_8 (1 mL). Both solutions were chilled at -35 °C (MeOH/H_2O dry ice bath). The latter solution ($AgBF_4$, 2.5 μmol, 50 μL) was then added to the solution of **1** (2.5 μmol, 0.5 mL) in a 4 mL vial at -35 °C. The mixture (0.55 mL) was quickly shaken, left in the cooling bath for 10 min, and transferred into an NMR tube capped with a rubber septum. Next, pentafluoroaniline (0.1 mL from a 15 mM stock solution in THF, 15 μmol, 6 equiv), and triethylamine (5 μL, 37.5 μmol, 15 equiv) were injected into the NMR tube sequentially at -78 °C. The reaction mixture was shaken gently for 1 min then a $^{31}P\{^1H\}$ NMR spectrum was acquired at -25 °C confirming formation of **35** (77%). Finally, a solution of PAd_3 (2.2 mg, 5.0 μmol, 2 equiv) in THF (0.1 mL) was injected into the NMR tube and the mixture was warmed to room temperature. After 1 h, ^{19}F and $^{31}P\{^1H\}$ NMR spectra were acquired that showed formation of only a trace of **4** (4%).

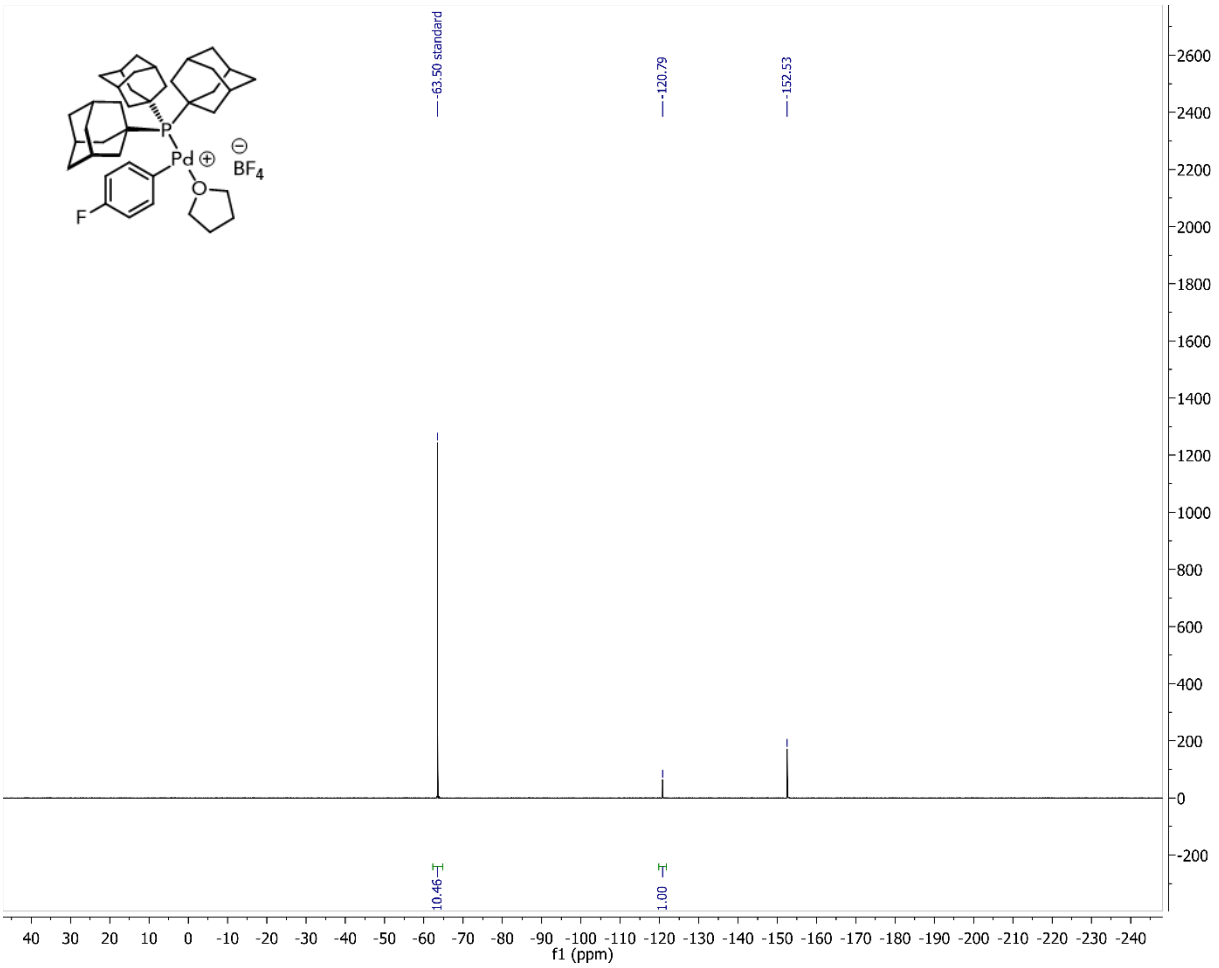

Figure S28. ^{19}F NMR spectrum (470 MHz, THF) of **33** prior to addition of Et_3N and formation of **35**.

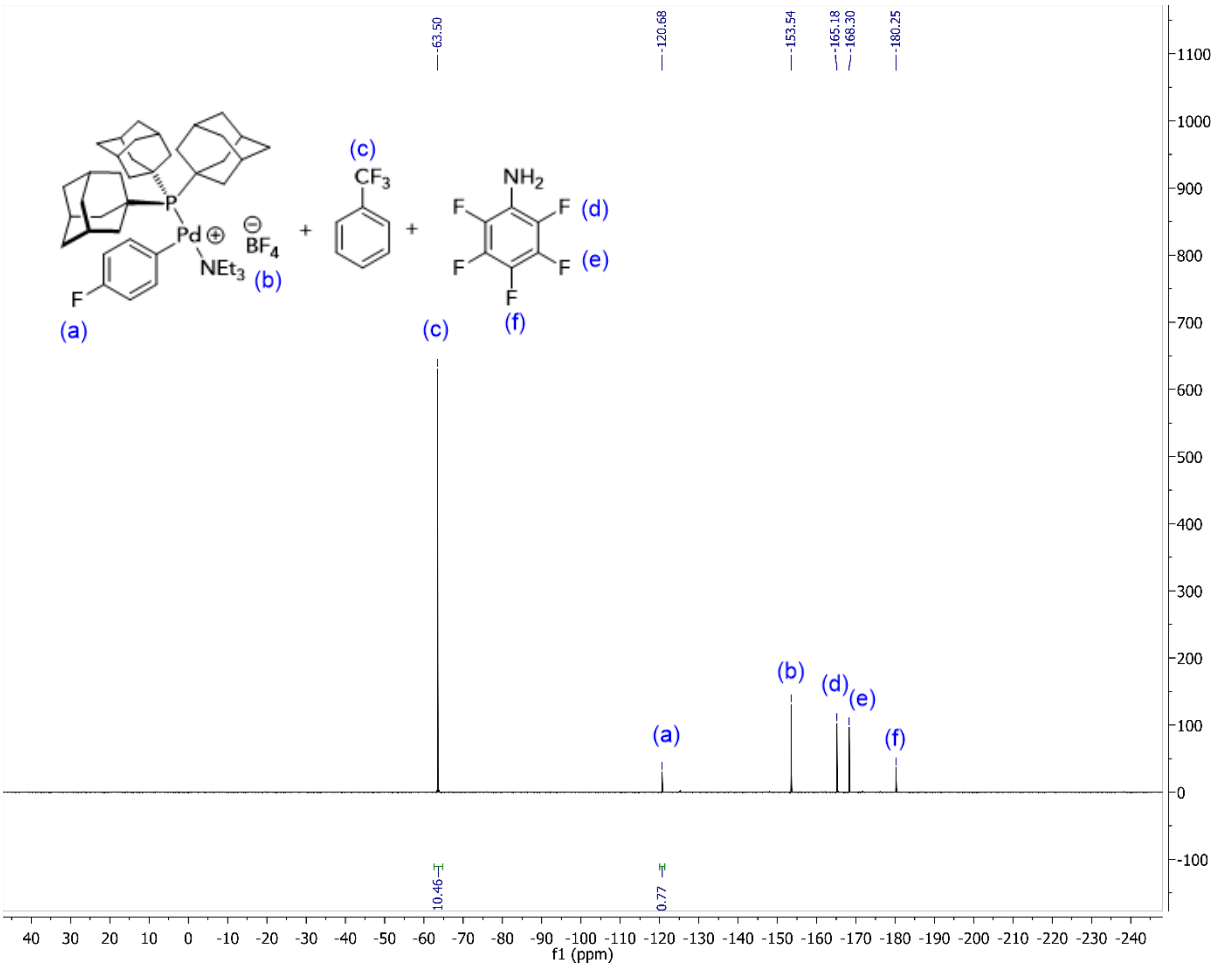

Figure S29. ^{19}F NMR spectrum (470 MHz, THF) of **35** in the presence of pentafluoroaniline, indicating the preference for coordination of Et_3N to Pd.

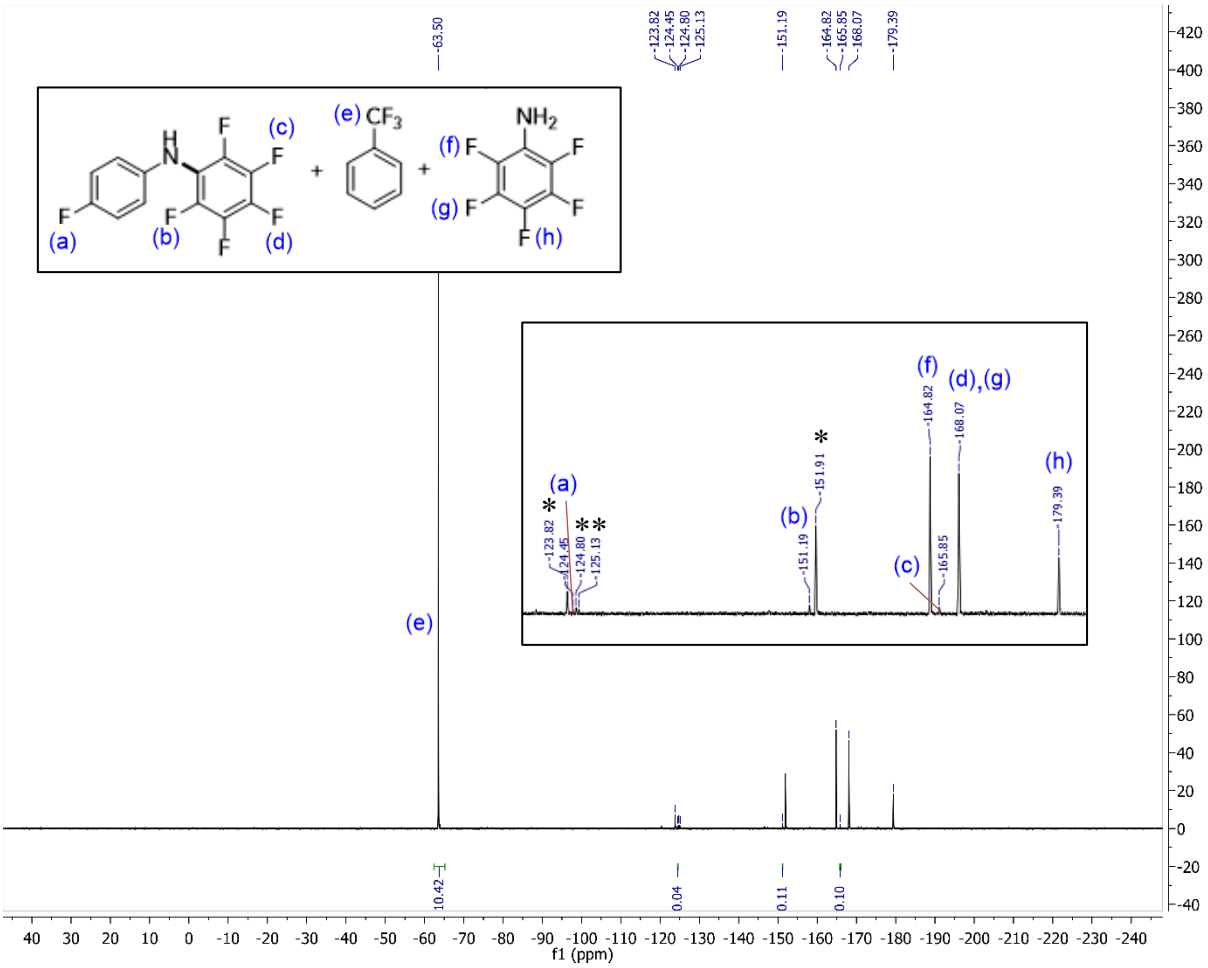

Figure S30. ^{19}F NMR spectrum (470 MHz, THF) of **35** after warming to RT for 1 h (* = unidentified).

Kinetic studies:

General procedure for determination of the rate dependence on [4-FC$_6$F$_4$Br]. The method of variable time normalization analysis (VTNA) was used to interpret kinetic data.[6] To an oven-dried 4 mL scintillation vial equipped with a stir bar was charged with 1-bromo-4-fluorobenzene (0.125 or 0.25 mmol), aniline (34 µL, 0.38 mmol), triethylamine (70 µL, 0.5 mmol), trifluorotoluene (internal standard, 10 µL, 83 µmol), **1** (1.8 mg, 2.5 µmol) and toluene (0.5 mL). The vial was capped with a puncturable PTFE-lined cap and was taken out of the glovebox. Under N_2 atmosphere, degassed deionized water (3 mL) was injected into the vial and the reaction mixture was left stirring vigorously at 80 °C for 160 minutes. Aliquots (20 µL) were taken at 5, 10, 20, 40, 80, and 160 min and were quenched by dilution in $CDCl_3$ (0.6 mL) at RT in an NMR tube. The yields were determined by ^{19}F NMR using a quantitative, single-scan experiment (acquisition time of 1.46 s and recycle delay time (d1) of 10 s). Both [**3**] vs. Σ([4-F-C$_6$F$_4$Br]^0*Δt) and [**3**] vs. Σ([4-F-C$_6$F$_4$Br]^1*Δt) were plotted where time (t) is in units of min, and the best overlay of data points was found for the zeroth-order plot with respect to the dependence of the rate on [4-F-C$_6$F$_4$Br]^n. Note that for the reaction using 0.25 mmol 4-F-C$_6$F$_4$Br, data were not plotted beyond 20 min because yield of **3** at this time was 94%.

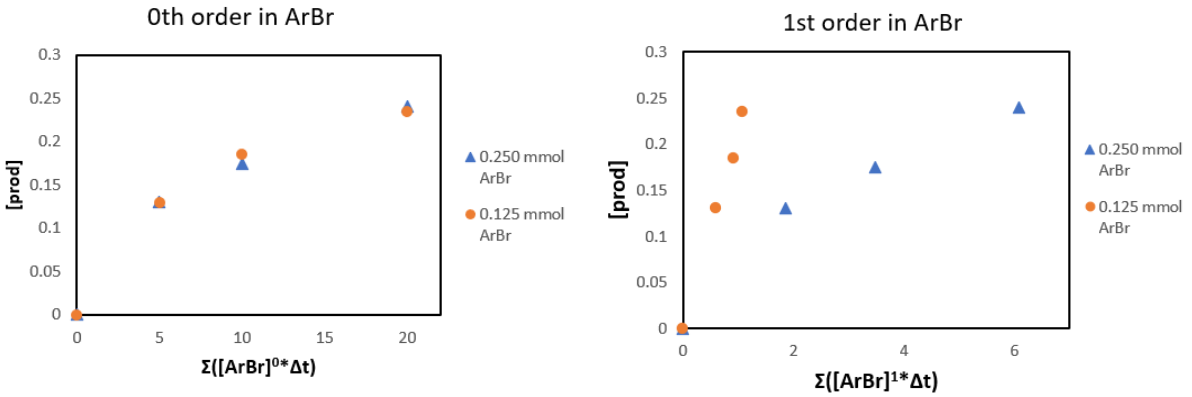

Figure S31. Variable time normalization analysis (VTNA) of reactions conducted at varying [4-F-C$_6$F$_4$Br].

General procedure for determination of the rate dependence on [$PhNH_2$]. The method of variable time normalization analysis (VTNA) was used to interpret kinetic data.[6] To an oven-dried 4 mL scintillation vial equipped with a stir bar was charged with 1-bromo-4-fluorobenzene (27 µL, 0.25 mmol, 1.0 equiv), aniline (0.38 mmol or 0.75 mmol), triethylamine (70 µL, 0.5 mmol), trifluorotoluene (internal standard, 10 µL, 83 µmol), **1** (1.8 mg, 2.5 µmol) and toluene (0.5 mL). The vial was capped with a puncturable PTFE-lined cap and was taken out of the glovebox. Under N_2 atmosphere, degassed deionized water (3 mL) was injected into the vial and the reaction mixture was left stirring vigorously at 80 °C for 160 minutes. Aliquots (20 µL) were taken at 5, 10, 20, 40, 80, and 160 minutes and were quenched by dilution into $CDCl_3$ (0.6 mL) at RT in an NMR tube. The yields were determined by ^{19}F NMR using a quantitative, single-scan experiment (acquisition time of 1.46 s and recycle delay time (d1) of 10 s). Both [**3**] vs. $\Sigma([PhNH_2]^0*\Delta t)$ and [**3**] vs. $\Sigma([PhNH_2]^1*\Delta t)$ were plotted where time (t) is in units of min, and the better overlay of data points was found for the zeroth-order plot with respect to the dependence of the rate on $[PhNH_2]^n$.

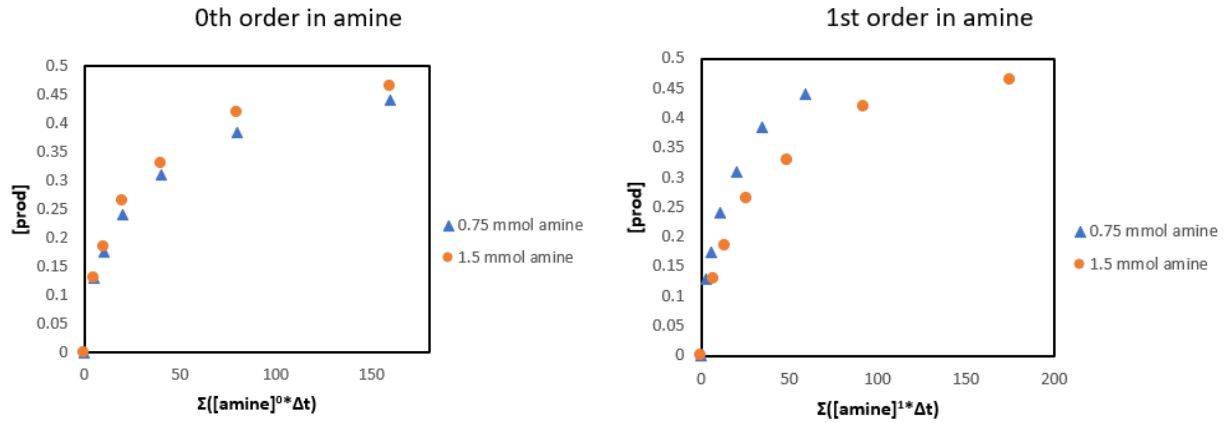

Figure S32. Variable time normalization analysis (VTNA) of reactions conducted at varying [$PhNH_2$].

General procedure for determination of the rate dependence on [Et_3N]. The method of variable time normalization analysis (VTNA) was used to interpret kinetic data.[6] To an oven-dried 4 mL scintillation vial equipped with a stir bar was charged with 1-bromo-4-fluorobenzene (27 µL, 0.25 mmol, 1.0 equiv), aniline (34 µL, 0.38 mmol), triethylamine (0.5 mmol or 1.0 mmol), trifluorotoluene (internal standard, 10 µL, 83 µmol), **1** (1.8 mg, 2.5 µmol) and toluene (0.5 mL). The vial was capped with a puncturable PTFE-lined cap and was taken out of the glovebox. Under N_2 atmosphere, degassed deionized water (3 mL) was injected into the vial and the reaction mixture was left stirring vigorously at 80 °C for 160 minutes. Aliquots (20 µL) were taken at 5, 10, 20, 40, 80, and 160 minutes and were quenched by dilution into $CDCl_3$ (0.6 mL) at RT in an NMR tube. The yields were determined by ^{19}F NMR using a quantitative, single-scan experiment (acquisition time of 1.46 s and recycle delay time (d1) of 10 s). Both [**3**] vs. $\Sigma([NEt_3]^0*\Delta t)$ and [**3**] vs. $\Sigma([NEt_3]^1*\Delta t)$ were plotted where time (t) is in units of min, and the better overlay of data points was found for the zeroth-order plot with respect to the dependence of the rate on $[Et_3N]^n$.

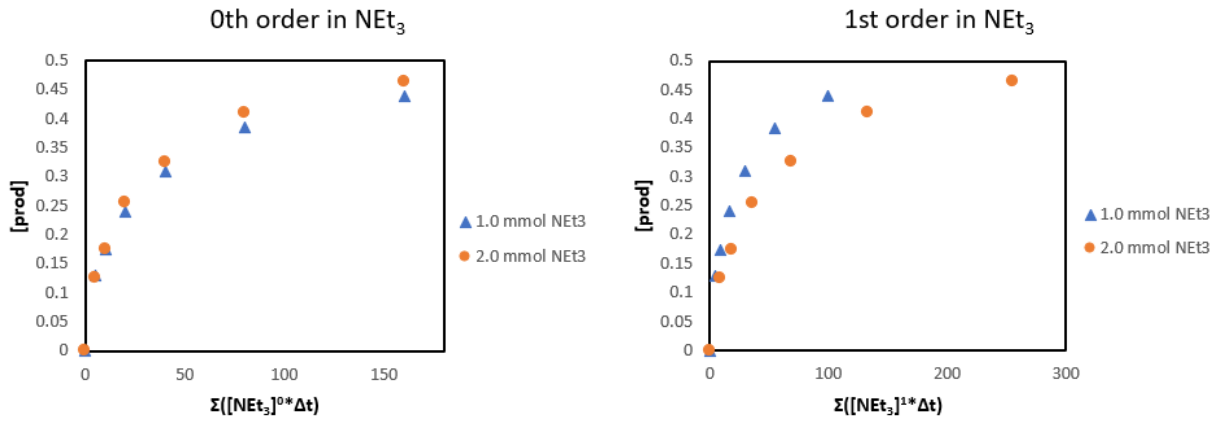

Figure S33. Variable time normalization analysis (VTNA) of reactions conducted at varying [Et_3N].

General procedure for determination of the rate dependence on [1]. The method of initial rates was used. To an oven-dried 4 mL scintillation vial equipped with a stir bar was charged with 1-bromo-4-fluorobenzene (27 µL, 0.25 mmol), aniline (34 µL, 0.375 mmol), triethylamine (70 µL, 0.5 mmol), trifluorotoluene (internal standard, 10 µL, 83 µmol), **1** (2.5 µmol or 5.0 µmol) and toluene (0.5 mL). The vial was capped with a puncturable PTFE-lined cap and was taken out of the glovebox. Under N_2 atmosphere, degassed deionized water (3 mL) was injected into the vial and the reaction mixture was left stirring vigorously at 80 °C. Aliquots (20 µL) were taken at 2, 4, 6, 8, and 10 minutes and were quenched by dilution into $CDCl_3$ (0.6 mL) at RT in an NMR tube. The yields at each time were determined by ^{19}F NMR using a quantitative, single-scan experiment (acquisition time of 1.46 s and recycle delay time (d1) of 10 s). Data were fit by linear regression analysis of plots of [**3**] vs. time at conversions of ≤30% yield. The dependence of the initial rate on [**1**] was calculated according to the following equations:

$$\left(\frac{[Pd]_2}{[Pd]_1}\right)^x = \left(\frac{slope\ 2}{slope\ 1}\right)$$

$$(2)^x = \left(\frac{0.028}{0.015}\right)$$

$$x = 0.90$$

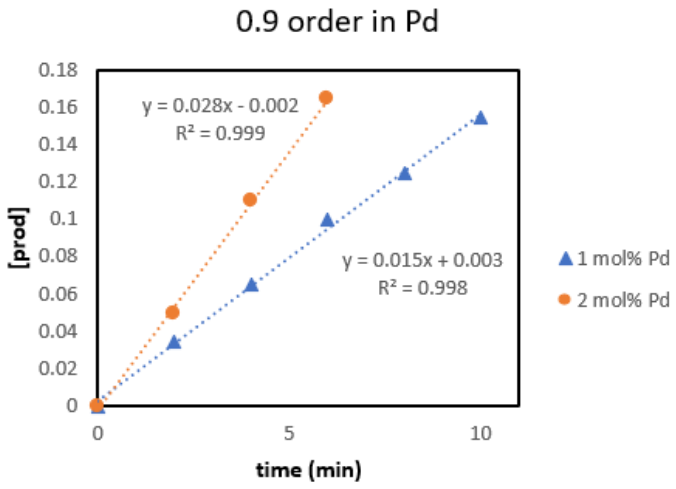

Figure S34. Initial rates during reactions conducted with either 2.5 µmol or 5.0 µmol of catalyst **1**.

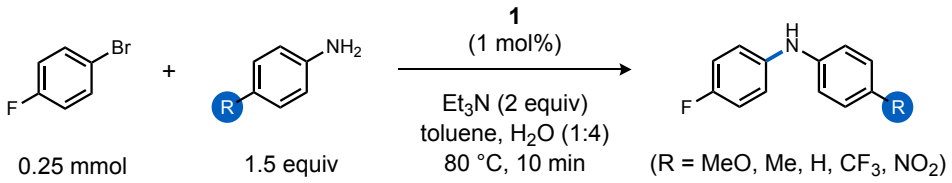

Linear free-energy relationship (LFER) studies with respect to *para*-substituted anilines. Five parallel reactions were performed using a *para*-substituted aniline (*p*-R-$C_6H_4NH_2$; R = MeO, Me, H, CF_3, or NO_2). To an oven-dried 4 mL scintillation vial equipped with a stir bar was charged with 1-bromo-4-fluorobenzene (27 µL, 0.25 mmol, 1.0 equiv), aniline (0.38 mmol), triethylamine (70 µL, 0.5 mmol), trifluorotoluene (internal standard, 10 µL, 83 µmol), **1** (1.8 mg, 2.5 µmol, 1 mol%), and toluene (0.5 mL). The vial was capped with a puncturable PTFE-lined cap and was taken out of the glovebox. Under N_2 atmosphere, degassed deionized water (3 mL) was injected into the vial and the reaction mixture was left stirring vigorously at 80 °C. Aliquots (20 µL) were taken at 2, 4, 6, 8, and 10 minutes and were quenched by dilution into $CDCl_3$ (0.6 mL) at RT in an NMR tube. The yields at each time were determined by ^{19}F NMR using a quantitative, single-scan experiment (acquisition time of 1.46 s and recycle delay time (d1) of 10 s). Data were fit by linear regression analysis of plots of [product] vs. time at conversions of ≤30% yield.[5, 7-10] A Hammett analysis was performed using the initial rates and corresponding substituent constants (σ_P).[11] A ρ value of +0.3 was determined from the slope of this plot.

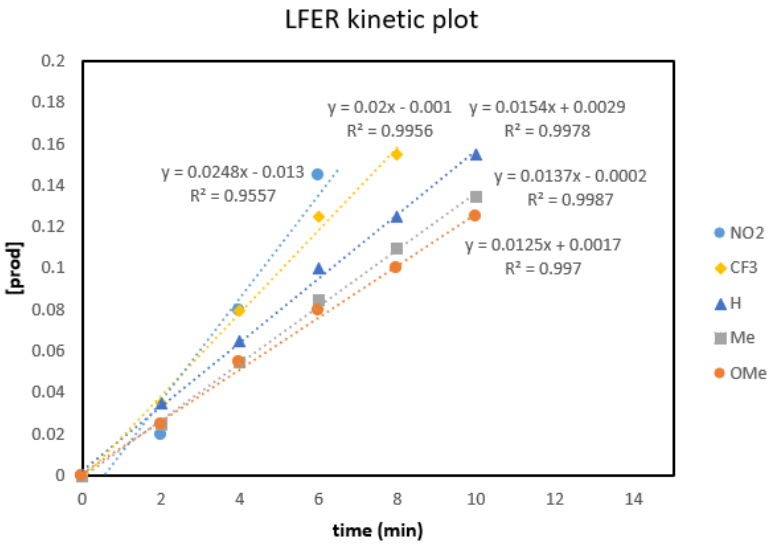

Figure S35. Determination of the initial rate of reactions between 4-FC_6H_4Br and a *para*-subsituted aniline under the conditions noted above.

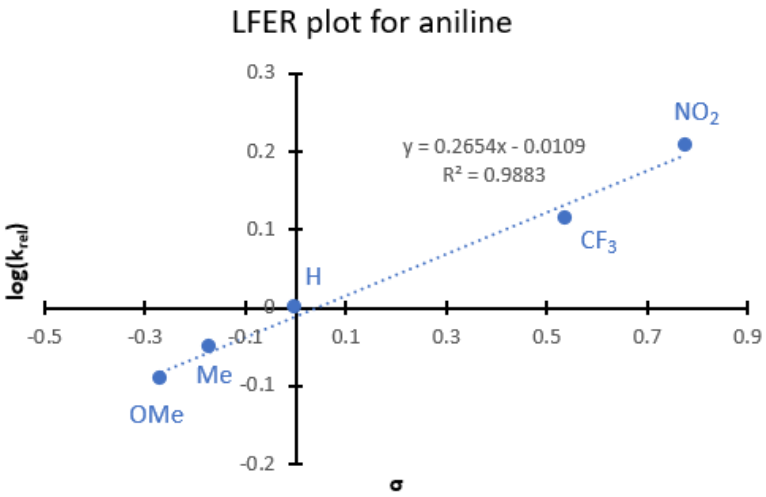

Figure S36. Hammett plot determined from initial rates of reactions between 4-FC_6H_4Br and a *para*-subsituted aniline under the conditions noted above.

$C_6H_5ND_2$. To a 20 mL scintillation vial equipped with a stir bar was charged with aniline (0.5 mL, 5.5 mmol), D_2O (5.0 mL, 0.28 mol, 51 equiv), and DCM (2 mL). The mixture was stirred at room temperature for 3 min. The organic layer was extracted with DCM and washed with D_2O (3 mL x 2), dried over sodium sulfate, and concentrated under reduced pressure. ^1H NMR taken in $CDCl_3$ indicated the absence of NH_2 resonances.

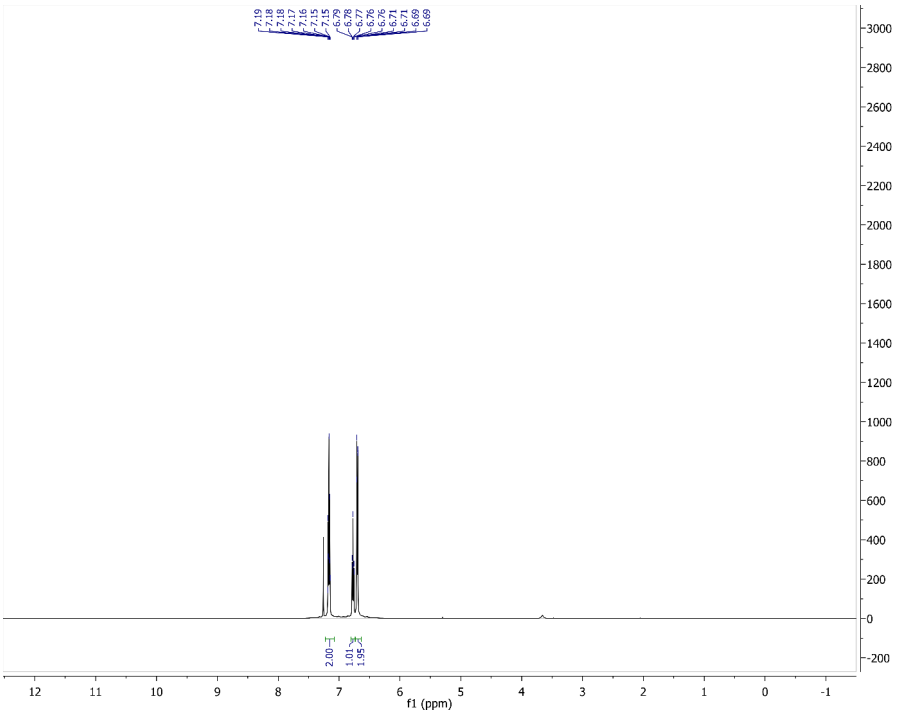

Figure S37. ^{1}H NMR spectrum (500 MHz, $CDCl_3$) of $C_6H_5ND_2$.

Kinetic isotope effect (KIE) experiments. To an oven-dried 4 mL scintillation vial equipped with a stir bar was charged with 1-bromo-4-fluorobenzene (27 µL, 0.25 mmol, 1.0 equiv), $C_6H_5NH_2$ (0.38 mmol), triethylamine (70 µL, 0.5 mmol), trifluorotoluene (internal standard, 10 µL, 83 µmol), **1** (1.8 mg, 2.5 µmol, 1 mol%), and toluene (0.5 mL). The vial was capped with a puncturable PTFE-lined cap and was taken out of the glovebox. Under N_2 atmosphere, degassed deionized water (3 mL) was injected into the vial and the reaction mixture was left stirring vigorously at 80 °C. Aliquots (20 µL) were taken at 2, 4, 6, 8, and 10 minutes and were quenched by dilution into $CDCl_3$ (0.6 mL) at RT in an NMR tube. The yields at each time were determined by ^{19}F NMR using a quantitative, single-scan experiment (acquisition time of 1.46 s and recycle delay time (d1) of 10 s). Data were fit by linear regression analysis of plots of [**3**] vs. time at conversions of ≤30% yield. The experiment and data analysis were repeated with substitution of $C_6H_5ND_2$ for $C_6H_5NH_2$ and D_2O for H_2O. The KIE was calculated according to the equation:

$$KIE = \frac{k_H}{k_D} = \frac{0.154}{0.127} = 1.2$$

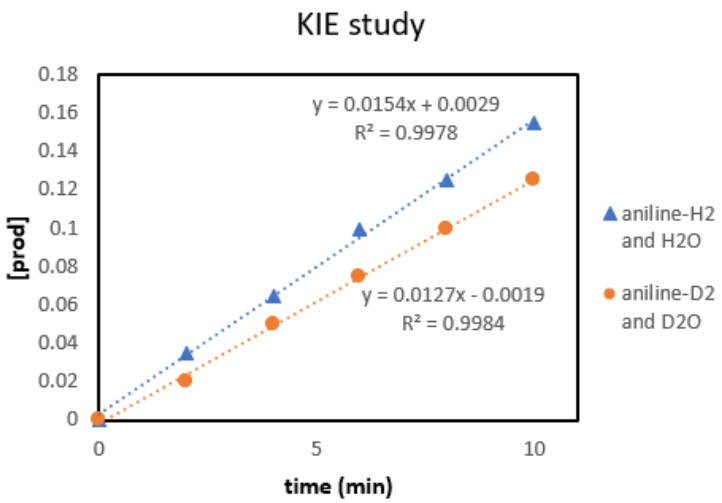

Figure S38. Plot of product (**3**) formation versus time during reacitons with aniline isotopologues.

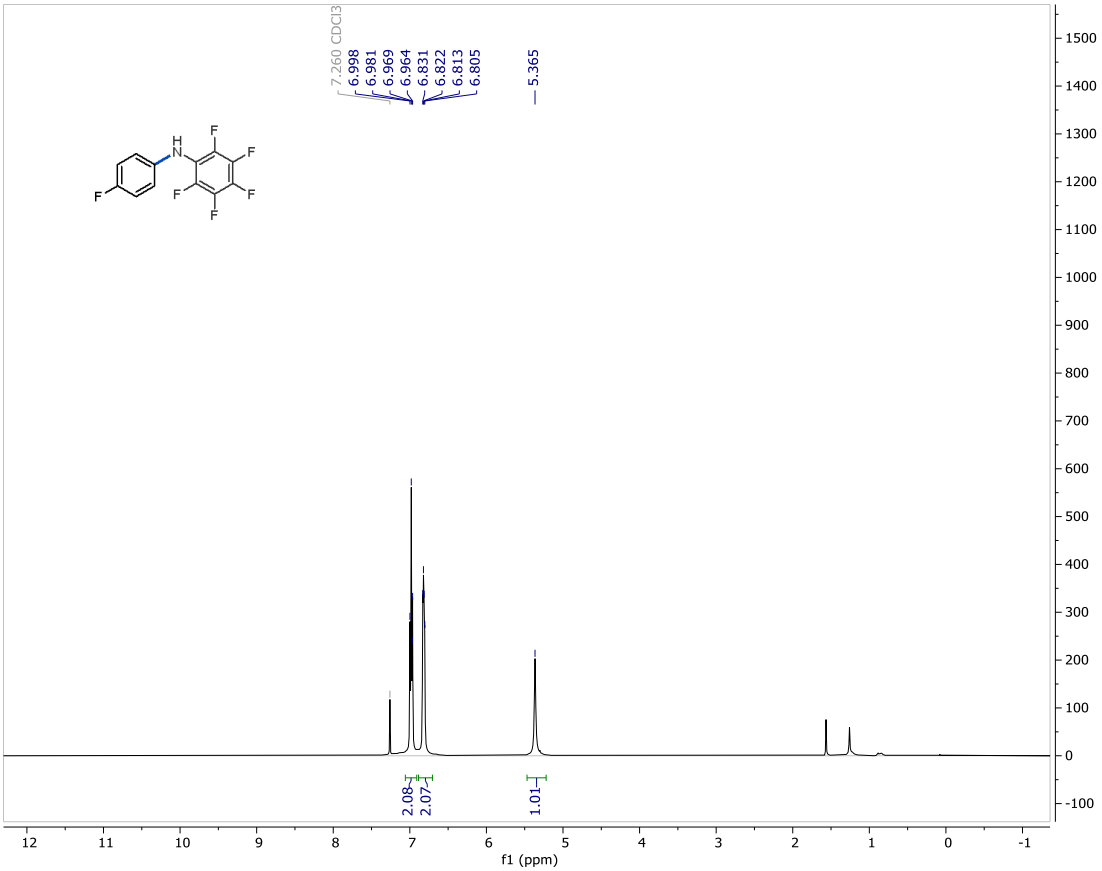

Figure S39. ^{1}H NMR (500 MHz, $CDCl_3$) of **4**.

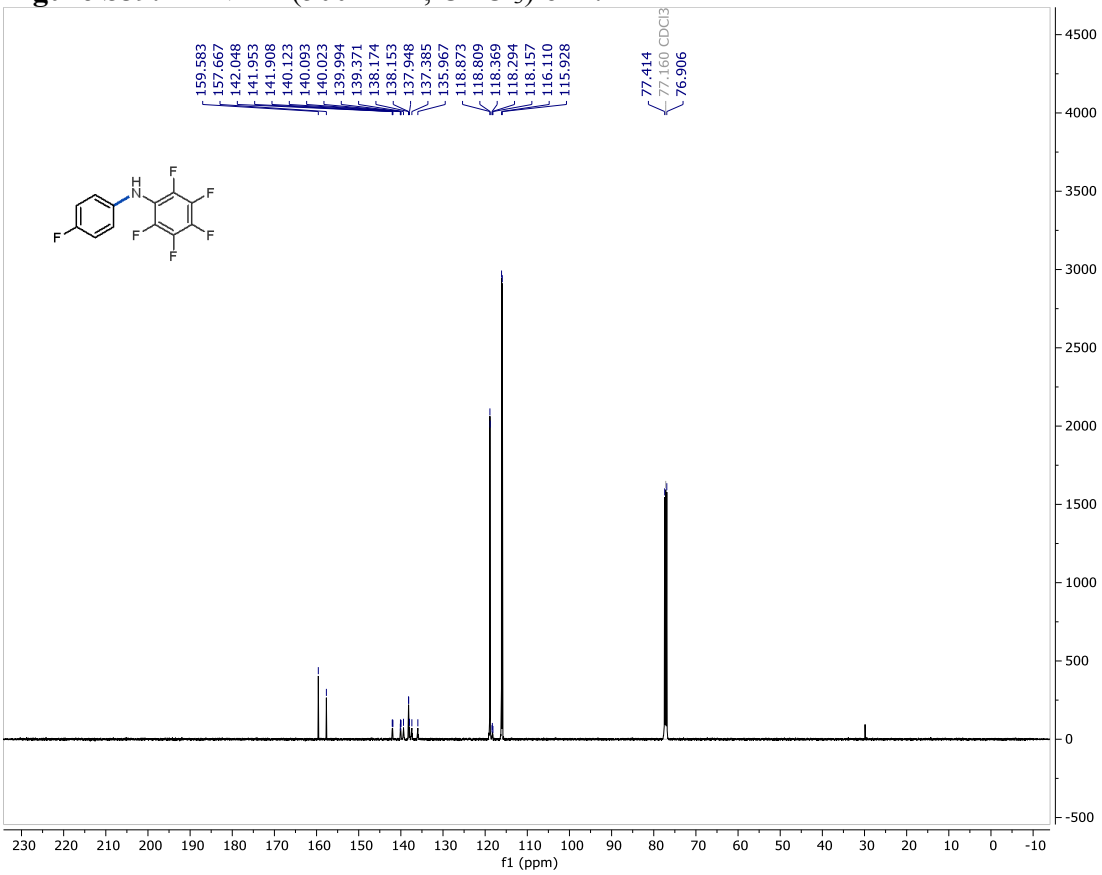

Figure S40. ^{13}C NMR (126 MHz, $CDCl_3$) of **4**.

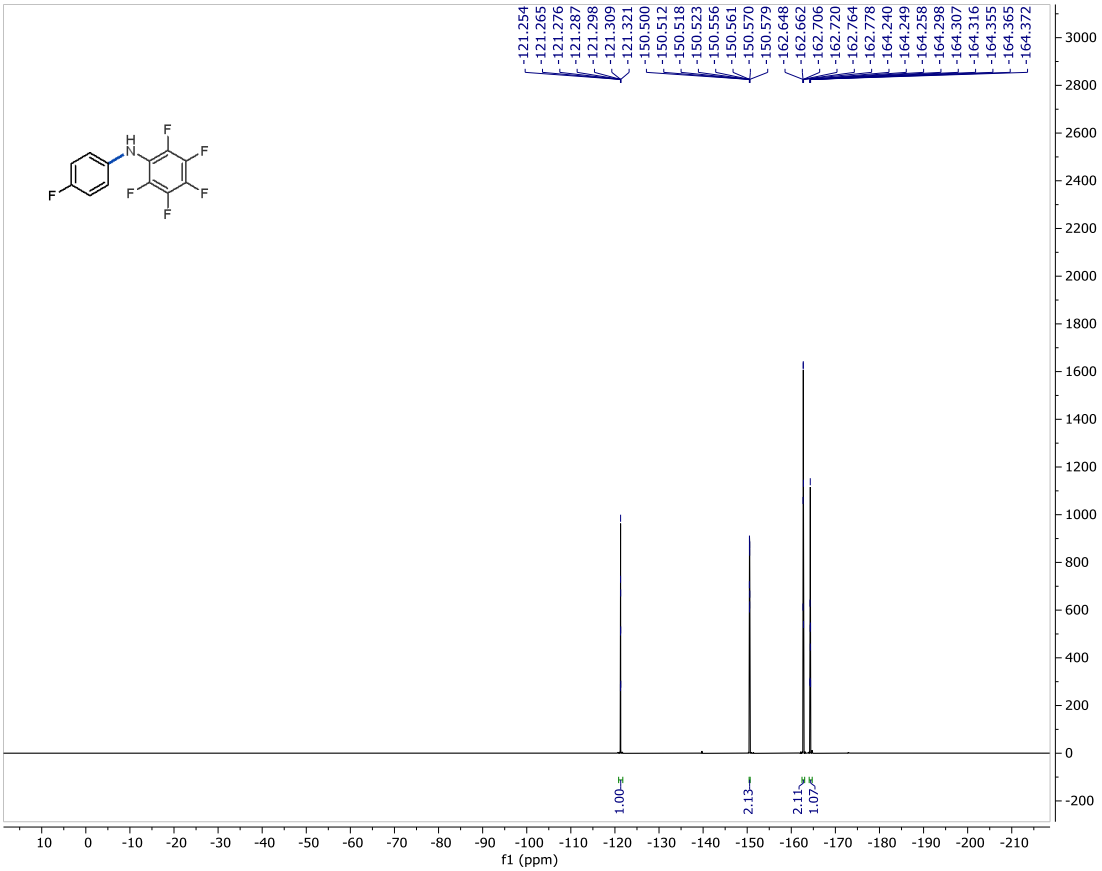

Figure S41. ^{19}F NMR (376 MHz, $CDCl_3$) of **4**.

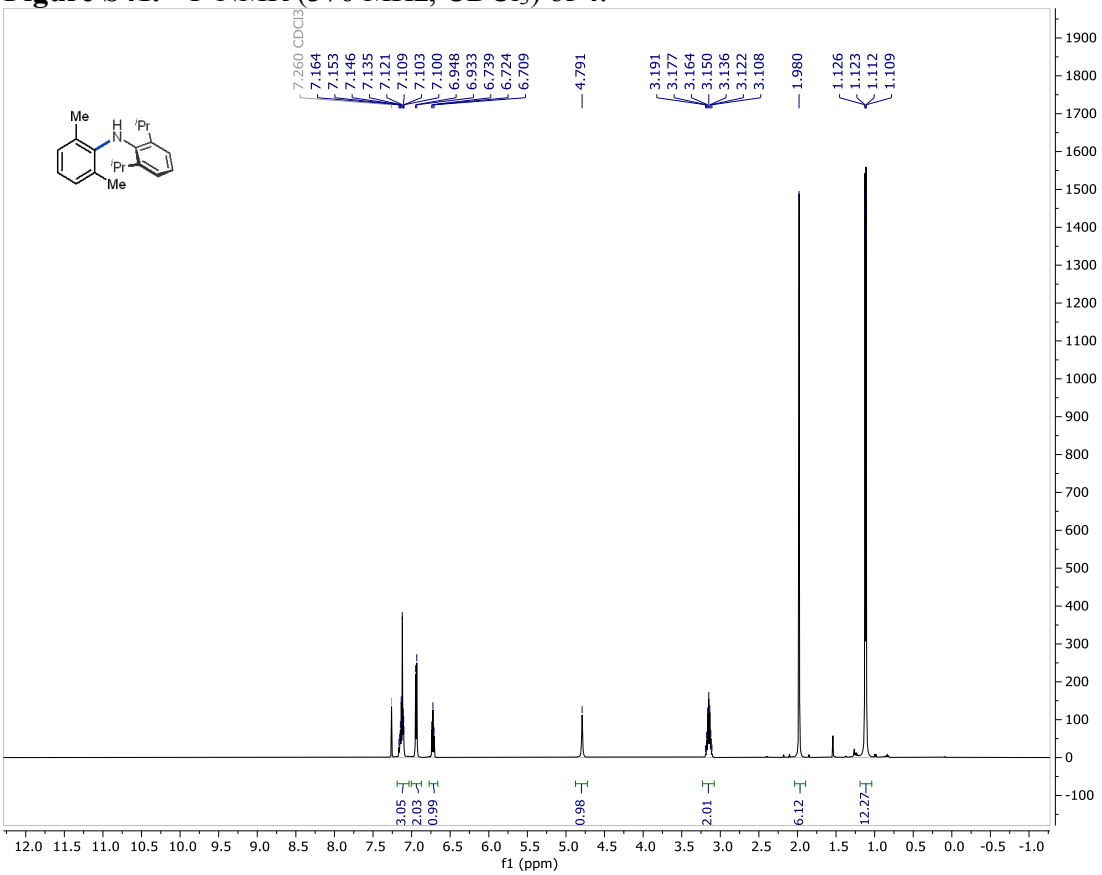

Figure S42. ^{1}H NMR (500 MHz, $CDCl_3$) of **5**.

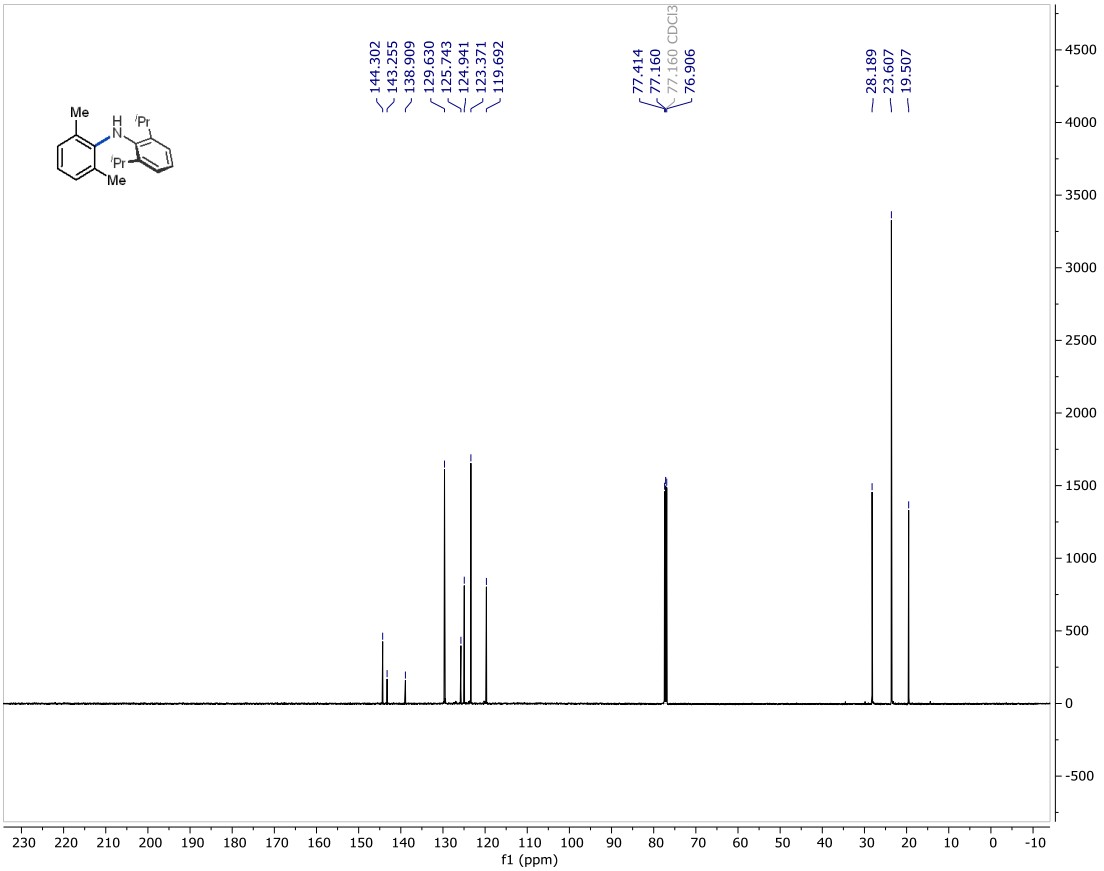

Figure S43. ^{13}C NMR (126 MHz, CDCl3) of **5**.

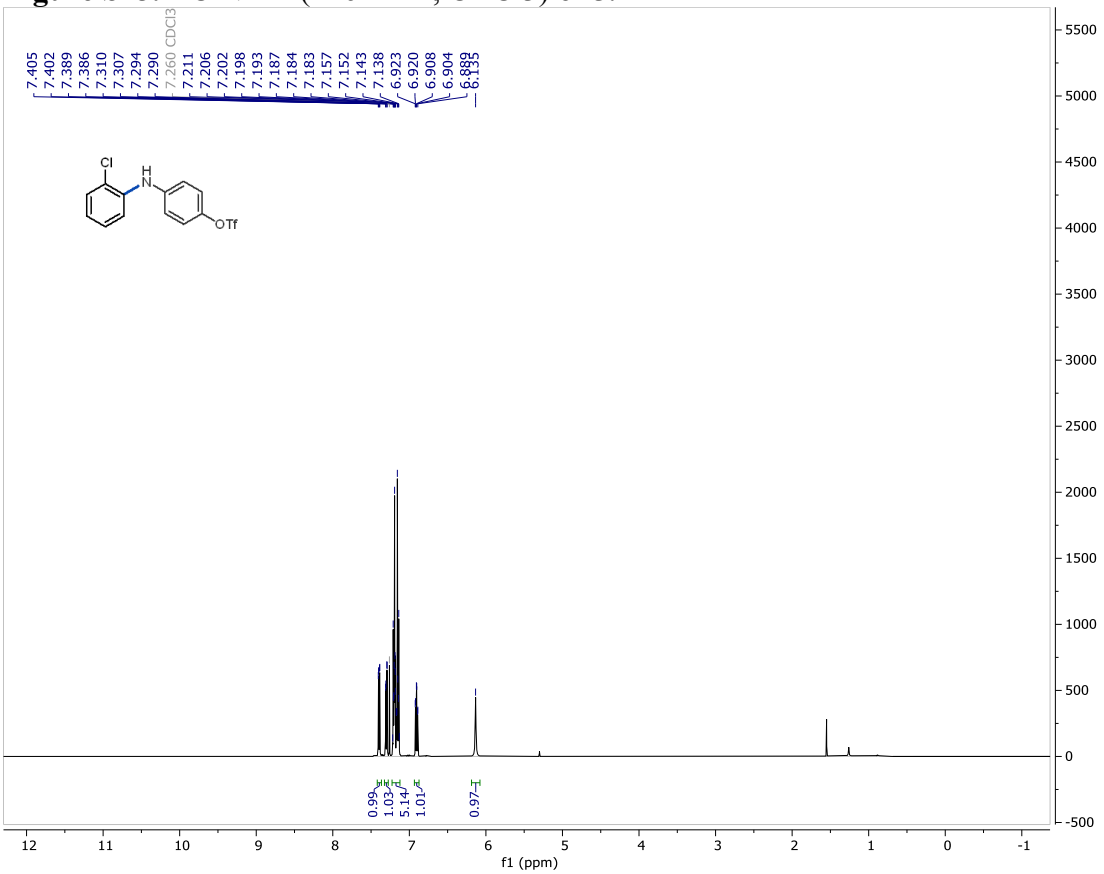

Figure S44. ^{1}H NMR (500 MHz, $CDCl_3$) of **6**.

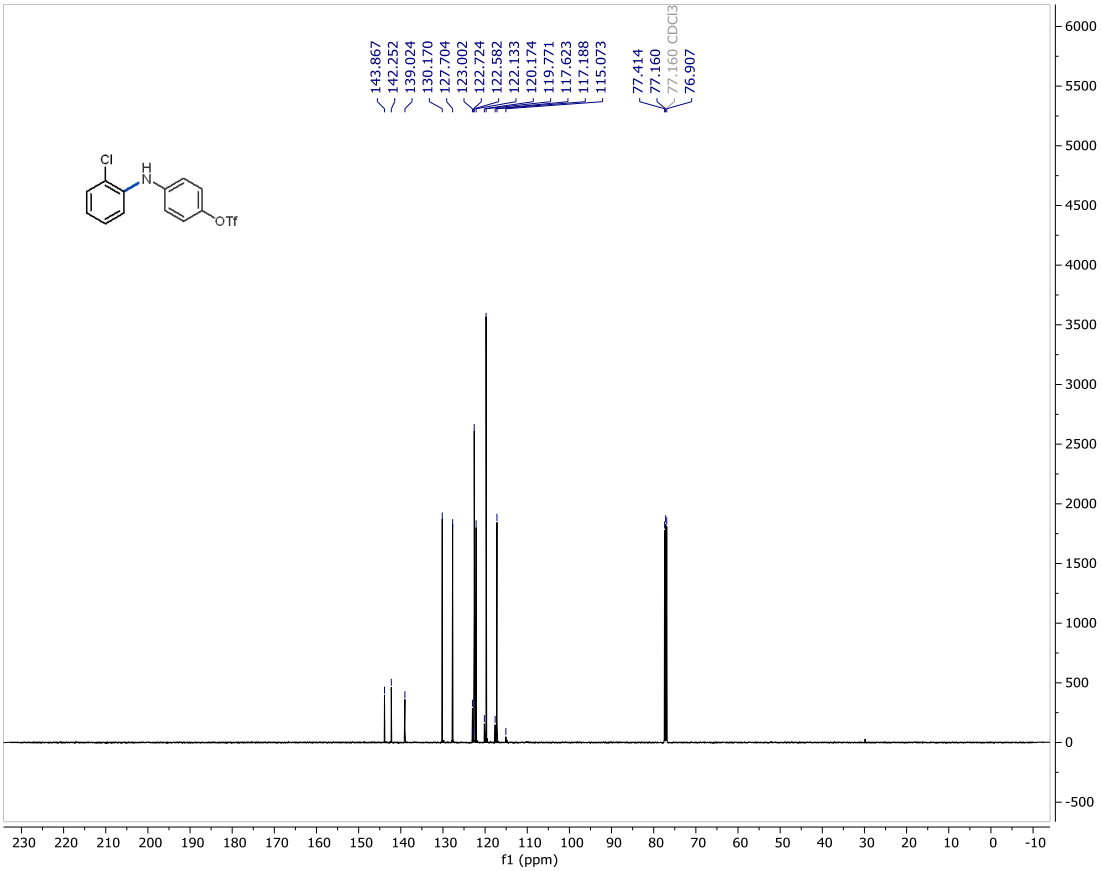

Figure S45. ^{13}C NMR (126 MHz, $CDCl_3$) of **6**.

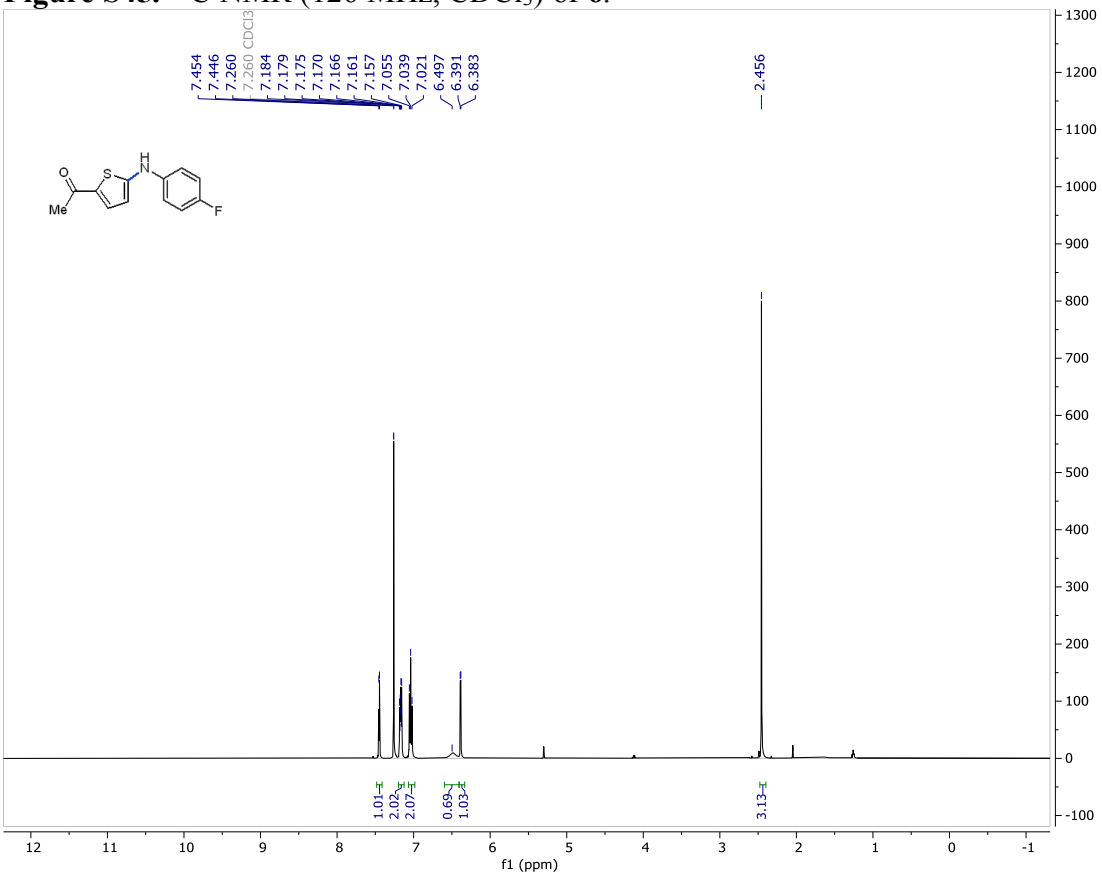

Figure S46. ^{1}H NMR (500 MHz, $CDCl_3$) of **7**.

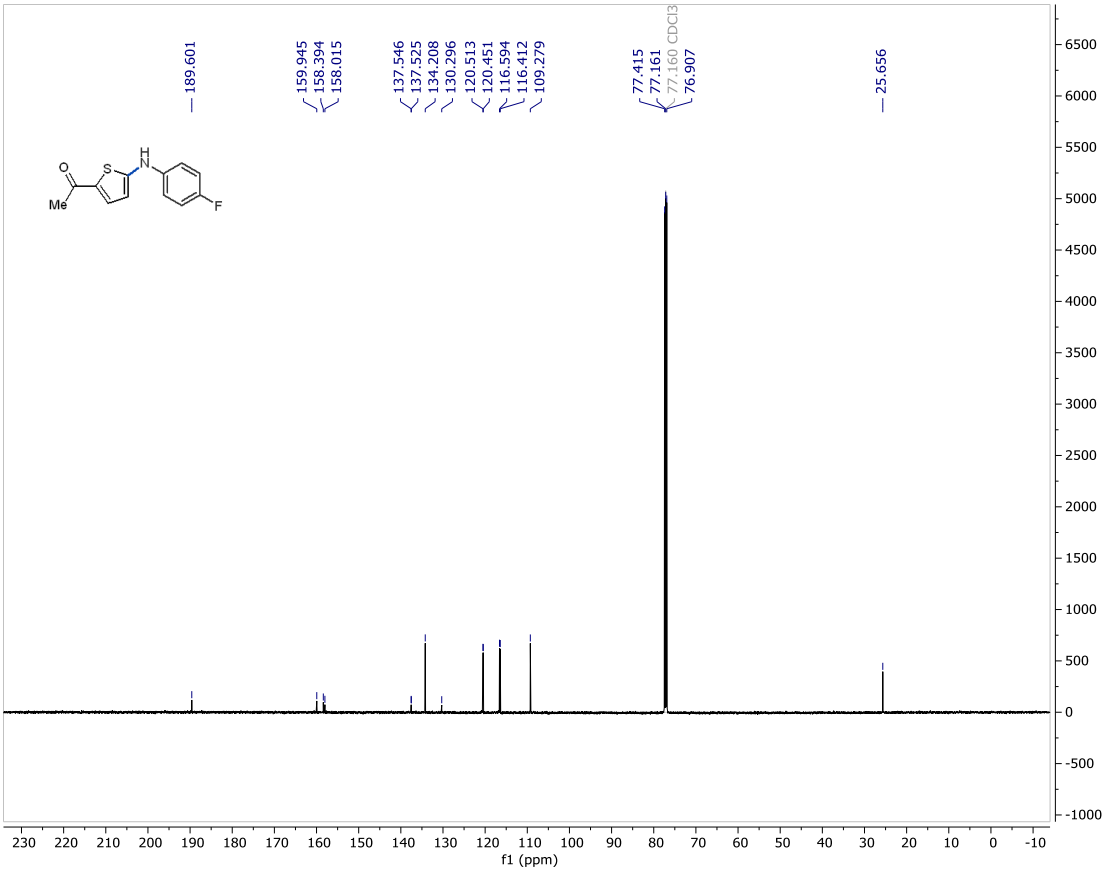

Figure S47. ^{13}C NMR (126 MHz, $CDCl_3$) of **7**.

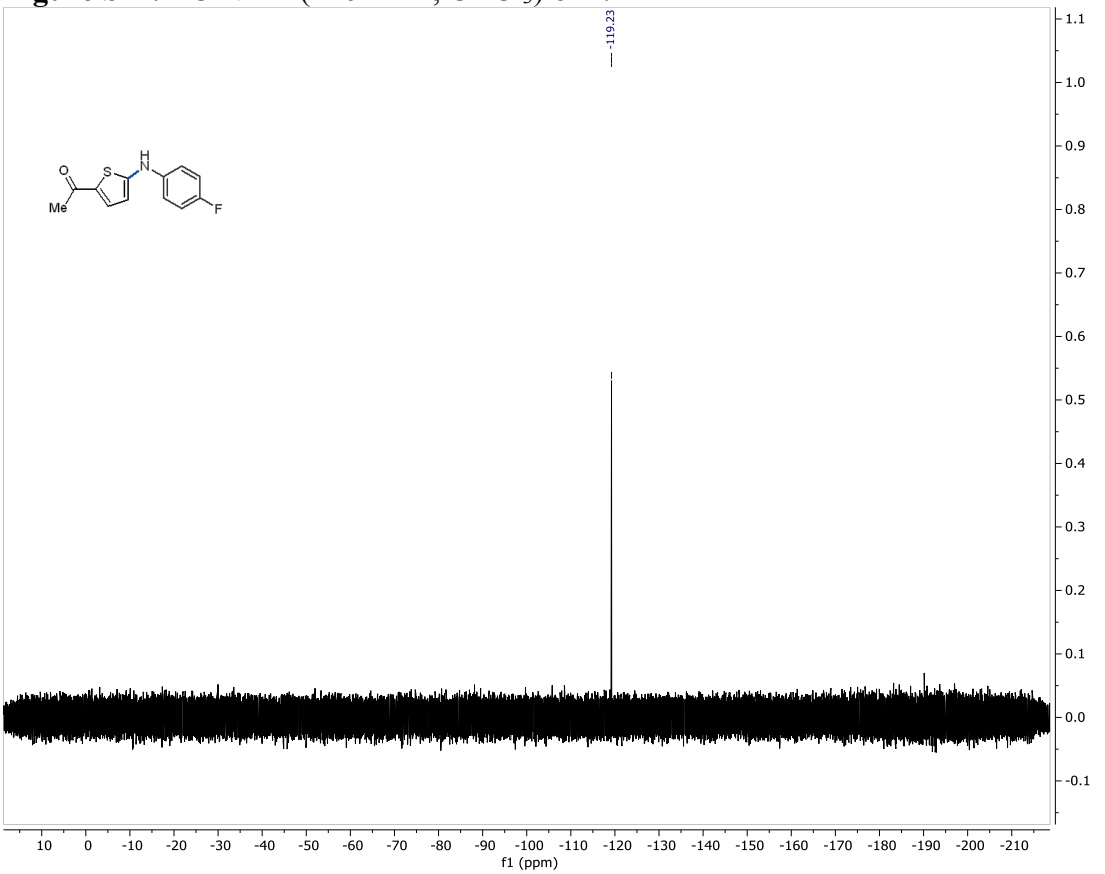

Figure S48. ^{19}F NMR (376 MHz, $CDCl_3$) of **7**.

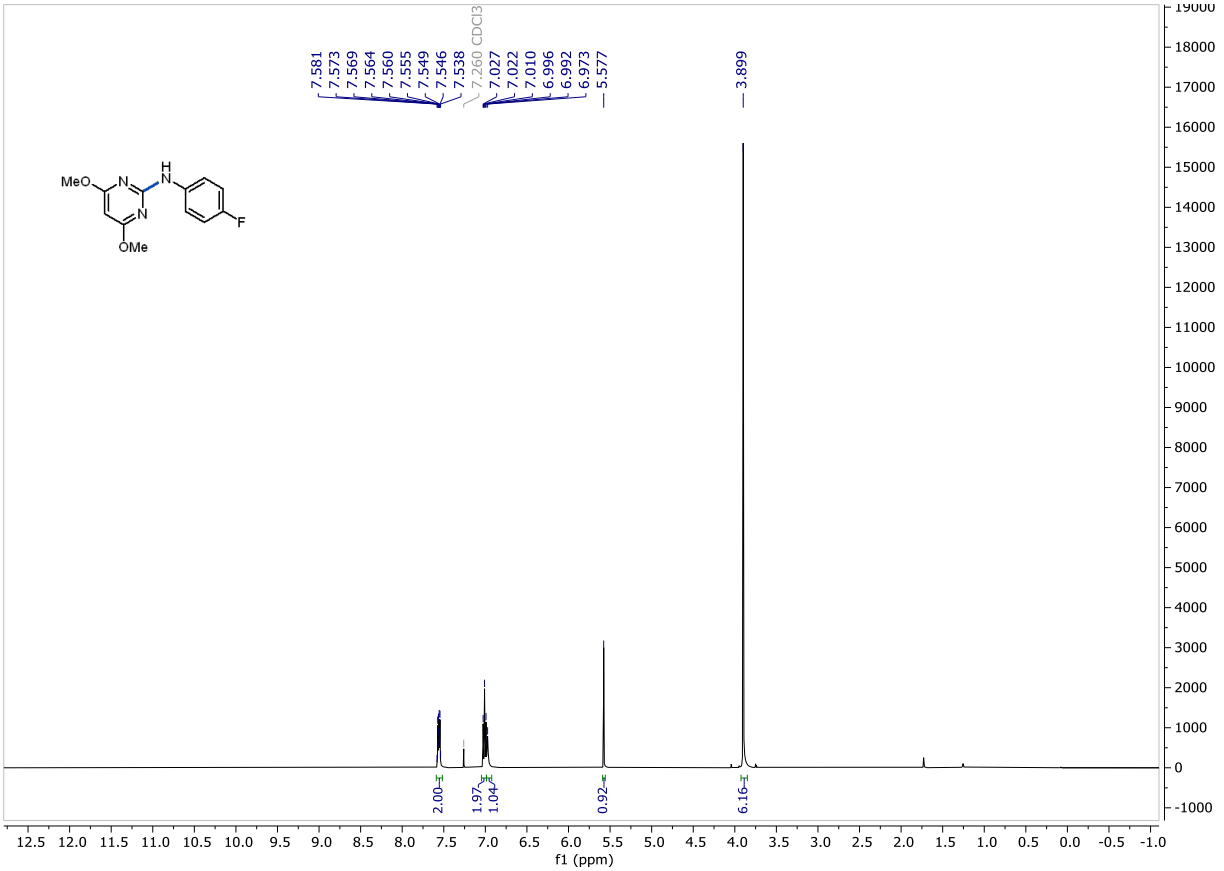

Figure S49. ^{1}H NMR (500 MHz, $CDCl_3$) of **8**.

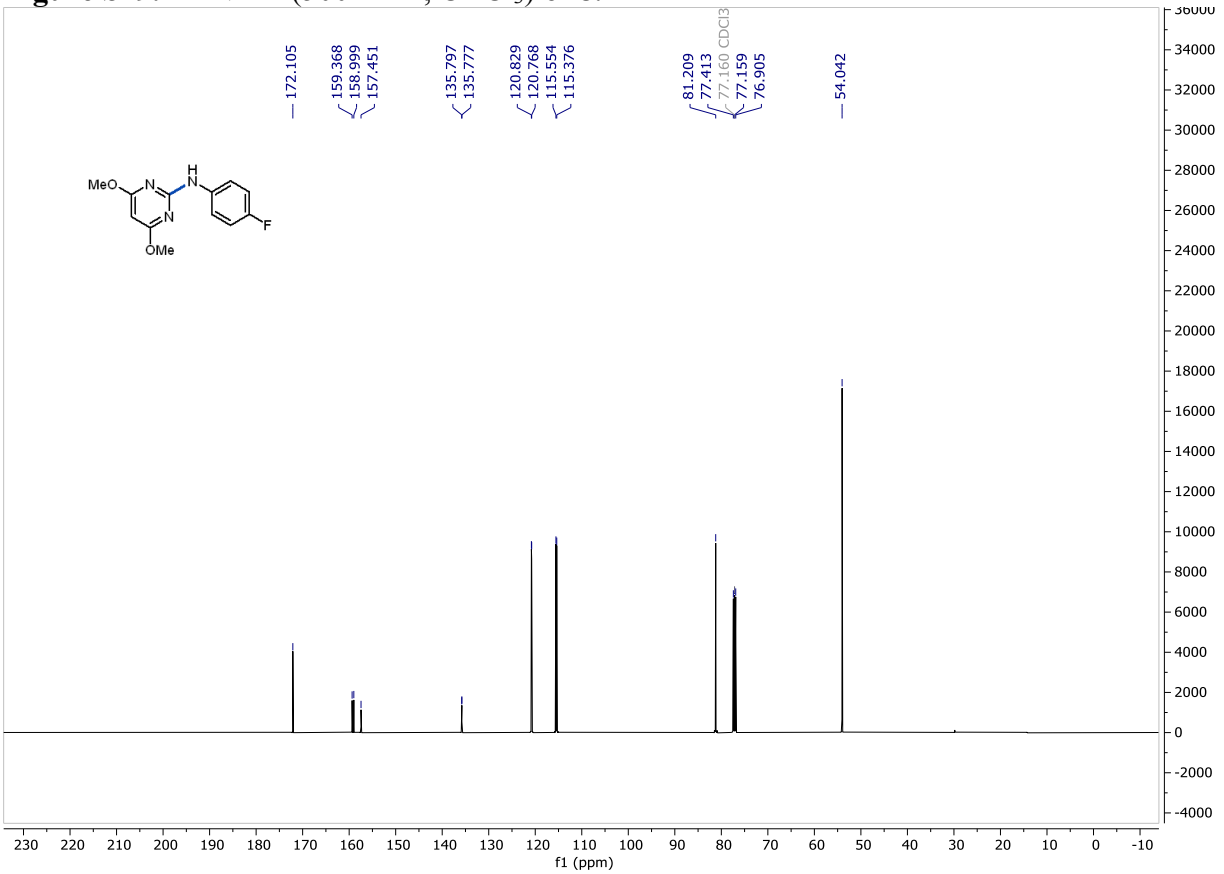

Figure S50. ^{13}C NMR (126 MHz, $CDCl_3$) of **8**.

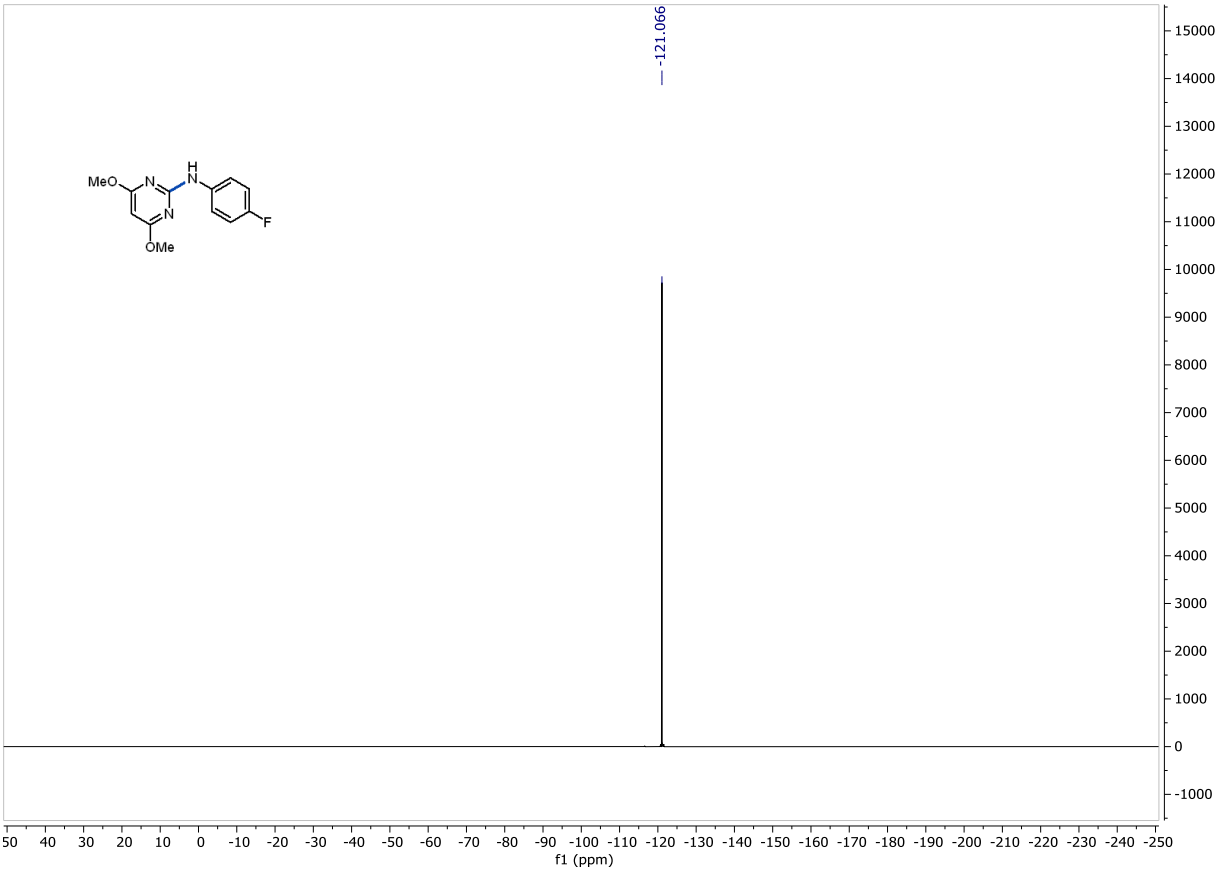

Figure S51. ^{19}F NMR (282 MHz, $CDCl_3$) of **8**.

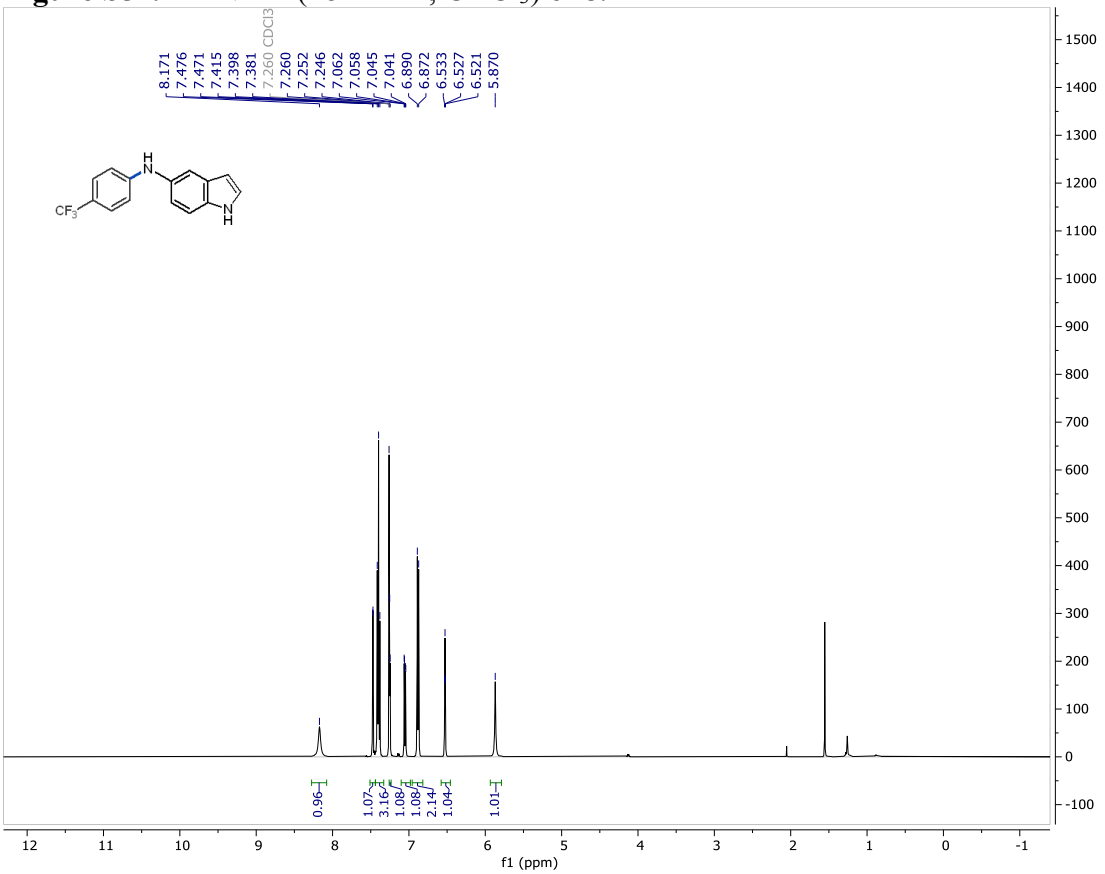

Figure S52. ^{1}H NMR (500 MHz, $CDCl_3$) of **9**.

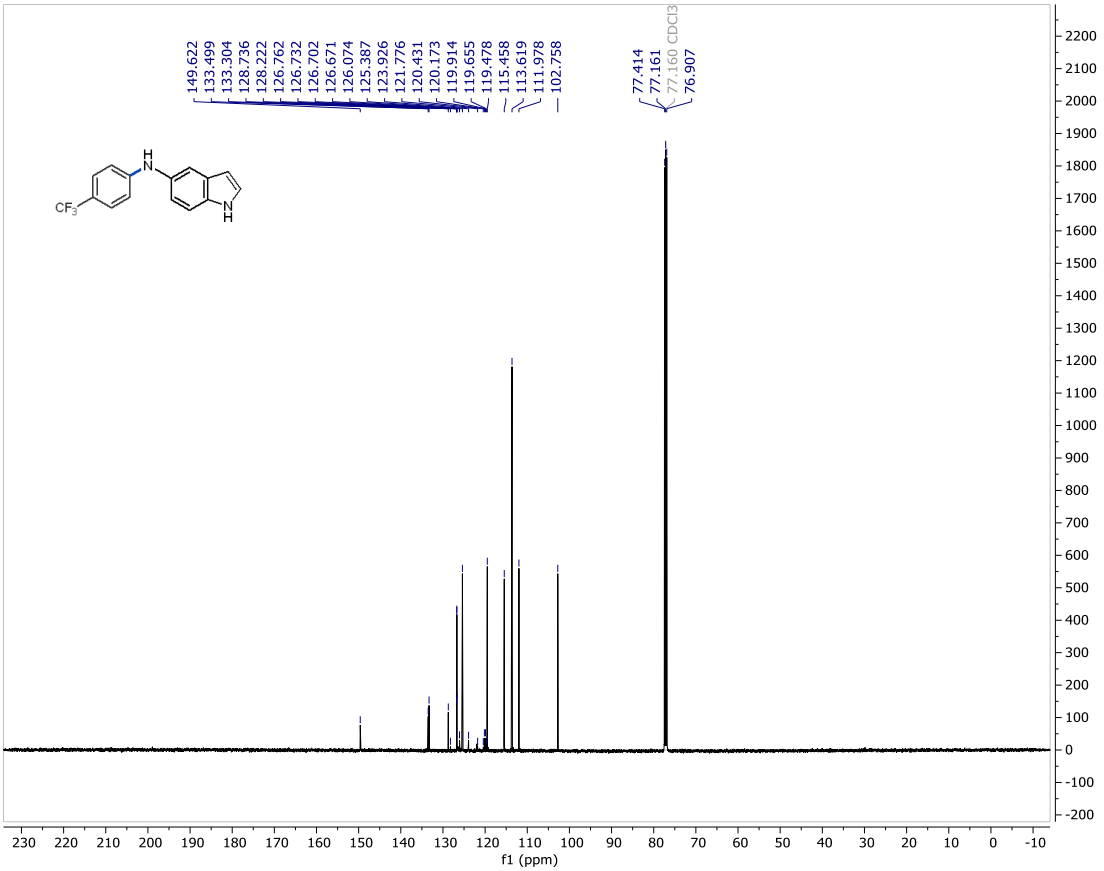

Figure S53. ^{13}C NMR (126 MHz, $CDCl_3$) of **9**.

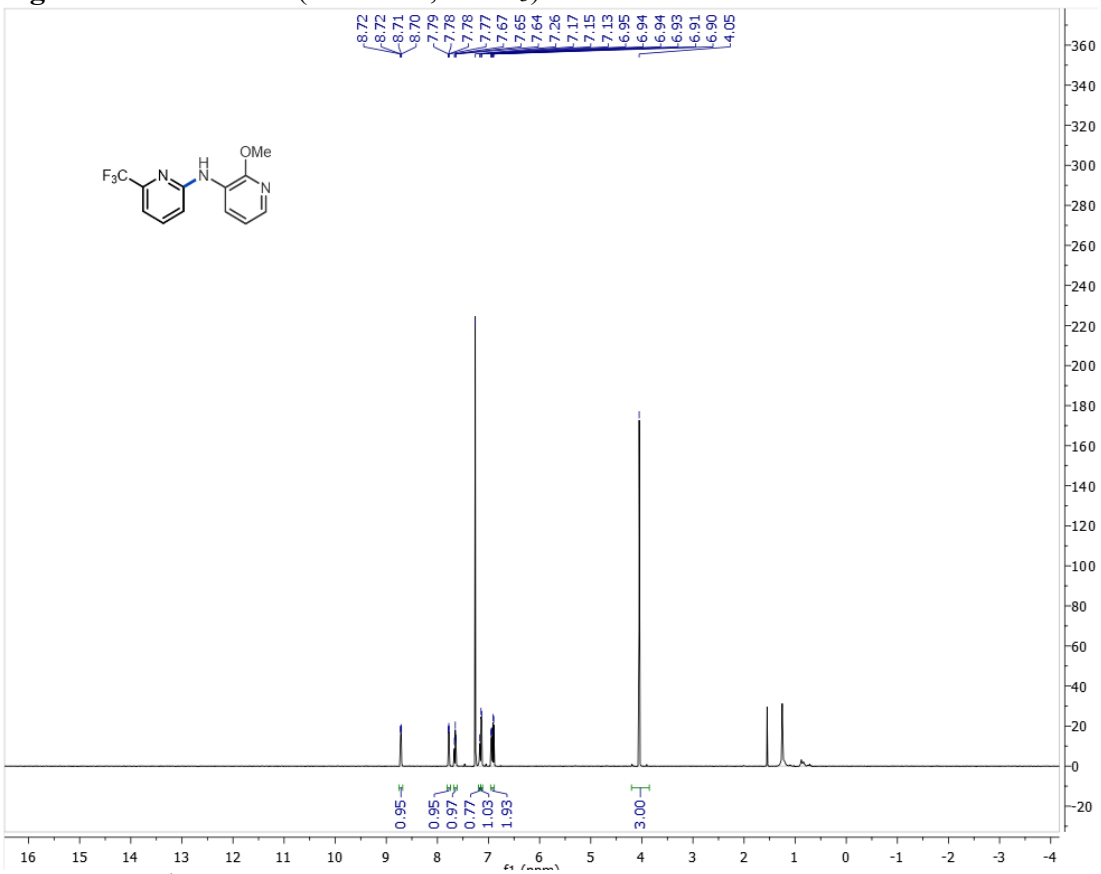

Figure S54. ^{1}H NMR (500 MHz, $CDCl_3$) of **10**.

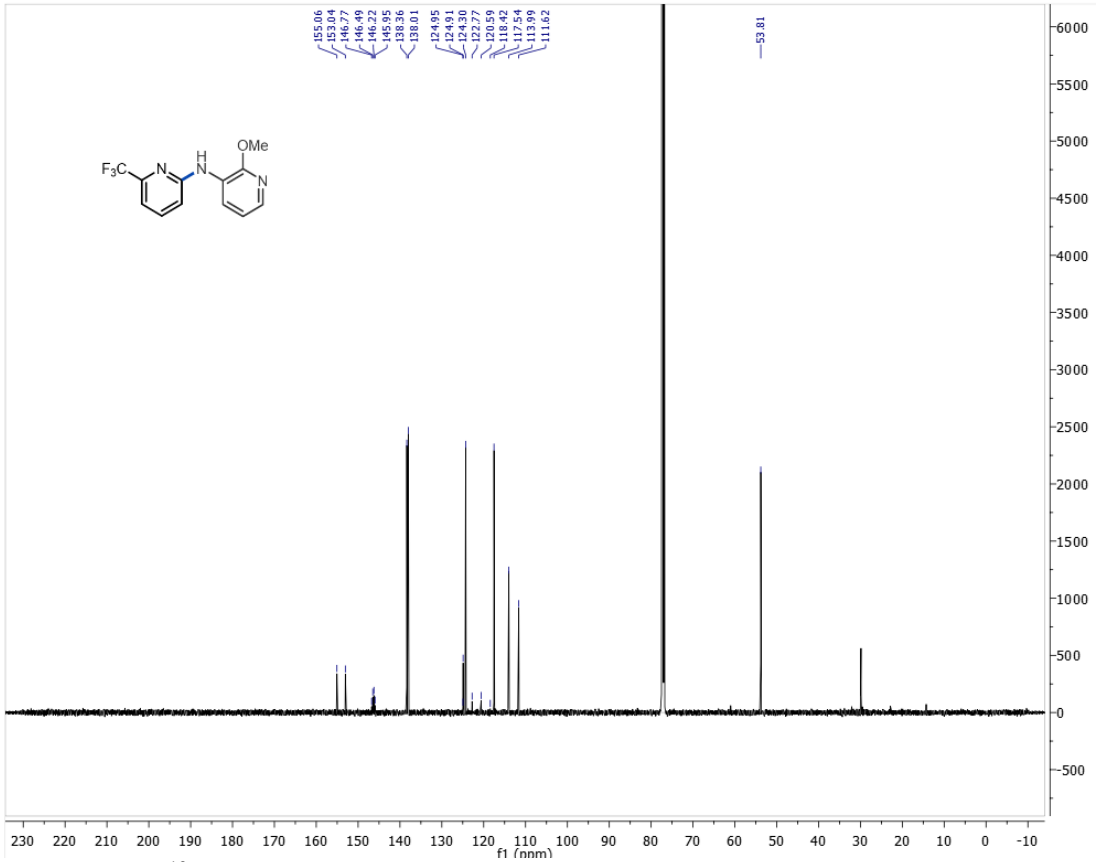

Figure S55. ^{13}C NMR (126 MHz, $CDCl_3$) of **10**.

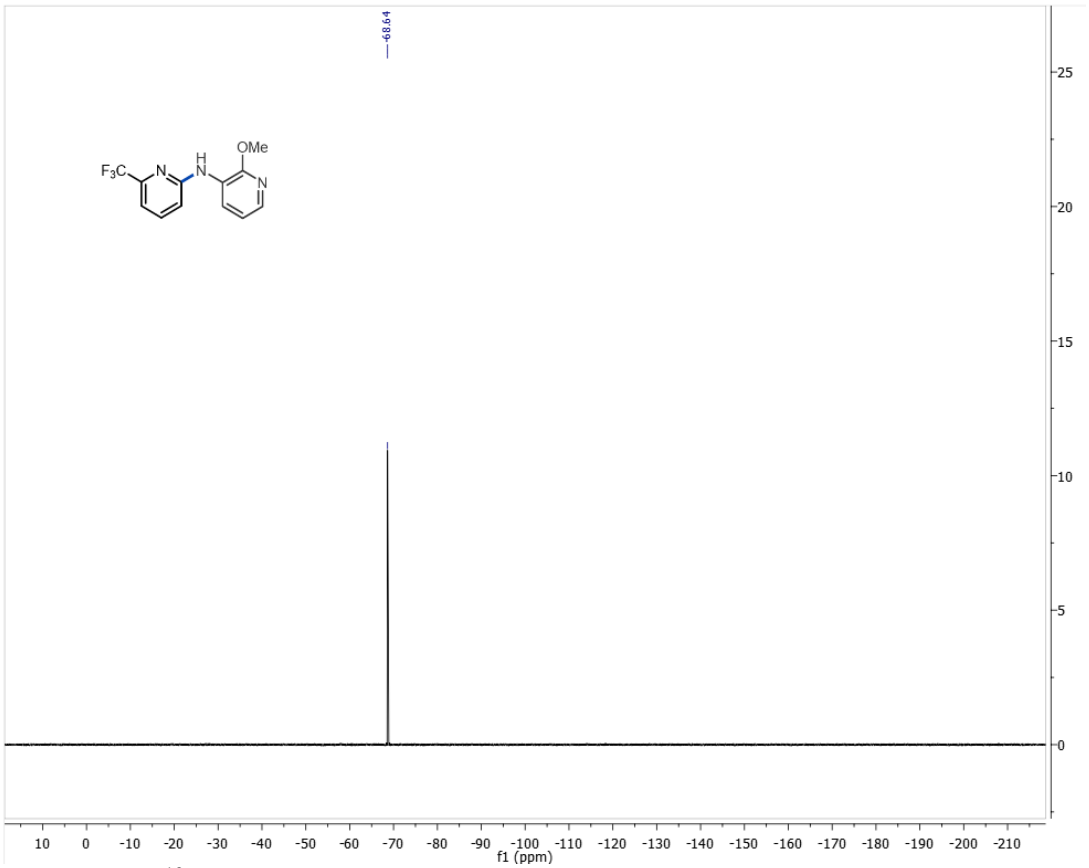

Figure S56. ^{19}F NMR (376 MHz, $CDCl_3$) of **10**.

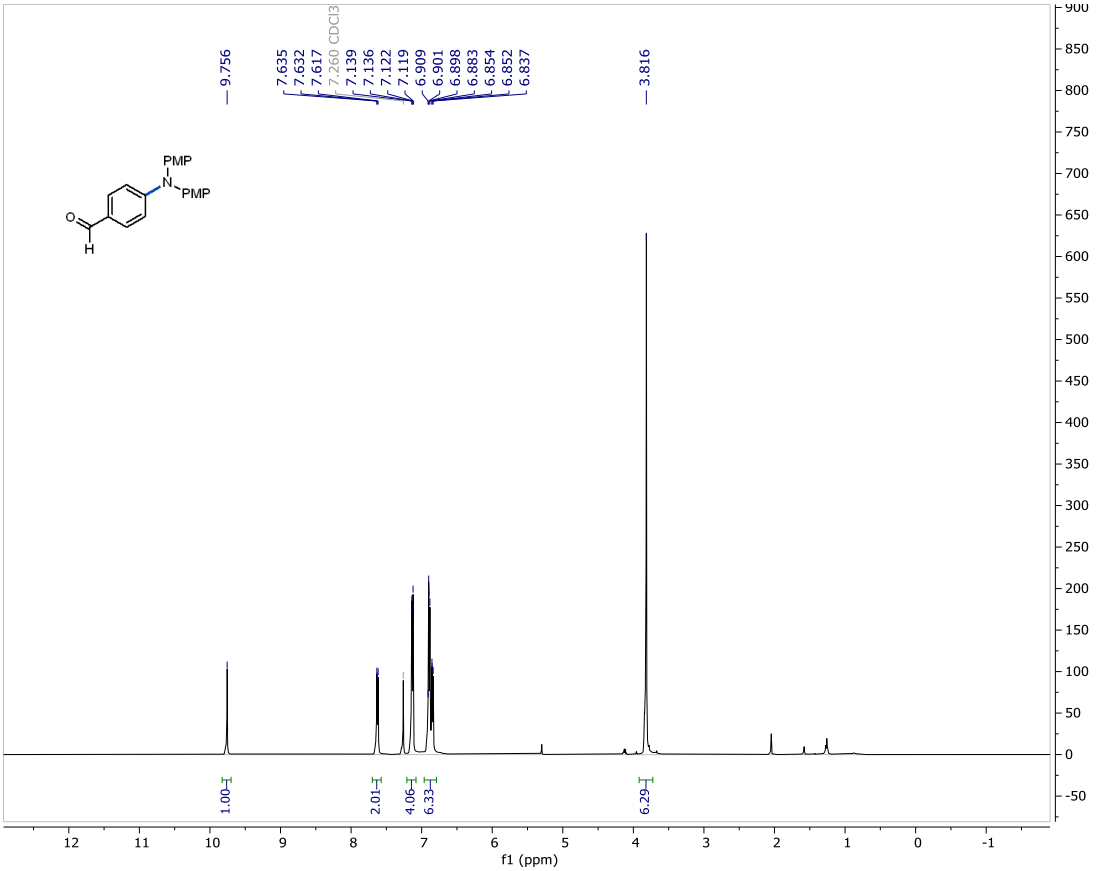

Figure S57. ^{1}H NMR (500 MHz, $CDCl_3$) of **11**.

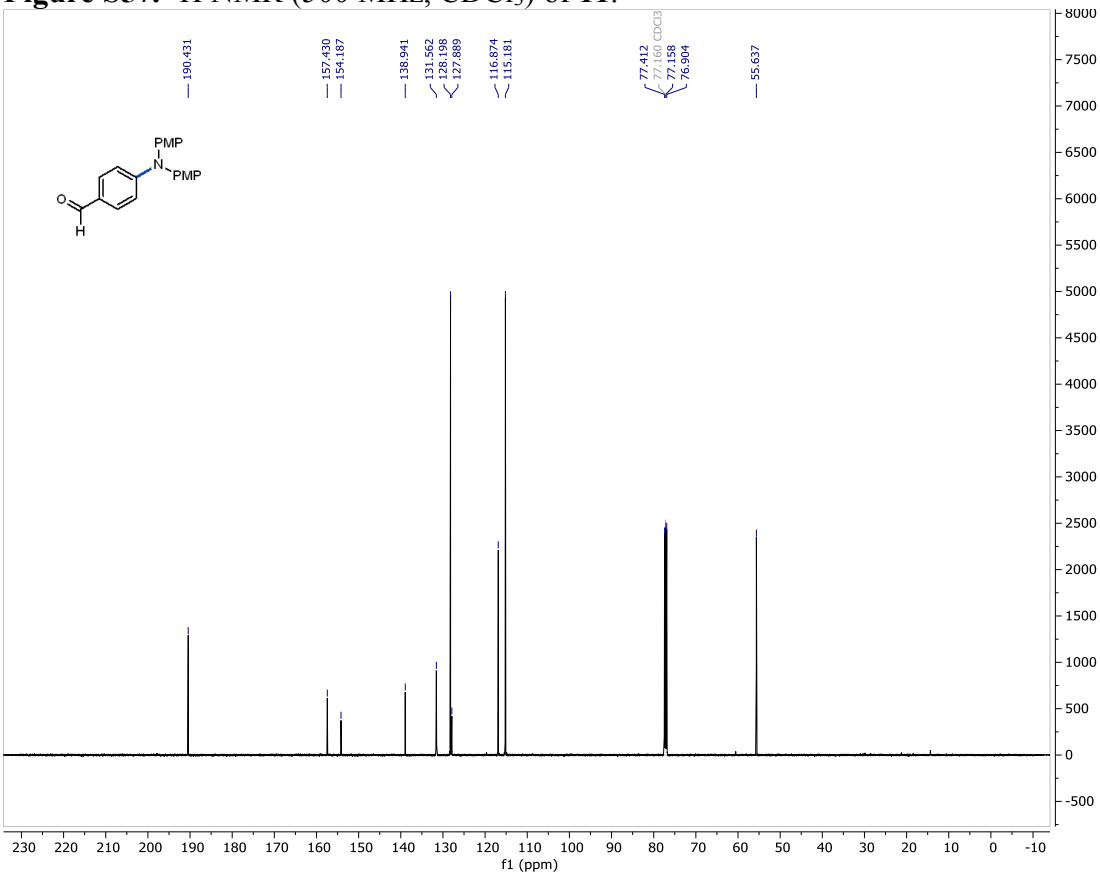

Figure S58. ^{13}C NMR (126 MHz, $CDCl_3$) of **11**.

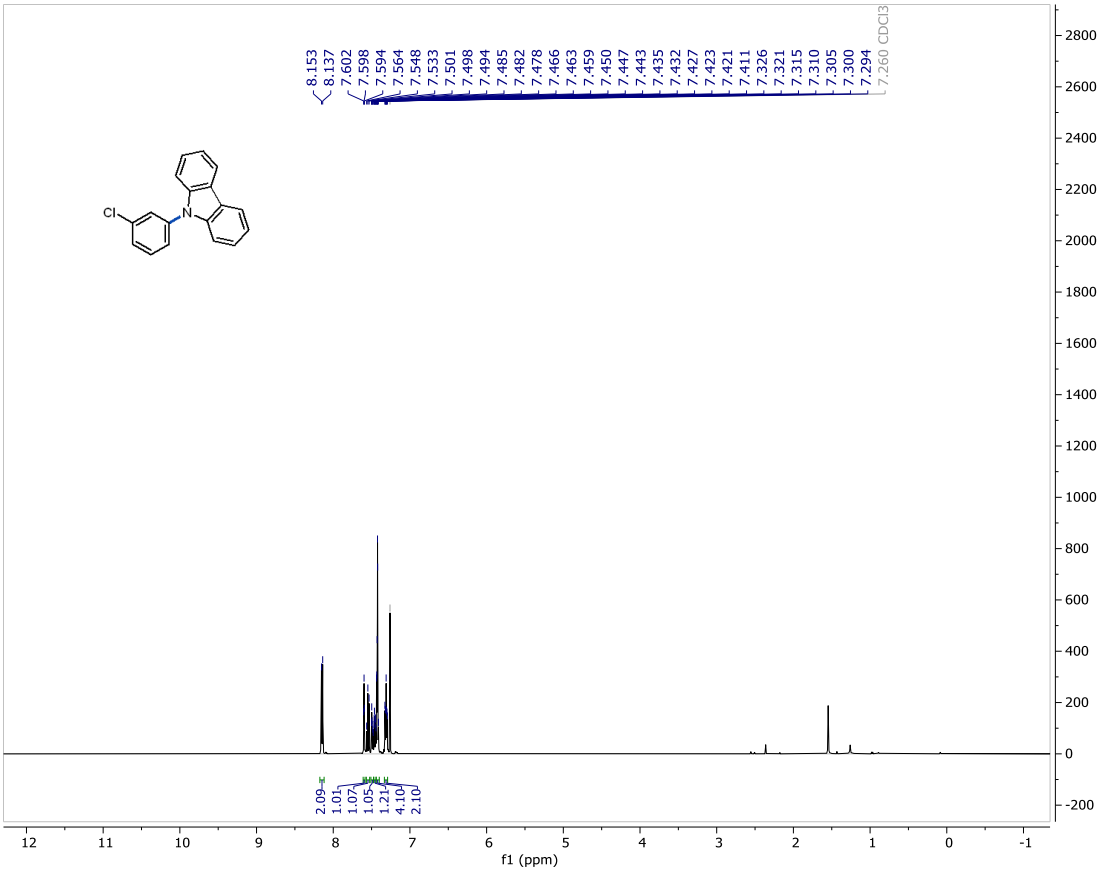

Figure S59. ^{1}H NMR (500 MHz, $CDCl_3$) of **12**.

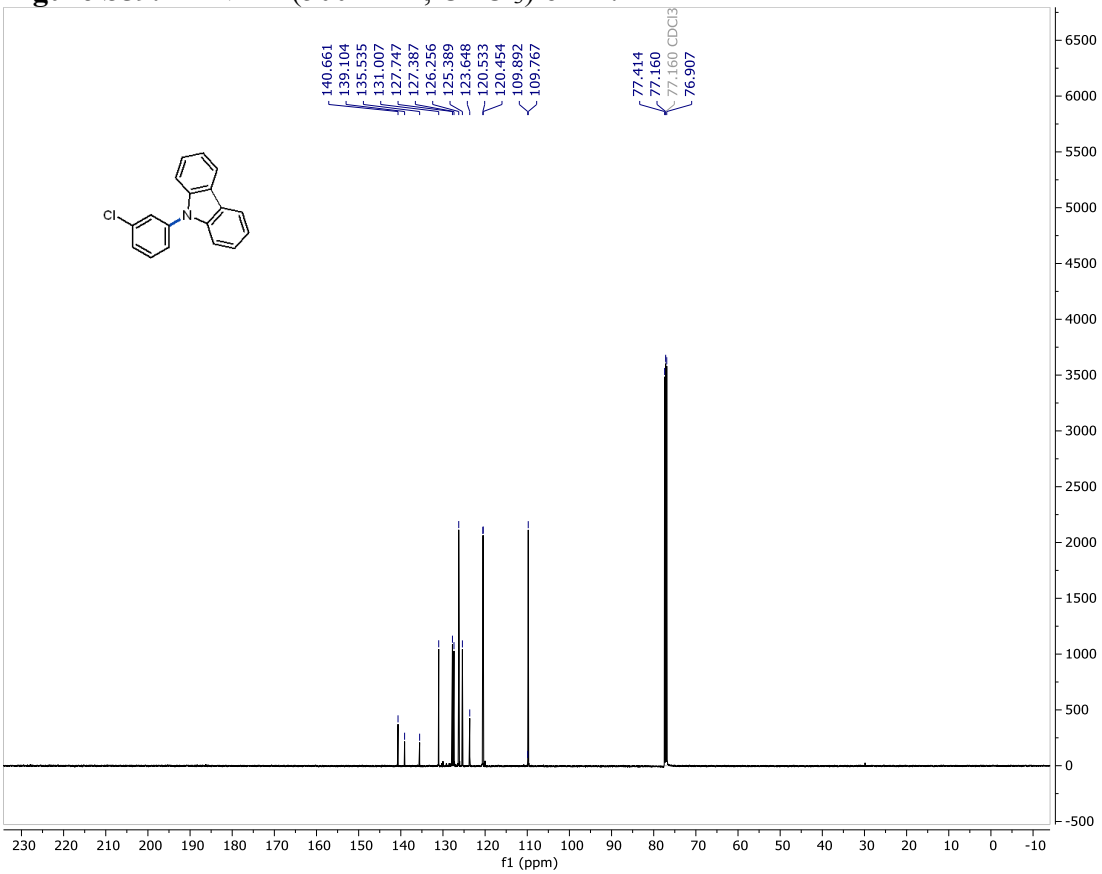

Figure S60. ^{13}C NMR (126 MHz, $CDCl_3$) of **12**.

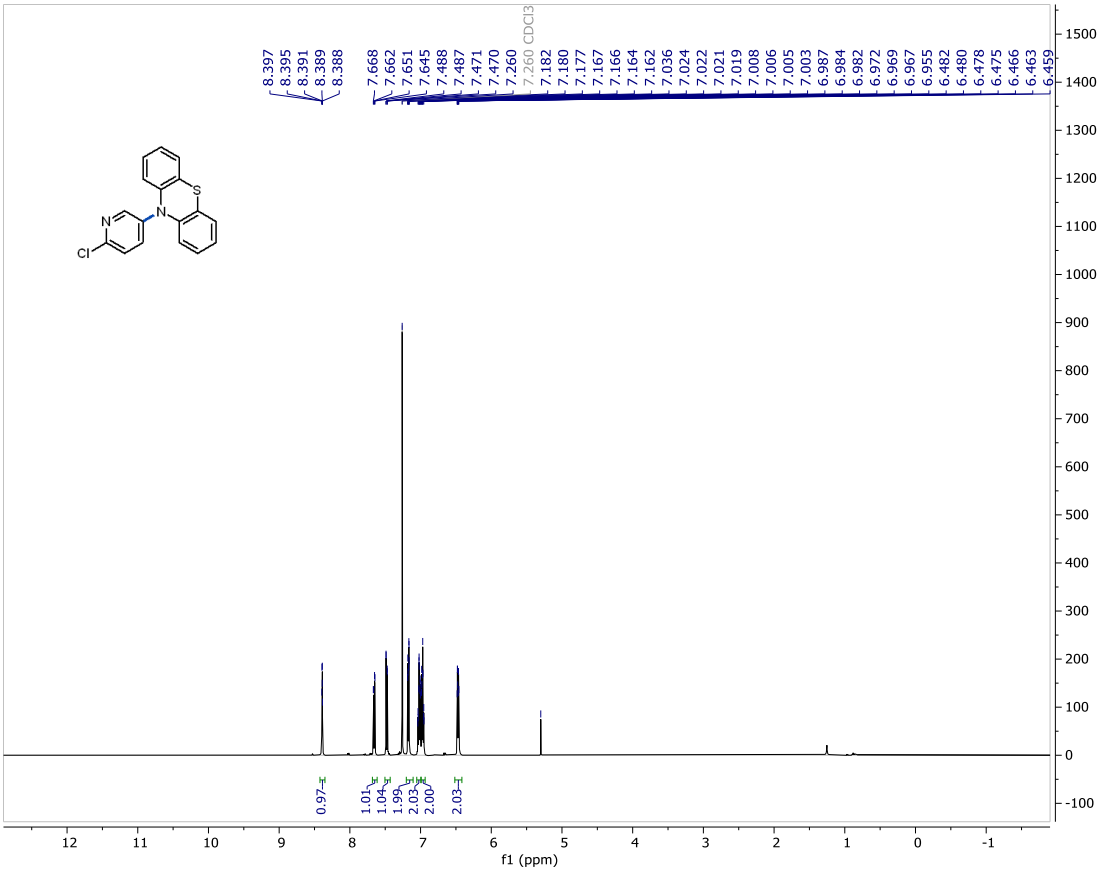

Figure S61. ^{1}H NMR (500 MHz, $CDCl_3$) of **13**.

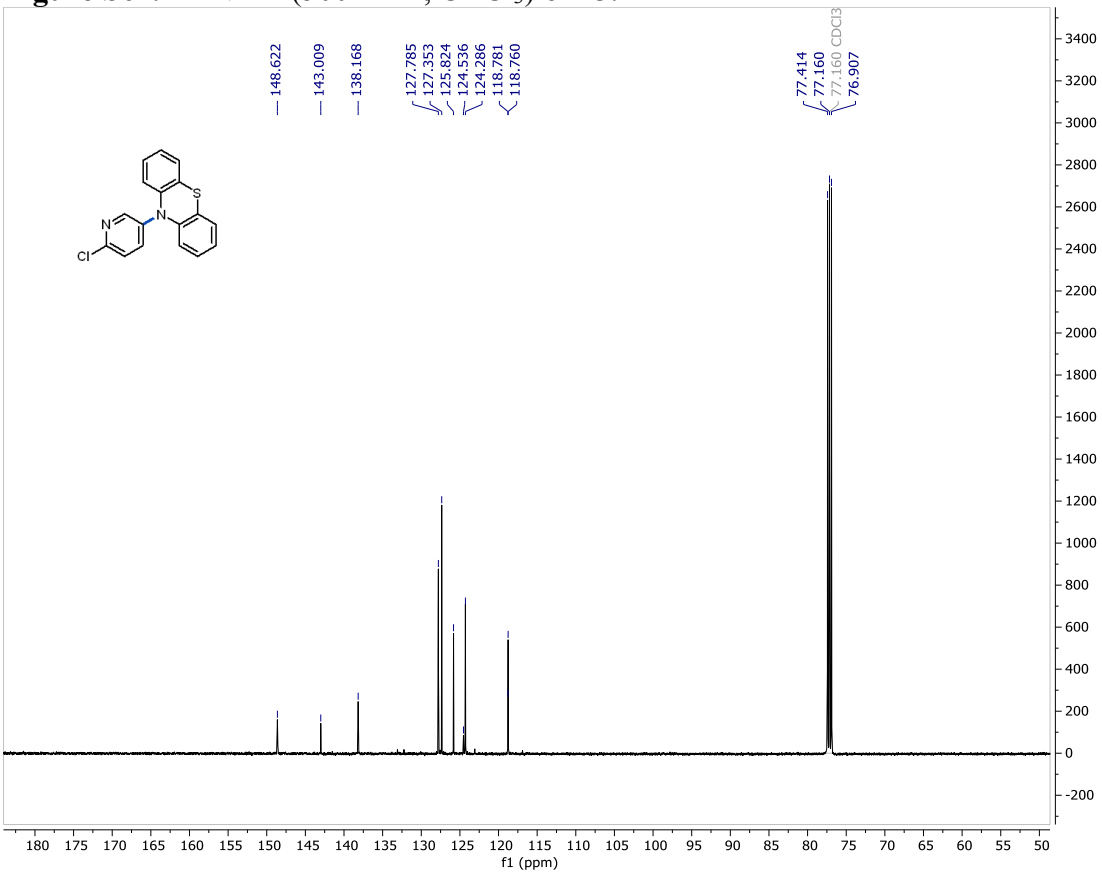

Figure S62. ^{13}C NMR (126 MHz, $CDCl_3$) of **13**.

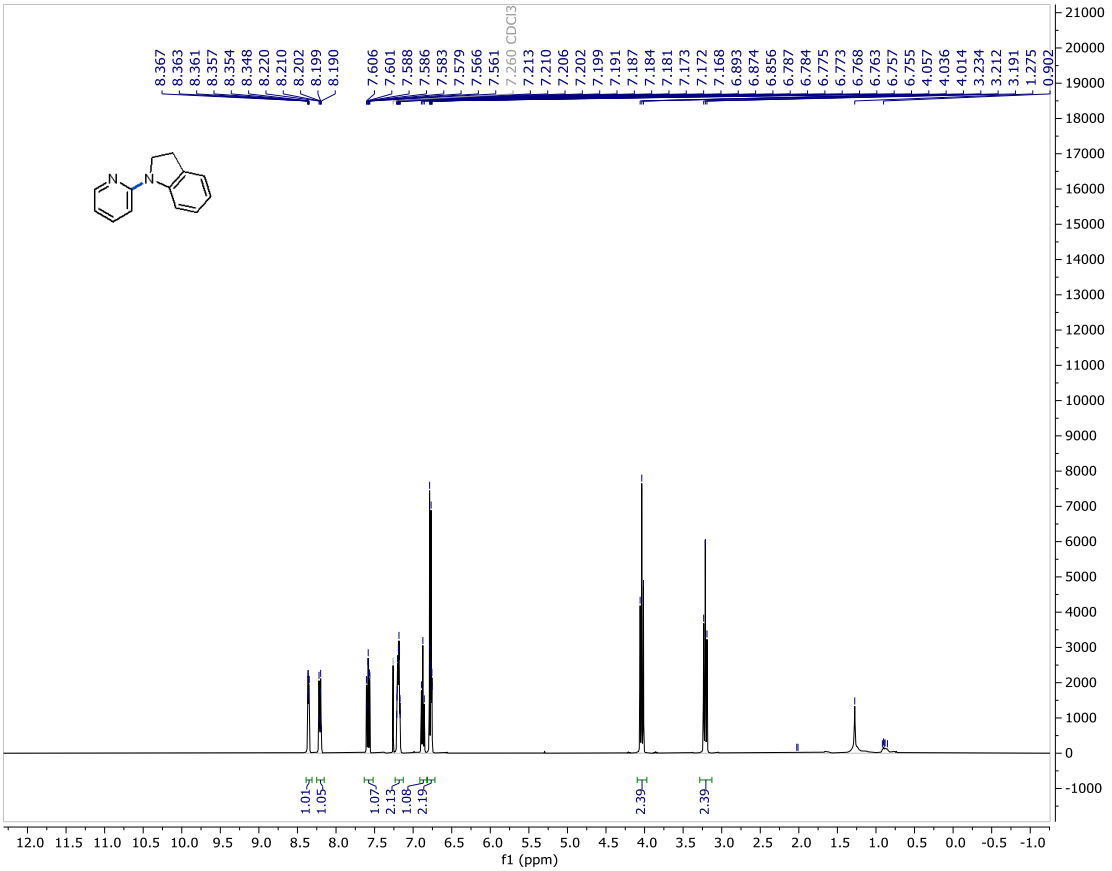

Figure S63. ^{1}H NMR (500 MHz, $CDCl_3$) of **14**.

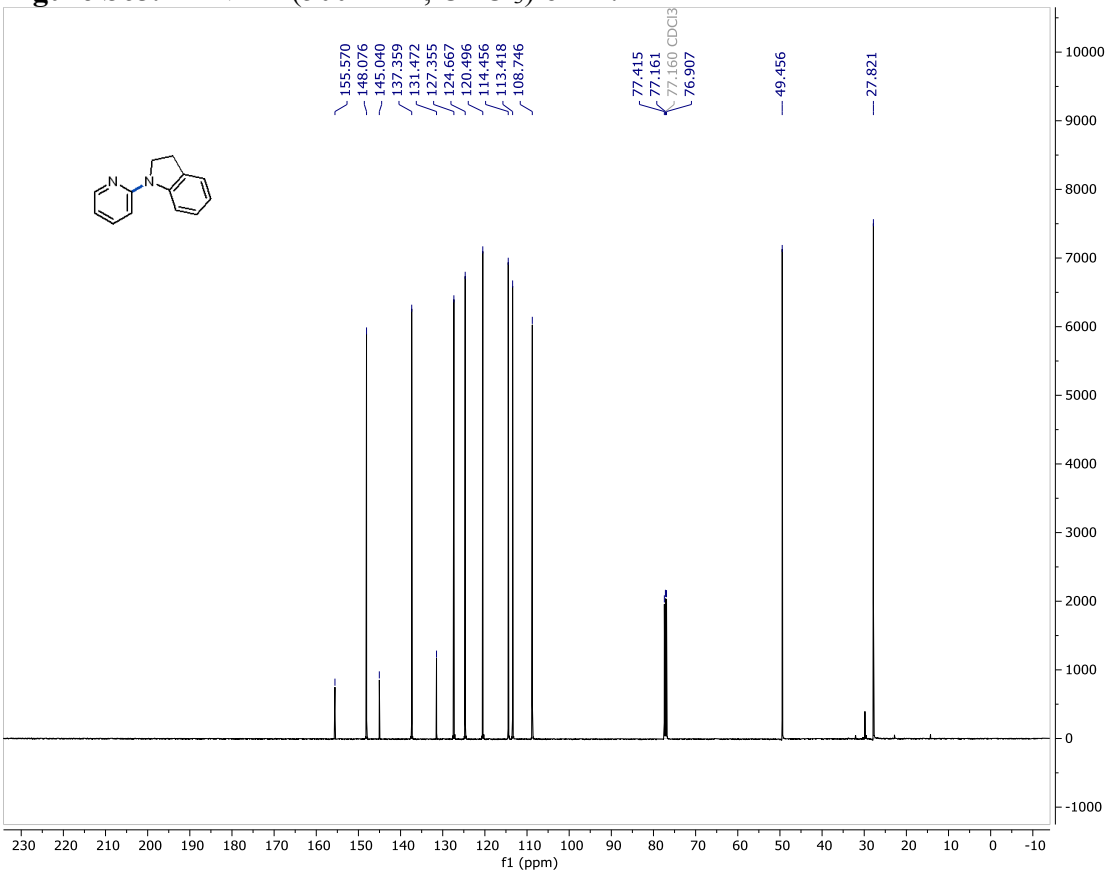

Figure S64. ^{13}C NMR (126 MHz, $CDCl_3$) of **14**.

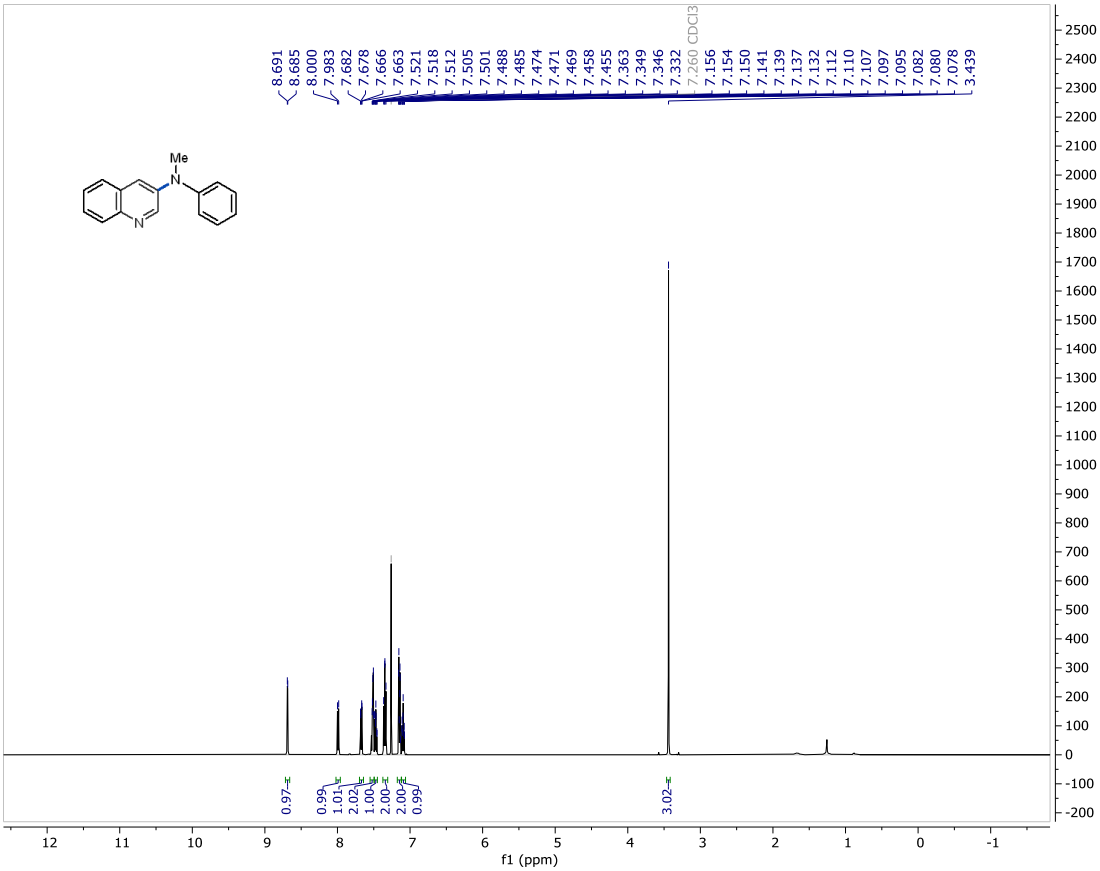

Figure S65. ^{1}H NMR (500 MHz, $CDCl_3$) of **15**.

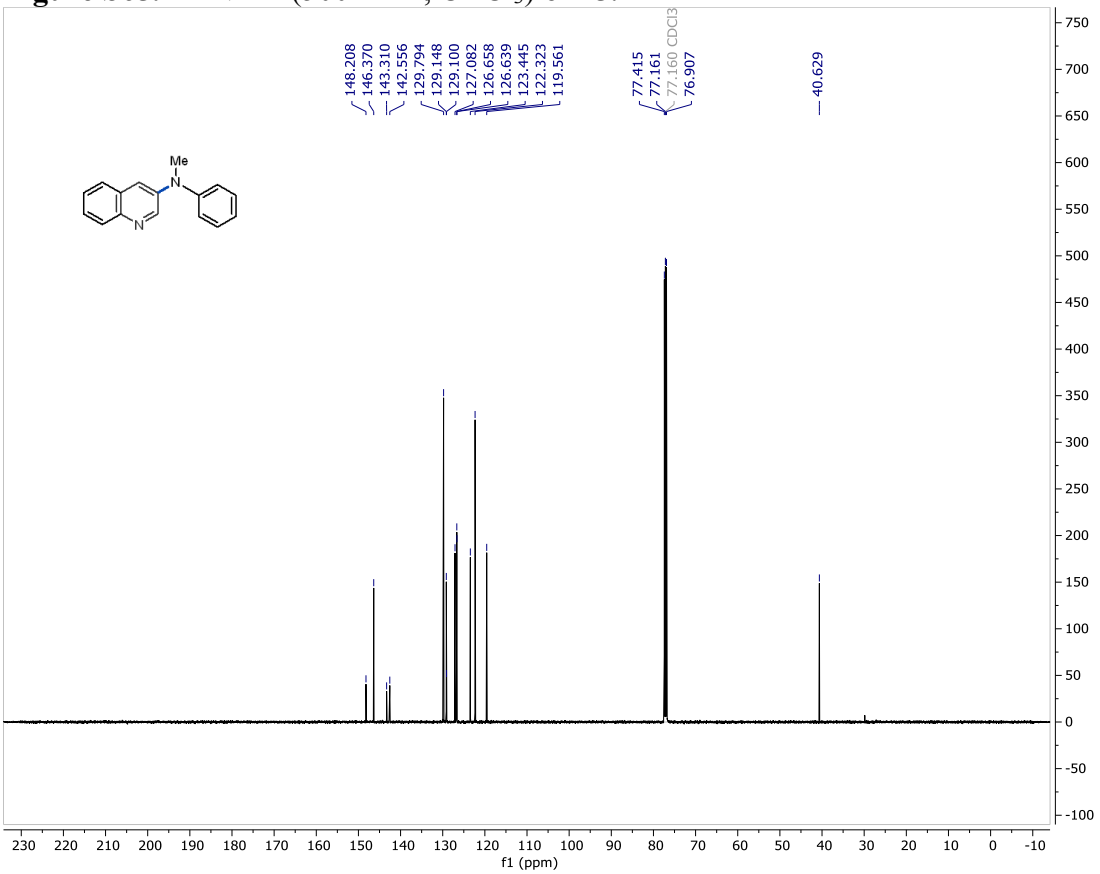

Figure S66. ^{13}C NMR (126 MHz, $CDCl_3$) of **15**.

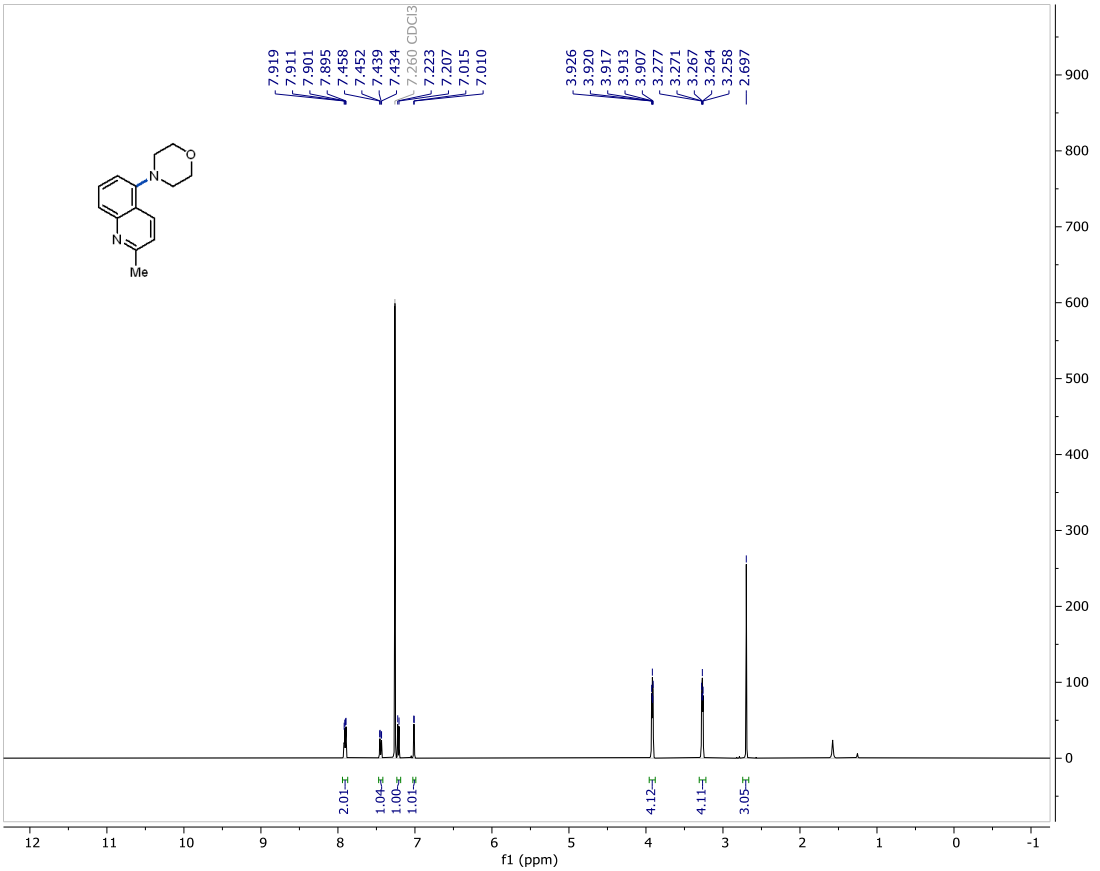

Figure S67. ^{1}H NMR (500 MHz, $CDCl_3$) of **16**.

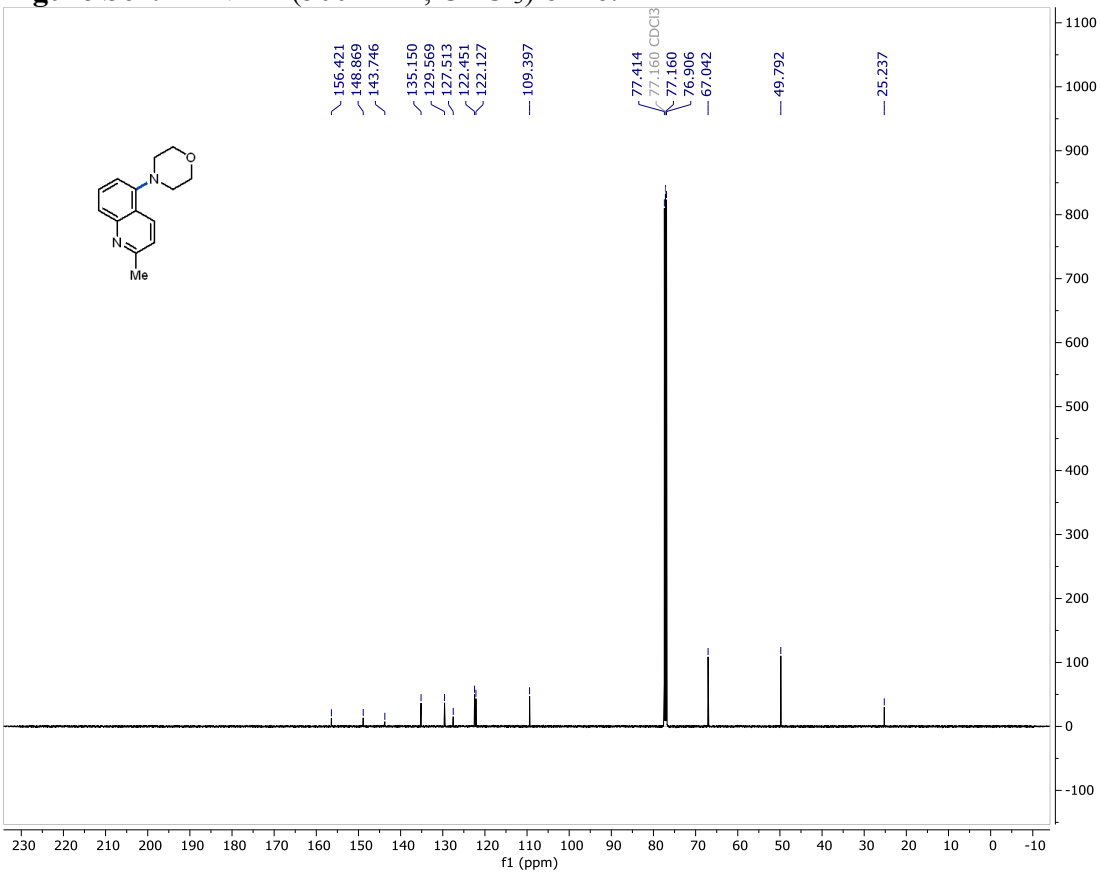

Figure S68. ^{13}C NMR (126 MHz, $CDCl_3$) of **16**.

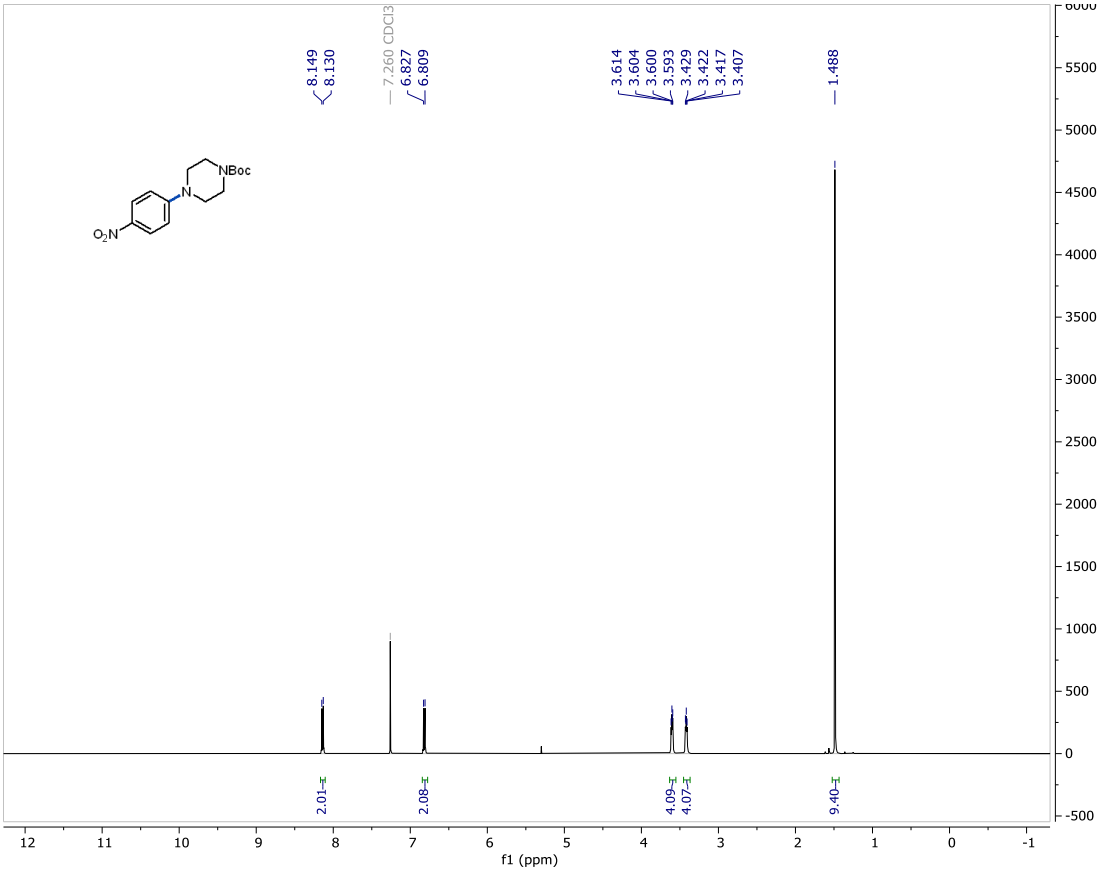

Figure S69. ^{1}H NMR (500 MHz, $CDCl_3$) of **17**.

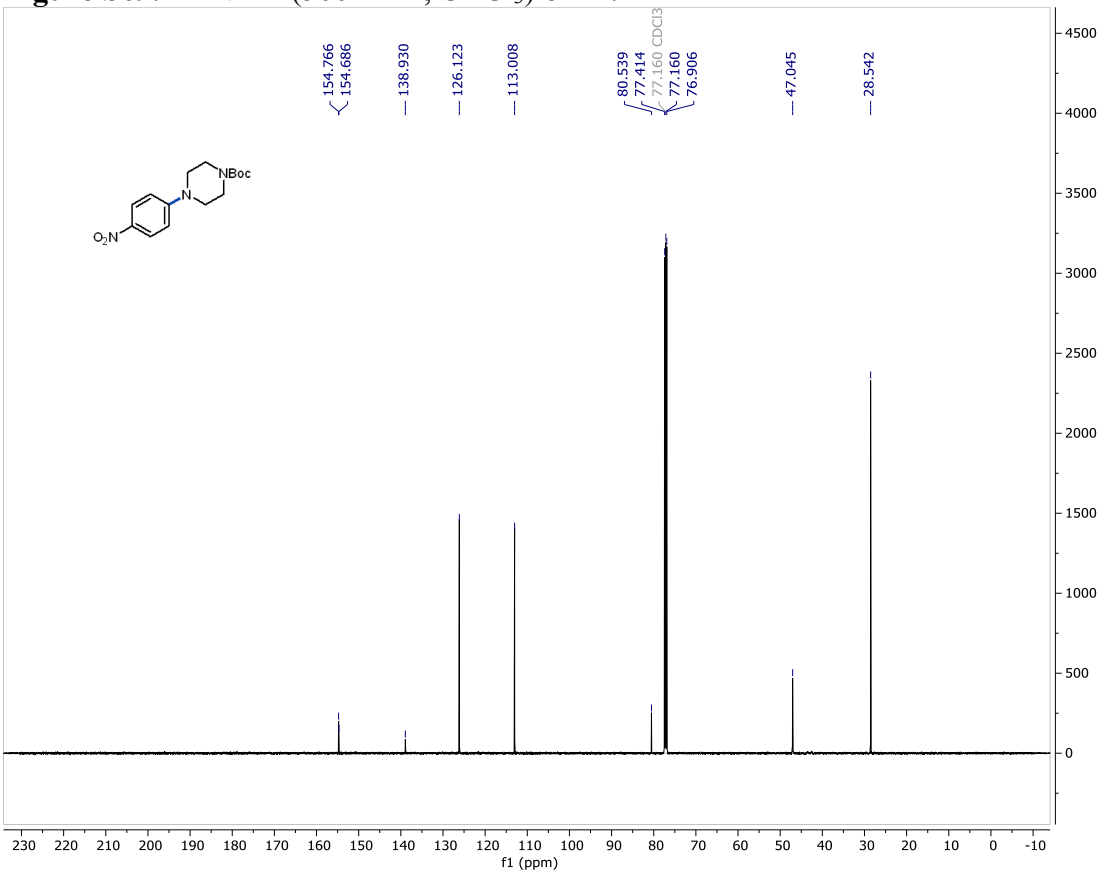

Figure S70. ^{13}C NMR (126 MHz, $CDCl_3$) of **17**.

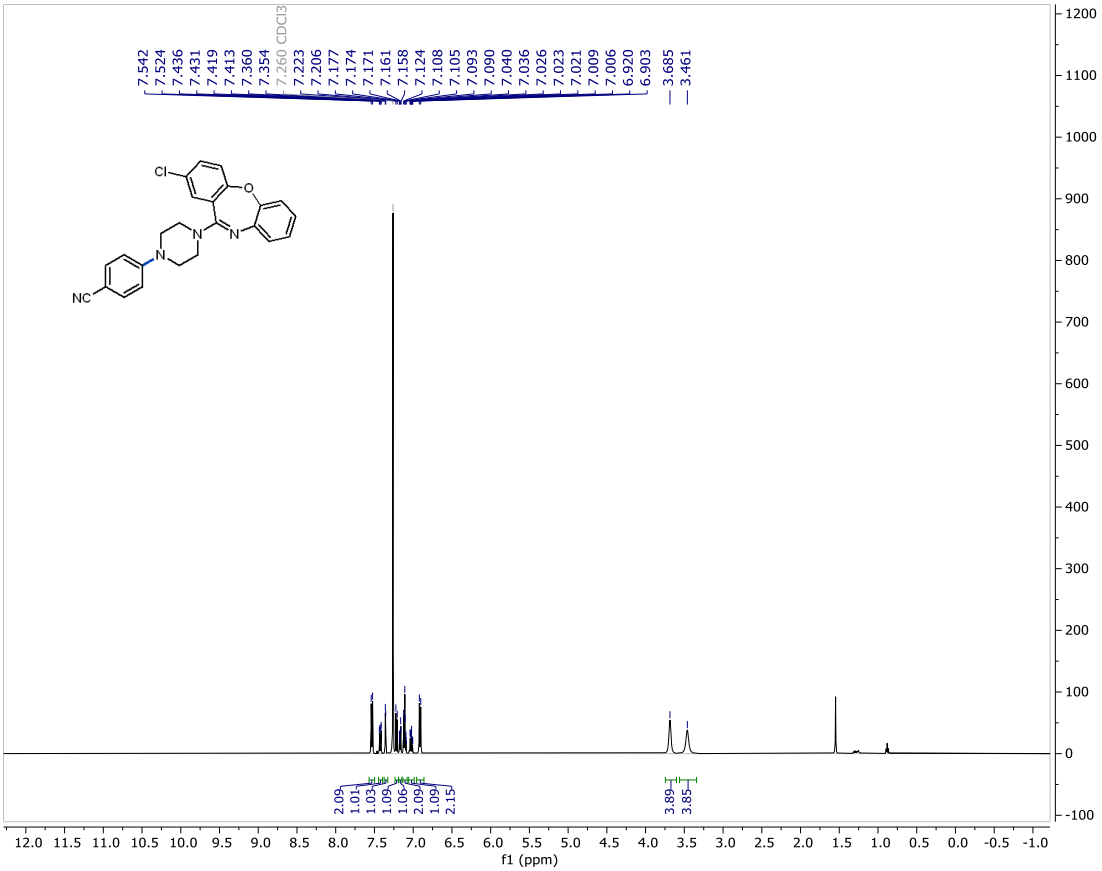

Figure S71. ^{1}H NMR (500 MHz, $CDCl_3$) of **18**.

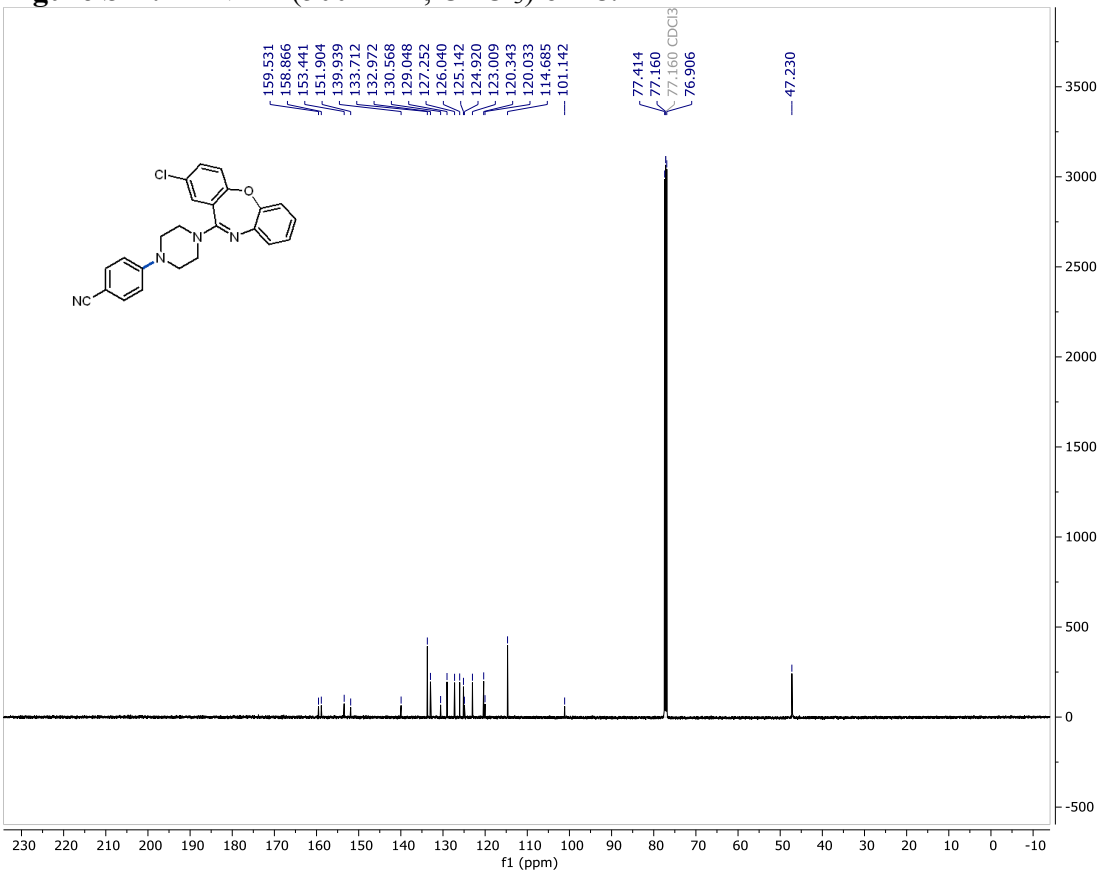

Figure S72. ^{13}C NMR (126 MHz, $CDCl_3$) of **18**.

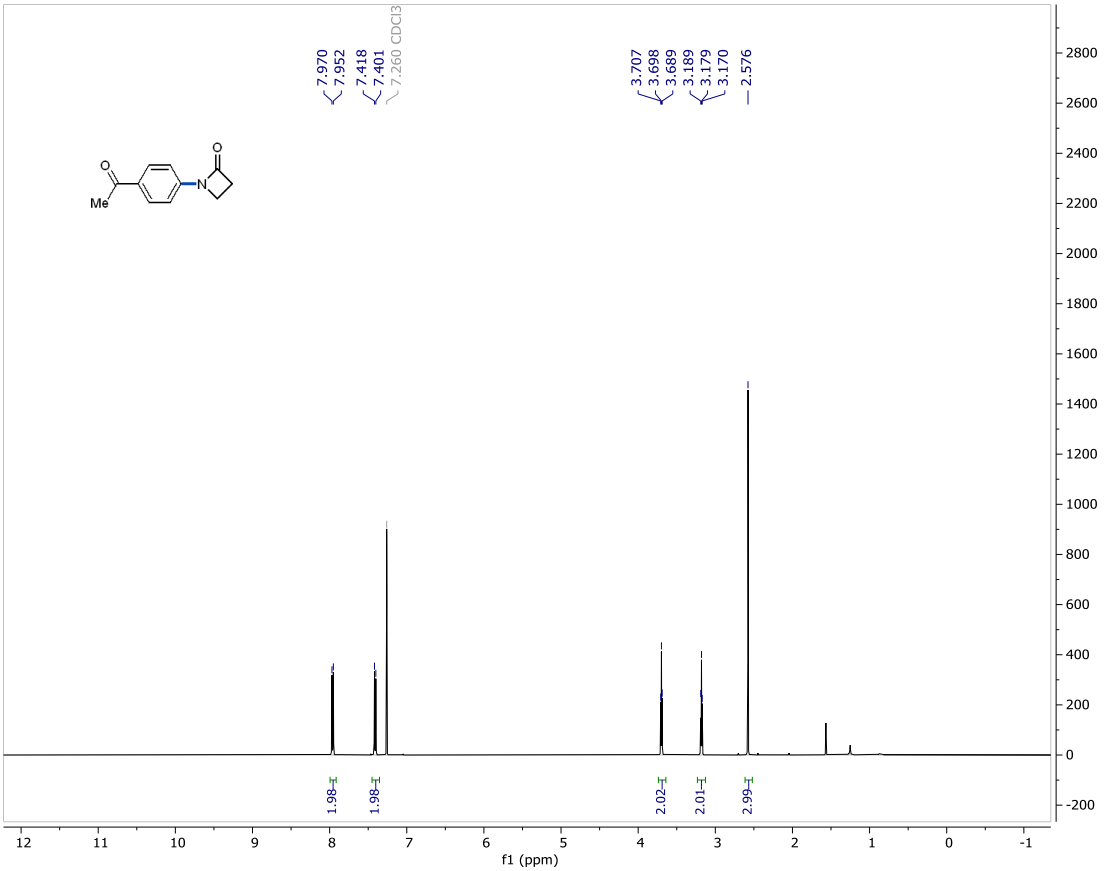

Figure S73. ^{1}H NMR (500 MHz, $CDCl_3$) of **19**.

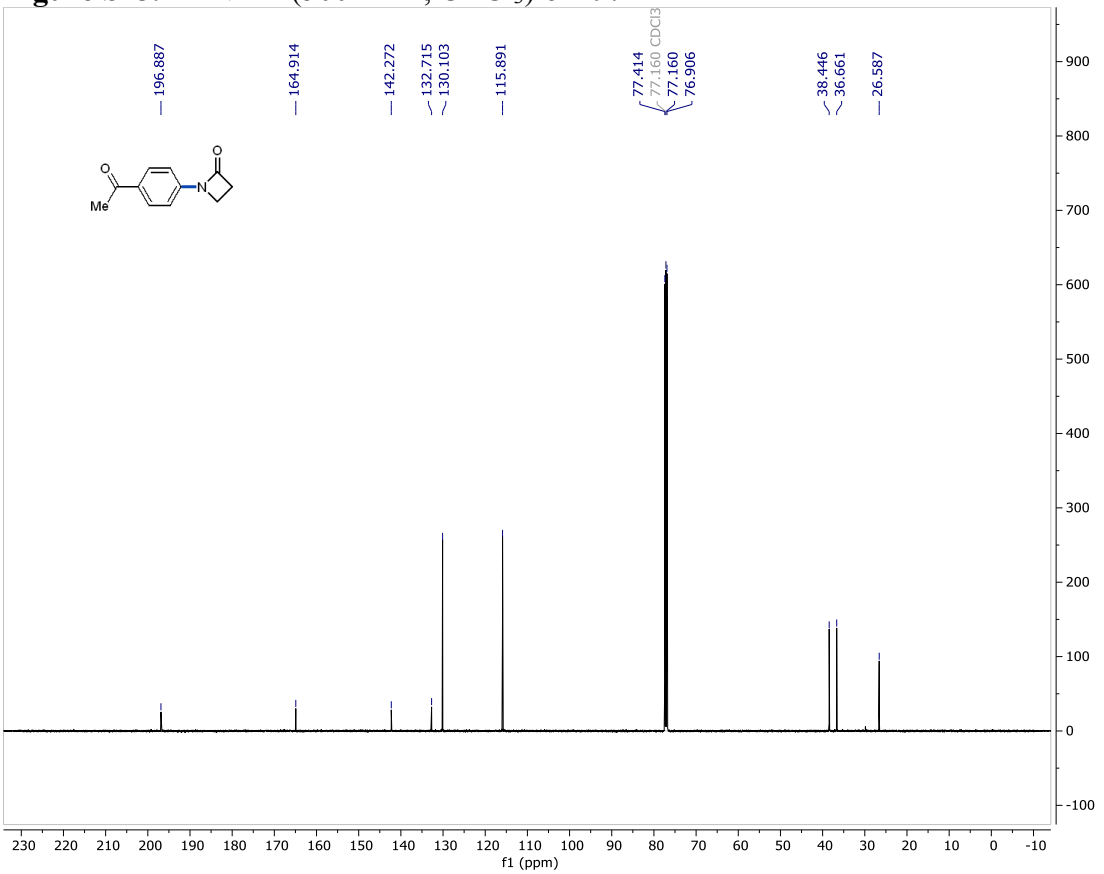

Figure S74. ^{13}C NMR (126 MHz, $CDCl_3$) of **19**.

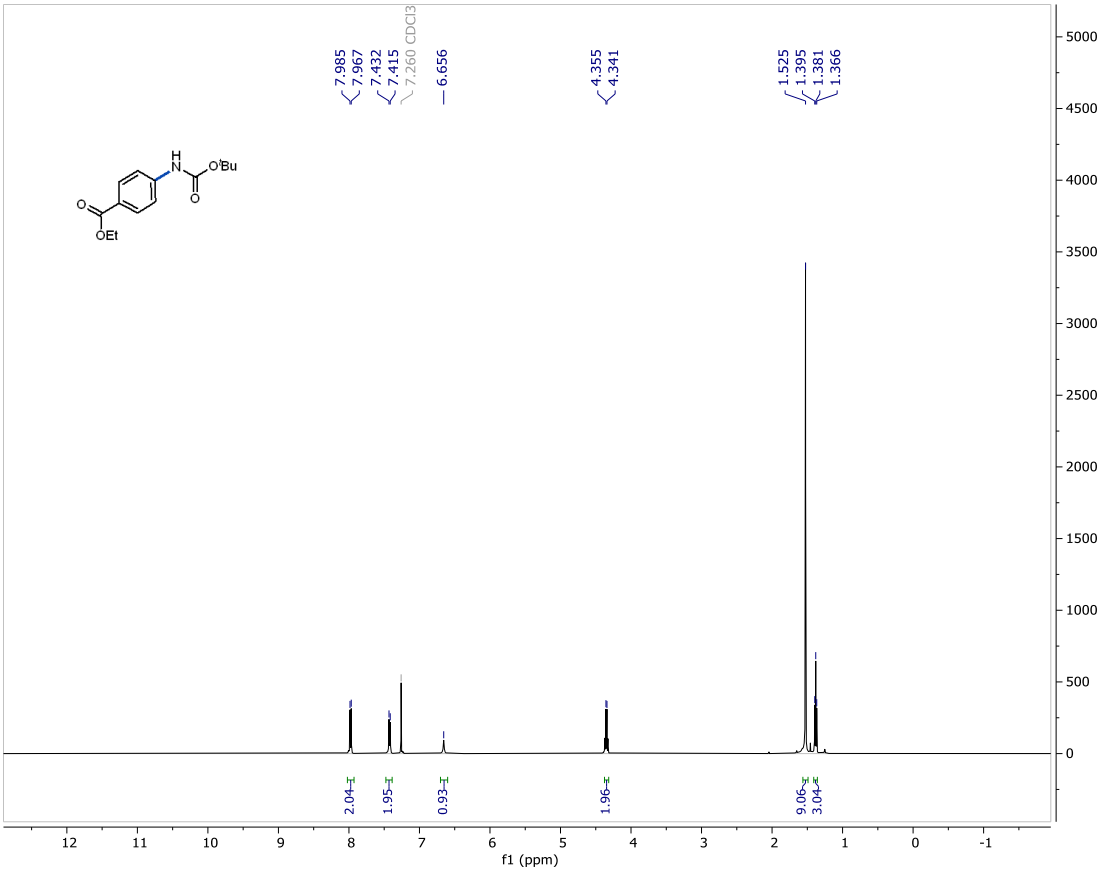

Figure S75. ^{1}H NMR (500 MHz, $CDCl_3$) of **20**.

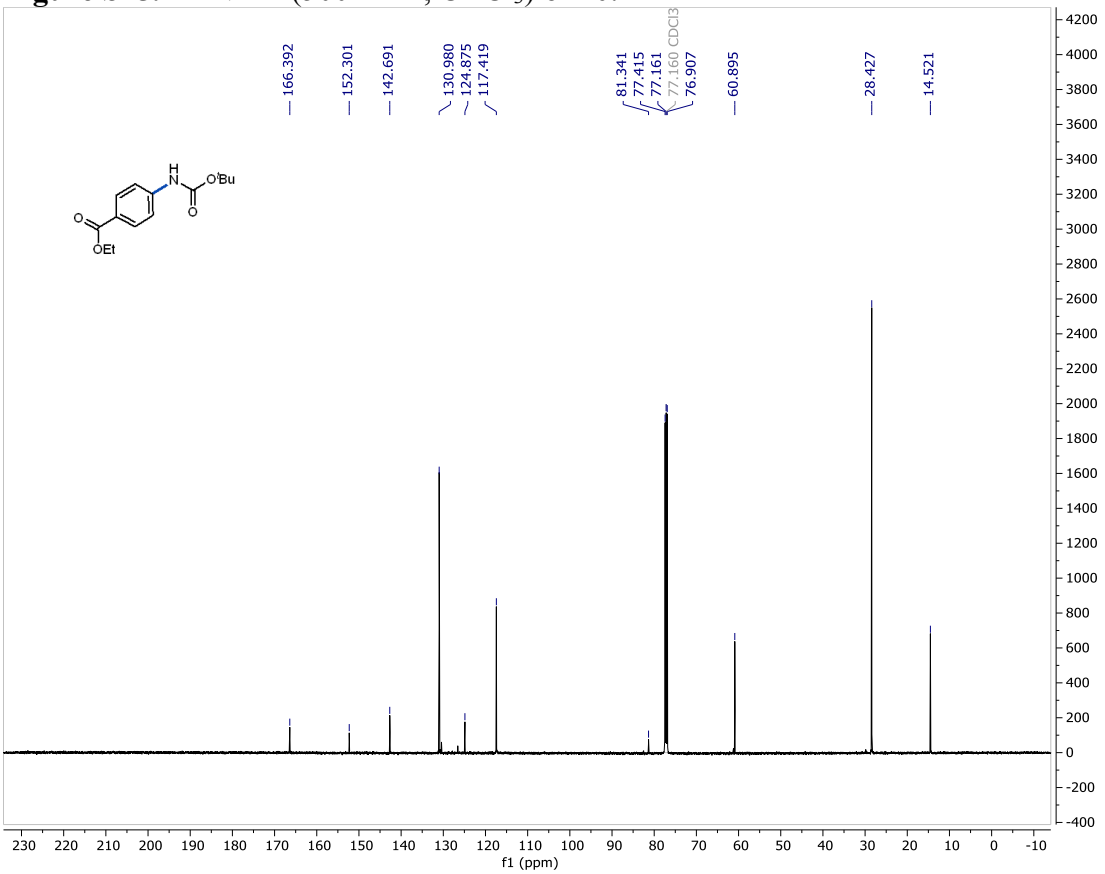

Figure S76. ^{13}C NMR (126 MHz, $CDCl_3$) of **20**.

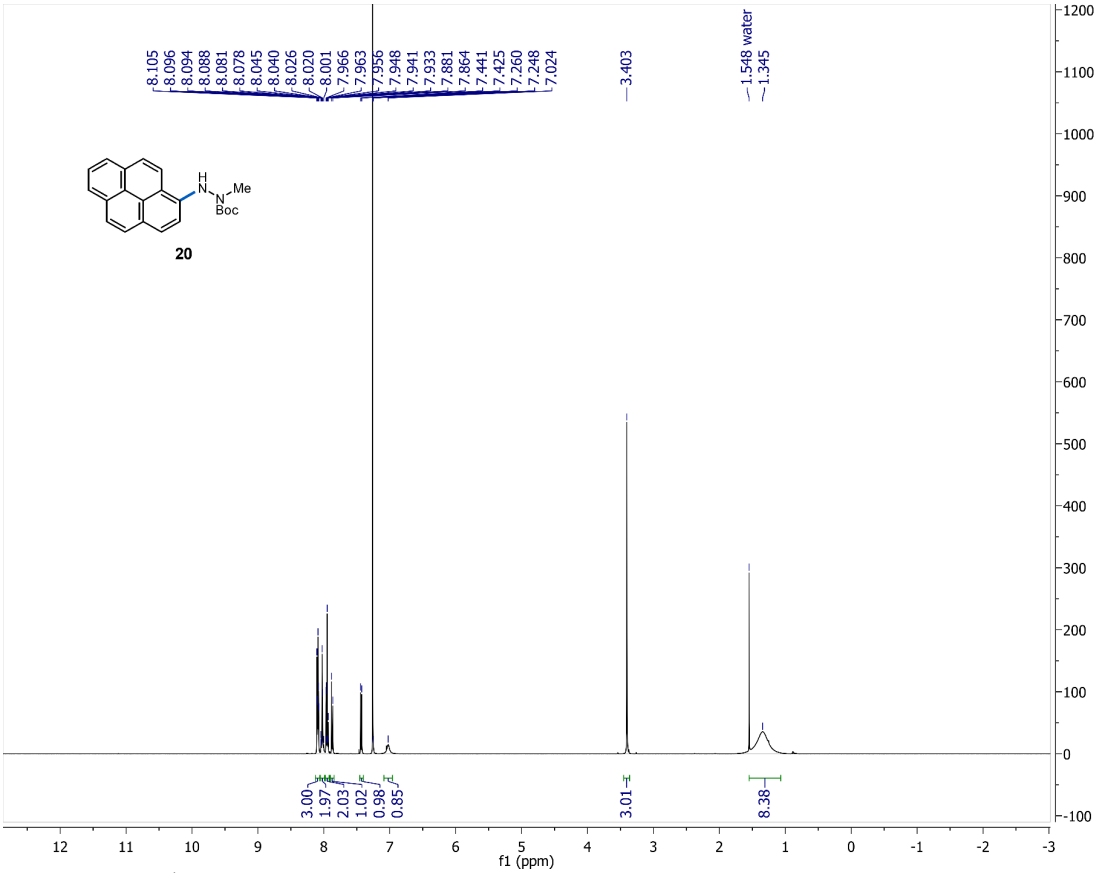

Figure S77. ^{1}H NMR (500 MHz, $CDCl_3$) of **21**.

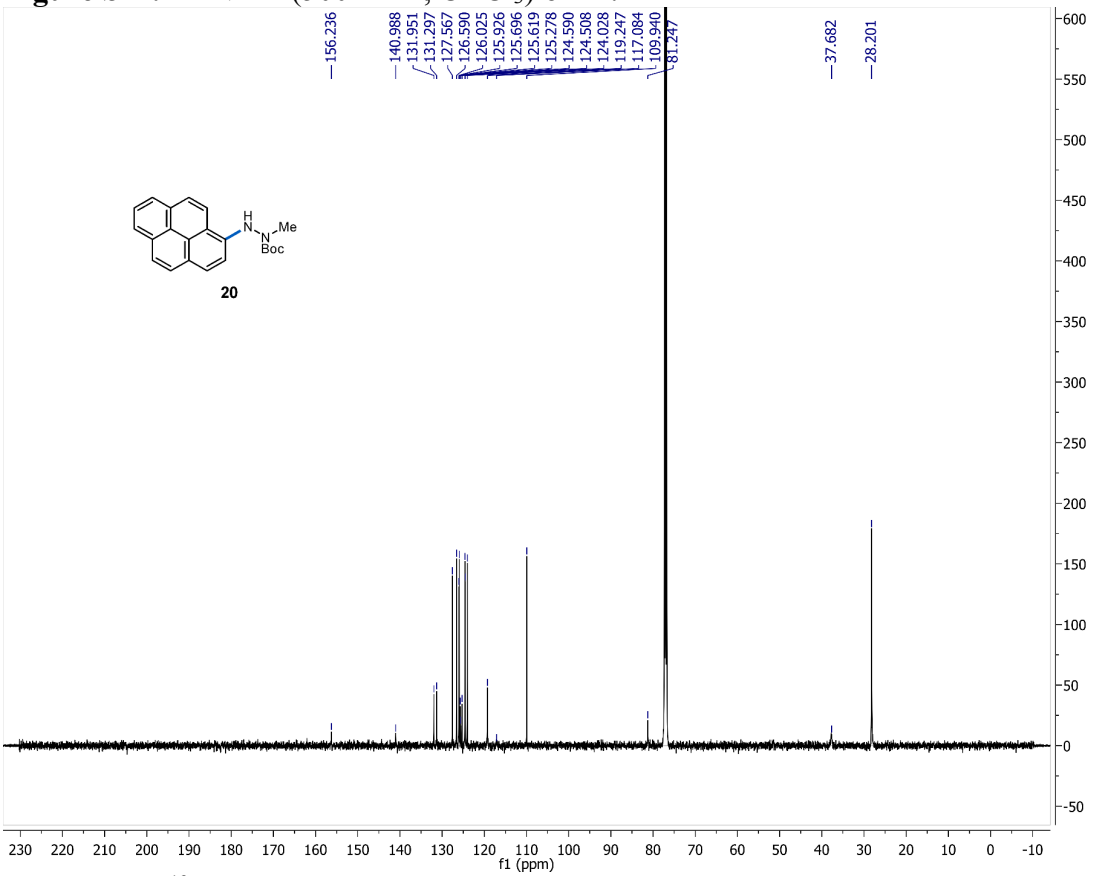

Figure S78. ^{13}C NMR (126 MHz, $CDCl_3$) of **21**.

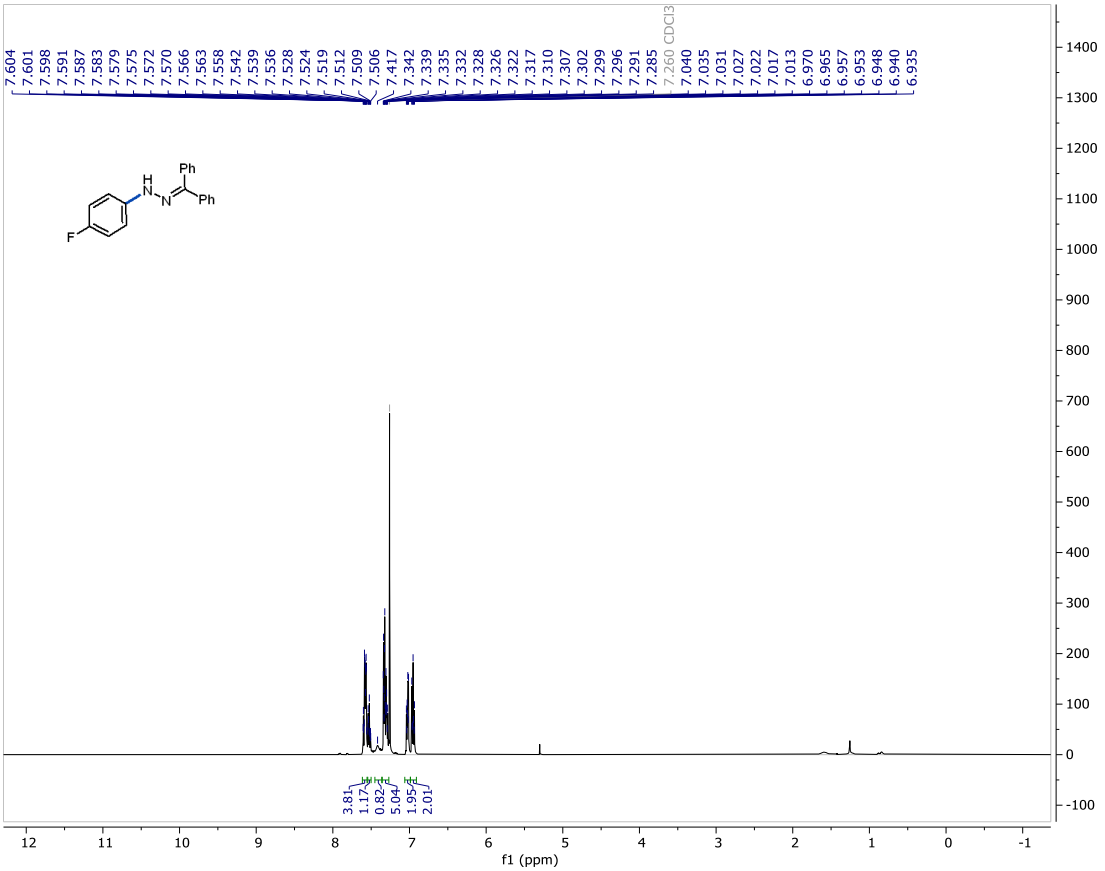

Figure S79. ^{1}H NMR (500 MHz, $CDCl_3$) of **22**.

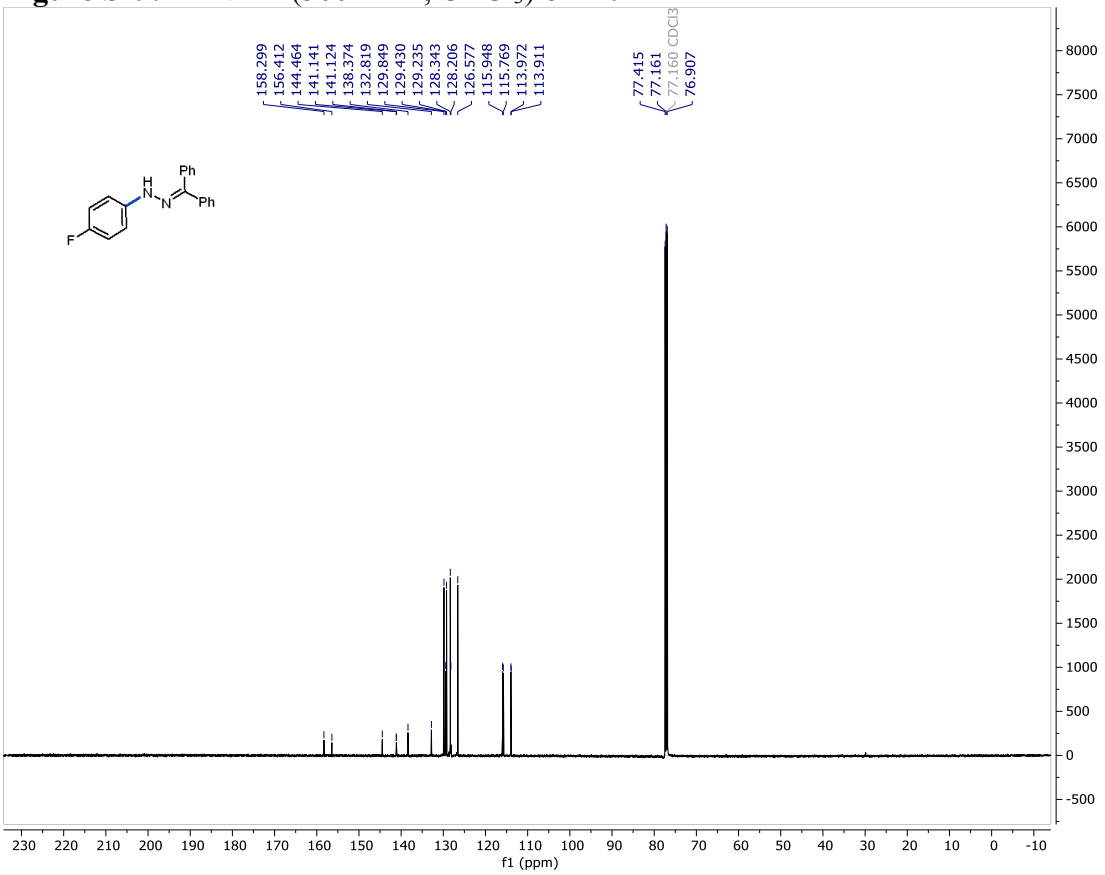

Figure S80. ^{13}C NMR (126 MHz, $CDCl_3$) of **22**.

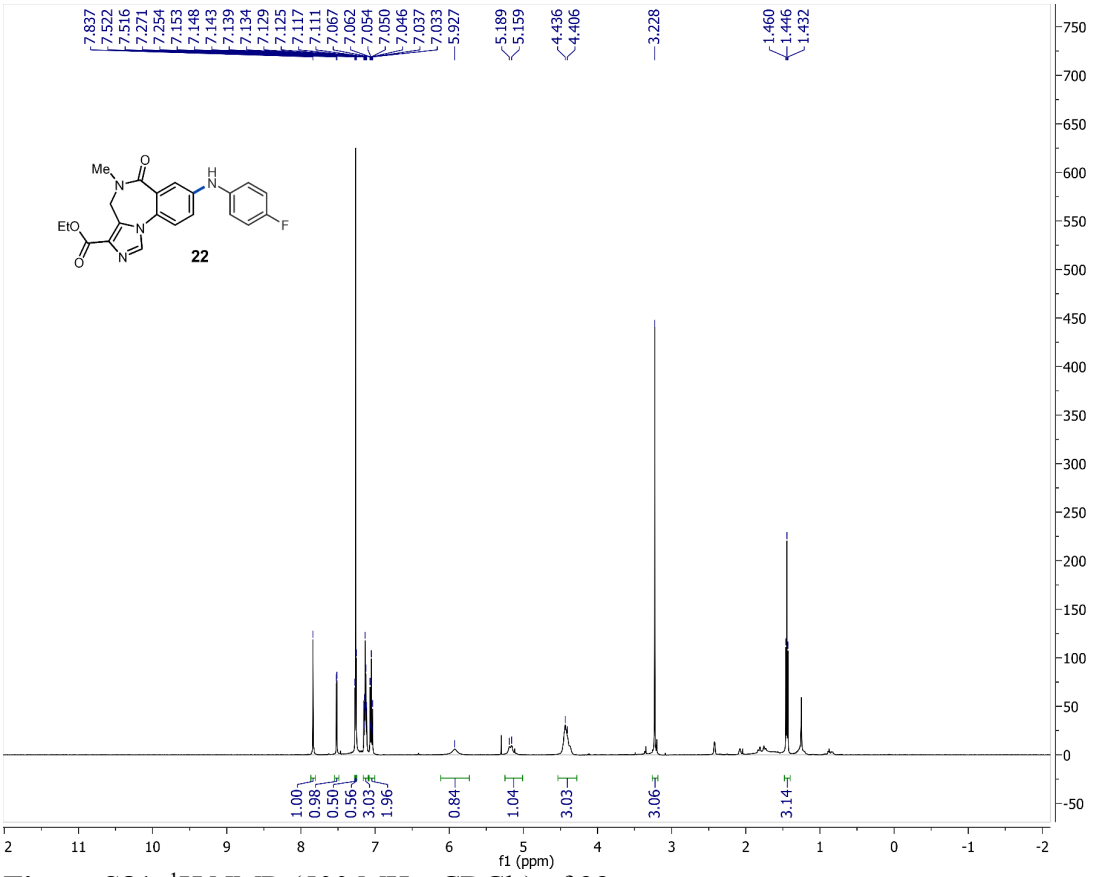

Figure S81. ^{1}H NMR (500 MHz, $CDCl_3$) of **23**.

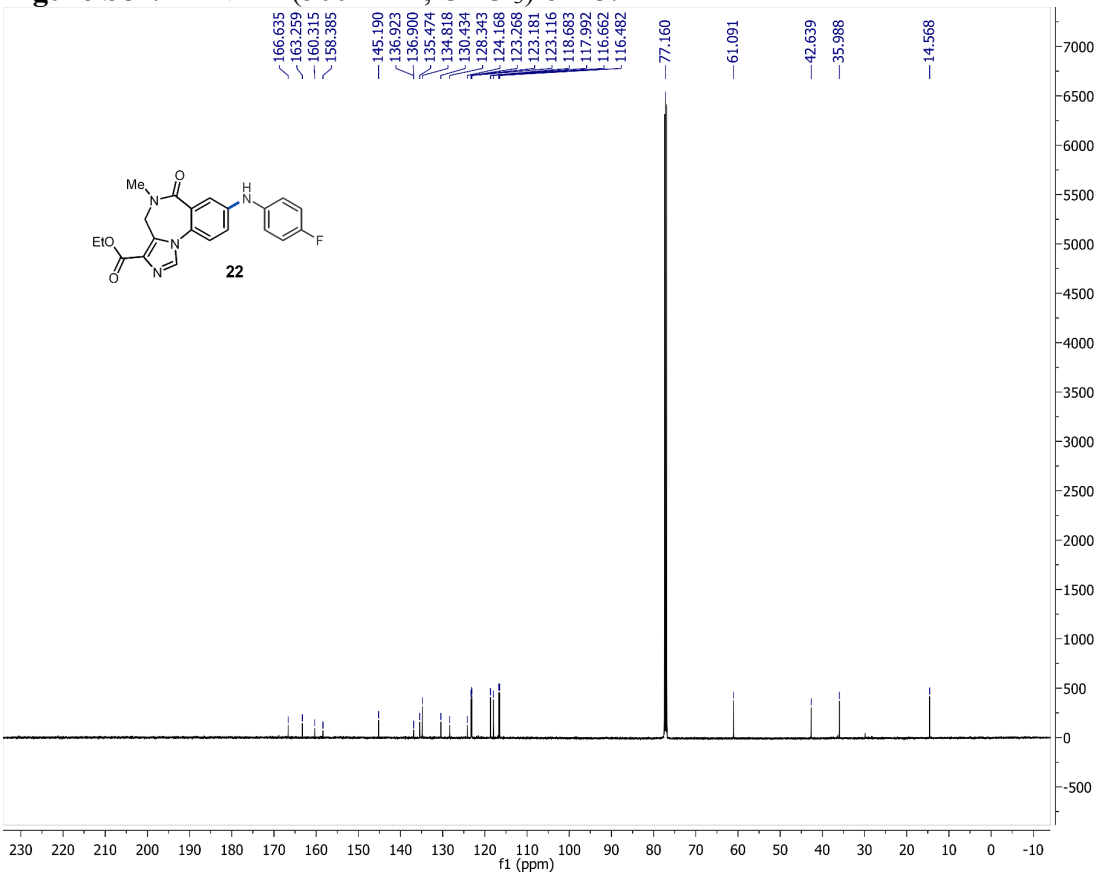

Figure S82. ^{13}C NMR (126 MHz, $CDCl_3$) of **23**.

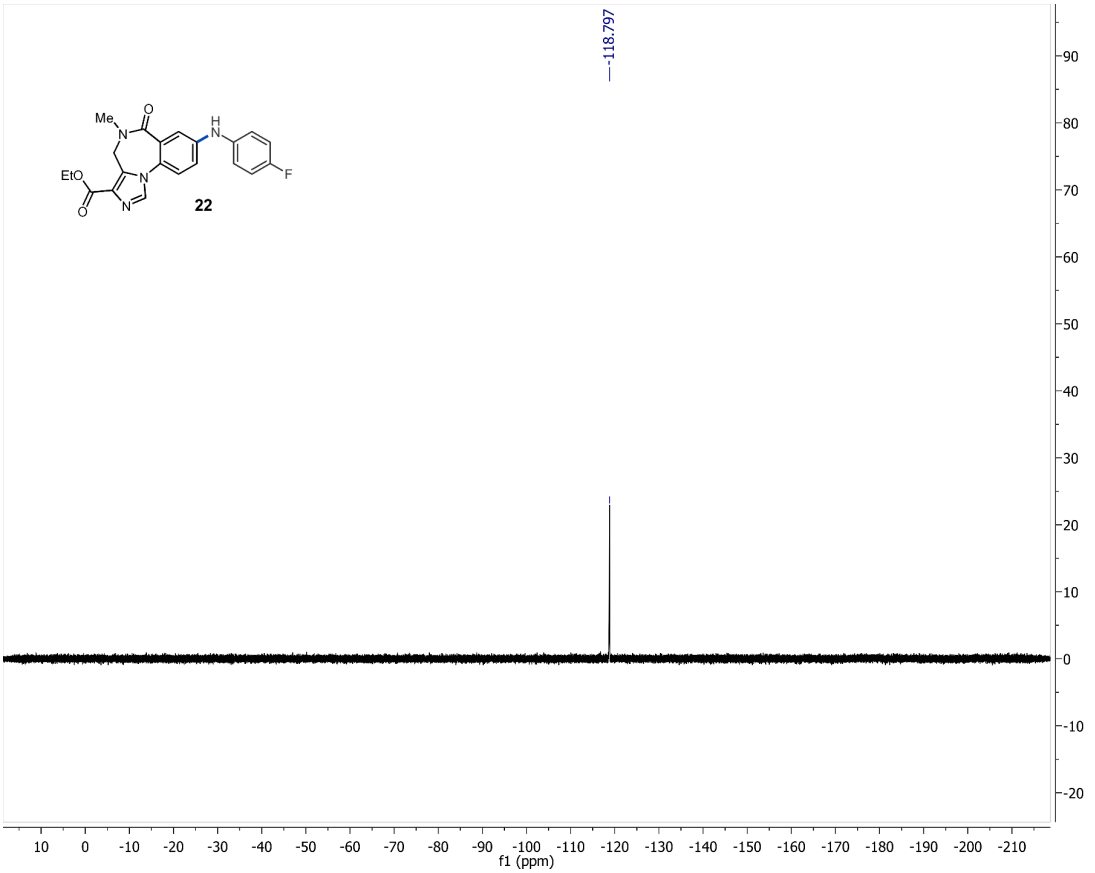

Figure S83. ^{19}F NMR (376 MHz, $CDCl_3$) of **23**.

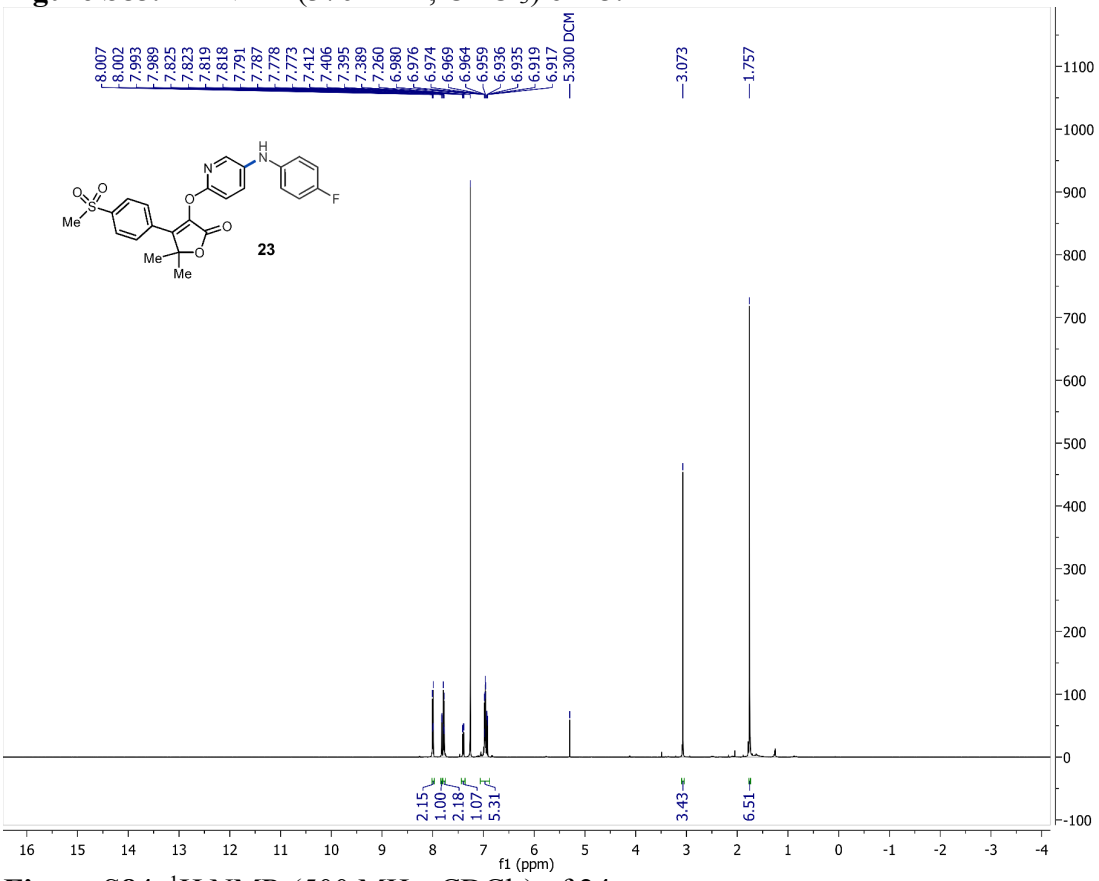

Figure S84. ^{1}H NMR (500 MHz, $CDCl_3$) of **24**.

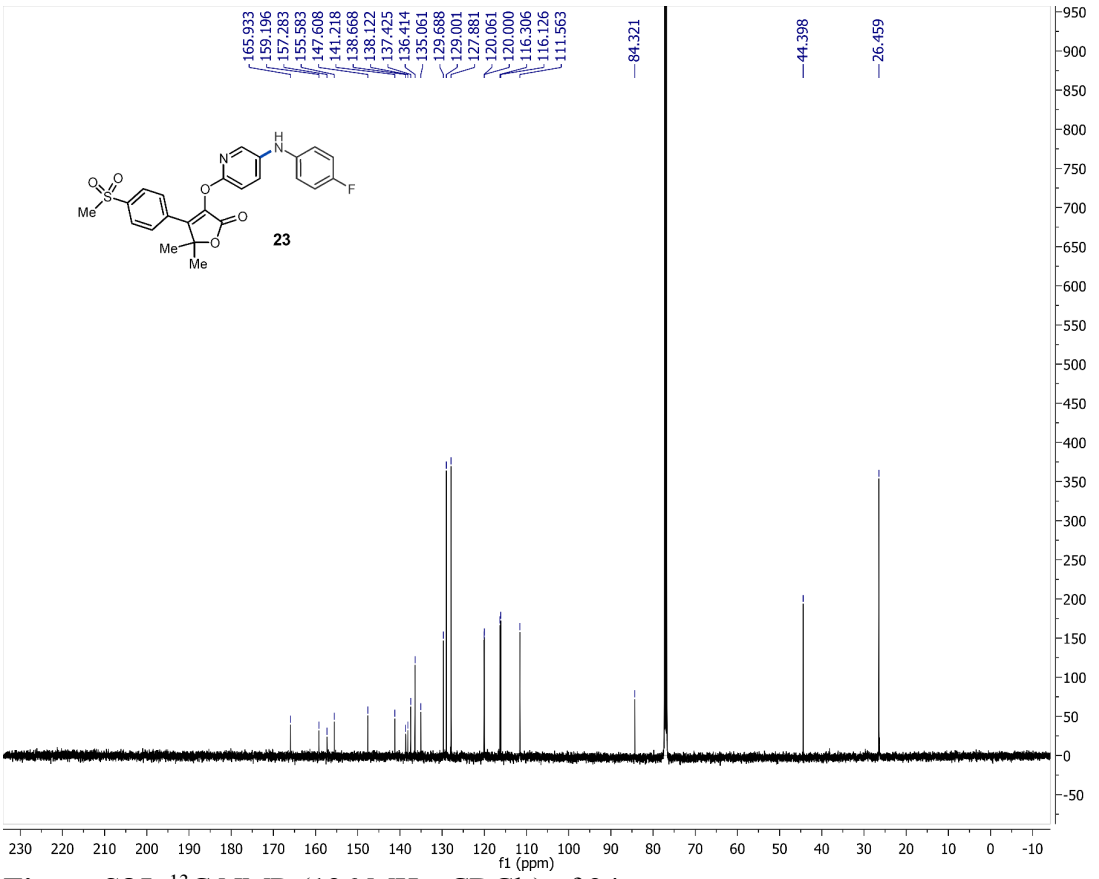

Figure S85. ^{13}C NMR (126 MHz, $CDCl_3$) of **24**.

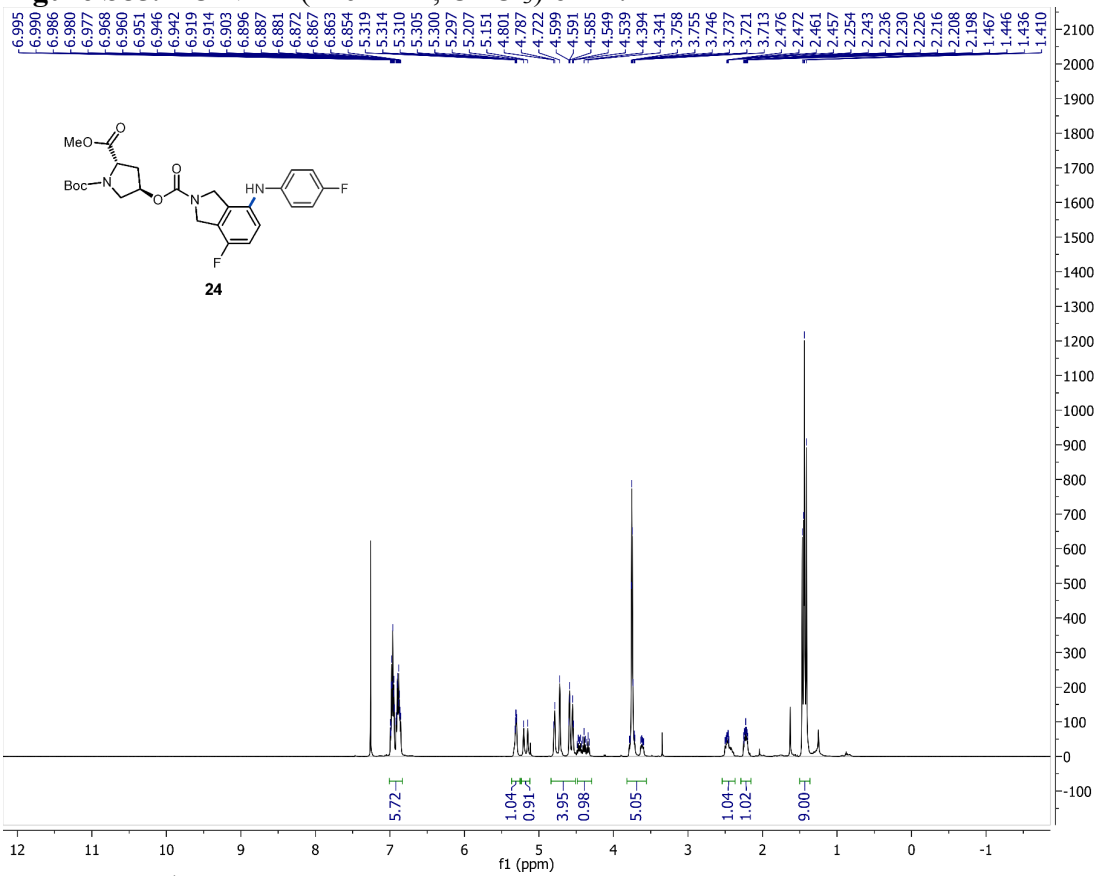

Figure S86. ^{1}H NMR (500 MHz, $CDCl_3$) of **25**.

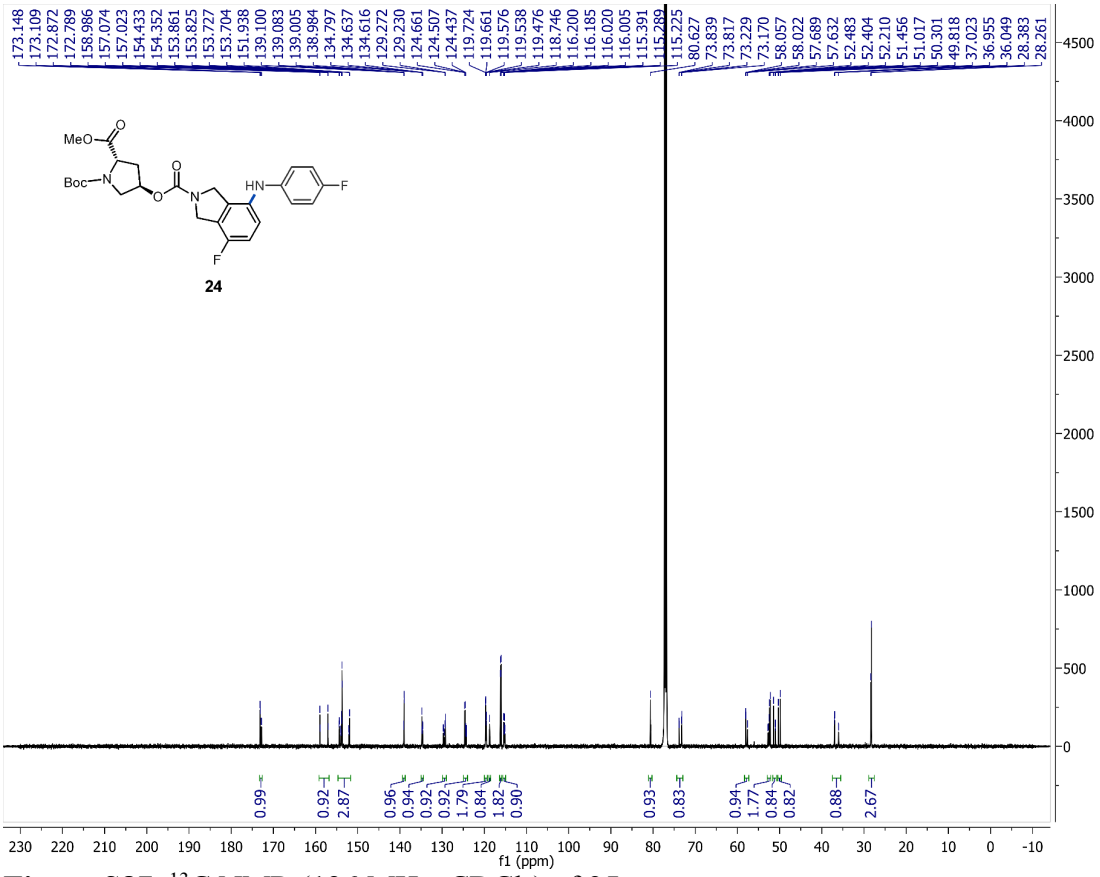

Figure S87. ^{13}C NMR (126 MHz, $CDCl_3$) of **25**.

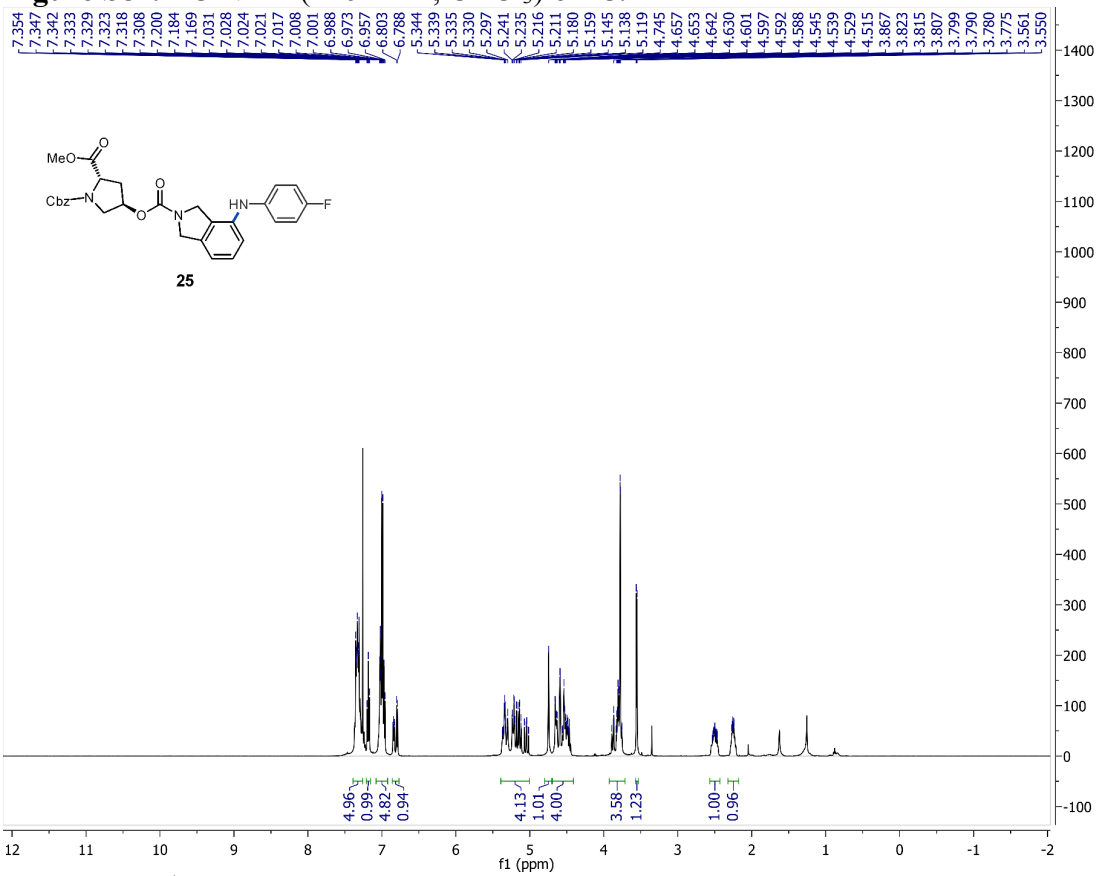

Figure S88. ^{1}H NMR (500 MHz, $CDCl_3$) of **26**.

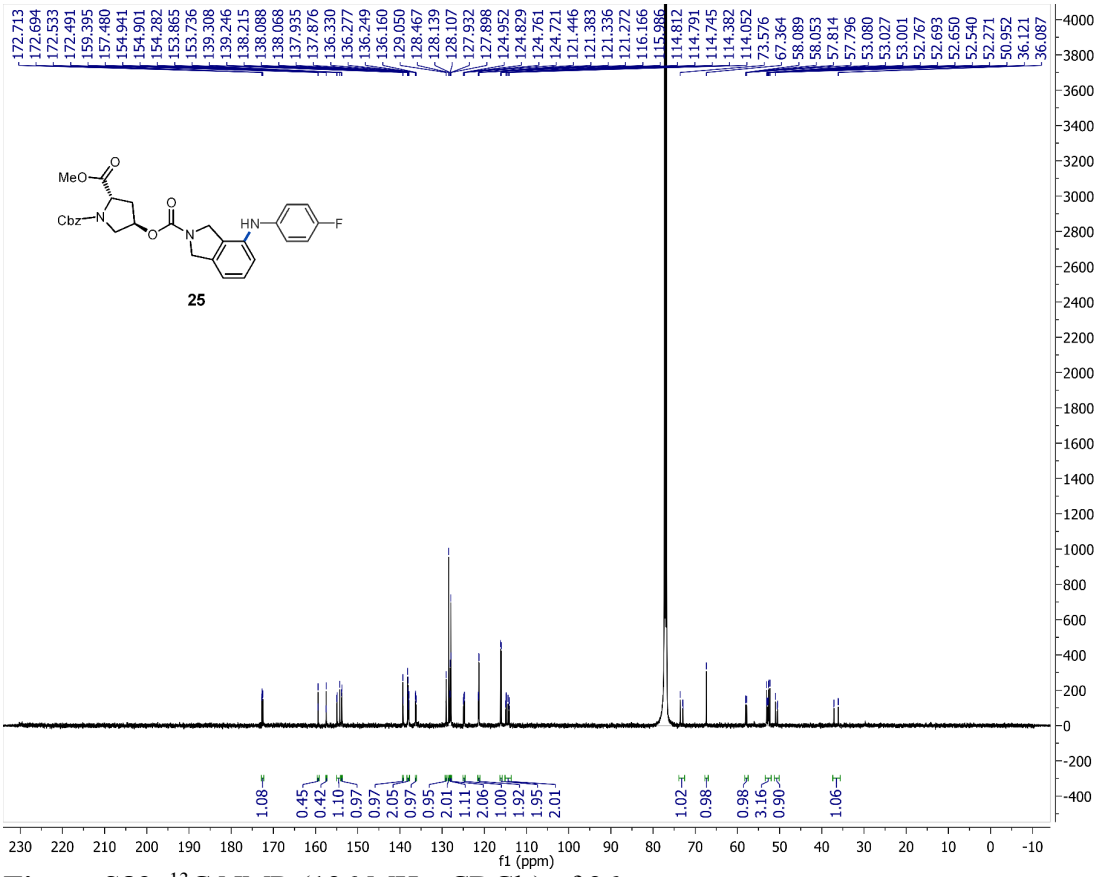

Figure S89. ^{13}C NMR (126 MHz, $CDCl_3$) of **26**.

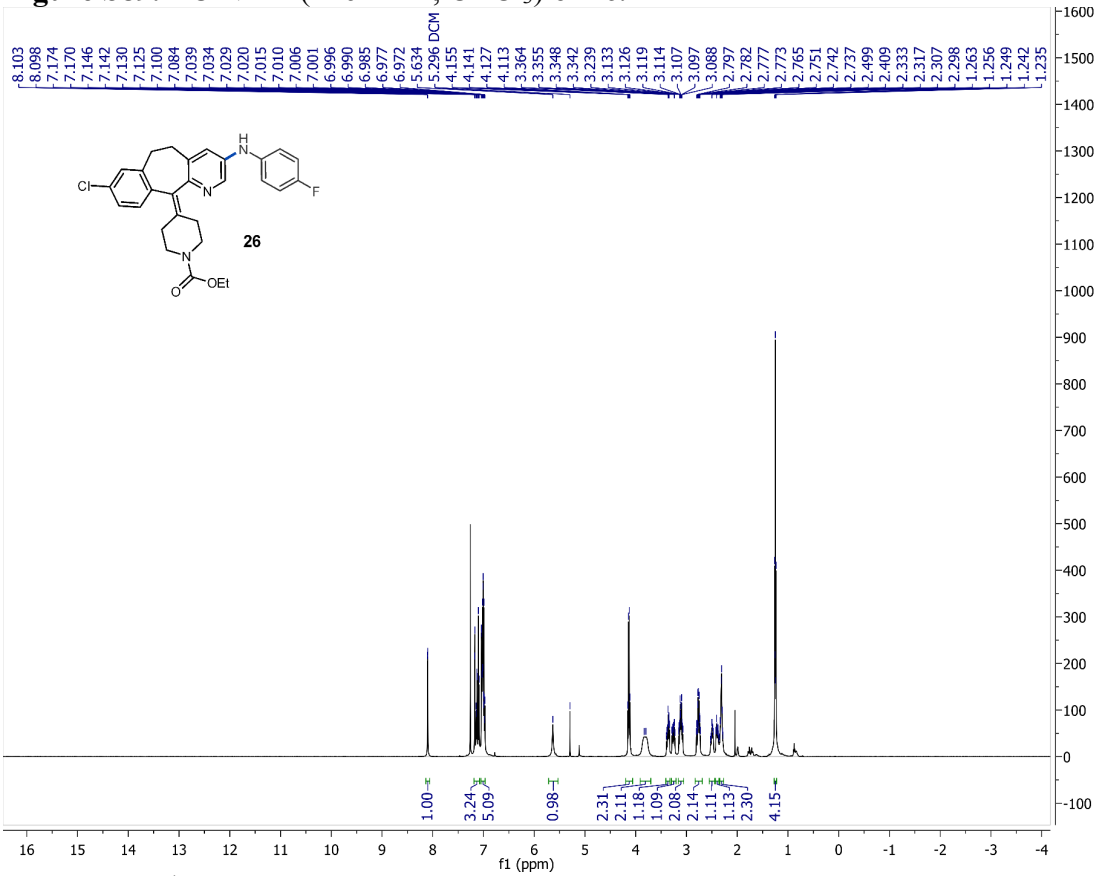

Figure S90. ^{1}H NMR (500 MHz, $CDCl_3$) of **27**.

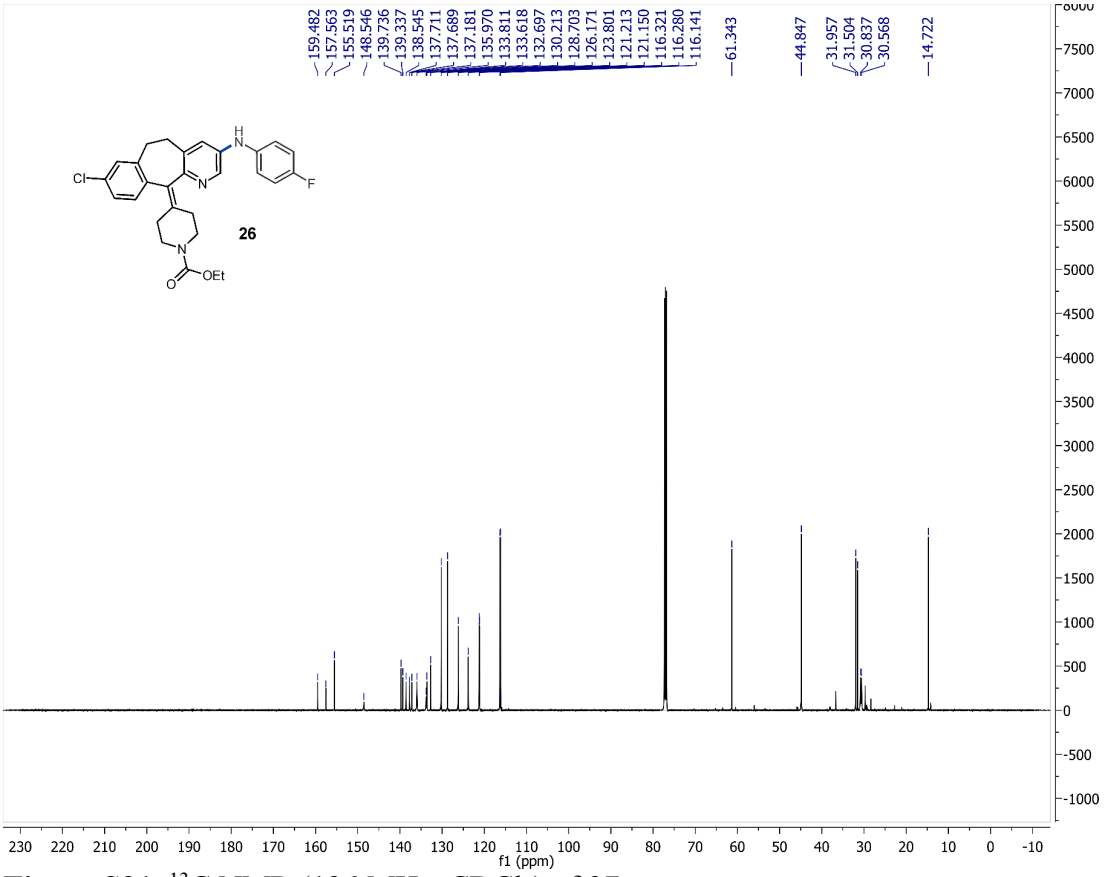

Figure S91. ^{13}C NMR (126 MHz, $CDCl_3$) of **27**.

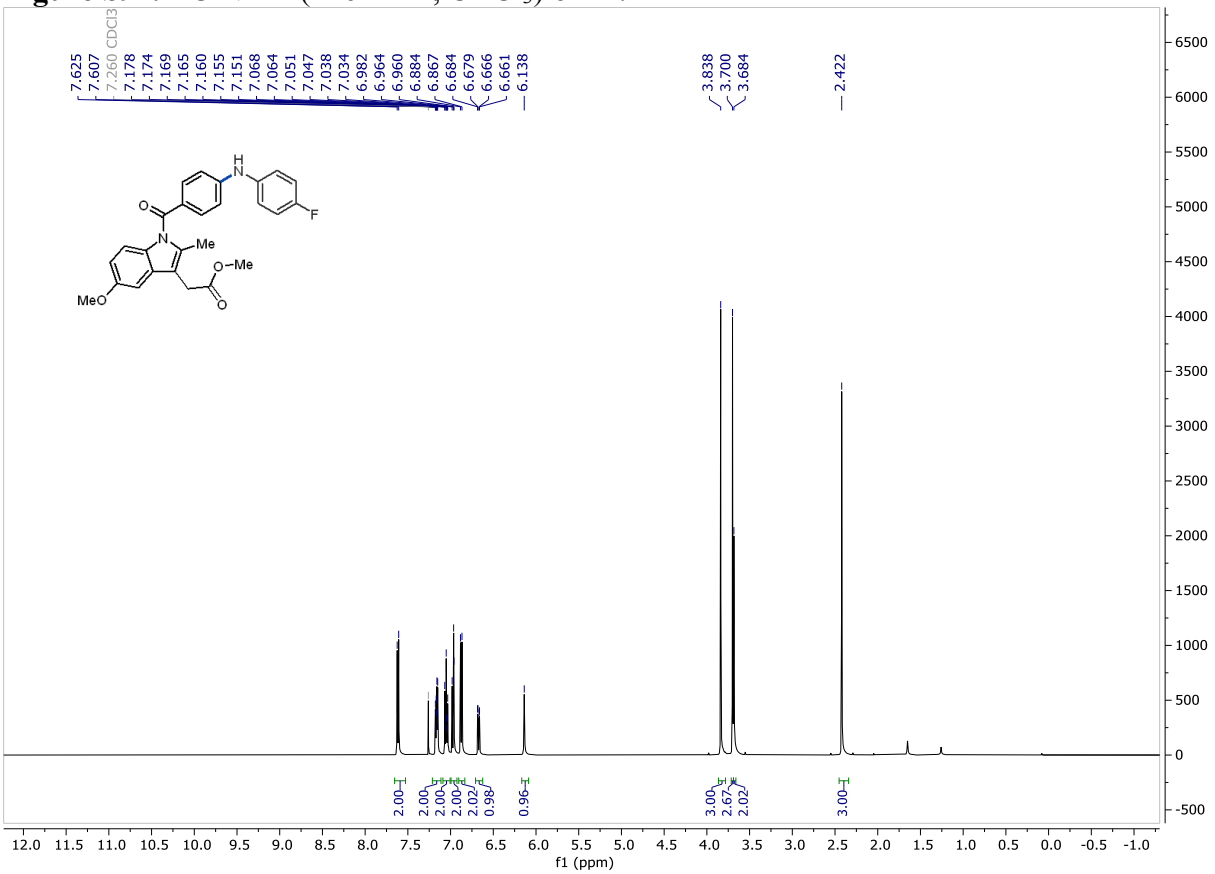

Figure S92. ^{1}H NMR (500 MHz, $CDCl_3$) of **28**.

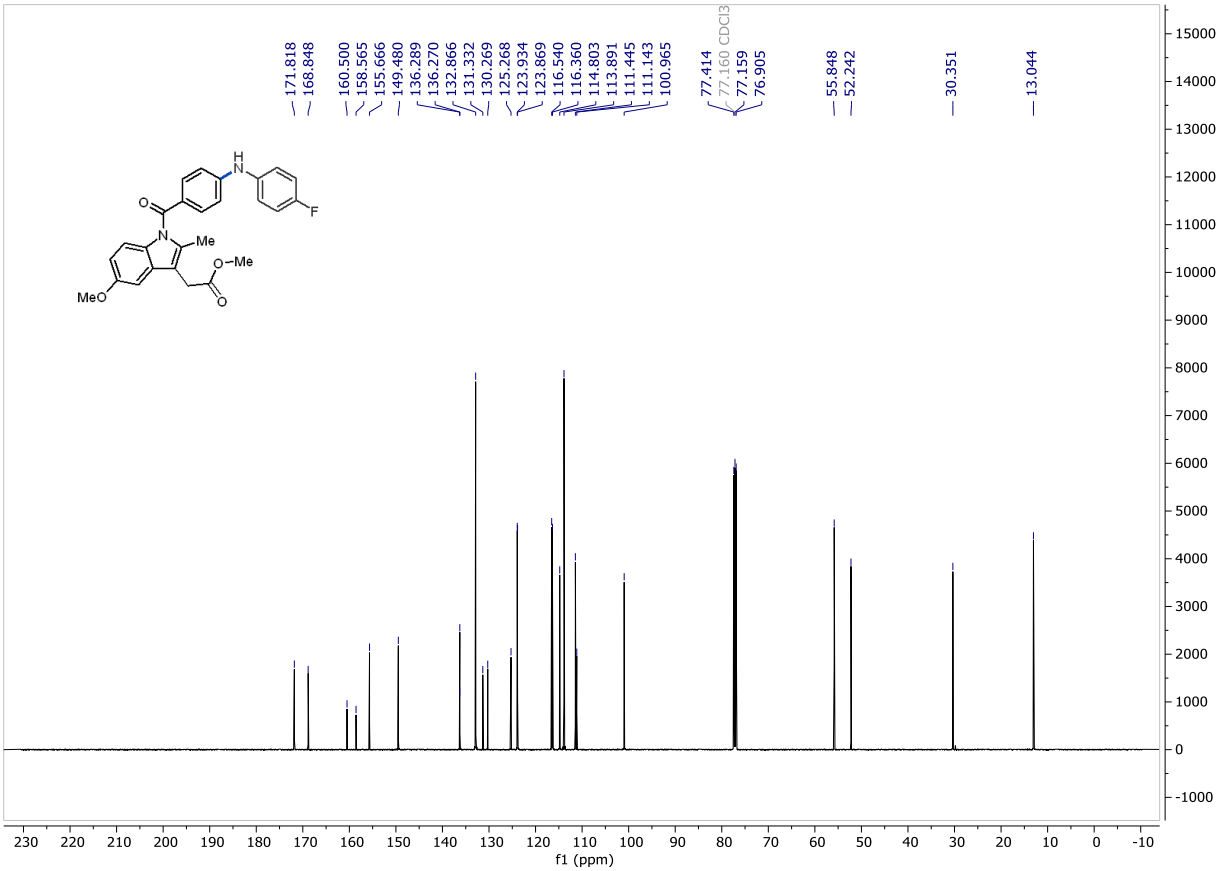

Figure S93. ^{13}C NMR (126 MHz, $CDCl_3$) of **28**.

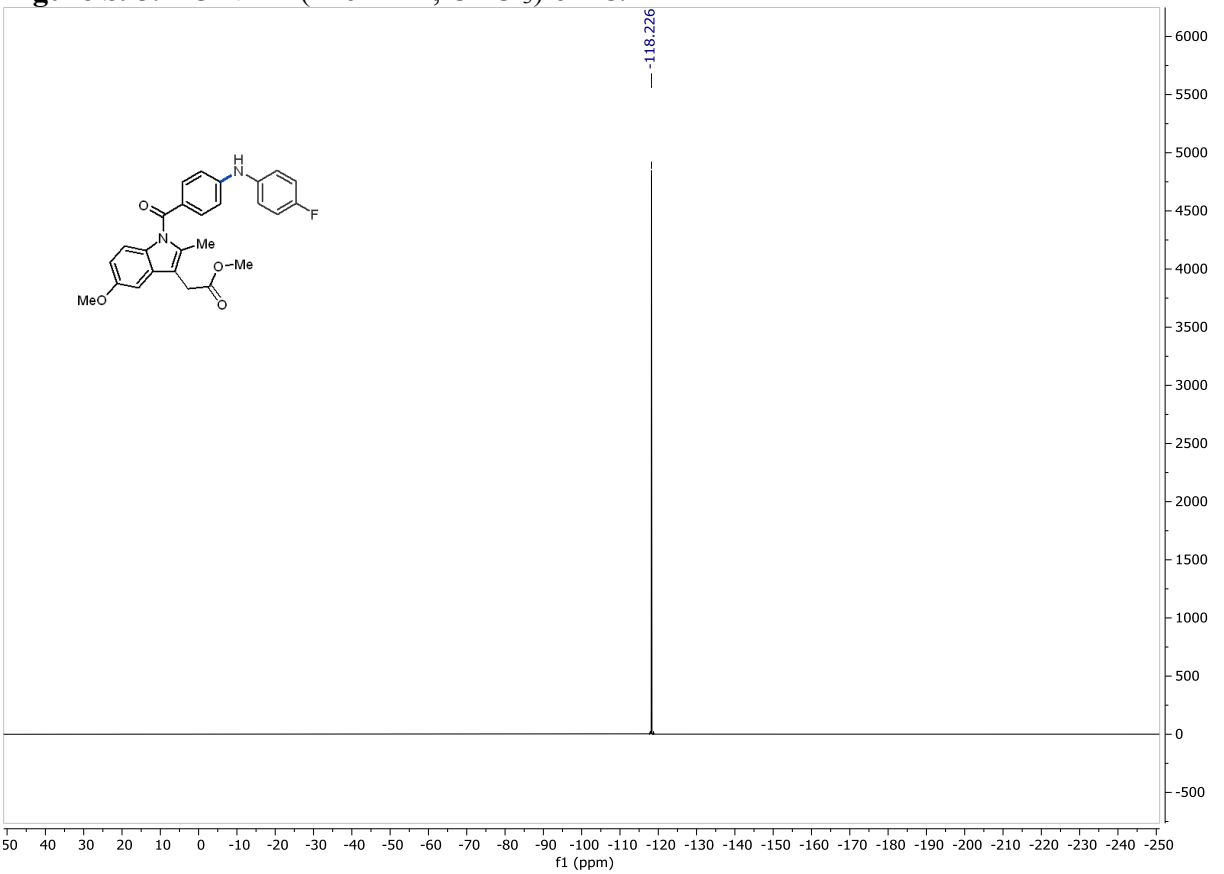

Figure S94. ^{19}F NMR (282 MHz, $CDCl_3$) of **28**.

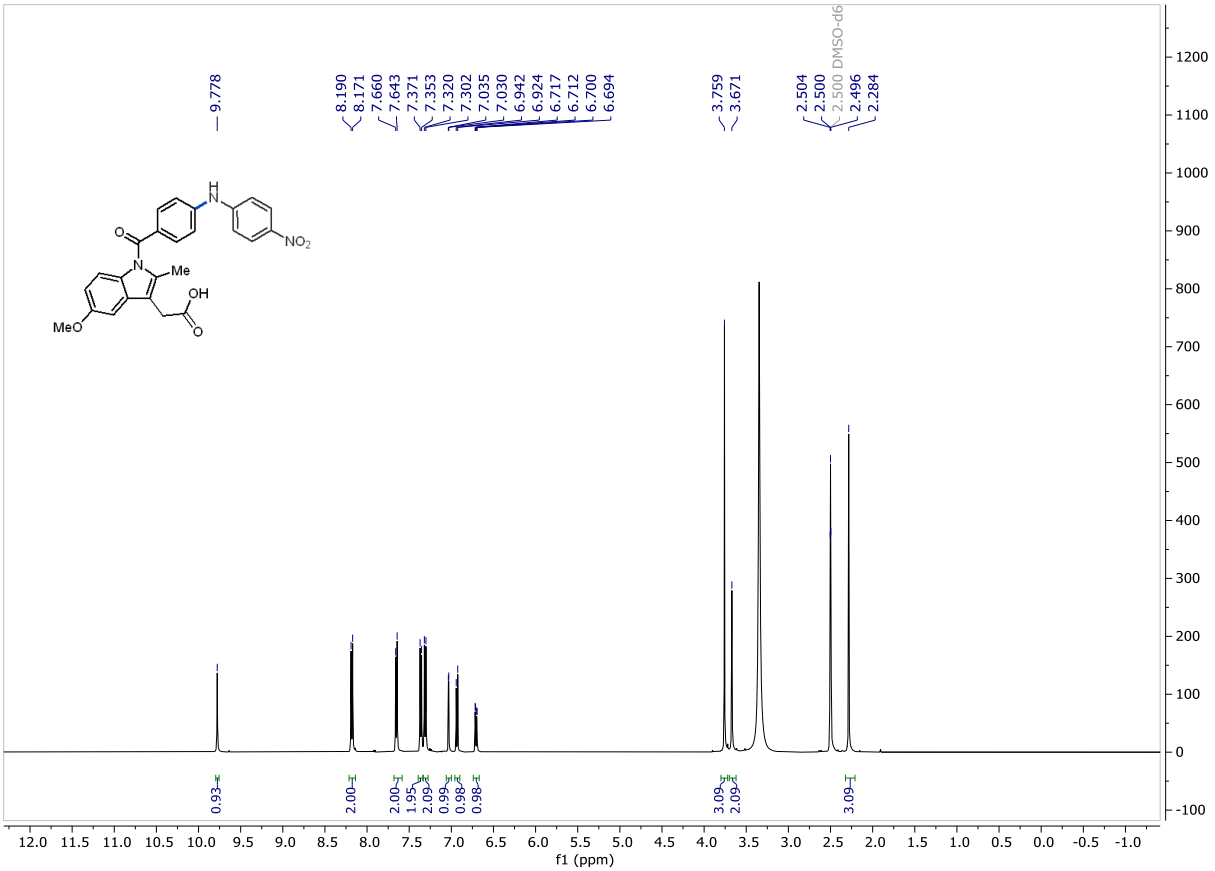

Figure S95. ^{1}H NMR (500 MHz, $CDCl_3$) of **29**.

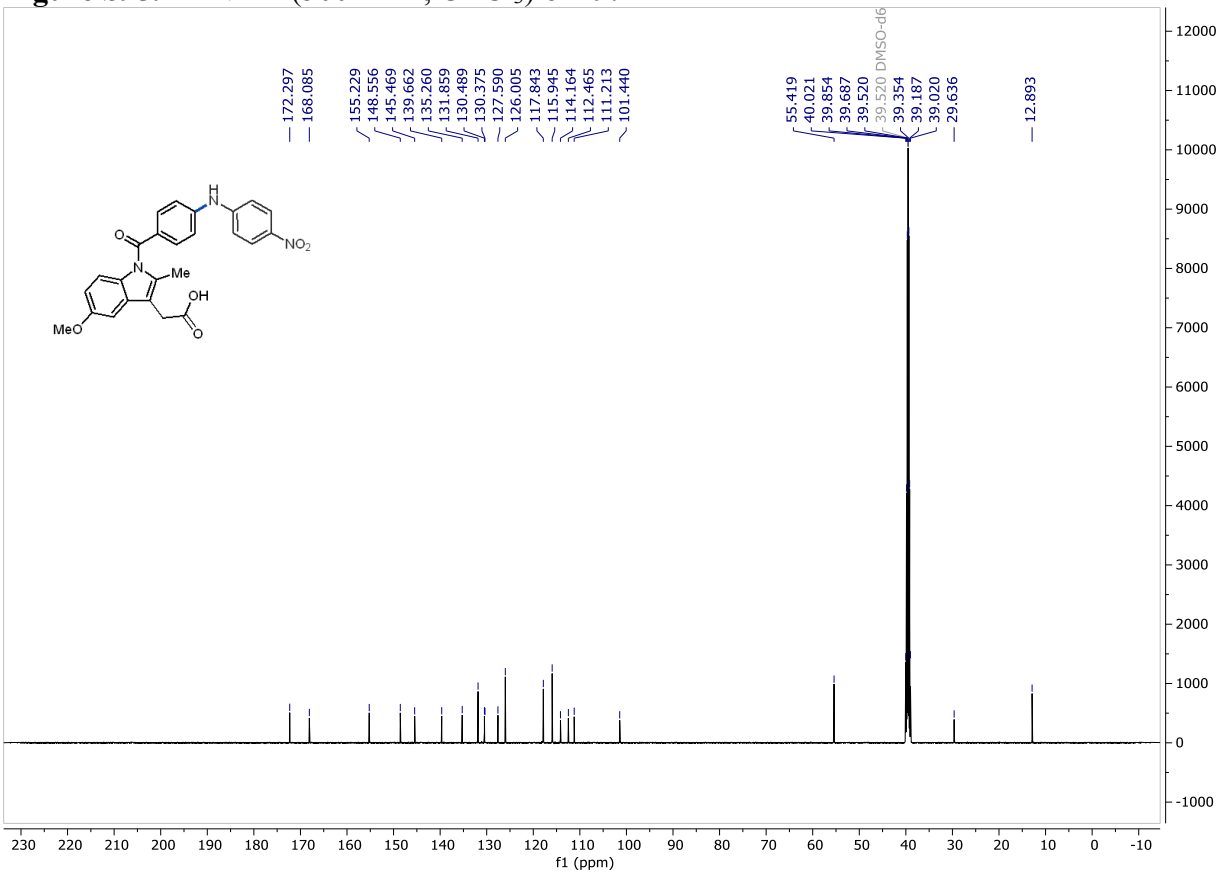

Figure S96. ^{13}C NMR (126 MHz, $CDCl_3$) of **29**.

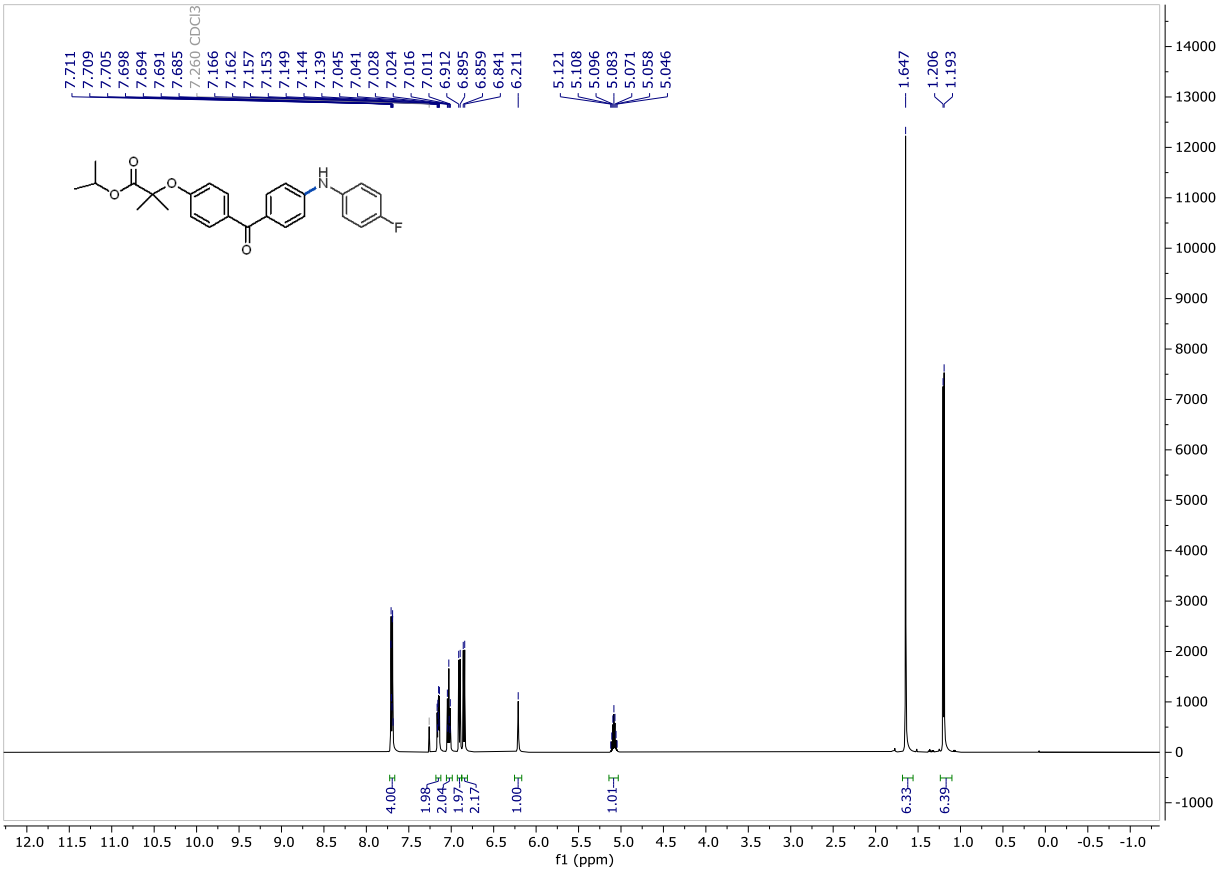

Figure S97. ^{1}H NMR (500 MHz, $CDCl_3$) of **30**.

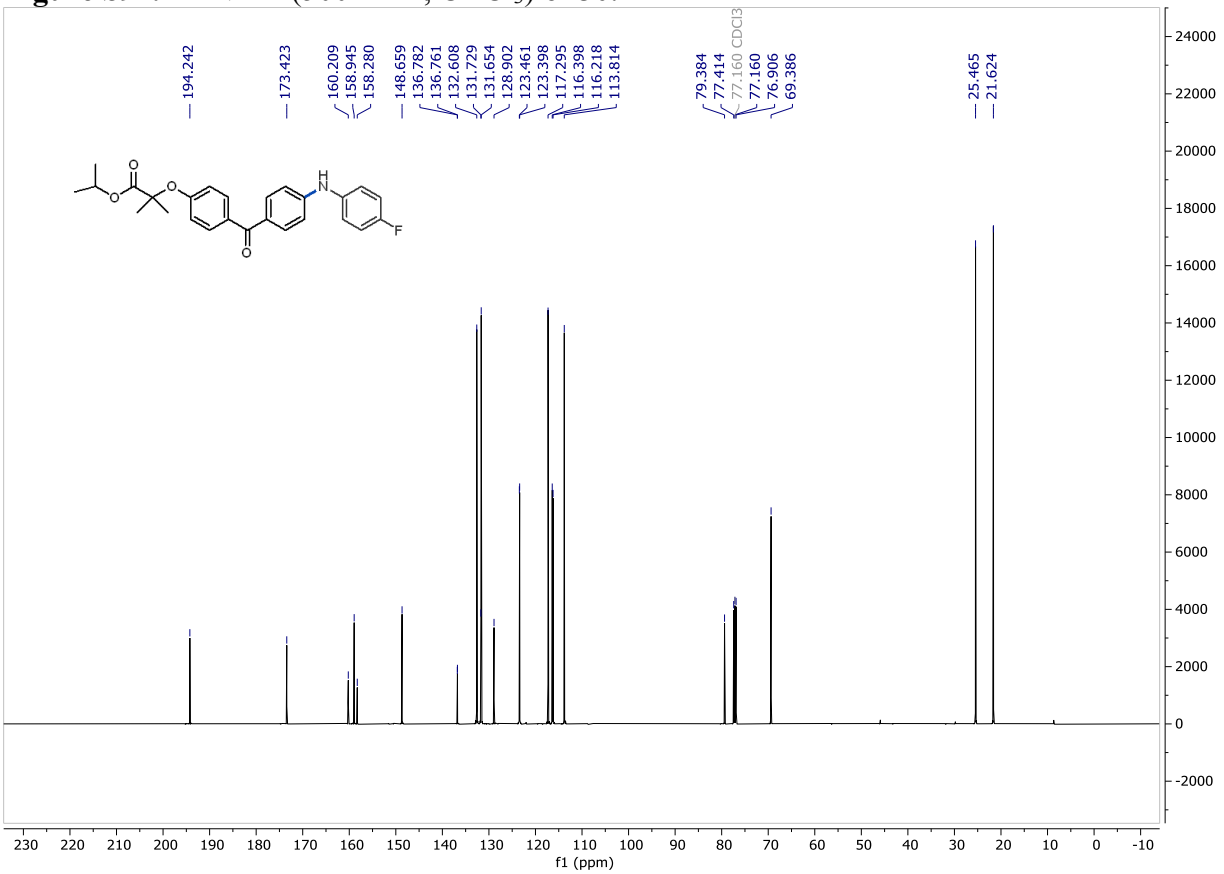

Figure S98. ^{13}C NMR (126 MHz, $CDCl_3$) of **30**.

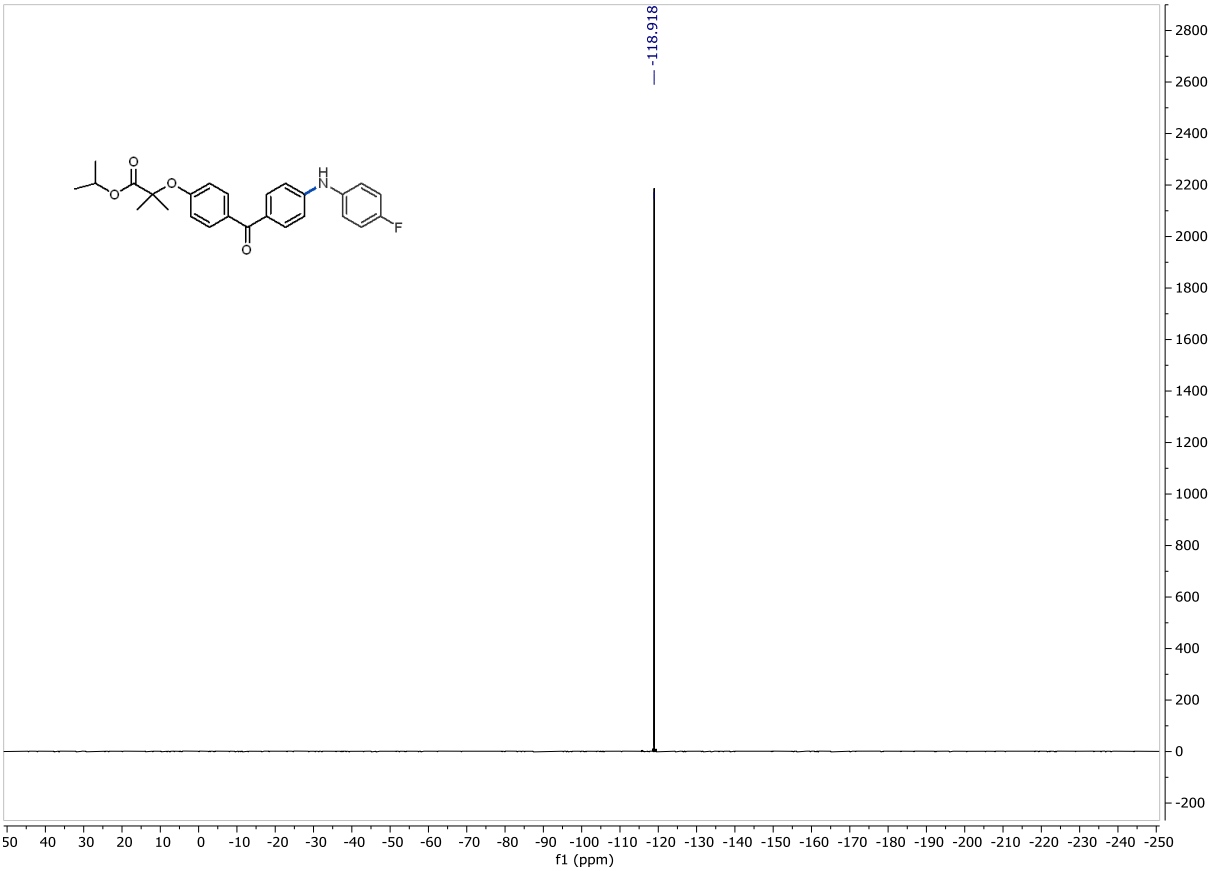

Figure S99. ^{19}F NMR (282 MHz, $CDCl_3$) of **30**.

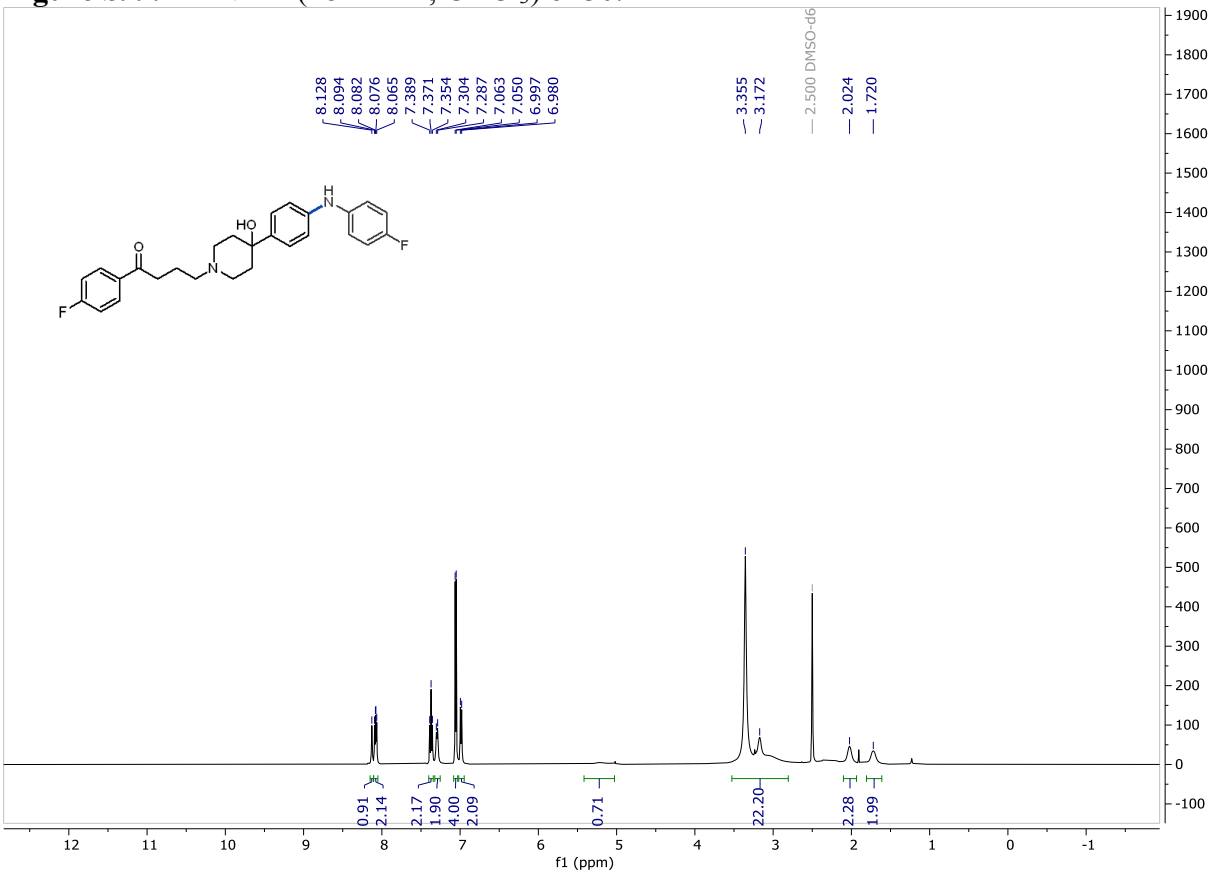

Figure S100. ^{1}H NMR (500 MHz, $CDCl_3$) of **31**.

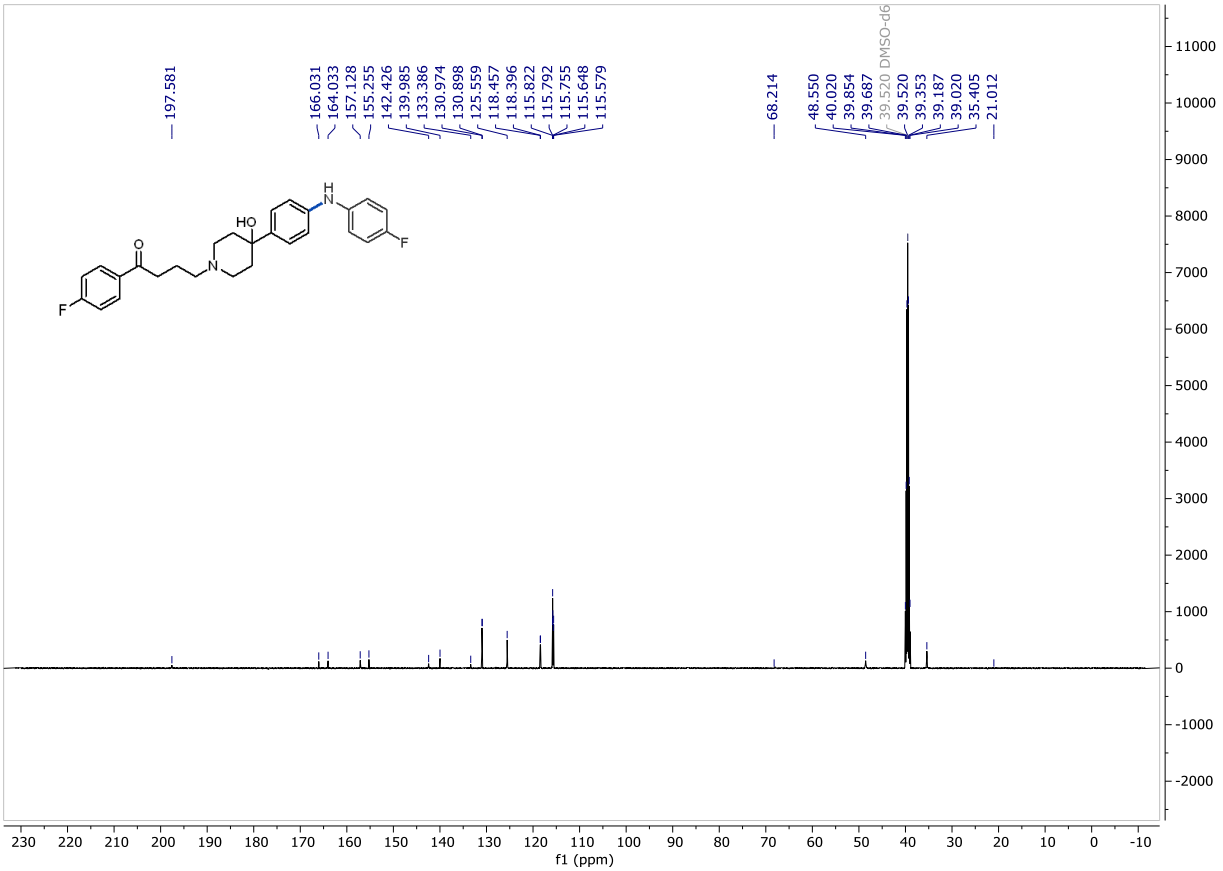

Figure S101. ^{13}C NMR (126MHz, $CDCl_3$) of **31**.

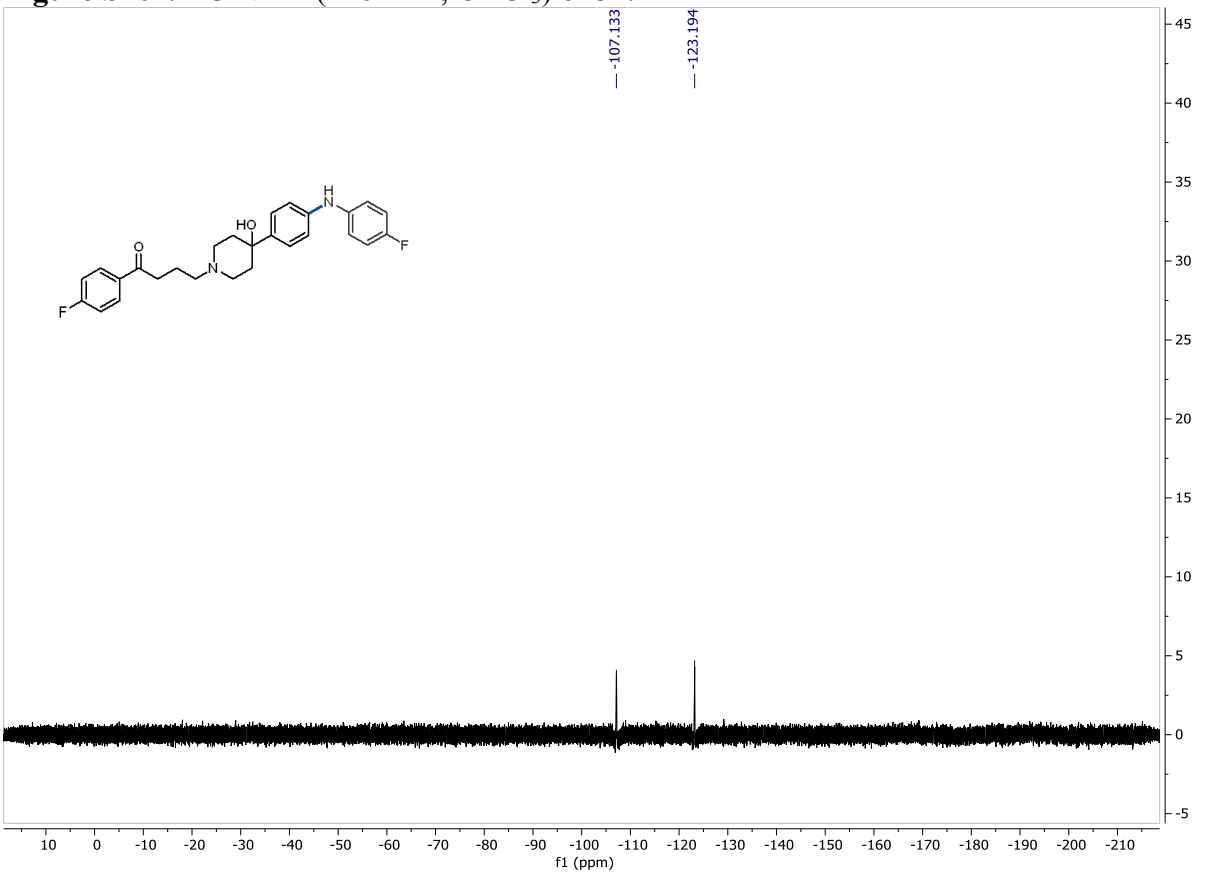

Figure S102. ^{19}F NMR (376 MHz, $CDCl_3$) of **31**.

References

1. Chen, L.; Ren, P.; Carrow, B. P., Tri(1-adamantyl)phosphine: Expanding the Boundary of Electron-Releasing Character Available to Organophosphorus Compounds. *J. Am. Chem. Soc.* **2016,** *138*, 6392-6395.
2. Chen, L.; Francis, H.; Carrow, B. P., An "On-Cycle" Precatalyst Enables Room-Temperature Polyfluoroarylation Using Sensitive Boronic Acids. *ACS Catal.* **2018,** *8*, 2989-2994.
3. Chen, L.; Sanchez, D. R.; Zhang, B.; Carrow, B. P., "Cationic" Suzuki–Miyaura Coupling with Acutely Base-Sensitive Boronic Acids. *J. Am. Chem. Soc.* **2017,** *139*, 12418-12421.
4. Fulmer, G. R.; Miller, A. J. M.; Sherden, N. H.; Gottlieb, H. E.; Nudelman, A.; Stoltz, B. M.; Bercaw, J. E.; Goldberg, K. I., NMR Chemical Shifts of Trace Impurities: Common Laboratory Solvents, Organics, and Gases in Deuterated Solvents Relevant to the Organometallic Chemist. *Organometallics* **2010,** *29*, 2176-2179.
5. Nykaza, T. V.; Yang, J.; Radosevich, A. T., PEt3-mediated deoxygenative CN coupling of nitroarenes and boronic acids. *Tetrahedron* **2019,** *75*, 3248-3252.
6. Burés, J., Variable Time Normalization Analysis: General Graphical Elucidation of Reaction Orders from Concentration Profiles. *Angew. Chem. Int. Ed.* **2016,** *55* 16084-16087.
7. Bastug, G.; Nolan, S. P., [Pd(IPr*OMe)(cin)Cl] (cin = Cinnamyl): A Versatile Catalyst for C–N and C–C Bond Formation. *Organometallics* **2014,** *33*, 1253-1258.
8. Akram, M. O.; Das, A.; Chakrabarty, I.; Patil, N. T., Ligand-Enabled Gold-Catalyzed C(sp2)–N Cross-Coupling Reactions of Aryl Iodides with Amines. *Org. Lett.* **2019,** *21*, 8101-8105.
9. Kampmann, S. S.; Sobolev, A. N.; Koutsantonis, G. A.; Stewart, S. G., Stable Nickel(0) Phosphites as Catalysts for C–N Cross-Coupling Reactions. *Adv. Syn. Catal.* **2014,** *356*, 1967-1973.
10. Kudisch, M.; Lim, C.-H.; Thordarson, P.; Miyake, G. M., Energy Transfer to Ni-Amine Complexes in Dual Catalytic, Light-Driven C–N Cross-Coupling Reactions. *J. Am. Chem. Soc.* **2019,** *141*, 19479-19486.
11. Hammett, L. P., The Effect of Structure upon the Reactions of Organic Compounds. Benzene Derivatives. *J. Am. Chem. Soc.* **1937,** *59*, 96-103.